Wave/Structure Interaction in Two-Layer Fluids

Jonathan R. Cadby

Doctoral Thesis.

Submitted in partial fulfilment of the requirements

for the award of

Doctor of Philosophy of Loughborough University

November 2000.

Supervisor: C.M. Linton, PhD. Loughborough University

Acknowledgements

I would like to thank Dr C.M. Linton for all his help and guidance during the last three years in which I have been producing the work presented in this thesis. I would also like to thank Dr M. McIver for her additional help.

The financial support of the Engineering and Physical Sciences Research Council through award reference 97004025 is gratefully acknowledged.

Finally I would also like to thank my parents for all their encouragement, patience and additional financial support over the course of this PhD.

Abstract

The main theme of this thesis is that of wave and submerged structure interaction in two-layer fluids. By a two-layer fluid we mean one which contains a layer of finite depth bounded above by a free surface and below by an infinite or finite layer of greater density. For such a situation time-harmonic waves can propagate with two different wavenumbers for a given frequency. One of these wavenumbers corresponds to waves where the motion is concentrated near the free surface and the other to waves near the interface between the two fluids.

All the problems that will be examined will be based on linear inviscid water wave theory. The work is separated into two parts; in part I three-dimensional problems involving spheres are investigated whereas part II is concerned with the two-dimensional problems of horizontal circular cylinders. All of the problems are solved using the method of multipole expansions.

In a single-layer fluid there are a number of reciprocity relations that exist which connect various hydrodynamic quantities. In chapter 2 we systematically extend all these relations to the three-dimensional two-layer fluid case. The radiation and scattering problems of a sphere in either the upper and lower layer are then solved. Chapter 3 examines the effect of a finite-depth lower layer on the radiation problem.

Chapters 4 and 5 investigate the transmission and reflection of incident waves by a horizontal circular cylinder. Chapter 4 contains the scattering problem where the lower layer is of finite depth whilst in chapter 5 obliquely incident waves are considered in a finite-depth single-layer fluid and then in a two-layer fluid. For the latter case, we find that there are frequencies at which complete reflection of the obliquely incident waves occurs.

Trapped modes above a horizontal circular cylinder are looked into in chapter 6. We first consider the single-layer problem for finite depth and then move onto the two-layer case. Using the fact that obliquely incident waves on a horizontal circular cylinder can be totally reflected we seek embedded trapped modes between a cylinder and a wall in chapter 7.

Contents

Chapter 1

Introduction

1.1 Historical review

This thesis is concerned with the interaction of surface gravity and internal waves with rigid bodies. Gravity waves are the type which occur on the surface of large bodies of water such as seas and lakes. The main restoring force of such waves is gravity, hence the name, and are generally generated by wind acting on the water surface. Internal waves occur along pycnoclines and thermoclines which are horizontal layers of sharp density stratification due to temperature and salinity variations. Gravity plays a role in the restoring force of the internal waves also.

One motivation for the study of the interaction of waves and structures in two-layer fluids is the suggestion by Friis, Grue & Palm (1991) that an underwater pipe bridge might be built across one of the Norwegian fjords. A fjord typically consists of a layer of fresh water about 10 m thick on top of a very deep body of salt water. A bridge would have a diameter large enough for a two-lane road, about 10 m, and would enter the water at a gentle slope passing through the free surface, the middle section being 40 m or so below the free surface, (and therefore totally within the lower layer), before rising through the upper layer and breaking the free surface on the other side of the fjord. A two-layer fluid model can also be used to investigate the effects of muddy water at the bottoms of channels and harbours on the hydrodynamic characteristics of ships. Over recent years a number of journal papers and conference proceedings have been written on the subject of waves in two-layer fluids.

We consider a fluid consisting of a layer of finite depth bounded above by a free surface and below by either a finite or infinite layer of fluid of greater density. There is

a density jump at the interface between the upper and lower fluids which represents an infinitely thin pycnocline. Although the largest currents which can occur in the fjords, around 1–2m/s, would cause some mixing of the layers at the interface, we will assume no mixing occurs.

The analysis of the effects of water waves upon structures was initiated well over a century ago by W Froude and A.N. Krylov. The interest in this area has become more widespread over the last half a century with investigators progressively becoming more ambitious. One reason for such interest in this field is the need to accurately predict the forces that will be exerted by waves on offshore structures placed in the sea. Such structures will move in response to waves incident on them and also radiate waves due to their motion. Solutions of such problems are extremely difficult even when the body geometry is simple.

In order to simplify the wave/structure interaction problems, we assume that the fluid is inviscid and incompressible which are good approximations in the case of water waves. The flow will be assumed to be irrotational such that potential theory can be employed. In wave-body interaction there are three relevant length scales; the characteristic body dimension a, the wavelength $2\pi/k$, and the wave amplitude A. These lengths can be combined to obtain two non-dimensional parameters, for example, kA and ka. We shall assume that the amplitude of the waves is much smaller than the wavelength so that $kA \ll 1$. Furthermore we shall assume that the body is large ($ka = O(1)$) such that its presence alters the pattern of wave propagation significantly and produces diffraction. Under these assumptions the equations of motion and boundary conditions can be linearised. Due to linearisation we can decompose the problem of waves incident on a moving body into two simpler problems; the radiation of waves due to a body oscillating in an otherwise still water and the scattering (or diffraction) of waves by a fixed body.

A rigid body in three dimensions has six degrees of freedom and thus six possible modes of motion. The three translational modes are referred to as sway, surge and heave while the three rotational modes are referred to as pitch, roll and yaw. In figure 1.1 these modes of motion are shown where the z-axis points directly upwards opposite in direction to the acceleration due to gravity. The solution to a problem in which an incident wave interacts with a body which is completely free to move requires the solution of seven separate problems; six radiation problems corresponding to each mode

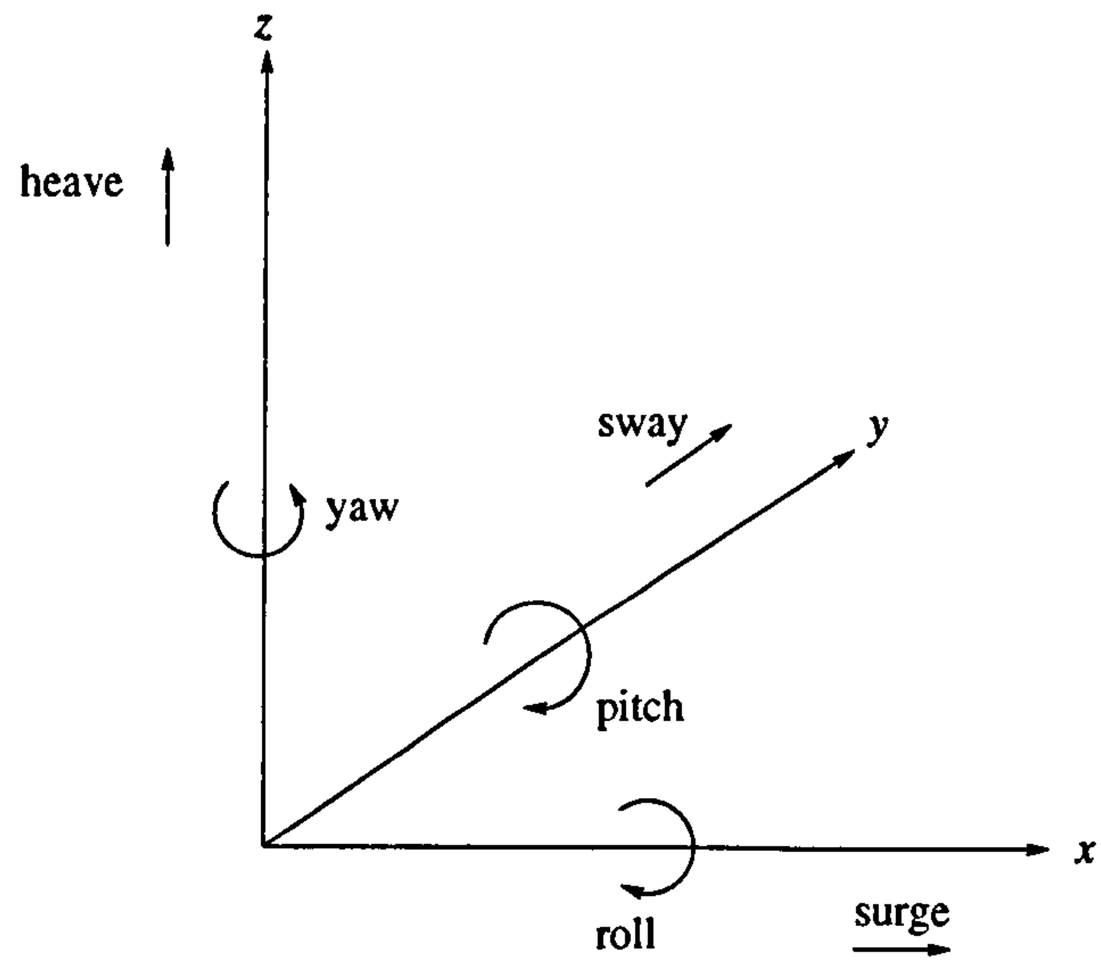

Figure 1.1: The components of motion.

of motion and a scattering problem. These problems can be solved separately but are not all independent and the various quantities which arise from the radiation and scattering problems are connected by a series of reciprocity relations. These relations have been derived by many authors over the years and can be obtained by applying Green's theorem to two different potentials corresponding to two different problems. A systematic derivation of all the first-order reciprocity relations is given by Newman (1976) for a body in a single-layer fluid in two and three dimensions.

When the problem is reduced to two dimensions there are only three possible modes of motion for the body (sway, heave and roll) which provides some simplification. Outgoing waves in two dimensions have constant amplitude far from a wave source which allows us to define reflection and transmission coefficients. These coefficients are the ratios of the amplitude of the reflected wave to that of the incident wave and the amplitude of the transmitted wave to that of the incident wave respectively. The general scattering problem in two dimensions was first considered by Kreisel (1949).

Simple geometries have to be considered for analytical progress to be made. In this thesis we will only be concerned with the interaction of waves with horizontal circular cylinders and spheres. We investigate cylinders because they represent a reasonable model of a pipe bridge. A sphere is used because it is one of the simplest three-dimensional geometries. Many authors have studied both types of structure in a single-layer fluid and it is interesting to investigate the corresponding situations in a two-layer fluid. Some of the previous research involving single-layer fluids and the

bodies we are considering is described below.

One of the most surprising results involving horizontal circular cylinders was discovered by Dean (1948), who used a conformal mapping technique to solve the problem of wave scattering by a submerged cylinder in infinite depth water. Dean showed that incident waves propagating perpendicular to the generator of the cylinder are completely transmitted. The only effect of the obstacle at a great distance is that there is a phase-difference between the incident and transmitted waves, their amplitudes being the same. This result was confirmed by Ursell (1950) and later by Ogilvie (1963). To solve the scattering problem Ursell invented the method of multipole expansions which will be used for all the problems in this thesis. Multipoles are singular solutions of the governing equation which satisfy all the boundary conditions except those on the body boundary and behave like outgoing waves far from the singular point. Ursell generated these multipoles by repeated differentiation of a wave source with respect to the source point. Thorne (1953) provided a different method for generating multipoles using complex analysis.

Levine (1965) investigated the scattering problem of waves obliquely incident on a horizontal circular cylinder in deep water. Using an integral equation technique he found that Dean's result of zero reflection does not occur for these waves. Work by Evans & Linton (1989) showed that normally incident waves in finite depth are also not completely transmitted.

The existence of trapped modes in a channel above a submerged horizontal cylinder spanning the sidewalls was first established by Ursell (1951) for when the radius of the cylinder is small compared to the length of the waves. By trapped modes we mean the free, time-harmonic oscillations of the fluid which decay to zero at infinity down the channel. Ursell showed that existence of the trapped modes depended upon the vanishing of a certain infinite determinant. Numerical results were obtained by McIver & Evans (1985) for trapped modes above a circular submerged cylinder. They found that only a single mode exists for a depth of submergence of the cylinder greater than about 1.07 of its radius. As the depth of submergence is decreased, further trapped modes appear.

There is much work on the radiation and scattering problems of waves by spherical objects in a single-layer fluid. Havelock (1955) solved the heave radiation problem for a half-immersed sphere in deep water and this work was later improved and extended by

Hulme (1982) to the case of sway motion. Numerical calculations of forces on a fixed sphere, both half-immersed and totally submerged, due to an incident wave in deep water, were made by Milgram & Halkyard (1971), and Gray (1978) solved the scattering problem for the submerged sphere, again in deep water, by formulating the problem as an integral equation and then expanding the Green's function and the velocity potential in spherical harmonics in order to reduce the problem to the solution of an infinite set of linear algebraic equations. The method of multipoles first used by Ursell (1950), which is much simpler than this, was used by Srokosz (1979) to solve the heave and sway radiation problems for a submerged sphere in deep water. More recently, Linton (1991) solved the radiation and scattering problems for a sphere submerged in finite depth again using multipole expansions.

The propagation of waves in a two-layer fluid which does not contain any bodies was first investigated by Stokes (1847) and a description of some of the types of linear motion which can occur is given in Lamb (1932) Art. 231. Very little work has been done on wave/structure interactions in two-layer fluids, except by approximating the free surface by a rigid lid. With this simplifying assumption Sturova (1994), for example, studied the radiation of waves by an oscillating cylinder which is moving uniformly in a direction perpendicular to its axis. Also Sturova (1999) considered the radiation and scattering problem for a cylinder in a two- and three-layer fluid which is bounded above and below by rigid horizontal walls. For the three-layer case the middle layer is linearly stratified representing a smooth pycnocline. Using the method of multipoles Sturova calculated the added-mass and damping coefficients of the radiation problem and the disturbing forces and scattering coefficients for the scattering problem. Further work investigating the smooth pycnocline was done by Gavrilov, Ermanyuk & Sturova (1999), again for a horizontal circular cylinder where the fluid is bounded above and below by rigid walls. A comparison of theoretical and experimental results was also given in Gavrilov et al. (1999) and they agreed quite well qualitatively but with notable quantitative disagreement. Other work on two-layer fluids includes Zilman & Miloh (1995) where the wave resistance due to a shallow layer of fluid mud is considered. Kassem (1982) developed two- and three-dimensional multipole expansions for the case of a two-layer fluid bounded above and below by rigid walls.

When the correct linear free-surface boundary condition is used, in the absence of obstacles, Lamb (1932) Art. 231 showed that the appropriate dispersion relation for a

two-layer fluid has two solutions for a given frequency. One of these solutions corresponds to waves where the majority of the disturbance is close to the free surface and the other to waves on the interface between the two fluid layers. More recently, Iooss (1999) has studied nonlinear periodic travelling waves in two dimensions, again in the absence of any obstacles.

When a wave is scattered by an obstacle there is the possibility that the wave energy will be transferred between the two modes. Nguyen & Yeung (1997) investigated the free-surface and internal waves due to a translating point source in a finite-depth two-layer fluid using Green's functions. In Barthélemy, Kabbaj & Germain (2000) the scattering of surface waves by a step bottom in a two-layer fluid was considered. This problem is of particular interest to understand how tides are scattered at the continental shelf break. A WKBJ technique, which approximates the solution by simple travelling waves locally, was employed to find the reflection and transmission coefficients of the surface waves past the step and the proportion of the surface motion transferred to the interface can be seen from the results.

Yeung & Nguyen (1999) solved the radiation and diffraction problems for a rectangular barge in a two-layer fluid using an integral-equation method. The symmetry relations for the added-mass and damping matrices and an analogue to the Haskind relations were given (see chapter 2 below).

The study of trapped modes in two-layer fluids has received very little attention. Kuznetsov (1993) investigated trapped modes in a channel spanned by a cylinder submerged in the lower fluid layer of a two-layer fluid. This work assumed the difference in density between the two fluid layers was small. Using a perturbation method Kuznetsov claimed to show that there were two sets of frequencies of trapped modes; one set corresponding to trapped modes on the free surface and the other to trapped modes on the interface. The work in chapter 6 of this thesis suggests that this is not actually the case. Only the set of interfacial modes exist, the frequencies at which the free-surface modes would exist are such that waves would propagate on the interface thus ruling out the possibility of the existence of a trapped mode.

Much of the research presented in this thesis is an extension of the work by Linton & McIver (1995) who looked at the scattering of waves by a submerged horizontal cylinder in a two-layer fluid where the lower layer has infinite depth. Following the approach of Newman (1976), all the first-order reciprocity relations for a two-layer fluid

were systematically derived using Green's theorem. The scattering problem was also solved using the method of multipoles and the transmission and reflection coefficients computed. It was shown that a cylinder in the (infinite) lower fluid of a two-layer fluid reflected no waves, extending the well-known result for the single-layer case. When the cylinder was positioned in the (finite) upper fluid zero reflection does not occur consistent with the interface acting as a rigid bottom when the density of the lower fluid tends to infinity.

Part I of this thesis is concerned with the three-dimensional problems of spheres submerged in a two-layer fluid. In chapter 2 we extend all the reciprocity relations for the two-layer fluid, given in Linton & McIver (1995), to three dimensions. The heave and sway radiation problems of a sphere entirely within the upper or lower fluid layers is solved and the added-mass and damping coefficients computed. The scattering problem is then solved and the exciting forces exerted on the sphere calculated. The results are compared to those found in Linton (1991). The work presented in chapter 2 has already been published and can be found in Cadby & Linton (2000). Chapter 3 considers the radiation problems for a sphere where the lower fluid is of finite depth.

Two-dimensional problems concerning submerged horizontal circular cylinders are considered in Part II of this thesis. In chapter 4 we investigate the effect of finite depth of the lower fluid layer on the scattering of waves by a cylinder submerged in the lower fluid. Chapter 5 solves the scattering problems of oblique waves by a cylinder; first in a single-layer finite-depth fluid and then in a two-layer infinite-depth fluid. Comparison with the results obtained by using the method given by Levine (1965) is included. We find that at certain frequencies, for a given submergence and depth of the upper fluid layer, zero transmission occurs.

Trapped modes above a cylinder are considered in chapter 6. We begin by extending the work by McIver & Evans (1985) of a cylinder in a single-layer fluid to finite-depth in section 6.1. In section 6.2 the trapped mode frequencies for a cylinder in the upper and lower fluid layers of a two-layer fluid are calculated. Free-surface and internal wave profiles are also presented confirming that the trapped mode waves for a cylinder submerged in the lower fluid layer are centred about the interface. For a cylinder in the upper fluid layer however we find that there can be waves on both surfaces.

Chapter 7 is devoted to finding embedded trapped modes between a wall and a cylinder in a two-layer fluid. These modes are called embedded trapped modes as the

frequencies at which the trapped mode waves occur are embedded in the continuous spectrum of a certain differential operator. Linton & Kuznetsov (1997) investigated these types of waves between a pair of identical surface piercing inclined barriers. Symmetry conditions were used such that the geometry was equivalent to a barrier next to a wall. An interesting hydrodynamic property of these barriers is that at a particular frequency, for a given inclination, the transmission coefficient is zero and a wave incident upon the plate is totally reflected. Linton & Kuznetsov (1997) used this property to seek frequencies of waves which are continually reflected between the two barriers leading to a trapped oscillation. Since we find that oblique waves incident upon a cylinder in a two-layer fluid can be totally reflecting we investigate these trapped modes between two identical cylinders submerged in the lower fluid layer.

1.2 Linear water wave theory

We shall first consider a single-layer fluid. We choose Cartesian coordinates such that x, y are horizontal and z is vertically upwards. The undisturbed air-water interface which will be called the mean free surface is positioned at $z = 0$. We assume that the fluid is inviscid and incompressible and the flow is irrotational (no local rotation). Due to irrotationality the velocity vector $\boldsymbol{u}$ of a point in the fluid can be expressed as the gradient of a scalar potential Φ

$$\boldsymbol{u}(x, y, z, t) = \nabla\Phi(x, y, z, t). \tag{1.2.1}$$

Conservation of mass, $\nabla \cdot \boldsymbol{u} = 0$, requires that the potential satisfies Laplace's equation

$$\nabla^2\Phi = 0 \qquad \text{in the fluid.} \tag{1.2.2}$$

There are at least three relevant length scales in wave-body interactions; a, a typical body dimension, λ, the wavelength and A, the wave amplitude. The wavenumber k is defined by $k\lambda = 2\pi$. These lengths can be combined to obtain two non-dimensional parameters for the problem, ka and kA. We shall assume that the wave-steepness $kA \ll 1$ which allows us to simplify some of the boundary conditions. The free surface is described by $z = H(x, y, t)$ and the linearised free-surface boundary conditions are

$$\frac{\partial H}{\partial t} = \frac{\partial \Phi}{\partial z}, \tag{1.2.3}$$

$$gH = -\frac{\partial \Phi}{\partial t}, \tag{1.2.4}$$

both applied on the undisturbed free surface. These can be combined to give

$$\frac{\partial^2\Phi}{\partial t^2} + g\frac{\partial\Phi}{\partial z} = 0 \qquad \text{on } z = 0. \tag{1.2.5}$$

The total pressure in the fluid is given by linearising Bernoulli's equation. Thus

$$P(x,y,z,t) = -\rho g z - \rho\frac{\partial\Phi}{\partial t}, \tag{1.2.6}$$

where the term $-\rho\partial\Phi/\partial t$ is called the dynamic pressure.

We shall further simplify things by considering monochromatic waves, i.e. waves at a single frequency, $\omega/2\pi$. We shall also assume that the constraints on any body are such as to produce a response at this frequency only. This requires the equations of motion of the body to be linear as well as the equations of fluid motion. For convenience we write

$$\Phi(x,y,z,t) = \Re\{\phi(x,y,z)e^{-i\omega t}\}, \tag{1.2.7}$$

$$H(x,y,t) = \Re\{\eta(x,y)e^{-i\omega t}\}, \tag{1.2.8}$$

$$P(x,y,z,t) = \Re\{p(x,y,z)e^{-i\omega t}\} - \rho g z. \tag{1.2.9}$$

Thus the conditions become

$$\nabla^2\phi = 0 \qquad \text{in the fluid,} \tag{1.2.10}$$

$$K\phi = \frac{\partial\phi}{\partial z} \qquad \text{on } z = 0\,, \tag{1.2.11}$$

where $K \equiv \omega^2/g$.

We shall now consider a two-layer fluid and derive the general linearised governing equations. Cartesian coordinates x, y, z are chosen with x, y horizontal and z vertically upwards. The undisturbed interface and free surface are at $z = 0$ and $z = d$ respectively. The upper fluid, $0 < z < d$, will be referred to as region I, whilst the lower fluid, $z < 0$, will be referred to as region II. The fluid velocity in the upper fluid (of density ρ^I) is $\boldsymbol{u}^I$ and that in the lower fluid (of density $\rho^{II} > \rho^I$) is $\boldsymbol{u}^{II}$. From now on in this chapter, for convenience, when a quantity appears without a superscript I or II then it refers to both.

As above, we assume the fluids are inviscid and incompressible, the motion is irrotational and the wave steepness is small. The free surface is described by $z = H_d(x,y,t)$ and the interface by $z = H_0(x,y,t)$. We have two velocity potentials describing the motion in the two fluid layers, both of which must satisfy Laplace's equation. The velocity

potential Φ^I for the upper fluid must satisfy the free-surface condition, at $z = d$. The continuity of the normal velocity and pressure at the interface are represented by

$$\frac{\partial H_0}{\partial t} = \frac{\partial \Phi^I}{\partial z} = \frac{\partial \Phi^{II}}{\partial z} \qquad \text{on } z = 0, \tag{1.2.12}$$

$$\frac{\rho^I}{\rho^{II}} \left(\frac{\partial \Phi^I}{\partial z} + gH_0 \right) = \frac{\partial \Phi^{II}}{\partial z} + gH_0 \qquad \text{on } z = 0. \tag{1.2.13}$$

The velocity potentials and pressure can be expressed in the same way as (1.2.7) and (1.2.9). The free surface and interface are given in a similar way

$$H_0(x, y, t) = \Re\{\eta_0(x, y)e^{-i\omega t}\}, \tag{1.2.14}$$

$$H_d(x, y, t) = \Re\{\eta_d(x, y)e^{-i\omega t}\}. \tag{1.2.15}$$

The conditions can be reduced to

$$\nabla^2 \phi = 0 \qquad \text{in the fluid,} \tag{1.2.16}$$

$$K\phi^I = \frac{\partial \phi^I}{\partial z} \qquad \text{on } z = d, \tag{1.2.17}$$

$$\frac{\partial \phi^I}{\partial z} = \frac{\partial \phi^{II}}{\partial z} \qquad \text{on } z = 0, \tag{1.2.18}$$

$$\frac{\rho^I}{\rho^{II}} \left(\frac{\partial \phi^I}{\partial z} - K\phi^I \right) = \frac{\partial \phi^{II}}{\partial z} - K\phi^{II} \qquad \text{on } z = 0. \tag{1.2.19}$$

Region II is of infinite depth which implies that

$$\nabla \phi^{II} \to 0 \qquad \text{as } z \to -\infty. \tag{1.2.20}$$

If region II has constant depth h then we would use the following alternative condition

$$\frac{\partial \phi^{II}}{\partial z} = 0 \qquad \text{on } z = -h. \tag{1.2.21}$$

1.3 The interaction of a body with an incident wave

Let us consider a moving body, with an impermeable surface, in the fluid. The velocity of the body at a point on its surface can be written as

$$\boldsymbol{V}(x, y, z, t) = \Re\{\boldsymbol{U}(x, y, z)e^{-iwt}\}. \tag{1.3.1}$$

The continuity of normal velocity implies that

$$\frac{\partial \phi}{\partial n} = \boldsymbol{U}.\boldsymbol{n} \qquad \text{on the body,} \tag{1.3.2}$$

where $\boldsymbol{n}$ is the inward unit normal to the body surface, i.e. the outward normal to the fluid. If we assume that the body motions are characterised by the same smallness parameter as for wave motions, (Ka), then we can linearise this condition by applying it on the fixed equilibrium position of the body.

When an incident wave, described by potential ϕ_{inc}, interacts with a body it diffracts to produce a scattered wave field, described by potential ϕ_S, and also sets the body in motion generating an additional radiated field, described by potential ϕ_R. In linear water wave theory the total effect can be determined by simply adding the various effects together. The total velocity potential can be written as

$$\phi = \phi_{\text{inc}} + \phi_S + \phi_R. \tag{1.3.3}$$

If we restrict our attention to rigid body motions, then the complex velocity of a point on the body surface, $\boldsymbol{U}$, defined in (1.3.1), can be written as

$$\boldsymbol{U} = (U_1, U_2, U_3) + (\Omega_1, \Omega_2, \Omega_3) \times \boldsymbol{r} \tag{1.3.4}$$

where U_1, U_2, U_3 are the components of velocity in surge, sway and heave; Ω_1, Ω_2, Ω_3 are the components of angular velocity in roll, pitch and yaw, and $\boldsymbol{r}$ is the position vector of the point on the body surface with the origin at the centre of rotation.

If we write

$$U_i = \quad \Omega_i \quad i = 4, 5, 6, \tag{1.3.5}$$

$$n_i = \quad \boldsymbol{n}.\boldsymbol{e}_i \quad i = 1, 2, 3, \tag{1.3.6}$$

$$n_i = \quad (\boldsymbol{r} \times \boldsymbol{n})_i \quad i = 4, 5, 6, \tag{1.3.7}$$

where $\boldsymbol{e}_i$, $i = 1, 2, 3$ are the unit vectors along the x, y, z axes respectively, then the body boundary condition, (1.3.2), becomes

$$\frac{\partial \phi}{\partial n} = \sum_{i=1}^{6} U_i n_i \tag{1.3.8}$$

and if ϕ_R is decomposed into six radiation potentials, one for each mode of motion, by

$$\phi_R = \sum_{i=1}^{6} U_i \phi_i \tag{1.3.9}$$

then the conditions satisfied by the various potentials on the body are

$$\frac{\partial \phi_S}{\partial n} = -\frac{\partial \phi_{\text{inc}}}{\partial n}, \tag{1.3.10}$$

$$\frac{\partial \phi_i}{\partial n} = n_i \qquad i = 1, \ldots, 6. \tag{1.3.11}$$

Far away from the body we require the potentials ϕ_S and ϕ_i, $i = 1, \ldots, 6$, to describe outgoing waves. The problems for ϕ_S and ϕ_i, $i = 1, \ldots, 6$, are all independent and can therefore be considered separately.

1.4 Hydrodynamic characteristics

From now on we shall restrict attention to bodies which are entirely within either the upper or the lower fluid layer. The case when a body straddles both fluid layers will not be considered. The force on a body in waves is made up of two components. The first is the hydrostatic force which is extremely important when studying floating bodies. In this thesis we will only be considering completely submerged bodies and so the hydrostatic forces will present no theoretical difficulty. A description of the hydrostatic forces is given in Newman (1977) but here we shall not discuss them. The second component of the force is that due to the motion of the waves, called the hydrodynamic force. The generalised hydrodynamic force on the body in the jth direction, F_j, is found by integrating the dynamic pressure times the appropriate component of the normal over the body surface. Thus

$$F_j(t) = \Re\{f_j e^{-i\omega t}\}, \tag{1.4.1}$$

where f_j is given by

$$f_j = i\rho\omega \int_{S_B} \phi n_j dS. \tag{1.4.2}$$

For $i = 4, 5, 6$ this will be a moment. Now $\phi = \phi_{\text{inc}} + \phi_S + \phi_R$ so we can write $f_j = f_j^S + f_j^R$, where

$$f_j^S = i\rho\omega \int_{S_B} (\phi_{\text{inc}} + \phi_S) n_j dS, \tag{1.4.3}$$

$$f_j^R = i\rho\omega \int_{S_B} \phi_R n_j dS \tag{1.4.4}$$

$$= \sum_{i=1}^{6} U_i T_{ij}, \tag{1.4.5}$$

and

$$T_{ij} = i\rho\omega \int_{S_B} \phi_i n_j dS. \tag{1.4.6}$$

The vector $\boldsymbol{f}^S$ having components f_j^S is called the exciting force on the stationary body due to the incident wave, whilst the matrix element T_{ij} represents the contribution to

the hydrodynamic force in the jth direction due to a unit velocity of the body in the ith mode of motion. The complex matrix T can be split into two real matrices, one in phase with the acceleration of the body, M, which is called the added mass matrix, and one in phase with the velocity of the body, B, which is called the radiation damping matrix. Thus if we write

$$T_{ij} = -B_{ij} + i\omega M_{ij} = i\rho\omega \int_{S_B} \phi_i n_j dS \tag{1.4.7}$$

then

$$f_j^R = \sum_{i=1}^{6} U_i(-B_{ij} + i\omega M_{ij}) \tag{1.4.8}$$

corresponding to the force

$$F_j^R(t) = -\sum_{i=1}^{6}[B_{ij}\Re\{U_i e^{-i\omega t}\} + M_{ij}\Re\{-i\omega U_i e^{-i\omega t}\}] \tag{1.4.9}$$

where the terms multiplying B_{ij} and M_{ij} are the velocity and acceleration of the body in the ith mode respectively. The matrices M and B are independent of the velocity of the body and depend solely on the geometry of the body and the frequency of the oscillation.

Part I

Submerged Spheres

Chapter 2

Infinite depth of lower fluid

2.1 Introduction

This chapter is concerned with three-dimensional wave/structure interaction in two-layer fluids. The work presented here has been published and can be found in Cadby & Linton (2000). General relations exist for water wave radiation and diffraction problems. They can be found by using Green's theorem with various pairings of radiation and scattering potentials, see Mei (1983) chapter 7. These relations were extended to two-layer fluids in two dimensions by Linton & McIver (1995). In this chapter I shall be extending their results to the three-dimensional case. All the identities found are useful in theoretical and practical argument and can be used to check calculations or reduce the numerical work of calculating certain quantities.

Srokosz (1979) used the multipole method to solve the heave and sway radiation problems of a sphere in deep water. Using the same method Linton (1991) examined the radiation and diffraction of waves by a sphere in finite-depth water. Here we will employ the multipole method to solve the radiation and scattering problems for a sphere submerged in a two-layer fluid. The added-mass and damping coefficients will be calculated for the radiation problems and the exciting forces on the sphere due to incident waves will be calculated for the scattering problems.

2.2 General relations between hydrodynamic quantities

Horizontal coordinates are x and y whilst the vertical coordinate z is measured upwards from the undisturbed interface between the two fluids, the free surface being linearised about $z = d$. Cylindrical polar coordinates defined by

$$x = R\cos\alpha, \qquad y = R\sin\alpha, \tag{2.2.1}$$

will also be used.

As described in chapter 1, the upper fluid, $0 < z < d$, will be referred to as region I, whilst the lower fluid, $z < 0$, will be referred to as region II. The potential in the upper fluid (of density ρ^I) is ϕ^I and that in the lower fluid (of density $\rho^{II} > \rho^I$) is ϕ^{II}. The motion is assumed to be irrotational and so both ϕ^I and ϕ^{II} satisfy Laplace's equation:

$$\nabla^2\phi^I = \nabla^2\phi^{II} = 0. \tag{2.2.2}$$

If we now define $\rho = \rho^I/\rho^{II}(< 1)$ (not to be confused with the notation in the previous chapter) then the linearised boundary conditions on the interface and free surface are

$$\phi^I_z = \phi^{II}_z \qquad \text{on } z = 0, \tag{2.2.3}$$

$$\rho(\phi^I_z - K\phi^I) = \phi^{II}_z - K\phi^{II} \qquad \text{on } z = 0, \tag{2.2.4}$$

$$\phi^I_z = K\phi^I \qquad \text{on } z = d, \tag{2.2.5}$$

where $K = \omega^2/g$, the time-dependence of $e^{-i\omega t}$ having been suppressed. The boundary conditions (2.2.3) and (2.2.4) represent the continuity of normal velocity and pressure at the interface respectively.

To derive the wave potentials which satisfy the above conditions we use standard three-dimensional water wave theory, for example Mei (1983) chapter 7, combined with two-dimensional two-layer fluid theory, Linton & McIver (1995). Thus in a two-layer fluid outgoing cylindrical waves have the form

$$\phi^I_i \sim \left(\frac{2}{\pi KR}\right)^{1/2} e^{iKR - i\pi/4} e^{Kz} A_i(\alpha) + \left(\frac{2}{\pi kR}\right)^{1/2} e^{ikR - i\pi/4} g(z) B_i(\alpha) \tag{2.2.6}$$

$$\phi^{II}_i \sim \left(\frac{2}{\pi KR}\right)^{1/2} e^{iKR - i\pi/4} e^{Kz} A_i(\alpha) + \left(\frac{2}{\pi kR}\right)^{1/2} e^{ikR - i\pi/4} e^{kz} B_i(\alpha) \tag{2.2.7}$$

as $KR \to \infty$, where

$$g(z) = \frac{K\sigma - k}{K(\sigma - 1)} e^{kz} + \frac{K - k}{K(\sigma - 1)} e^{-kz} \tag{2.2.8}$$

$$= \frac{\rho^{-1}}{1 - e^{2kd}} e^{kz} + \frac{\rho^{-1} - 1 + e^{2kd}}{1 - e^{2kd}} e^{-kz}, \tag{2.2.9}$$

$\sigma = (1 + \rho)/(1 - \rho)$ and $A_i(\alpha)$, $B_i(\alpha)$ are the far field amplitudes of the waves of wavenumbers K, k respectively . The dispersion relation is given by

$$(u - K)(K(\sigma + e^{-2ud}) - u(1 - e^{-2ud})) = 0. \tag{2.2.10}$$

It follows that either $u = K$ or $u = k$ where

$$K(\sigma + e^{-2kd}) = k(1 - e^{-2kd}). \tag{2.2.11}$$

This has exactly one positive root k which lies in the range

$$K\sigma < k < \frac{K(\sigma + 1)}{1 - e^{-2Kd\sigma}}. \tag{2.2.12}$$

An incident plane wave making an angle α_{inc} with the positive x-axis with wavenumber k has the form

$$\phi^I_{\text{inc}} = g(z) e^{ikR\cos(\alpha - \alpha_{\text{inc}})}, \tag{2.2.13}$$

$$\phi^{II}_{\text{inc}} = e^{kz} e^{ikR\cos(\alpha - \alpha_{\text{inc}})}. \tag{2.2.14}$$

An incident wave of wavenumber K has the form

$$\phi_{\text{inc}} = e^{Kz} e^{iKR\cos(\alpha - \alpha_{\text{inc}})} \tag{2.2.15}$$

in both the upper and lower fluids.

Now consider a situation in which there are a number of bodies, some in the upper layer, some in the lower layer, and some straddling the two. The boundaries of those bodies in the upper fluid will be denoted by B^I and those in the lower fluid by B^{II}. Assume that ϕ and ψ are solutions to two different problems, with $\partial\phi/\partial n$ and $\partial\psi/\partial n$ given on the boundaries B^I and B^{II}. Now apply Green's theorem, which for harmonic functions ϕ and ψ takes the form

$$\int_s \left(\phi \frac{\partial \psi}{\partial n} - \psi \frac{\partial \phi}{\partial n} \right) dS = 0, \tag{2.2.16}$$

where S is the boundary of a fluid region completely contained in one of the fluid layers and $\partial/\partial n$ is the derivative with respect to the outward normal. In region I, S is

composed of the free surface, the boundary of the bodies B^I, the interface Γ, and a cylinder S^I_∞ whose radius is sufficiently large for the asymptotic forms of the potentials to be used. In region II, S is composed of a surface parallel to the interface whose depth will be made to tend to infinity, the boundary of the bodies B^{II}, the interface Γ, and a cylinder of large radius S^{II}_∞. Using (2.2.3) and (2.2.4) we obtain

$$\begin{aligned} \rho(\psi^I_z - K\psi^I)\phi^I_z &= (\psi^{II}_z - K\psi^{II})\phi^{II}_z \\ \text{and} \qquad \rho(\phi^I_z - K\phi^I)\psi^I_z &= (\phi^{II}_z - K\phi^{II})\psi^{II}_z \end{aligned}$$

on $z = 0$. Subtracting these two equations gives

$$\rho\left(\phi^I\frac{\partial\psi^I}{\partial z} - \psi^I\frac{\partial\phi^I}{\partial z}\right) = \phi^{II}\frac{\partial\psi^{II}}{\partial z} - \psi^{II}\frac{\partial\phi^{II}}{\partial z} \tag{2.2.17}$$

on $z = 0$. Using Green's theorem in region I, and noting that the integral along the free surface disappears due to (2.2.5), gives

$$\begin{aligned} \int_{S^I_\infty}\left(\phi^I\frac{\partial\psi^I}{\partial R} - \psi^I\frac{\partial\phi^I}{\partial R}\right)dS - \int_\Gamma\left(\phi^I\frac{\partial\psi^I}{\partial z} - \psi^I\frac{\partial\phi^I}{\partial z}\right)dS \\ + \int_{B^I}\left(\phi^I\frac{\partial\psi^I}{\partial n} - \psi^I\frac{\partial\phi^I}{\partial n}\right)dS = 0. \end{aligned} \tag{2.2.18}$$

In region II the integral on the surface at depth infinity disappears, and so Green's theorem yields

$$\begin{aligned} \int_{S^{II}_\infty}\left(\phi^{II}\frac{\partial\psi^{II}}{\partial R} - \psi^{II}\frac{\partial\phi^{II}}{\partial R}\right)dS + \int_\Gamma\left(\phi^{II}\frac{\partial\psi^{II}}{\partial z} - \psi^{II}\frac{\partial\phi^{II}}{\partial z}\right)dS \\ + \int_{B^{II}}\left(\phi^{II}\frac{\partial\psi^{II}}{\partial n} - \psi^{II}\frac{\partial\phi^{II}}{\partial n}\right)dS = 0. \end{aligned} \tag{2.2.19}$$

Multiplying (2.2.18) by ρ, adding to (2.2.19) and using (2.2.17) gives

$$\begin{aligned} \rho\int_{B^I}\left(\phi^I\frac{\partial\psi^I}{\partial n} - \psi^I\frac{\partial\phi^I}{\partial n}\right)dS + \int_{B^{II}}\left(\phi^{II}\frac{\partial\psi^{II}}{\partial n} - \psi^{II}\frac{\partial\phi^{II}}{\partial n}\right)dS \\ = -\rho\int_{S^I_\infty}\left(\phi^I\frac{\partial\psi^I}{\partial R} - \psi^I\frac{\partial\phi^I}{\partial R}\right)dS - \int_{S^{II}_\infty}\left(\phi^{II}\frac{\partial\psi^{II}}{\partial R} - \psi^{II}\frac{\partial\phi^{II}}{\partial R}\right)dS. \end{aligned} \tag{2.2.20}$$

By using this equation with radiation and scattering potentials for ϕ and ψ we can obtain a number of relations between various hydrodynamic quantities.

2.3 Two radiation potentials

First let's consider the case of two radiation potentials. For the rest of this chapter we shall restrict our attention to a single body with boundary S_B. Let $\phi = \phi_i$ and $\psi = \phi_j$,

where ϕ_i, ϕ_j are two radiation potentials whose behaviour in the far field is given by (2.2.6) and (2.2.7). Now

$$\rho \int_0^d e^{Kz} g(z) dz = \frac{\rho}{K(\sigma-1)} \int_0^d \left[(K\sigma - k) e^{(K+k)z} + (K-k) e^{(K-k)z} \right] dz \tag{2.3.1}$$

$$= \frac{\rho}{K(\sigma-1)} \left[\frac{K\sigma - k}{K+k} \left(e^{(K+k)d} - 1 \right) + e^{(K-k)d} - 1 \right]. \tag{2.3.2}$$

This can be simplified using (2.2.11) to give

$$\rho \int_0^d e^{Kz} g(z) dz = - \frac{\rho}{K(\sigma-1)} \left[\frac{K\sigma - k}{K+k} + 1 \right] \tag{2.3.3}$$

$$= - \frac{\rho(\sigma+1)}{(\sigma-1)(K+k)} \tag{2.3.4}$$

$$= - \frac{1}{K+k} \tag{2.3.5}$$

$$= - \int_{-\infty}^0 e^{(K+k)z} dz. \tag{2.3.6}$$

Noting the above and using (2.2.20) we see that the right-hand side equates to zero leaving

$$\delta \int_{S_B} \left(\phi_i \frac{\partial \phi_j}{\partial n} - \phi_j \frac{\partial \phi_i}{\partial n} \right) dS = 0, \tag{2.3.7}$$

where $\delta = \rho$ if bodies are in fluid I or $\delta = 1$ if bodies are in fluid II. Since $\partial \phi_i / \partial n = n_i$, see equation (1.3.10), on the body, where n_i is the normal of the body in the ith direction, the above gives

$$\int_{S_B} \phi_i n_j dS = \int_{S_B} \phi_j n_i dS. \tag{2.3.8}$$

It follows from this and (1.4.7) that the added-mass and damping matrices are symmetric as was found for the two-dimensional case by Linton & McIver (1995). This is a classical result which has been derived in different contexts by many authors.

Suppose now we use $\psi = \overline{\phi_j}$. The function $\overline{\phi_j}$ satisfies the complex conjugate of the equations governing ϕ_j and describes an incoming cylindrical wave far from the body. Thus, using the fact that the n_i are real, (2.2.20) becomes

$$\delta \int_{S_B} (\phi_i n_j - \overline{\phi_j} n_i) dS = 2i\delta \Im \int_{S_B} \phi_i n_j dS$$

$$= \frac{2i}{\pi} \left(J_K \int_0^{2\pi} A_i(\alpha) \overline{A_j}(\alpha) d\alpha + J_k \int_0^{2\pi} B_i(\alpha) \overline{B_j}(\alpha) d\alpha \right), \tag{2.3.9}$$

where

$$J_K = \frac{1}{K} + 2\rho \int_0^d e^{2Kz} dz \tag{2.3.10}$$

$$= \frac{1}{K} \left(1 + \rho(e^{2Kd} - 1)\right), \tag{2.3.11}$$

$$J_k = \frac{1}{k} + 2\rho \int_0^d [g(z)]^2 dz \tag{2.3.12}$$

$$= \frac{1}{k} + \frac{2\rho}{K^2(\sigma-1)^2} \left[\frac{(K\sigma - k)^2}{2k} (e^{2kd} - 1) \right.$$

$$\left. + 2(K\sigma - k)(K - k)d - \frac{(K-k)^2}{2k} (e^{-2kd} - 1) \right]. \tag{2.3.13}$$

Thus the damping coefficient B_{ij} can be found in terms of the far-field behaviour

$$B_{ij} = -\Re i \rho^{II} \delta\omega \int_{S_B} \phi_i n_j dS \tag{2.3.14}$$

$$= \frac{\rho^{II}\omega}{\pi} \left[J_K \int_0^{2\pi} A_i(\alpha)\overline{A_j}(\alpha) d\alpha + J_k \int_0^{2\pi} B_i(\alpha)\overline{B_j}(\alpha) d\alpha \right]. \tag{2.3.15}$$

This is an interesting result as we have the damping coefficient related to the amplitude of the waves radiated away from the body which is not physically obvious. For the special case of (2.3.15) where $j = i$ we find that the diagonal elements of the damping coefficient matrix are proportional to the energy radiated away from the body. The time-averaged energy flux, $\tilde{E}$, of outgoing waves of the form (2.2.6) and (2.2.7) is given by

$$\tilde{E} = -\left\{ \rho^I \int_{S_\infty^I} + \rho^{II} \int_{S_\infty^{II}} \right\} \frac{\partial\Phi}{\partial t} \frac{\partial\Phi}{\partial n} dS \tag{2.3.16}$$

$$= \frac{\rho^{II}\omega}{2\pi} \left[J_K \int_0^{2\pi} A_i(\alpha)\overline{A_j}(\alpha) d\alpha + J_k \int_0^{2\pi} B_i(\alpha)\overline{B_j}(\alpha) d\alpha \right]. \tag{2.3.17}$$

Equation (2.3.15) is a useful method of calculating the damping coefficient which does not require integrating the potential over the body surface. Later we will calculate the damping coefficient with (2.3.14) and use (2.3.15) to provide a numerical check for the results.

2.4 A radiation and a scattering potential

Suppose now we use $\phi = \phi_{\text{inc}} + \phi_S$ and $\psi = \phi_i$, where ϕ_{inc} is an incident wave and ϕ_S is the scattered field potential. The left hand side of (2.2.20) will be

$$\delta \int_{S_B} \left(\phi_{\text{inc}} \frac{\partial\phi_i}{\partial n} - \phi_i \frac{\partial\phi_{\text{inc}}}{\partial n} \right) dS + \delta \int_{S_B} \left(\phi_S \frac{\partial\phi_i}{\partial n} - \phi_i \frac{\partial\phi_S}{\partial n} \right) dS. \tag{2.4.1}$$

Since ϕ_i and ϕ_S both represent outgoing cylindrical waves the contribution in the far field due to the second integral will disappear, leaving just the contribution due to the radiation and incident potentials in the far field. Now consider the case of an incident wave of wavenumber K making an angle α_{inc} with the positive x-axis. Using (2.2.20) and noting that $\partial\phi/\partial n = 0$ and $\partial\phi_i/\partial n = n_i$ on the body, we get

$$\delta \int_{S_B} \phi n_i dS = \lim_{KR\to\infty} \left[-iJ_K \left(\frac{KR}{2\pi}\right)^{1/2} e^{-i\pi/4} \right.$$
$$\left. \times \int_0^{2\pi} (1-\cos(\alpha-\alpha_{\text{inc}})) e^{iKR(1+\cos(\alpha-\alpha_{\text{inc}}))} A_i(\alpha) d\alpha \right]. \quad (2.4.2)$$

Using stationary phase arguments, see appendix A, this evaluates to

$$\delta \int_{S_B} \phi n_i dS = -2iJ_K A_i(\alpha_{\text{inc}} + \pi). \quad (2.4.3)$$

Doing the same but with an incident wave of wavenumber k gives

$$\delta \int_{S_B} \phi n_i dS = -2iJ_k B_i(\alpha_{\text{inc}} + \pi). \quad (2.4.4)$$

The hydrodynamic force on the body in the jth mode of motion is given by $F_j(t) = \Re\{f_j e^{-i\omega t}\}$ where f_j is found by integrating the dynamic pressure times the appropriate component of the normal over the body surface. In other words

$$f_j = i\delta\rho^{II}\omega \int_{S_B} \phi n_j dS, \quad (2.4.5)$$

which when combined with (2.4.3) gives the exciting force in the jth direction due to an incident wave of wavenumber K as

$$f_j = 2\rho^{II}\omega J_K A_j(\alpha_{\text{inc}} + \pi). \quad (2.4.6)$$

The same can be done with an incident wave of wavenumber k using (2.4.4) to give

$$f_j = 2\rho^{II}\omega J_k B_j(\alpha_{\text{inc}} + \pi). \quad (2.4.7)$$

In both cases the exciting force is related to the amplitude of the radiated wave with the same wavenumber as the incident wave in the direction opposite to that of the incident wave. These formulas represent extensions to two-layer fluids of the Haskind relations (see Newman (1976)). These relations are particularly useful as the exciting forces can be derived from the properties of the radiation problem making it unnecessary to solve the scattering problem for these forces. We will use these relations to verify numerical calculations of the exciting forces found from (2.4.5).

2.5 Two scattering potentials

If ϕ and ψ in (2.2.20) are both potentials of the form $\phi_{\text{inc}} + \phi_S$ for diffracted incident waves then the body surface integrals will be zero leaving

$$-\rho \int_{S_\infty^I} \left(\phi^I \frac{\partial \psi^I}{\partial R} - \psi^I \frac{\partial \phi^I}{\partial R} \right) dS - \int_{S_\infty^{II}} \left(\phi^{II} \frac{\partial \psi^{II}}{\partial R} - \psi^{II} \frac{\partial \phi^{II}}{\partial R} \right) dS = 0. \tag{2.5.1}$$

We will use the notation $\phi(u, \alpha_i)$ to represent a scattering potential for which the incident wave has wavenumber u and makes an angle α_i with the positive x-axis. In the far field such a potential takes the form

$$\phi^I(u, \alpha_i) \sim \phi^I_{\text{inc}} + \left(\frac{2}{\pi KR} \right)^{1/2} e^{iKR - i\pi/4} e^{Kz} A_u^{(i)}(\alpha) + \left(\frac{2}{\pi kR} \right)^{1/2} e^{ikR - i\pi/4} g(z) B_u^{(i)}(\alpha) \tag{2.5.2}$$

$$\phi^{II}(u, \alpha_i) \sim \phi^{II}_{\text{inc}} + \left(\frac{2}{\pi KR} \right)^{1/2} e^{iKR - i\pi/4} e^{Kz} A_u^{(i)}(\alpha) + \left(\frac{2}{\pi kR} \right)^{1/2} e^{ikR - i\pi/4} e^{kz} B_u^{(i)}(\alpha) \tag{2.5.3}$$

with the appropriate form for the incident wave depending on its wavenumber. Using (2.5.1) with $\phi = \phi(K, \alpha_1)$ and $\psi = \phi(K, \alpha_2)$ we will only get a contribution from the incident waves with the scattering potentials, leaving

$$A_K^{(2)}(\alpha_1 + \pi) = A_K^{(1)}(\alpha_2 + \pi). \tag{2.5.4}$$

With $\phi = \phi(k, \alpha_1)$ and $\psi = \phi(k, \alpha_2)$ we get

$$B_k^{(2)}(\alpha_1 + \pi) = B_k^{(1)}(\alpha_2 + \pi). \tag{2.5.5}$$

In other words, if we have two incident waves of wavenumber K (k) the amplitude of the first scattered wave with wavenumber K (k) towards the second incident wave is the same as that of the second scattered wave towards the first. In particular, taking $\alpha_2 = \alpha_1 + \pi$, it follows that for an incident wave of wavenumber K (k) the amplitude of the scattered wave with wavenumber K (k) in the same direction as the incident wave is unchanged if the direction of the incident wave is reversed. With $\phi = \phi(K, \alpha_1)$ and $\psi = \phi(k, \alpha_2)$, (2.5.1) reduces to

$$A_k^{(2)}(\alpha_1 + \pi) = J B_K^{(1)}(\alpha_2 + \pi), \tag{2.5.6}$$

where $J = J_k / J_K$. Equations (2.5.4)–(2.5.6) are the three-dimensional analogues of equations (2.27)–(2.32) from Linton & McIver (1995). They are useful because they relate the scattered wave amplitudes from one problem to another.

The complex conjugate of a scattering potential satisfies the same condition on the body boundary and so (2.2.20) still applies if either or both of ϕ and ψ are of this form. With $\phi = \phi(K, \alpha_1)$ and $\psi = \overline{\phi}(K, \alpha_2)$ we obtain, after considerable algebra,

$$\pi\overline{A_K^{(2)}}(\alpha_1) + \pi A_K^{(1)}(\alpha_2) + \int_0^{2\pi} A_K^{(1)}(\alpha)\overline{A_K^{(2)}}(\alpha)d\alpha + J\int_0^{2\pi} B_K^{(1)}(\alpha)\overline{B_K^{(2)}}(\alpha)d\alpha = 0, \quad (2.5.7)$$

and with $\phi = \phi(k, \alpha_1)$ and $\psi = \overline{\phi}(k, \alpha_2)$ the result is

$$\pi J\overline{B_k^{(2)}}(\alpha_1) + \pi J B_k^{(1)}(\alpha_2) + \int_0^{2\pi} A_k^{(1)}(\alpha)\overline{A_k^{(2)}}(\alpha)d\alpha + J\int_0^{2\pi} B_k^{(1)}(\alpha)\overline{B_k^{(2)}}(\alpha)d\alpha = 0. \quad (2.5.8)$$

Finally, with $\phi = \phi(K, \alpha_1)$ and $\psi = \overline{\phi}(k, \alpha_2)$ we get

$$\pi\overline{A_k^{(2)}}(\alpha_1) + \pi J B_K^{(1)}(\alpha_2) + \int_0^{2\pi} A_K^{(1)}(\alpha)\overline{A_k^{(2)}}(\alpha)d\alpha + J\int_0^{2\pi} B_K^{(1)}(\alpha)\overline{B_k^{(2)}}(\alpha)d\alpha = 0. \quad (2.5.9)$$

These last three relations are the three-dimensional analogues of equations (2.38)–(2.43) from Linton & McIver (1995). Putting $\alpha_2 = \alpha_1$ into equations (2.5.7) and (2.5.8) gives

$$\Re\{A_K^{(1)}(\alpha_1)\} = -\frac{1}{\pi}\left(\int_0^{2\pi} |A_K^{(1)}(\alpha)|^2 d\alpha + J\int_0^{2\pi} |B_K^{(1)}(\alpha)|^2 d\alpha\right), \quad (2.5.10)$$

$$\Re\{B_k^{(1)}(\alpha_1)\} = -\frac{1}{\pi}\left(\int_0^{2\pi} |A_k^{(1)}(\alpha)|^2 d\alpha + J\int_0^{2\pi} |B_k^{(1)}(\alpha)|^2 d\alpha\right). \quad (2.5.11)$$

Similar relations are well known in quantum mechanics and other physical contexts as the optical theorem. These equations imply that for an incident wave of wavenumber K (k) the total energy of the scattered waves can be found from the amplitude of the scattered wave with wavenumber K (k) in the forward direction alone.

To complete the reciprocity relations the two-layer equivalent of the three-dimensional Bessho-Newman relations can be derived. The potential $\phi_i - \overline{\phi_i}$, where ϕ_i is a radiation potential whose behaviour in the far field is given by (2.2.6) and (2.2.7) and which satisfies the body boundary condition given in (1.3.10), has zero normal derivative on the body boundary (since n_i is real) and is thus an appropriate potential to use in (2.2.20). We apply (2.2.20) to the potential $\phi = \phi_i - \overline{\phi_i}$ and each of the scattering potentials $\psi = \phi(K, \alpha_{\text{inc}})$ (for which the scattering amplitudes will be labelled $A_K(\alpha)$ and $B_K(\alpha)$) and $\psi = \phi(k, \alpha_{\text{inc}})$ (for which the scattering amplitudes will be labelled $A_k(\alpha)$ and $B_k(\alpha)$) in turn. The three-dimensional equivalents of Linton & McIver (1995), equations (2.69)–(2.72), can thus be shown to be

$$\pi A_i(\alpha_{\text{inc}} + \pi) + \pi\overline{A_i}(\alpha_{\text{inc}}) + \int_0^{2\pi} A_K(\alpha)\overline{A_i}(\alpha)d\alpha + J\int_0^{2\pi} B_K(\alpha)\overline{B_i}(\alpha)d\alpha = 0 \quad (2.5.12)$$

and

$$\int_0^{2\pi} A_k(\alpha)\overline{A_i}(\alpha)d\alpha + J\left(\pi B_i(\alpha_{\text{inc}}+\pi) + \pi\overline{B_i}(\alpha_{\text{inc}}) + \int_0^{2\pi} B_k(\alpha)\overline{B_i}(\alpha)d\alpha\right) = 0. \tag{2.5.13}$$

Although not used in this thesis these Bessho-Newman relations can be used to determine relationships between the phase angles of certain hydrodynamic quantities as was done by Newman (1976) for the single fluid case.

2.6 Heave and sway radiation problems

To illustrate the general theory of the three-dimensional wave/structure interactions in two-layer fluids we will solve various problems involving submerged spheres. Radiation and scattering problems for such geometries can be solved using multipole expansions, the technique having been used to solve similar problems in unstratified fluids by Srokosz (1979) (deep water) and Linton (1991) (finite depth). The centre of the sphere will be at $x = y = 0$, $z = f$ so that if $f < 0$ the sphere is in the lower layer, whereas if $f > 0$ the sphere is in the upper layer. We will use spherical coordinates (r, θ, α) centred on the sphere defined by

$$x = r\cos\alpha\sin\theta, \qquad y = r\sin\alpha\sin\theta, \qquad z - f = r\cos\theta, \tag{2.6.1}$$

as illustrated in figure 2.1, with $r = a$ being the sphere surface. If $f < 0$ we require $a < |f|$, whereas if $f > 0$ we need $a < \min(d - f, f)$.

2.6.1 Sphere in lower fluid layer

Multipole expansions

Multipoles are singular solutions of the governing equation which satisfy all the boundary conditions of the problem except that on the sphere and behave like outgoing waves far from the singular point. For the case of a sphere centred at $(0, 0, f)$, $f < 0$ of radius a $(< |f|)$ we need to develop multipoles singular at $z = f$. A solution of Laplace's equation singular at $z = f$ is $r^{-n-1}P_n^m(\cos\theta)\cos m\alpha$, $n \geq m \geq 0$, and this has the integral representation, valid for $z > f$,

$$\frac{P_n^m(\cos\theta)}{r^{n+1}}\cos m\alpha = \frac{\cos m\alpha}{(n-m)!}\int_0^\infty u^n e^{-u(z-f)}J_m(uR)du, \tag{2.6.2}$$

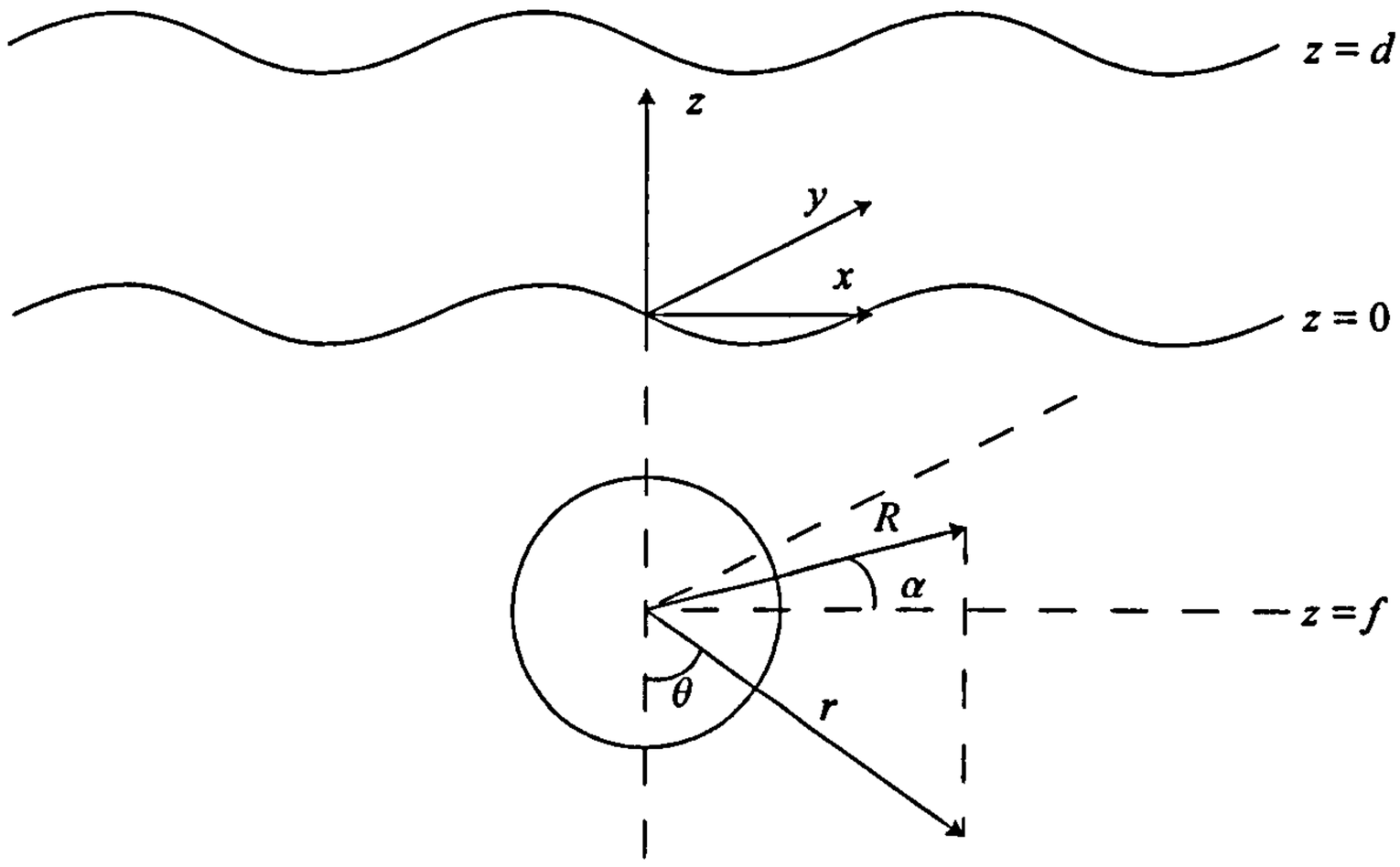

Figure 2.1: Definition sketch

see Gray & Matthews (1952) page 100 equation (6). Note the definition of P_n^m used here corresponds to that in Thorne (1953): $P_n^m(\cos\theta) = \sin^m\theta d^m P_n(\cos\theta)/d(\cos\theta)^m$, which differs from a factor of $(-1)^m$ from that used by some other authors. Multipoles can be constructed from the solution of Laplace's equation

$$\phi_n^{Im} = \frac{a^{n+2}\cos m\alpha}{(n-m)!}\int_0^\infty u^n[A_L(u)e^{uz} + B_L(u)e^{-uz}]J_m(uR)du \tag{2.6.3}$$

$$\phi_n^{IIm} = a^{n+2}\cos m\alpha\left[\frac{P_n^m(\cos\theta)}{r^{n+1}} + \frac{1}{(n-m)!}\int_0^\infty u^n C_L(u)e^{uz}J_m(uR)du\right]. \tag{2.6.4}$$

To find the functions $A(u)$, $B(u)$ and $C(u)$ the multipole functions must satisfy the boundary conditions below

$$\phi_z^{Im} = \phi_z^{IIm} \qquad \text{on } z = 0, \tag{2.6.5}$$

$$\rho(\phi_z^{Im} - K\phi^{Im}) = \phi_z^{IIm} - K\phi^{IIm} \qquad \text{on } z = 0, \tag{2.6.6}$$

$$\phi_z^{Im} = K\phi^{Im} \qquad \text{on } z = d. \tag{2.6.7}$$

After applying these conditions to the multipoles we obtain expressions involving $A_L(u)$, $B_L(u)$ and $C_L(u)$ which are

$$A_L(u) \qquad -B_L(u) - C_L(u) = -e^{uf}, \tag{2.6.8}$$

$$\rho A_L(u) \qquad -\rho\frac{u+K}{u-K}B_L(u) - C_L(u) = -\frac{u+K}{u-K}e^{uf}, \tag{2.6.9}$$

$$A_L(u) - e^{-2ud}\frac{u+K}{u-K}B_L(u) \qquad = \quad 0. \tag{2.6.10}$$

When the above equations are solved we obtain the following functions

$$A_L(u) = K(1+\sigma)(u+K)e^{u(f-2d)}/(u-K)h(u), \tag{2.6.11}$$

$$B_L(u) = K(1+\sigma)e^{uf}/h(u), \tag{2.6.12}$$

$$C_L(u) = (u+K)e^{uf}[(u+K\sigma)e^{-2ud} - u + K]/(u-K)h(u), \tag{2.6.13}$$

where

$$h(u) = (u+K)e^{-2ud} - u + K\sigma, \tag{2.6.14}$$

such that $h(k) = 0$, from the dispersion relation. The multipole functions (2.6.11)–(2.6.13) are identical to (3.7)–(3.9) in Linton & McIver (1995). We now notice that these functions have poles so the multipoles should be written as

$$\phi_n^{Im} = \frac{a^{n+2}\cos m\alpha}{(n-m)!} \int_0^\infty u^n [A_L(u)e^{uz} + B_L(u)e^{-uz}] J_m(uR)du \tag{2.6.15}$$

$$\phi_n^{IIm} = a^{n+2}\cos m\alpha \left[\frac{P_n^m(\cos\theta)}{r^{n+1}} + \frac{1}{(n-m)!} \int_0^\infty u^n C_L(u) e^{uz} J_m(uR)du \right], \tag{2.6.16}$$

where the path of integration is indented to pass beneath the poles of the integrand at $u = K$ and $u = k$ so that the multipoles behave like outgoing waves as $KR \to \infty$. If the integrand were to pass above the poles the multipoles would behave like incoming waves far away from the sphere.

The far-field form of ϕ_n^m, in the lower fluid, is (see appendix B for details)

$$\phi_n^{IIm} \sim -\frac{(-i)^{m+1}a^{n+2}\cos m\alpha}{(n-m)!} \left(\frac{2\pi}{R}\right)^{1/2} \times \left(K^{n-1/2} e^{iKR} C_L^K e^{Kz} + k^{n-1/2} e^{ikR} C_L^k e^{kz} \right) e^{-i\pi/4}, \tag{2.6.17}$$

as $KR \to \infty$, where C_L^K and C_L^k are the residues of $C_L(u)$ at $u = K$ and $u = k$ respectively, which are given by

$$C_L^K = \frac{2K(1+\sigma)e^{K(f-2d)}}{2e^{-2Kd} - 1 + \sigma} \tag{2.6.18}$$

$$\text{and} \qquad C_L^k = \frac{(K+k)e^{kf}\left[(K\sigma+k)e^{-2kd} - k + K\right]}{(k-K)\left[(1-2d(K+k))e^{-2kd} - 1\right]}. \tag{2.6.19}$$

The multipoles defined by (2.6.15) and (2.6.16) can be expanded about $r = 0$ in spherical coordinates by using the identity (see Thorne (1953))

$$e^{\pm u(z-f)} J_m(uR) = (\pm)^m \sum_{s=m}^{\infty} \frac{(\pm ur)^s}{(s+m)!} P_s^m(\cos\theta). \tag{2.6.20}$$

This gives

$$\phi_n^{IIm} = a\cos m\alpha \left[\left(\frac{a}{r}\right)^{n+1} P_n^m(\cos\theta) + \sum_{s=m}^{\infty} A_{ns}^m \left(\frac{r}{a}\right)^s P_s^m(\cos\theta) \right] \tag{2.6.21}$$

where

$$A_{ns}^m = \frac{a}{(n-m)!(s+m)!} \oint_0^{\infty} (au)^{n+s} e^{uf} C_L(u) du. \tag{2.6.22}$$

For computational purposes we note that the contour integral in the above expression can be written

$$\oint_0^{\infty} (au)^{n+s} e^{uf} C_L(u) du + \pi i (Ka)^{n+s} e^{Kf} C_L^K + \pi i (ka)^{n+s} e^{kf} C_L^k \tag{2.6.23}$$

and that the principal-value integral can be evaluated using the method described in appendix C.

Formulation of problem

The solutions to the problems of heave and sway will be denoted by ϕ^0 and ϕ^1 respectively. In the case of heave the body velocity is given by $\boldsymbol{U}^0 = \Re\{Ue^{-iwt}\}\boldsymbol{e}_3$, where $\boldsymbol{e}_3$ is a unit vector in the z-direction, whereas in sway the body velocity is $\boldsymbol{U}^1 = \Re\{Ue^{-iwt}\}\boldsymbol{e}_1$, where $\boldsymbol{e}_1$ is a unit vector in the x-direction. Hence for the heave and sway problems we have the following boundary conditions on the body

$$\frac{\partial \phi^0}{\partial r} = U\cos\theta \qquad \text{on } r = a,\ 0 \le \theta \le \pi,\ 0 \le \alpha \le 2\pi, \tag{2.6.24}$$

$$\frac{\partial \phi^1}{\partial r} = U\sin\theta\cos\alpha \qquad \text{on } r = a,\ 0 \le \theta \le \pi,\ 0 \le \alpha \le 2\pi. \tag{2.6.25}$$

These body boundary conditions can be written in terms of associated Legendre functions, noting that $P_1^0(\cos\theta) = \cos\theta$ and $P_1^1(\cos\theta) = \sin\theta$, giving

$$\frac{\partial \phi^m}{\partial r} = U P_1^m(\cos\theta)\cos m\alpha \qquad \text{on } r = a,\ 0 \le \theta \le \pi,\ 0 \le \alpha \le 2\pi,\ m = 0, 1. \tag{2.6.26}$$

In order to solve the heave and sway problems the velocity potential is expanded in multipole potentials as follows:

$$\phi^m = U \sum_{n=1}^{\infty} b_n^m \phi_n^m \qquad m = 0, 1, \tag{2.6.27}$$

for some unknown coefficients b_n^m. Note that the $n = 0$ term which could appear in the expansion for ϕ^0 has been omitted. This term corresponds to a r^{-1} singularity at the

centre of the sphere which is physically unacceptable, as it would imply an instantaneous flux of fluid across the surface of the sphere.

The expansion of ϕ^m satisfies all the conditions of the problem except that on the body surface (2.6.26). By applying this condition to (2.6.27) we obtain

$$\sum_{n=1}^{\infty} b_n^m \left[-(n+1)P_n^m(\cos\theta) + \sum_{s=1}^{\infty} sA_{ns}^m P_s^m(\cos\theta) \right] = P_1^m(\cos\theta) \qquad m = 0, 1. \quad (2.6.28)$$

Using the orthogonality relations of the Legendre Functions

$$\int_0^{\pi} P_i^m(\cos\theta) P_j^m(\cos\theta) \sin\theta d\theta = \delta_{ij} \begin{cases} 2/(2j+1) & m = 0 \\ 2j(j+1)/(2j+1) & m = 1 \end{cases} \quad (2.6.29)$$

where δ_{ij} is the Kronecker delta, we can reduce equation (2.6.28) to

$$b_s^m - \left[\frac{s}{s+1} \right] \sum_{n=1}^{\infty} A_{ns}^m b_n^m = -\delta_{1s}/2 \qquad s = 1, 2, \ldots \qquad m = 0, 1, \quad (2.6.30)$$

which is an infinite system of linear equations in an infinite number of unknowns. When computing the solution of this the system is truncated into an $N \times N$ system and then approximations to the finite set of coefficients $b_s^m, s = 1, 2, \ldots, N$ computed. For the results presented here I have used a 4×4 system which gives results correct to 3 decimal places. The hydrodynamic force on the sphere in the direction of motion is $F^m = \Re\{f^m e^{-i\omega t}\}$ where f^m is given by

$$f^m = \rho^{II} \omega i \int_0^{2\pi} \int_0^{\pi} \phi^m(a, \theta, \alpha) P_1^m(\cos\theta) \cos m\alpha \, a^2 \sin\theta d\theta d\alpha \qquad m = 0, 1, \quad (2.6.31)$$

from (1.4.4). Using (2.6.21), (2.6.27) and (2.6.29), we can reduce this to

$$f^m = \frac{4}{3}\pi a^3 U \rho^{II} \omega i \left[b_1^m + \sum_{n=1}^{\infty} A_{n1}^m b_n^m \right]. \quad (2.6.32)$$

This can be simplified by using (2.6.30) with $s = 1$. If the force is non-dimensionalised with respect to the mass of the fluid displaced by the sphere and the maximum acceleration of the sphere ($U\omega$), we get expressions for the non-dimensionalised added-mass and damping coefficients μ^m and ν^m (the diagonal entries in the added-mass and damping matrices), which are

$$\mu^m + i\nu^m = -(1 + 3b_1^m) \qquad m = 0, 1. \quad (2.6.33)$$

We note that equations (2.6.30), (2.6.32) and (2.6.33) are the same as the respective equations (13), (15) and (16) in Linton (1991). The form of A_{ns}^m differs and hence so do the coefficients b_n^m.

The damping coefficient B_{ii} is related to the energy radiated to infinity, see equation (2.3.14), given by

$$B_{ii} = \frac{4}{3}\pi\rho^{II}a^3\omega\nu^m = \frac{\rho^{II}\omega}{\pi}\left[J_K\int_0^{2\pi}|A^m(\alpha)|^2d\alpha + J_k\int_0^{2\pi}|B^m(\alpha)|^2d\alpha\right] \tag{2.6.34}$$

where $A^m(\alpha)$ and $B^m(\alpha)$ are the far-field coefficients of wavenumbers K and k respectively in ϕ^m. The far-field form for ϕ^m, in the lower fluid layer, can be written as

$$U^{-1}\phi^m \sim \left(\frac{2}{\pi KR}\right)^{1/2} e^{iKR-i\pi/4}e^{Kz}A^m(\alpha) + \left(\frac{2}{\pi kR}\right)^{1/2} e^{ikR-i\pi/4}e^{kz}B^m(\alpha) \tag{2.6.35}$$

as $KR \to \infty$. We use this form as opposed to the form in the upper fluid layer because it does not contain the $g(z)$ function so it is simpler to extract the $A^m(\alpha)$ and $B^m(\alpha)$ coefficients. From (2.6.17) and (2.6.27) we have that

$$|A^m(\alpha)|^2 = \left|\sum_{n=1}^{\infty}\frac{(Ka)^n b_n^m}{(n-m)!}\right|^2 (\pi a^2 C_L^K \cos m\alpha)^2 \tag{2.6.36}$$

$$|B^m(\alpha)|^2 = \left|\sum_{n=1}^{\infty}\frac{(ka)^n b_n^m}{(n-m)!}\right|^2 (\pi a^2 C_L^k \cos m\alpha)^2. \tag{2.6.37}$$

Any numerical results produced by solving (2.6.30) can then be checked against the following identity

$$\Im(b_1^m) = -\frac{\pi a}{2\epsilon_m}\left(J_K\left|\sum_{n=1}^{\infty}\frac{(Ka)^n b_n^m}{(n-m)!}C_L^K\right|^2 + J_k\left|\sum_{n=1}^{\infty}\frac{(ka)^n b_n^m}{(n-m)!}C_L^k\right|^2\right) \tag{2.6.38}$$

where $\epsilon_0 = 1$, $\epsilon_m = 2$ for $m \geq 1$, which follows from (2.6.34) using (2.6.33) and (2.6.36)–(2.6.37). The results produced by (2.6.33) were checked using (2.6.38) and agreed in all cases.

Results

Curves of added-mass and damping coefficients for spheres in the lower fluid layer in both heave and sway are shown in figures 2.2–2.5. In all the curves $\rho(=\rho^I/\rho^{II})$ is 0.95 and the ratio of the depth of the upper fluid layer to the radius of sphere, d/a, is 2.0. Each plot shows the results obtained for four different submersion depths, f/a, of the sphere, -1.1, -1.5, -2 and -3. The case $f/a = -1.1$ represents a sphere close to the interface between the two fluid layers, with $|f/a|$ increasing as the sphere becomes more deeply submerged.

Figures 2.2 and 2.3 show the damping coefficients for heave and sway respectively and it can be seen that in each case there are two local maximums. These occur near $ka = 1$,

which corresponds to $Ka \approx 0.025$, and $Ka = 1$ and in order to satisfactorily illustrate both of them on the same figure we have plotted the results (here and subsequently) on a log scale. The damping coefficient is proportional to the radiated energy, see (2.6.34), and the local maximum around $ka = 1$ corresponds to the sphere's increased ability to make waves on the interface at this frequency, whereas the local maximum around $Ka = 1$ corresponds to the sphere's increased free surface wave-making ability (see, for example, Linton (1991)). As one would expect, the closer the sphere is to the interface the greater the wave-making capability and hence the greater the damping coefficient. Since the sphere is in the lower layer it affects the interface a lot more than the free surface and so the variation in the damping coefficient near $ka = 1$ is greater than that near $Ka = 1$. In all cases the heave damping coefficient is greater than the sway damping coefficient, just as was reported in Srokosz (1979) for the single-layer fluid case.

Figures 2.4 and 2.5 show the added-mass coefficients for heave and sway respectively. As the immersion depth increases the added-mass curves tend towards the constant value of 1/2, which is the added-mass of a sphere oscillating in an infinite expanse of fluid. When the sphere is close to the interface, the deviation from 1/2 is greater in the case of heave. It is again noticeable that there is an effect due to the presence of the free surface near $Ka = 1$. In the limit as $Ka \to 0$, the interface boundary conditions (2.2.3) and (2.2.4) reduce to $\phi_z^{II} = 0$ and we get the same results in the long-wave limit as if the interface were the free-surface in a single-layer fluid. Thus the solid curve in figure 2 of Linton (1991) tends to the same value as $Ka \to 0$ as the $f/a = -1.5$ curve in figure 2.4 here.

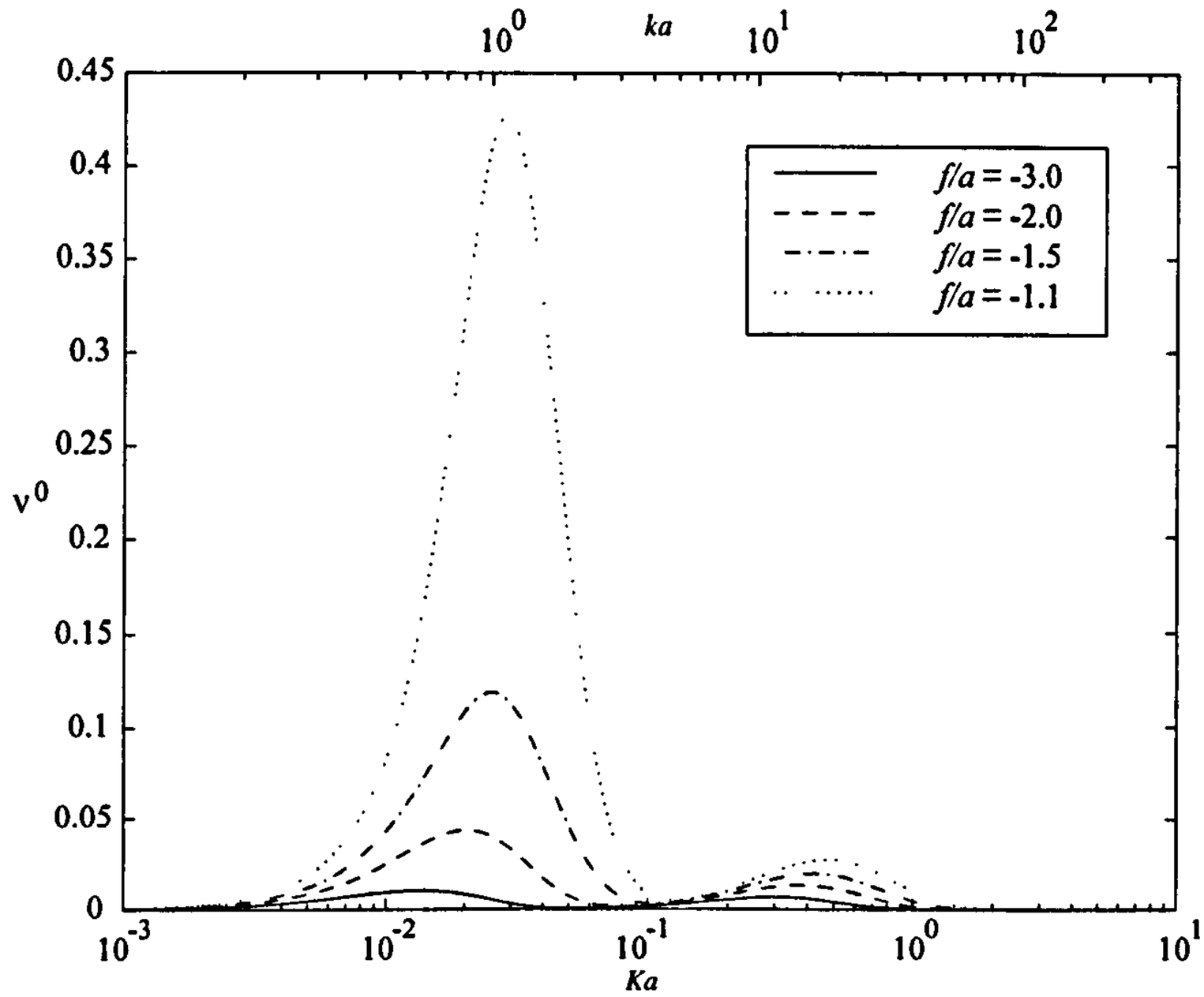

Figure 2.2: Damping coefficient ν^0 (heave) plotted against Ka for a submerged sphere at different depths in the lower fluid layer; $\rho = 0.95$ and $d/a = 2.0$.

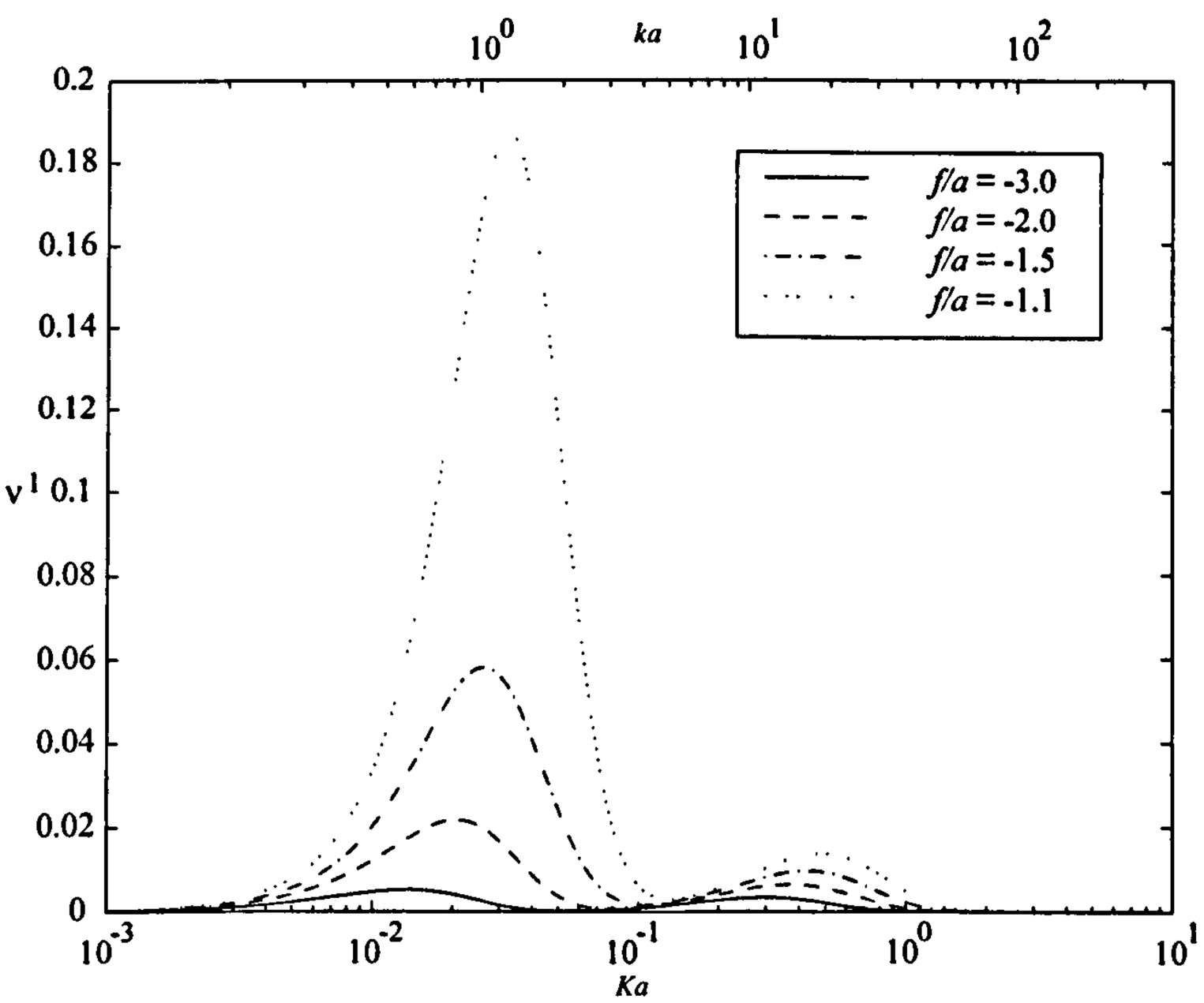

Figure 2.3: Damping coefficient ν^1 (sway) plotted against Ka for a submerged sphere at different depths in the lower fluid layer; $\rho = 0.95$ and $d/a = 2.0$.

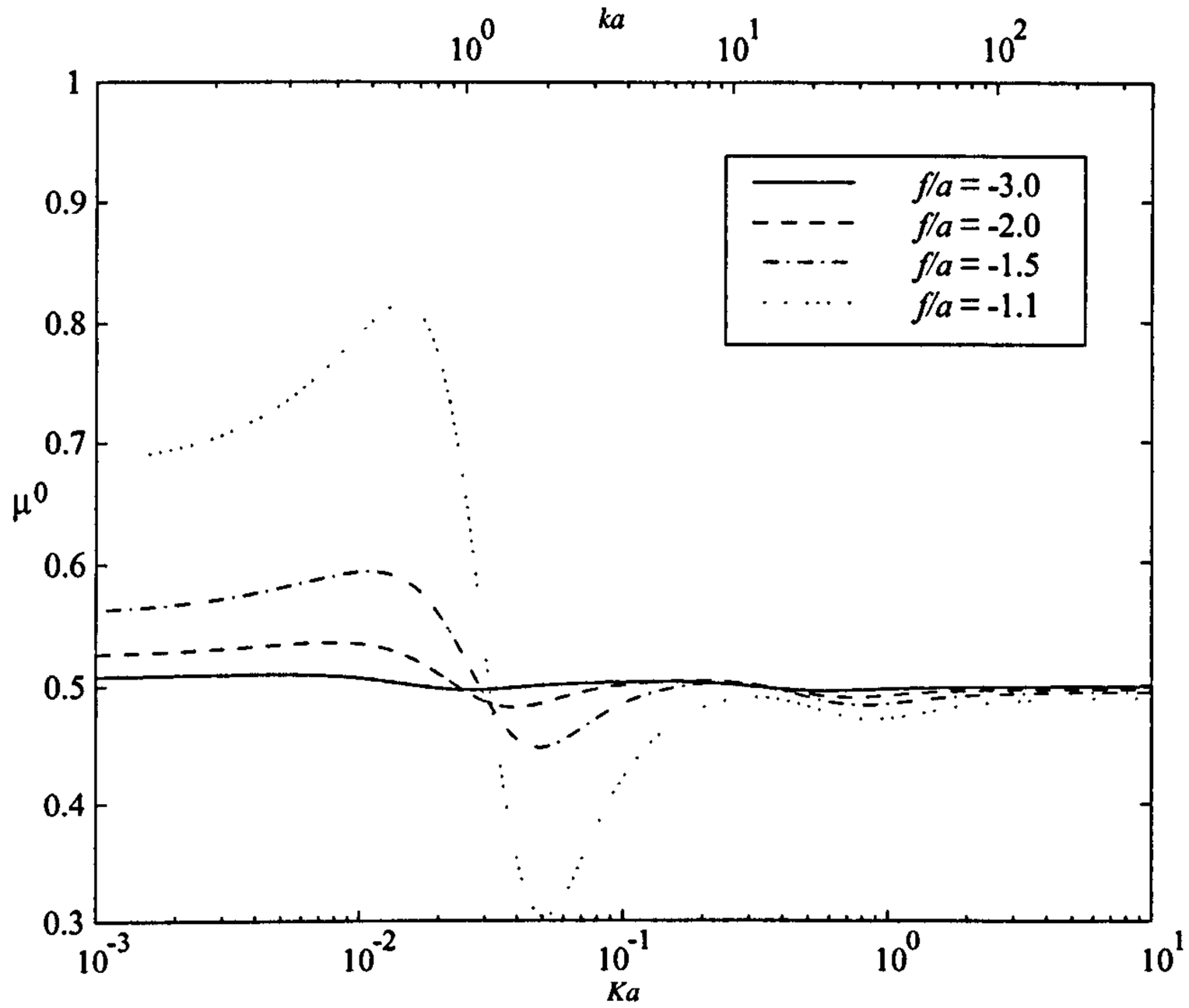

Figure 2.4: Added mass coefficient μ^0 (heave) plotted against Ka for a submerged sphere at different depths in the lower fluid layer; $\rho = 0.95$ and $d/a = 2.0$.

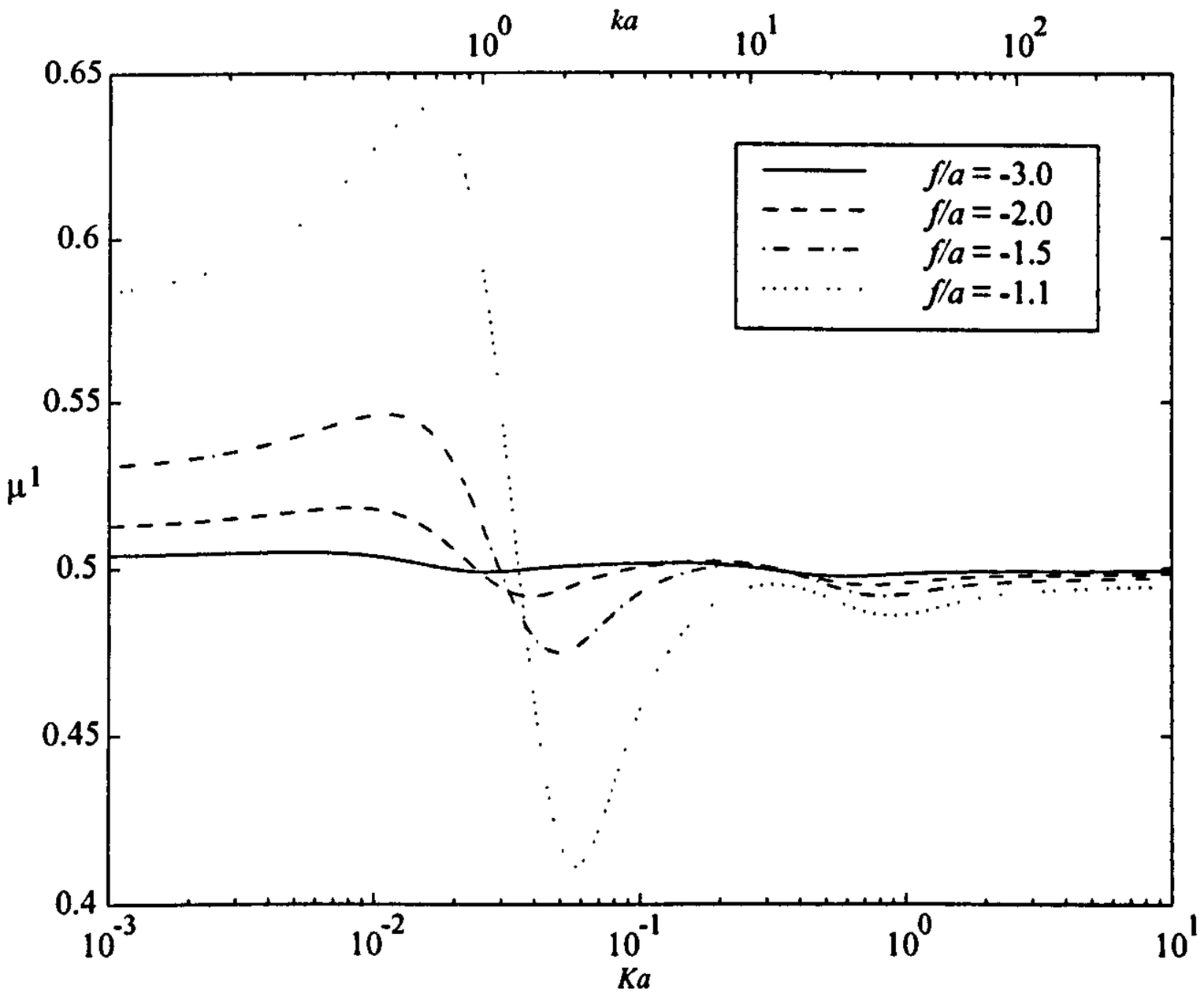

Figure 2.5: Added mass coefficient μ^1 (sway) plotted against Ka for a submerged sphere at different depths in the lower fluid layer; $\rho = 0.95$ and $d/a = 2.0$.

2.6.2 Sphere in upper fluid layer

Multipole expansions

For problems involving a sphere in the upper fluid layer we need to develop multipoles singular at $z = f > 0$. To do so we require in addition to the integral representation (2.6.2), the following representation valid for $z < f$:

$$\frac{P_n^m(\cos\theta)}{r^{n+1}} = \frac{(-1)^{m+n}}{(n-m)!}\int_0^\infty u^n e^{u(z-f)} J_m(uR)du. \tag{2.6.39}$$

This is derived from (2.6.2) by replacing θ by $\pi - \theta$ and so $z - f$ $(= r\cos\theta)$ is replaced by $f - z$ and also the following identity is used

$$P_n^m(-\cos\theta) = (-1)^{m+n} P_n^m(\cos\theta). \tag{2.6.40}$$

Suitable multipoles are of the form

$$\begin{aligned}\phi_n^{Im} =& a^{n+2}\cos m\alpha\left[\frac{P_n^m(\cos\theta)}{r^{n+1}} + \right.\\ &\left.\frac{(-1)^{m+n}}{(n-m)!}\int_0^\infty u^n[A_U(u)e^{uz} + B_U(u)e^{-uz}]J_m(uR)du\right] \qquad (2.6.41)\\ \phi_n^{IIm} =& \frac{(-1)^{m+n}a^{n+2}\cos m\alpha}{(n-m)!}\int_0^\infty u^n J_m(uR)C_U(u)e^{uz}du. \qquad (2.6.42)\end{aligned}$$

After application of (2.6.5)–(2.6.7) we get equations involving $A_U(u)$, $B_U(u)$ and $C_U(u)$ which are

$$\begin{aligned} A_U(u) \qquad\qquad -B_U(u) \quad -C_U(u) &= \qquad -e^{-uf}, \qquad (2.6.43)\\ \rho A_U(u) - \rho\frac{u+K}{u-K}B_U(u) \quad -C_U(u) &= \qquad -\rho e^{-uf}, \qquad (2.6.44)\\ \frac{u-K}{u+K}e^{2ud}A_U(u) \qquad\qquad -B_U(u) &= (-1)^{m+n}e^{uf}. \qquad (2.6.45)\end{aligned}$$

Solving the above gives expressions for the multipole functions which are

$$\begin{aligned} A_U(u) =& (u+K)e^{-2ud}[(-1)^{m+n+1}(u-K\sigma)e^{uf} - (u-K)e^{-uf}]/(u-K)h(u), \qquad (2.6.46)\\ B_U(u) =& [(-1)^{m+n+1}(u+K)e^{u(f-2d)} - (u-K)e^{-uf}]/h(u), \qquad (2.6.47)\\ C_U(u) =& K(1-\sigma)B_U(u)/(u-K). \qquad (2.6.48)\end{aligned}$$

We note that the functions (2.6.46)–(2.6.48) are the same as (4.7)–(4.9) in Linton & McIver (1995) with q replaced by m. The multipoles are expanded about $r = 0$ by using

(2.6.20) and we obtain

$$\phi_n^{Im} = \left\{ \frac{P_n^m(\cos\theta)}{r^{n+1}} + \sum_{s=m}^{\infty} \frac{(-1)^{m+n}}{(n-m)!} \oint_0^{\infty} u^n [A_U(u) e^{uf} (ur)^s + (-1)^{m+s} B_U(u) e^{-uf} (ur)^s] du \frac{P_s^m(\cos\theta)}{(s+m)!} \right\} a^{n+2} \cos m\alpha. \quad (2.6.49)$$

The above can be written as

$$\phi_n^{Im} = \left[\left(\frac{a}{r}\right)^{n+1} P_n^m(\cos\theta) + \sum_{s=m}^{\infty} \left(\frac{r}{a}\right)^s B_{ns}^m P_s^m(\cos\theta) \right] a \cos m\alpha \quad (2.6.50)$$

where

$$B_{ns}^m = \frac{(-1)^{m+n} a}{(n-m)!(s+m)!} \oint_0^{\infty} (au)^{n+s} [e^{uf} A_U(u) + (-1)^{m+s} e^{-uf} B_U(u)] du. \quad (2.6.51)$$

The far-field form of ϕ_n^m, in the lower fluid, is given by

$$\phi_n^m \sim \frac{(-1)^n i^{m+1} a^{n+2} \cos m\alpha}{(n-m)!} \left(\frac{2\pi}{R}\right)^{1/2} \times \left(K^{n-1/2} e^{iKR} C_U^K e^{Kz} + k^{n-1/2} e^{ikR} C_U^k e^{kz} \right) e^{-i\pi/4}, \quad (2.6.52)$$

as $KR \to \infty$, where

$$C_U^K = \frac{(-1)^{m+n+1} 2K(1-\sigma) e^{K(f-2d)}}{2e^{-2ud} - 1 + \sigma}, \quad (2.6.53)$$

$$C_U^k = \frac{K(1-\sigma)[(-1)^{m+n+1}(K+k)e^{k(f-2d)} - (k-K)e^{-kf}]}{(k-K)[(1-2d(K+k))e^{-2kd} - 1]}. \quad (2.6.54)$$

Formulation of problem

First express the velocity potential in terms of the multipoles as in (2.6.27)

$$\phi^m = U \sum_{n=1}^{\infty} b_n^m \phi_n^m \qquad m = 0, 1, \quad (2.6.55)$$

and then apply the body boundary condition (2.6.26) to give

$$\sum_{n=1}^{\infty} b_n^m \left[-(n+1) P_n^m(\cos\theta) + \sum_{s=1}^{\infty} s B_{ns}^m P_s^m(\cos\theta) \right] = P_1^m(\cos\theta) \qquad m = 0, 1. \quad (2.6.56)$$

Using the orthogonality of the Legendre functions we can reduce this to

$$b_s^m - \left[\frac{s}{s+1}\right] \sum_{n=1}^{\infty} B_{ns}^m b_n^m = -\delta_{1s}/2 \qquad s = 1, 2, \ldots \qquad m = 0, 1, \quad (2.6.57)$$

which, as before, is an infinite system of linear equations in an infinite number of unknowns. Equation (2.6.57) is the same as (2.6.30) with A_{ns}^m replaced with B_{ns}^m. The force f^m, from (1.4.4), is given by

$$f^m = \rho^I \omega i \int_0^{2\pi} \int_0^{\pi} \phi^m(a, \theta, \alpha) P_1^m(\cos\theta) \cos m\alpha \, a^2 \sin\theta \, d\theta \, d\alpha \qquad m = 0, 1. \quad (2.6.58)$$

Using (2.6.50), (2.6.55) and (2.6.29), this reduces to

$$f^m = \frac{4}{3}\pi a^3 U \rho^I \omega i \left[b_1^m + \sum_{n=1}^{\infty} B_{n1}^m b_n^m \right] \tag{2.6.59}$$

which can be simplified by using (2.6.57) with $s = 1$. By non-dimensionalising with respect to the mass of fluid displaced by the sphere and the maximum acceleration of the sphere ($U\omega$), we get expressions for the non-dimensionalised added-mass and damping coefficients μ^m and ν^m. These are

$$\mu^m + i\nu^m = -(1 + 3b_1^m) \qquad m = 0, 1. \tag{2.6.60}$$

We again notice the similarities with the single-layer formulas as in Linton (1991). The damping coefficient ν^m is related to the energy radiated to infinity, equation (2.3.14), given by

$$B_{ii} = \frac{4}{3}\pi \rho^I a^3 \omega \nu^m = \frac{\rho^{II}\omega}{\pi} \left[J_K \int_0^{2\pi} |A^m(\alpha)|^2 d\alpha + J_k \int_0^{2\pi} |B^m(\alpha)|^2 d\alpha \right]. \tag{2.6.61}$$

Now $A^m(\alpha)$ and $B^m(\alpha)$ can be found using (2.6.35), (2.6.52) and (2.6.27). They are

$$|A^m(\alpha)|^2 = \left| \sum_{n=1}^{\infty} \frac{(-Ka)^n b_n^m}{(n-m)!} C_U^K \right|^2 (a^2 \pi \cos m\alpha)^2 \tag{2.6.62}$$

$$|B^m(\alpha)|^2 = \left| \sum_{n=1}^{\infty} \frac{(-ka)^n b_n^m}{(n-m)!} C_U^k \right|^2 (a^2 \pi \cos m\alpha)^2 \tag{2.6.63}$$

Note the residues of C_U are included in the summation because they depend on n. The numerical check for results of added-mass and damping coefficients with the sphere in the upper fluid is now

$$\Im(b_1^m) = -\frac{\pi a}{2\epsilon_m \rho} \left(J_K \left| \sum_{n=1}^{\infty} \frac{(-Ka)^n b_n^m}{(n-m)!} C_U^K \right|^2 + J_k \left| \sum_{n=1}^{\infty} \frac{(-ka)^n b_n^m}{(n-m)!} C_U^k \right|^2 \right) \tag{2.6.64}$$

which follows from (2.6.61) using (2.6.60) and (2.6.62)–(2.6.63). The results presented below, produced by (2.6.60), were checked using the identity (2.6.64) and agreed in all cases.

Results

Curves of added-mass and damping coefficients for spheres in the upper fluid layer are shown in figures 2.6–2.9. In all the curves ρ is 0.95 and d/a is 4.0. Each plot shows the results obtained for four different submersion depths, f/a, of the sphere. The values of f/a have been chosen so there are results close to the interface ($f/a = 1.1$), close to the free surface ($f/a = 2.9$) and at two intermediate values ($f/a = 1.7$ and 2.3).

Figures 2.6 and 2.7 show the damping coefficients for heave and sway motion respectively. The two cases lead to similar results, but those for heave motion are greater than those obtained for sway. As with the results for the sphere in the lower region there are two local maximums, one near $ka = 1$ which corresponds to waves being generated on the interface and one near $Ka = 1$ which corresponds to waves on the free surface. When the sphere is close to the interface ($f/a = 1.1$) the first local maximum is the greatest as more waves are generated on the interface than on the free surface. As the sphere approaches the free surface the ability to make waves on the interface decreases whilst it becomes easier to generate waves on the free surface. The maximum value of the damping coefficient is greater when $f/a = 2.9$ (when the distance of the sphere's surface is $0.1a$ from the free surface) than for the case $f/a = 1.1$ (when the distance of the sphere's surface is $0.1a$ from the interface) showing that the ability to make waves on the free-surface is greater than that on the interface. It is also noteworthy that the range of values of Ka over which there is a noticeable effect on the free surface is an order of magnitude bigger than the range for which the interface is affected.

The added-mass coefficients for heave and sway are shown in figures 2.8 and 2.9 respectively and again the deviations from the infinite fluid value of 1/2 are greater for heave motion than for sway motion. The effect of the interface is pronounced when $f/a = 1.1$ as can be seen by the fact that large variations occur in the added-mass around $ka = 1$ ($Ka \approx 0.025$) whereas for $f/a = 2.9$ it is the free-surface effect which dominates with large variations around $Ka = 1$. In the limit as $Ka \to 0$ the problem reduces to that of a sphere oscillating between parallel planes and so we get the same limiting value for $f/a = 1.1$ and 2.9 (as in each case the sphere's surface is a distance $0.1a$ from one of the walls) and similarly the same limiting value is obtained for $f/a = 1.7$ and 2.3 (in each case the sphere's surface is a distance $0.7a$ from one of the walls). Though not present on these figures, negative added-mass can occur for the heave problem when the sphere is either very close to the free surface or to the interface. This phenomenon, which does not appear to occur for sway, or when the sphere is below the interface is discussed by McIver & Evans (1984).

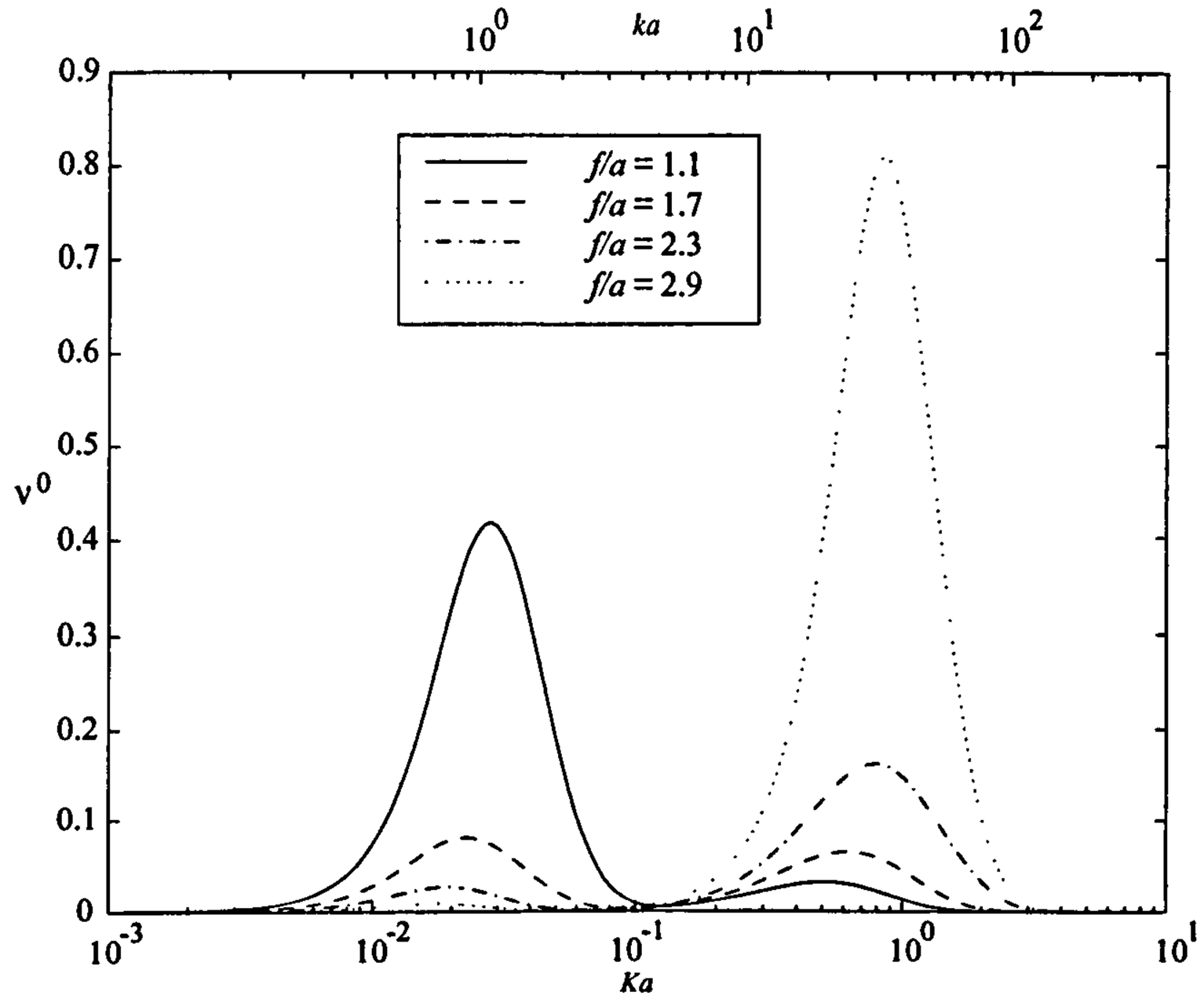

Figure 2.6: Damping coefficient ν^0 (heave) plotted against Ka for a submerged sphere at different depths in the upper fluid layer; $\rho = 0.95$ and $d/a = 4.0$.

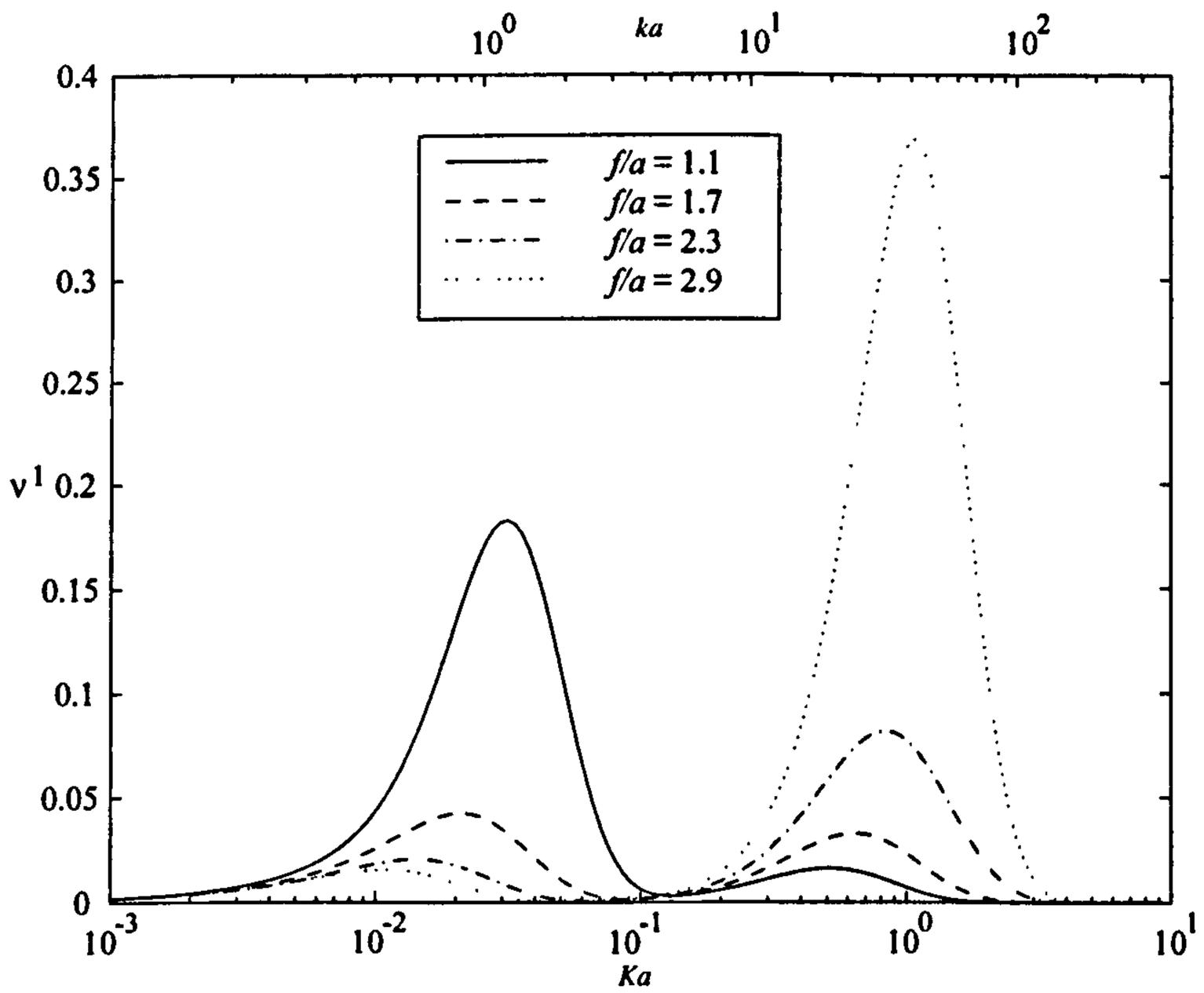

Figure 2.7: Damping coefficient ν^1 (sway) plotted against Ka for a submerged sphere at different depths in the upper fluid layer; $\rho = 0.95$ and $d/a = 4.0$.

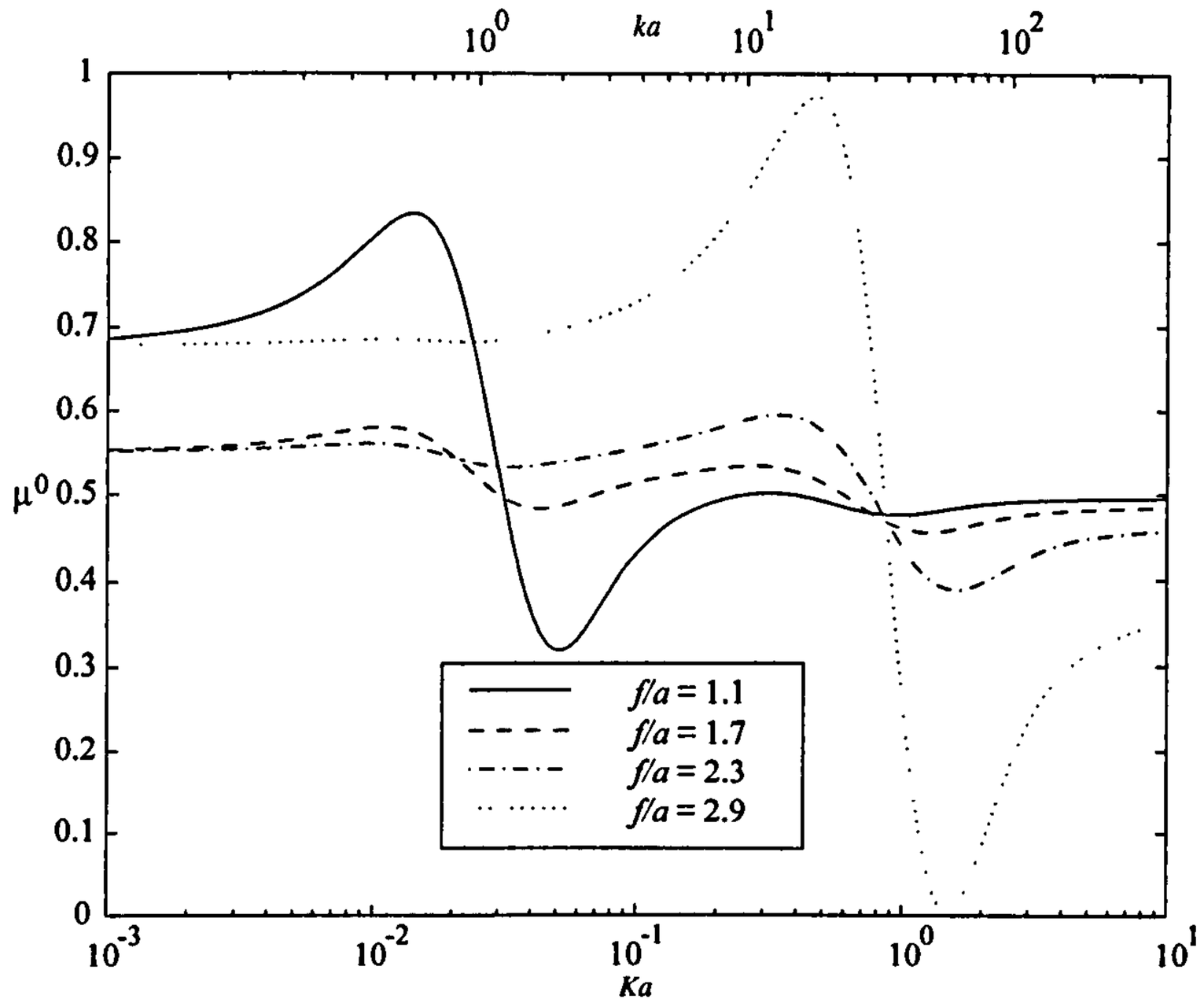

Figure 2.8: Added mass coefficient μ^0 (heave) plotted against Ka for a submerged sphere at different depths in the upper fluid layer; $\rho = 0.95$ and $d/a = 4.0$.

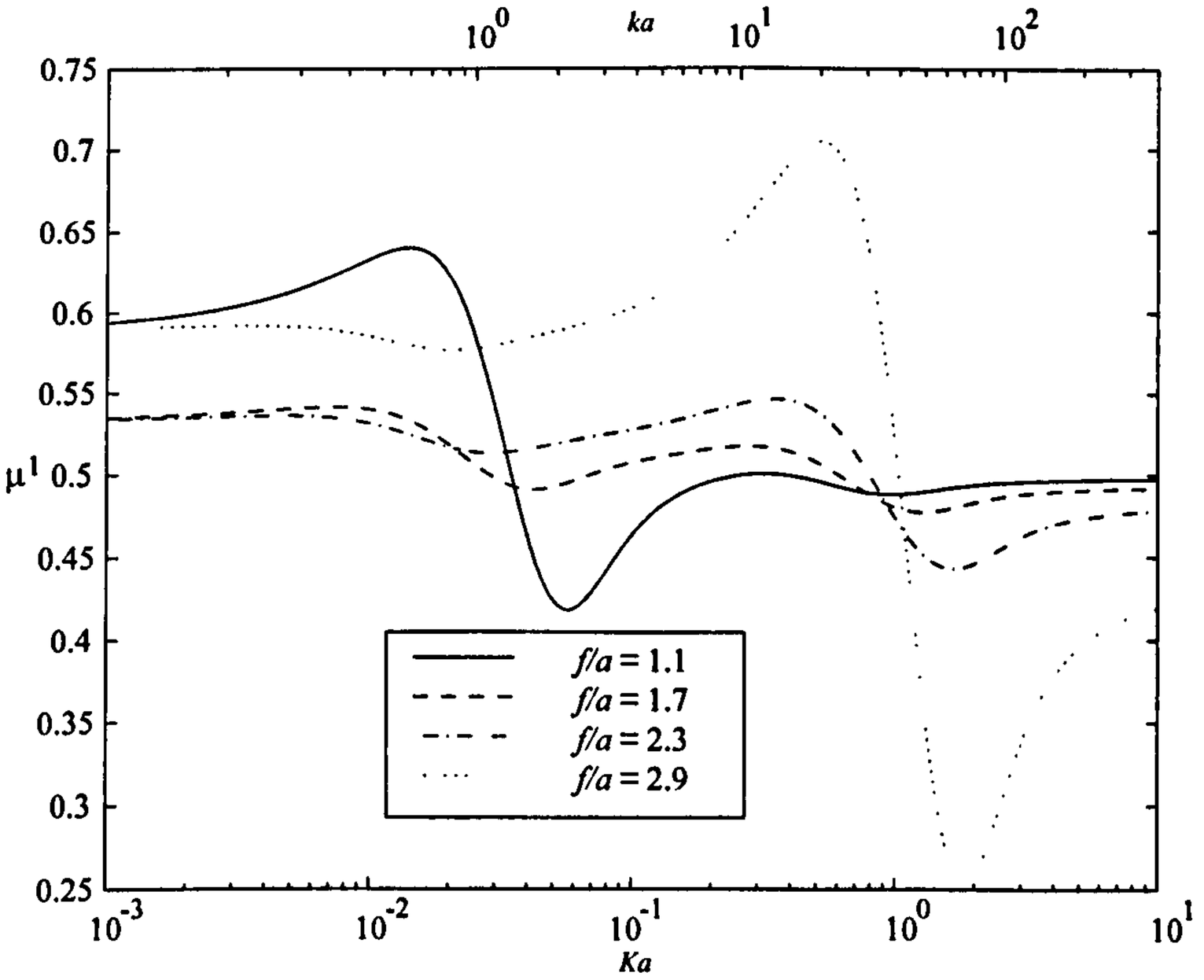

Figure 2.9: Added mass coefficient μ^1 (sway) plotted against Ka for a submerged sphere at different depths in the upper fluid layer; $\rho = 0.95$ and $d/a = 4.0$.

2.7 Scattering problem

In this section we will solve the problem of the scattering of an incident plane wave, of wavenumber either K or k, by a submerged sphere, first situated in the lower layer and then above the interface. In each case the total scattering potential can be decomposed into two parts:

$$\phi = \phi_{\text{inc}} + \phi_S \tag{2.7.1}$$

where ϕ_{inc} is the potential representing the incident plane wave (given, up to an arbitrary multiplicative constant by (2.2.15) if the incident wave has wavenumber K and by (2.2.13) and (2.2.14) if the incident wave has wavenumber k) and ϕ_S therefore must satisfy (2.2.2)–(2.2.5), the body boundary condition

$$\frac{\partial \phi_S}{\partial r} = -\frac{\partial \phi_{\text{inc}}}{\partial r} \qquad \text{on } r = a, \tag{2.7.2}$$

and behave as an outgoing cylindrical wave far from the sphere. Without loss of generality we can assume that the incident wave is from $x = -\infty$ so that $\alpha_{\text{inc}} = 0$.

2.7.1 Sphere in lower fluid layer

Incident wavenumber K

First we consider an incident plane wave of wavenumber K and amplitude A on the free surface ($z = d$). The time independent free-surface elevation, η_d, of such a wave is

$$\eta_d = Ae^{iKR\cos\alpha} \tag{2.7.3}$$

where the velocity potential, ϕ_{inc}, of the wave is given, up to a constant B, by

$$\phi_{\text{inc}} = Be^{Kz}e^{iKR\cos\alpha} \tag{2.7.4}$$

from (2.2.15). To find the constant B we apply the free-surface condition $g\eta_d = i\omega\phi$, on $z = d$ which gives

$$B = -\frac{igA}{\omega}e^{-Kd} \tag{2.7.5}$$

so we can now write the potential as

$$\phi_{\text{inc}} = -\frac{igA}{\omega}e^{K(z-d)}e^{iKR\cos\alpha}. \tag{2.7.6}$$

This potential can be expanded in spherical polar coordinates using Abramowitz & Stegun (1965), equations (9.1.44), (9.1.45), and (2.6.20) from earlier, to give

$$\phi_{\text{inc}} = -\frac{igA}{\omega} e^{K(z-d)} e^{iKR\cos\alpha} \tag{2.7.7}$$

$$= -\frac{igA}{\omega} e^{K(z-d)} \sum_{m=0}^{\infty} \epsilon_m i^m J_m(KR) \cos m\alpha \tag{2.7.8}$$

$$= -\frac{igA}{\omega} e^{K(f-d)} \sum_{m=0}^{\infty} \epsilon_m i^m \cos m\alpha \sum_{s=m}^{\infty} \frac{(Kr)^s}{(s+m)!} P_s^m(\cos\theta). \tag{2.7.9}$$

where $\epsilon_0 = 1$, $\epsilon_m = 2$ for $m \geq 1$.

For the radiation problems considered in the previous section the dependence on the azimuthal angle α was known, but here it is not (apart from the fact that its even) and so we must use a more general multipole expansion. We write

$$\phi_S = -\frac{igA}{a\omega} \sum_{m=0}^{\infty} \sum_{n=m_1}^{\infty} c_n^m \phi_n^m, \tag{2.7.10}$$

where $m_1 = \max(m, 1)$ and ϕ_n^m is given (in the lower fluid layer) by (2.6.21). If we then apply the boundary condition (2.7.2) we obtain

$$\sum_{m=0}^{\infty} \sum_{n=m_1}^{\infty} c_n^m \cos m\alpha \left[(n+1) P_n^m(\cos\theta) - \sum_{s=m}^{\infty} s A_{ns}^m P_s^m(\cos\theta) \right]$$

$$= e^{K(f-d)} \sum_{m=0}^{\infty} \epsilon_m i^m \cos m\alpha \sum_{s=m}^{\infty} s \frac{(Ka)^s}{(s+m)!} P_s^m(\cos\theta). \tag{2.7.11}$$

Integrating the above equation from 0 to 2π with respect to α gives,

$$\sum_{n=1}^{\infty} c_n^0 \left[(n+1) P_n^0(\cos\theta) - \sum_{s=0}^{\infty} s A_{ns}^0 P_s^0(\cos\theta) \right] = e^{K(f-d)} \sum_{s=0}^{\infty} \frac{s(Ka)^s}{s!} P_s^0(\cos\theta). \tag{2.7.12}$$

Using the orthogonality of the Legendre functions (2.6.29) yields an infinite system of equations for the set of coefficients c_n^0, $n = 1, 2, \ldots$, which is

$$c_s^0 - \left[\frac{s}{s+1} \right] \sum_{n=1}^{\infty} c_n^0 A_{ns}^0 = e^{K(f-d)} \frac{s(Ka)^s}{(s+1)!} \qquad s = 1, 2, \ldots . \tag{2.7.13}$$

Now if (2.7.11) is multiplied by $\cos m\alpha$, $m \geq 1$, and integrated from 0 to 2π with respect to α we obtain

$$\sum_{n=m_1}^{\infty} c_n^m \left[(n+1) P_n^m(\cos\theta) - \sum_{s=m}^{\infty} s A_{ns}^m P_s^m(\cos\theta) \right]$$

$$= 2 i^m e^{K(f-d)} \sum_{s=m}^{\infty} \frac{s(Ka)^s}{(s+m)!} P_s^m(\cos\theta). \tag{2.7.14}$$

Then by using the orthogonality of the Legendre functions again we get an infinite system of equations for the set of coefficients c_n^m, $n = 1, 2, \ldots$ for each $m = 1, 2, \ldots$ which is

$$c_s^m - \left[\frac{s}{s+1}\right] \sum_{n=m_1}^{\infty} A_{ns}^m c_n^m = 2 \left[\frac{s}{s+1}\right] i^m e^{K(f-d)} \frac{(Ka)^s}{(s+m)!} \qquad s = 1, 2, \ldots . \tag{2.7.15}$$

It is clear that the systems c_n^0 and c_n^m can be represented with one equation which is

$$c_s^m - \left[\frac{s}{s+1}\right] \sum_{n=m_1}^{\infty} A_{ns}^m c_n^m = \epsilon_m \left[\frac{s}{s+1}\right] i^m e^{K(f-d)} \frac{(Ka)^s}{(s+m)!}, \tag{2.7.16}$$

for $s \geq m_1$. These systems can be solved by truncation with an additional truncation parameter being the number of systems that are solved. In computations presented below two 4×4 systems were solved.

The vertical and horizontal exciting forces on the sphere due to an incident wave of wavenumber K, f_K^0 and f_K^1, can be calculated from

$$f_K^0 = -\rho^{II} \omega i \int_0^{2\pi} \int_0^{\pi} \phi(a, \theta, \alpha) P_1^0(\cos\theta) a^2 \sin\theta d\theta d\alpha \tag{2.7.17}$$

and

$$f_K^1 = -\rho^{II} \omega i \int_0^{2\pi} \int_0^{\pi} \phi(a, \theta, \alpha) P_1^1(\cos\theta) \cos\alpha \; a^2 \sin\theta d\theta d\alpha. \tag{2.7.18}$$

Performing the integration gives

$$f_K^0 = -\frac{4}{3} \pi a^2 \rho^{II} g A \left[e^{K(f-d)} Ka + c_1^0 + \sum_{n=1}^{\infty} A_{n1}^0 c_n^0 \right] \tag{2.7.19}$$

and

$$f_K^1 = -\frac{4}{3} \pi a^2 \rho^{II} g A \left[i e^{K(f-d)} Ka + c_1^1 + \sum_{n=1}^{\infty} A_{n1}^1 c_n^1 \right]. \tag{2.7.20}$$

These can be simplified using (2.7.13) and (2.7.15) giving

$$f_K^0 = -4\pi a^2 \rho^{II} g A c_1^0,$$
$$f_K^1 = -4\pi a^2 \rho^{II} g A c_1^1, \tag{2.7.21}$$

and after non-dimensionalising we are led to the results

$$\overline{f_K^0} = |f_K^0/(a^2 \rho^{II} g A)| = 4\pi |c_1^0|, \tag{2.7.22}$$

$$\overline{f_K^1} = |f_K^1/(a^2 \rho^{II} g A)| = 4\pi |c_1^1|. \tag{2.7.23}$$

Note that $\overline{f_K^m}$ does not mean the complex conjugate of f_K^m here. Equations (2.7.22) and (2.7.23) are the same as the single fluid case as in Linton (1991) equations (28a) and (28b). Now, from (2.4.6), the expression that relates the exciting forces on a fixed body due to an incident wave of wavenumber K to that wave field radiated by the same body in motion is

$$f^m = 2\rho^{II}\omega J_K A^m(\alpha_{\text{inc}} + \pi). \tag{2.7.24}$$

The vertical and horizontal forces are found by using heave and sway radiation potentials respectively. So, with $\alpha_{\text{inc}} = 0$, we have

$$f_K^0 = 2\rho^{II}\omega J_K A^0(\pi), \tag{2.7.25}$$

$$f_K^1 = 2\rho^{II}\omega J_K A^1(\pi), \tag{2.7.26}$$

where A^m is found from the far-field behaviour of the multipole given by (2.6.17) and (2.6.27). Substituting A^m into f_K^0 and f_K^1 and using (2.7.21) gives

$$c_1^0 = -\frac{J_K}{2} e^{-Kd} C_L^K \sum_{n=1}^{\infty} \frac{b_n^0 (Ka)^n}{n!}, \tag{2.7.27}$$

$$c_1^1 = -\frac{iJ_K}{2} e^{-Kd} C_L^K \sum_{n=1}^{\infty} \frac{b_n^1 (Ka)^n}{(n-1)!}, \tag{2.7.28}$$

where the coefficients b_n^m are the solutions of (2.6.30). These identities were used as a numerical check on the results obtained from the radiation and scattering problems.

Incident wavenumber k

Next we consider the case of an incident plane wave of amplitude A on the interface ($z = 0$) with wavenumber k. The time independent interfacial elevation, η_0, of such a wave is written as

$$\eta_0 = Ae^{ikR\cos\alpha} \tag{2.7.29}$$

and the velocity potential, up to a constant B, is

$$\phi_{\text{inc}}^I = Bg(z)e^{ikR\cos\alpha}, \tag{2.7.30}$$

$$\phi_{\text{inc}}^{II} = Be^{kz}e^{ikR\cos\alpha}, \tag{2.7.31}$$

from (2.2.13)–(2.2.14). To find B we apply the interface condition $-i\omega\eta_0 = \partial\phi_{\text{inc}}/\partial z$, on $z = 0$ which gives

$$B = -\frac{i\omega A}{k} = -\frac{igAK}{\omega k}. \tag{2.7.32}$$

The incident wave potential can now be written as

$$\phi^I_{\text{inc}} = -\frac{igAK}{\omega k} g(z) e^{ikR\cos\alpha} \tag{2.7.33}$$

$$\phi^{II}_{\text{inc}} = -\frac{igAK}{\omega k} e^{kz} e^{ikR\cos\alpha}. \tag{2.7.34}$$

In region II this incident wave is similar to that of an incident wave of wavenumber K and so the analysis above can be closely followed. We use the same expansion for ϕ_S as before, (2.7.10), but denote the unknown coefficients by d^m_n and we obtain the infinite systems of equations

$$d^m_s - \left[\frac{s}{s+m}\right] \sum_{n=m_1}^{\infty} A^m_{ns} d^m_n = \left[\frac{s}{s+1}\right] \frac{\epsilon_m i^m s K a (ka)^{s-1} e^{kf}}{(s+m)!} \qquad s \geq m_1, \tag{2.7.35}$$

for each $m \geq 0$. The vertical and horizontal exciting forces are given by

$$f^0_k = -4\pi a^2 \rho^{II} g A d^0_1, \tag{2.7.36}$$

$$f^1_k = -4\pi a^2 \rho^{II} g A d^1_1, \tag{2.7.37}$$

and after non-dimensionalising we get

$$\overline{f^0_k} = |f^0_k/(a^2\rho^{II} g A)| = 4\pi |d^0_1|, \tag{2.7.38}$$

$$\overline{f^1_k} = |f^1_k/(a^2\rho^{II} g A)| = 4\pi |d^1_1|. \tag{2.7.39}$$

Now, from (2.4.7), the relation between the forces on the body due to an incident wave of wavenumber k and the wave field radiated by the body is

$$f^m = 2\rho^{II}\omega J_k B^m(\alpha_{\text{inc}} + \pi). \tag{2.7.40}$$

Where $B^m(\alpha)$ is from the far-field form of ϕ^m, from (2.6.52) and (2.6.55), and is the amplitude of the radiated waves of wavenumber k. The formulas connecting this scattering problem to the heave and sway radiation problems are

$$d^0_1 = -\frac{J_k}{2} C^k_L \sum_{n=1}^{\infty} \frac{b^0_n K a (ka)^{n-1}}{n!} \tag{2.7.41}$$

$$d^1_1 = -\frac{iJ_k}{2} C^k_L \sum_{n=1}^{\infty} \frac{b^1_n K a (ka)^{n-1}}{(n-1)!}. \tag{2.7.42}$$

Equations (2.7.41) and (2.7.42) were used as numerical checks on the results obtained from the radiation and scattering problem.

Equations (2.6.33), (2.7.22), (2.7.23), (2.7.27), (2.7.28), (2.7.38), (2.7.39), (2.7.41) and (2.7.42) can be combined with (2.6.38) with $m = 0$ and 1 to give

$$\nu^m = \frac{3a}{8\pi\epsilon_m} \left(\frac{e^{2Kd}}{J_K} \overline{f^m_K}^2 + \frac{k^2}{K^2 J_k} \overline{f^m_k}^2 \right) \tag{2.7.43}$$

which relates the heave and sway damping coefficients to the vertical and horizontal exciting forces respectively. Equation (2.7.43) was used as an extra check on the radiation and scattering results shown in this chapter.

Results

Figures 2.10–2.13 show curves of $\overline{f^0}$ and $\overline{f^1}$ plotted against Ka for both scattering problems considered above. In each figure there are four curves corresponding to different immersion depths of the sphere in the lower region. These immersion depths, $f/a = -1.1$, -1.5, -2 and -3 are the same as those used in the lower fluid radiation problems as are the values $\rho = 0.95$ and $d/a = 2.0$.

Figures 2.10 and 2.11 show, respectively, the non-dimensionalised vertical and horizontal exciting forces on the sphere due to an incident wave of wavenumber K. The two sets of curves are very similar and show that, as one would expect, the forces increase the closer the sphere is to the interface (and hence to the free surface). This is simply because there is more motion occuring higher up in the fluid, especially on the free surface due to the incident wave.

Figures 2.12 and 2.13 show curves for the case of an incident wave of wavenumber k. Again, the figures for the vertical and horizontal forces look similar but the results obtained for $\overline{f_k^0}$ are greater that those for $\overline{f_k^1}$. The exciting forces increase as the surface of the sphere approaches the interface. These forces are an order of magnitude smaller than those for an incident wave of wavenumber K.

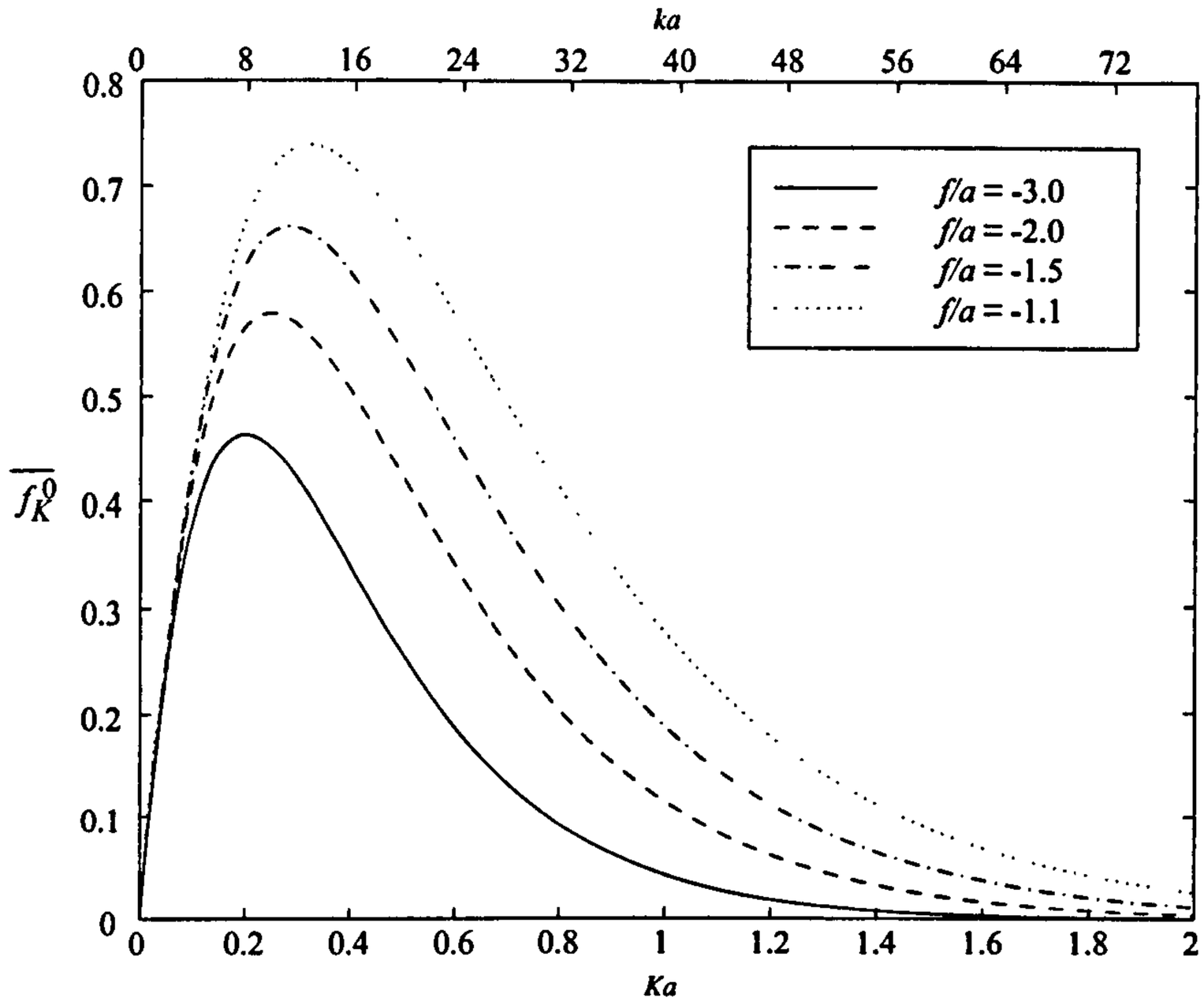

Figure 2.10: Non-dimensionalised vertical force $\overline{f_K^0}$ by incident wave of wavenumber K on sphere plotted against Ka for different submersion depths in the lower fluid layer; $\rho = 0.95$ and $d/a = 2.0$.

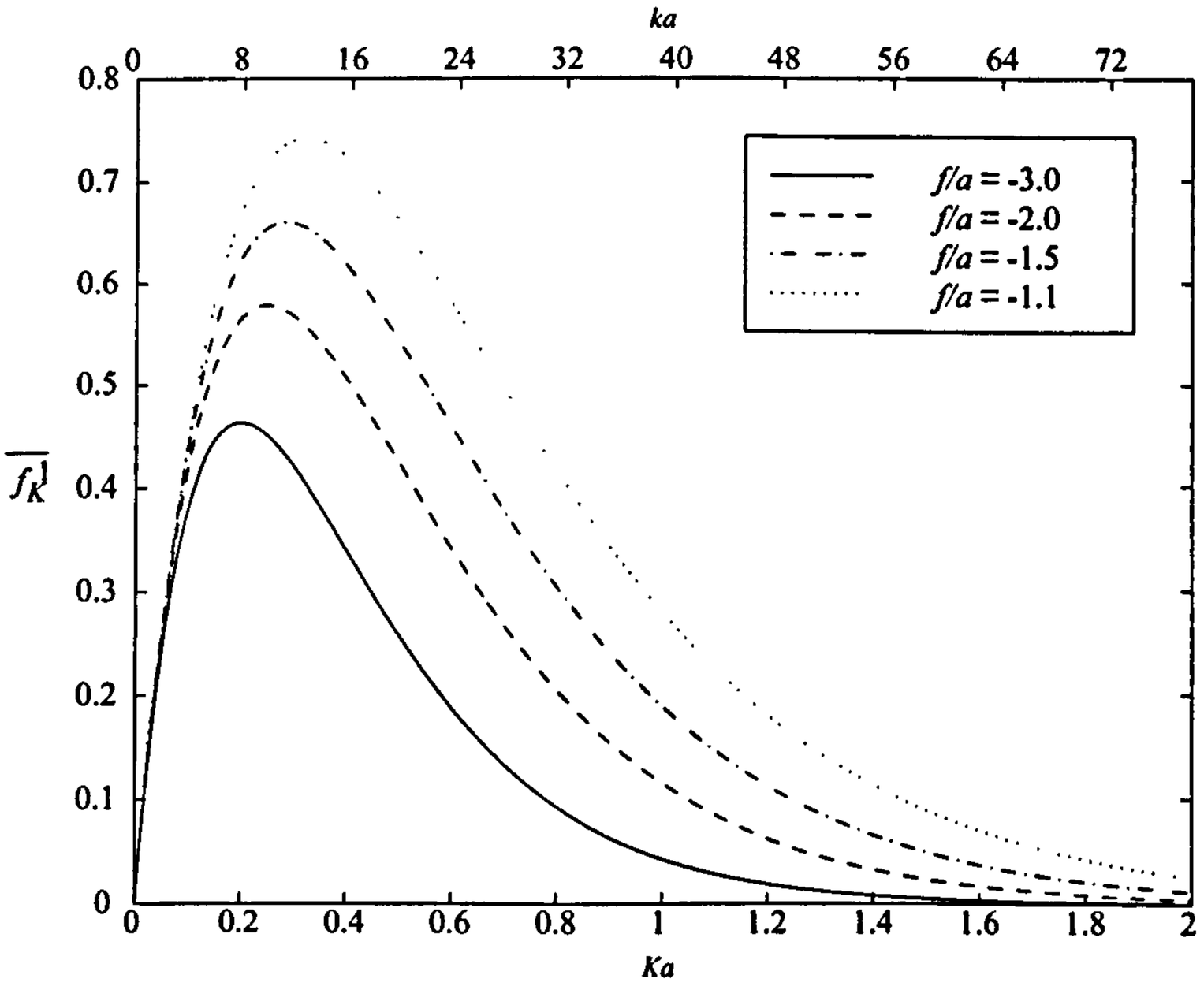

Figure 2.11: Non-dimensionalised horizontal force $\overline{f_K^1}$ by incident wave of wavenumber K on sphere plotted against Ka for different submersion depths in the lower fluid layer; $\rho = 0.95$ and $d/a = 2.0$.

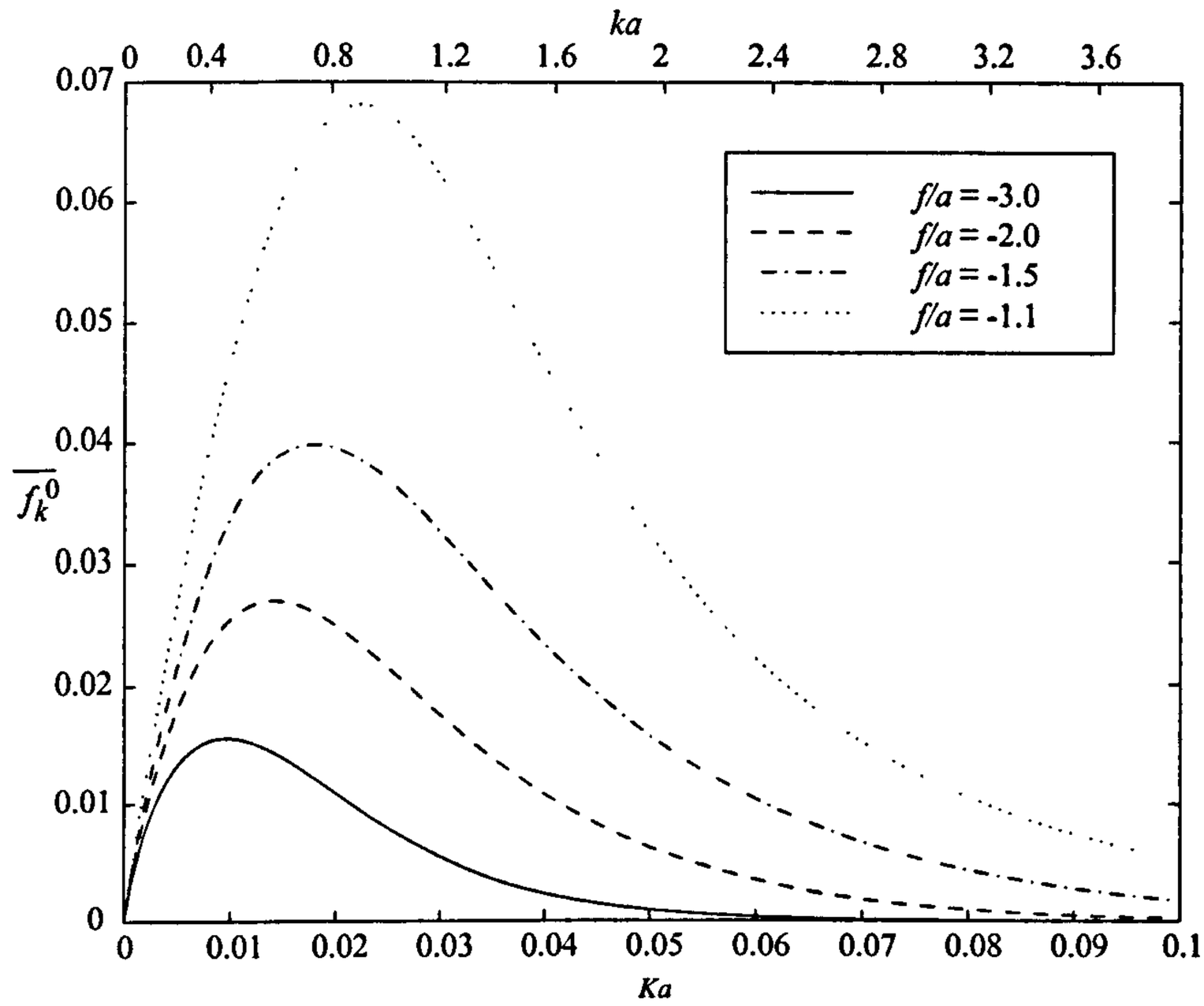

Figure 2.12: Non-dimensionalised vertical force $\overline{f_k^0}$ by incident wave of wavenumber k on sphere plotted against Ka for different submersion depths in the lower fluid layer; $\rho = 0.95$ and $d/a = 2.0$.

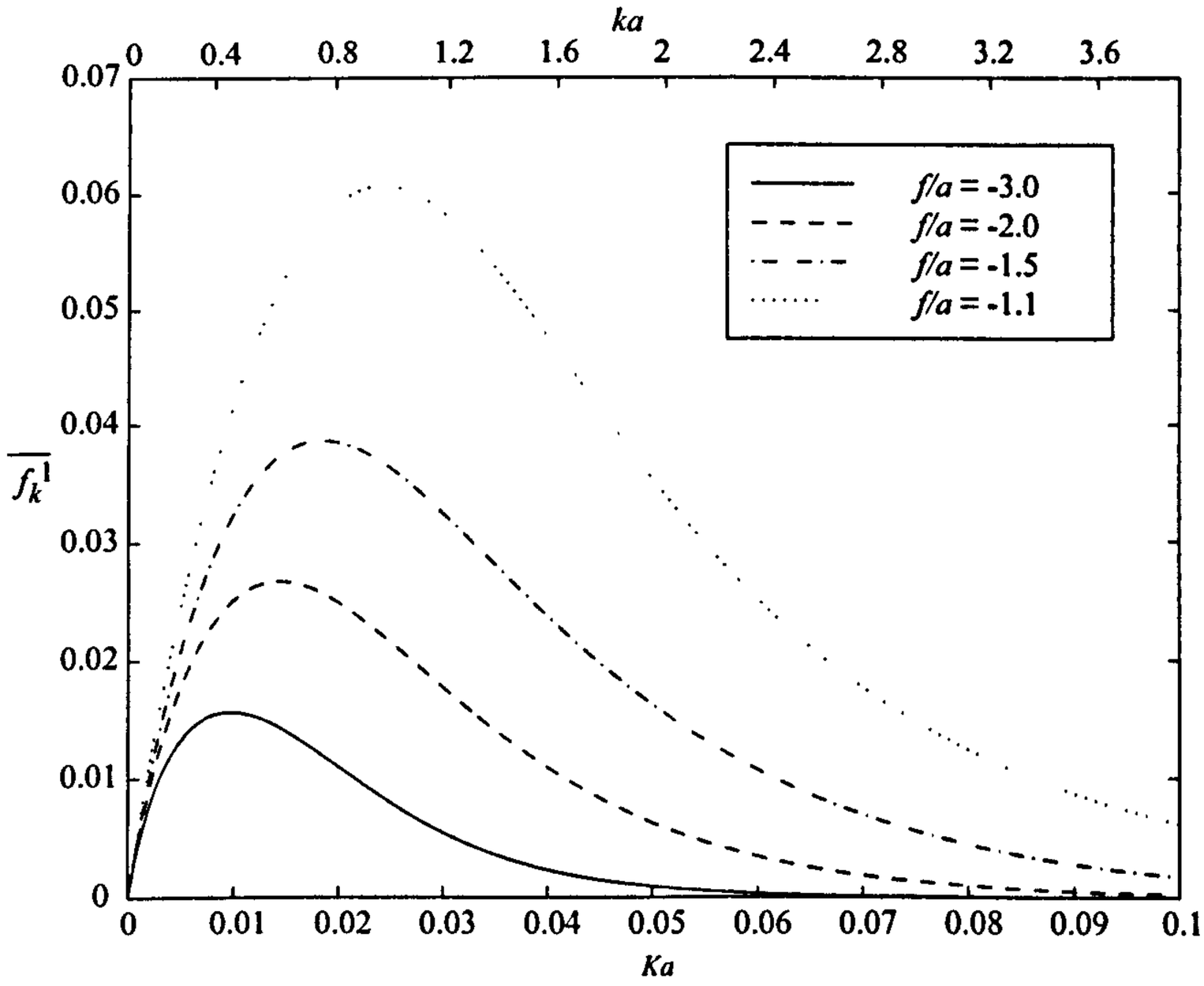

Figure 2.13: Non-dimensionalised horizontal force $\overline{f_k^1}$ by incident wave of wavenumber k on sphere plotted against Ka for different submersion depths in the lower fluid layer; $\rho = 0.95$ and $d/a = 2.0$.

2.7.2 Sphere in upper fluid layer

Incident wavenumber K

An incident plane wave of wavenumber K and amplitude A on the free surface ($z = d$) has the same form in the upper layer as in the lower layer, given by (2.7.9). The form for ϕ_S is the same as (2.7.10) but we now use the multipole expansions developed for the upper fluid layer, (2.6.50). As before we let $\alpha_{\text{inc}} = 0$ and then apply the body boundary condition (2.7.2) to get

$$\sum_{m=0}^{\infty}\sum_{n=m_1}^{\infty} c_n^m \cos m\alpha \left[(n+1)P_n^m(\cos\theta) - \sum_{s=m}^{\infty} sB_{ns}^m P_s^m(\cos\theta)\right]$$
$$= e^{K(f-d)} \sum_{m=0}^{\infty} \epsilon_m i^m \cos m\alpha \sum_{s=m}^{\infty} s\frac{(Ka)^s}{(s+m)!} P_s^m(\cos\theta). \quad (2.7.44)$$

Again using the orthogonality of the functions $\cos m\alpha, m = 0, 1, ...$ and of the Legendre functions we obtain the infinite systems of equations for the coefficients c_n^m, $m \geq 0$ which is

$$c_s^m - \left[\frac{s}{s+1}\right] \sum_{n=m_1}^{\infty} B_{ns}^m c_n^m = \epsilon_m \left[\frac{s}{s+1}\right] i^m e^{K(f-d)} \frac{(Ka)^s}{(s+m)!}, \quad (2.7.45)$$

for $s \geq m_1$. We note that this is the same as equation (2.7.16), for the sphere in the lower fluid, with A_{ns}^m replaced with B_{ns}^m. The vertical and horizontal exciting forces on the sphere in the upper fluid layer can be calculated from

$$f_K^0 = -\rho^I \omega i \int_0^{2\pi}\int_0^{\pi} \phi(a,\theta,\alpha) P_1^0(\cos\theta) a^2 \sin\theta d\theta d\alpha \quad (2.7.46)$$

and

$$f_K^1 = -\rho^I \omega i \int_0^{2\pi}\int_0^{\pi} \phi(a,\theta,\alpha) P_1^1(\cos\theta)\cos\alpha\, a^2 \sin\theta d\theta d\alpha. \quad (2.7.47)$$

Performing the integration and simplifying gives

$$f_K^0 = -4\pi a^2 \rho^I g A c_1^0, \quad (2.7.48)$$

$$f_K^1 = -4\pi a^2 \rho^I g A c_1^1, \quad (2.7.49)$$

and after non-dimensionalising this gives

$$\overline{f_K^0} = |f_K^0/(a^2\rho^I g A)| = 4\pi|c_1^0,| \quad (2.7.50)$$

$$\overline{f_K^1} = |f_K^1/(a^2\rho^I g A)| = 4\pi|c_1^1|. \quad (2.7.51)$$

The vertical and horizontal exciting forces on the sphere can be found from the wave field radiated by the sphere in heave and sway motion respectively from (2.4.6). Using this with the far-field form of the multipoles from (2.6.52) and (2.6.55) we obtain the following numerical checks

$$c_1^0 = -\frac{J_K}{2\rho} e^{-Kd} \sum_{n=1}^{\infty} \frac{b_n^0 (-Ka)^n}{n!} C_U^K, \tag{2.7.52}$$

$$c_1^1 = \frac{iJ_K}{2\rho} e^{-Kd} \sum_{n=1}^{\infty} \frac{b_n^1 (-Ka)^n}{(n-1)!} C_U^K, \tag{2.7.53}$$

which were used on the results calculated.

Incident wavenumber k

For the case of an incident wave of wavenumber k (and amplitude A on the interface $z = 0$) we note that in region I this takes the form

$$\phi_{\text{inc}}^I = -\frac{igAK}{\omega k} g(z) e^{ikR\cos\alpha} \tag{2.7.54}$$

$$= -\frac{igA}{\omega k} \left[\frac{K\sigma - k}{(\sigma - 1)} e^{kz} + \frac{K - k}{(\sigma - 1)} e^{-kz} \right] e^{ikR\cos\alpha}. \tag{2.7.55}$$

Expanding this into spherical polar coordinates gives

$$\phi_{\text{inc}} = -\frac{igA}{\omega k(\sigma - 1)} \sum_{m=0}^{\infty} \epsilon_m i^m \cos m\alpha$$

$$\times \sum_{s=m}^{\infty} \left[(K\sigma - k) e^{kf} + (-1)^{m+s} (K - k) e^{-kf} \right] \frac{(kr)^s}{(s+m)!} P_s^m(\cos\theta). \tag{2.7.56}$$

The expansion for ϕ_S with unknowns d_n^m, $m \geq 0$ is used and the body boundary condition, (2.7.2), on the sphere is applied. Using the orthogonality of the functions $\cos m\alpha, m = 0, 1, \ldots$ on $(0, 2\pi)$ and that of the Legendre functions we obtain the infinite system of equations for d_n^m which is

$$d_s^m - \frac{s}{s+1} \sum_{n=m_1}^{\infty} B_{ns}^m d_n^m$$

$$= \frac{\epsilon_m i^m s (ka)^s}{(s+1)(s+m)!} \frac{(K\sigma - k) e^{kf} + (-1)^{m+s} (K - k) e^{-kf}}{k(\sigma - 1)}, \qquad s \geq m_1. \tag{2.7.57}$$

The vertical and horizontal exciting forces can be calculated from (2.7.46) and (2.7.47) respectively, and after simplification one obtains

$$f_k^0 = -4\pi a^2 \rho^I g A d_1^0, \tag{2.7.58}$$

$$f_k^1 = -4\pi a^2 \rho^I g A d_1^1. \tag{2.7.59}$$

After non-dimensionalising these become

$$\overline{f_k^0} = |f_k^0/(a^2\rho^I g A)| = 4\pi|d_1^0|, \tag{2.7.60}$$

$$\overline{f_k^1} = |f_k^1/(a^2\rho^I g A)| = 4\pi|d_1^1|. \tag{2.7.61}$$

The vertical and horizontal exciting forces on the sphere can be found from the wave field radiated by the sphere in heave and sway motion respectively from (2.4.7). Using this with the far-field form of the multipoles from (2.6.52) and (2.6.55) we obtain numerical checks for d_1^0 and d_1^1 which are

$$d_1^0 = -\frac{KJ_k}{2\rho k}\sum_{n=1}^{\infty}\frac{b_n^0(-ka)^n}{n!}C_U^k, \tag{2.7.62}$$

$$d_1^1 = \frac{iKJ_k}{2\rho k}\sum_{n=1}^{\infty}\frac{b_n^1(-ka)^n}{(n-1)!}C_U^k, \tag{2.7.63}$$

which were employed on the results shown below.

Equations (2.6.60), (2.7.50)–(2.7.53), (2.7.60)–(2.7.63) can be combined with (2.6.64) with $m = 0$ and 1 to give

$$\nu^m = \frac{3a\rho}{8\epsilon_m\pi}\left(\frac{e^{2Kd}}{J_K}\overline{f_K^m}^2 + \frac{k^2}{K^2J_k}\overline{f_k^m}^2\right) \tag{2.7.64}$$

which is the upper fluid equivalent of (2.7.43). This can be used to solve the radiation problem of a sphere in the upper fluid layer using the results obtained from the corresponding scattering problem as well as a numerical check on both results. Equation (2.7.64) was used to check the results for the radiation and scattering problems shown in this chapter.

Results

Figures 2.14–2.17 show curves of $\overline{f^0}$ and $\overline{f^1}$ plotted against Ka for incident wavenumbers K and k when $\rho = 0.95$ and $d/a = 4.0$. For each figure there are four curves corresponding to the immersion depths $f/a = 1.1$, 1.7, 2.3 and 2.9. These immersion depths are the same as those used in the upper region radiation problem.

Figures 2.14 and 2.15 show, respectively, the non-dimensionalised vertical and horizontal exciting forces on the sphere due to an incident wave of wavenumber K. The values obtained for $\overline{f_K^0}$ are larger than those for $\overline{f_K^1}$ and the curves are very similar (apart from the Ka values) to those shown in figures 2.12 and 2.13 in which the incident wave is associated with the interface and the sphere is in the lower fluid. As one would expect the forces are greater the closer the sphere is to the free surface.

Figures 2.16 and 2.17 show curves for the case of an incident wave of wavenumber k. Again, the values obtained for the vertical forces are greater that those for the horizontal forces but this time the forces increase as the surface of the sphere approaches the interface.

2.8 Conclusion

In this chapter we have examined the relationships that exist between the solutions to three-dimensional radiation and scattering problems in two-layer fluids where the upper fluid is bounded above by a free surface and the lower (denser) fluid is infinite in extent. In such a situation propagating waves can exist at two different wavenumbers for any given frequency. A systematic derivation, using Green's theorem, of all the reciprocity relations for such problems has been carried out including extensions to the two-fluid case of the Haskind and Bessho-Newman relations. We have then used multipole expansions to solve radiation and scattering problems for a sphere situated entirely within either the upper of lower fluid layer.

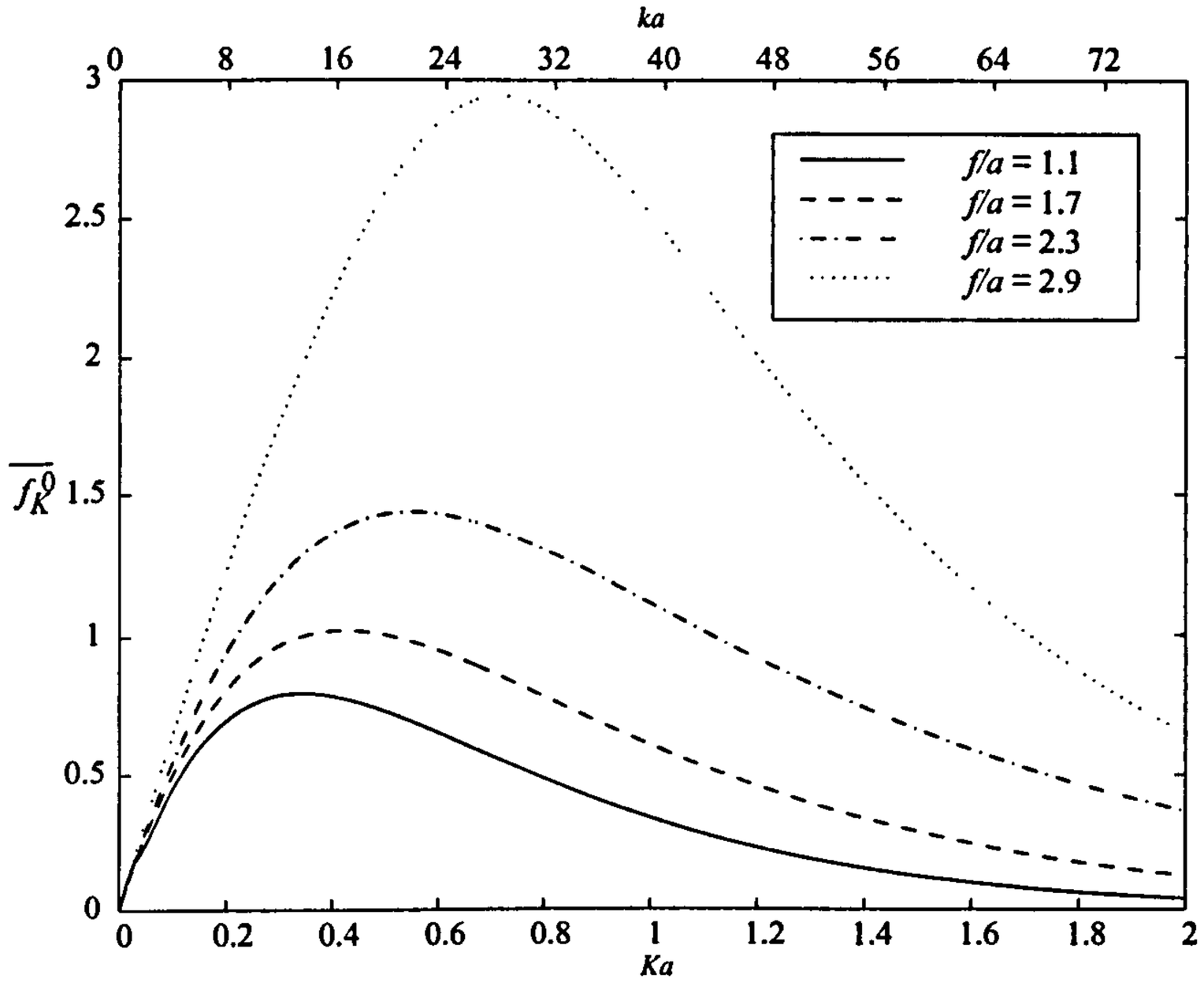

Figure 2.14: Non-dimensionalised vertical force $\overline{f_K^0}$ by incident wave of wavenumber K on sphere plotted against Ka for different submersion depths in the upper fluid layer; $\rho = 0.95$ and $d/a = 4.0$.

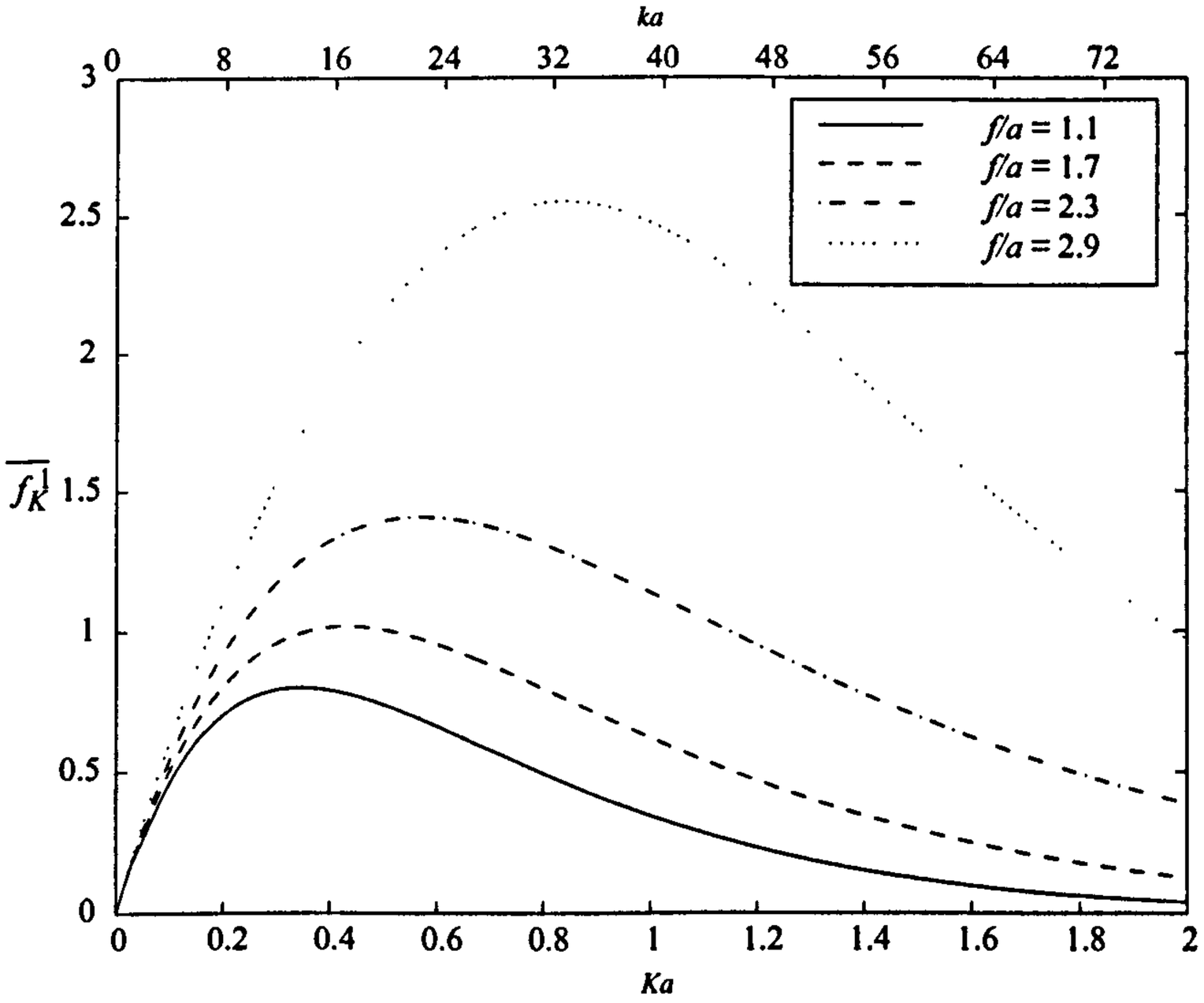

Figure 2.15: Non-dimensionalised horizontal force $\overline{f_K^1}$ by incident wave of wavenumber K on sphere plotted against Ka for different submersion depths in the upper fluid layer; $\rho = 0.95$ and $d/a = 4.0$.

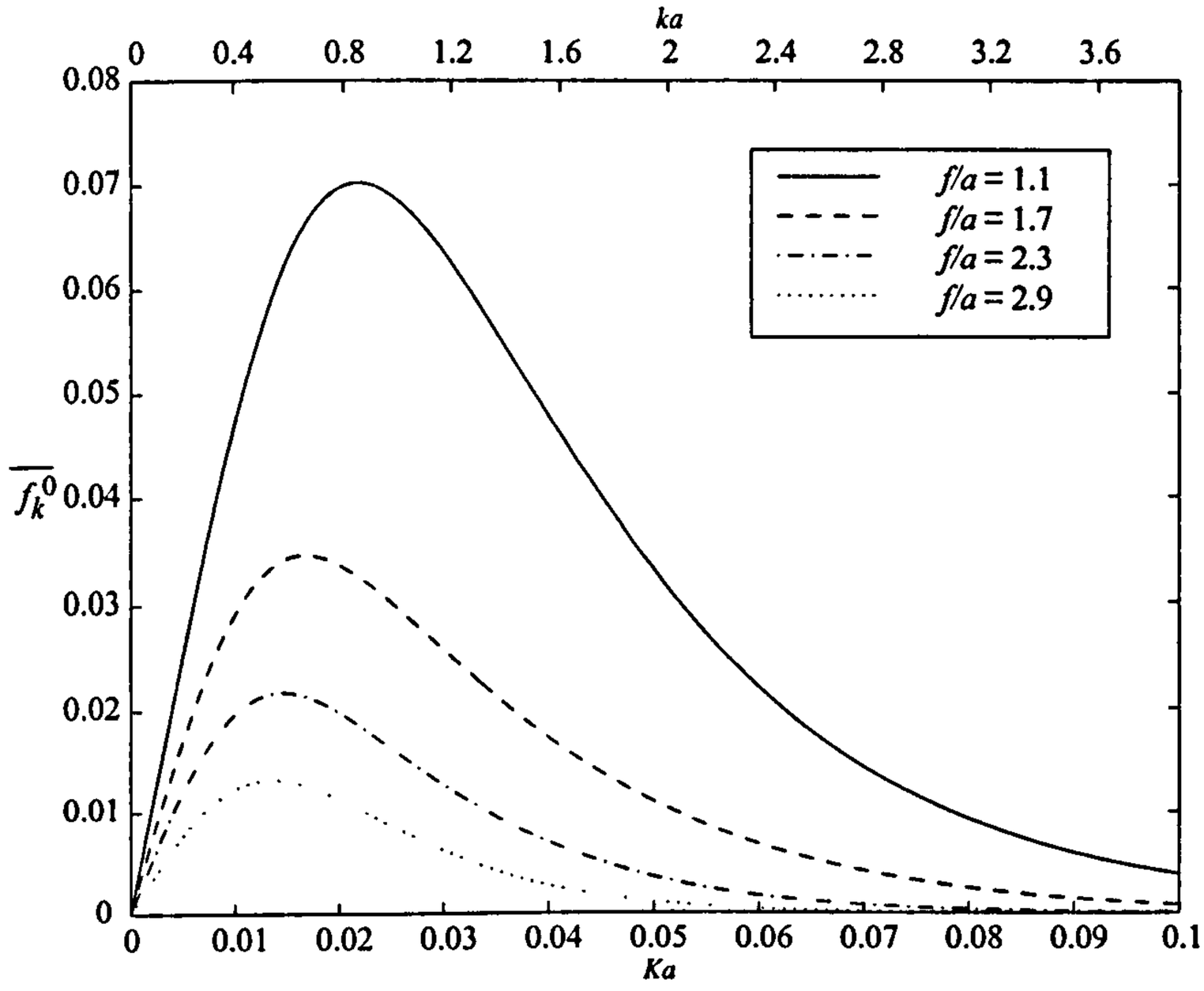

Figure 2.16: Non-dimensionalised vertical force $\overline{f_k^0}$ by incident wave of wavenumber k on sphere plotted against Ka for different submersion depths in the upper fluid layer; $\rho = 0.95$ and $d/a = 4.0$.

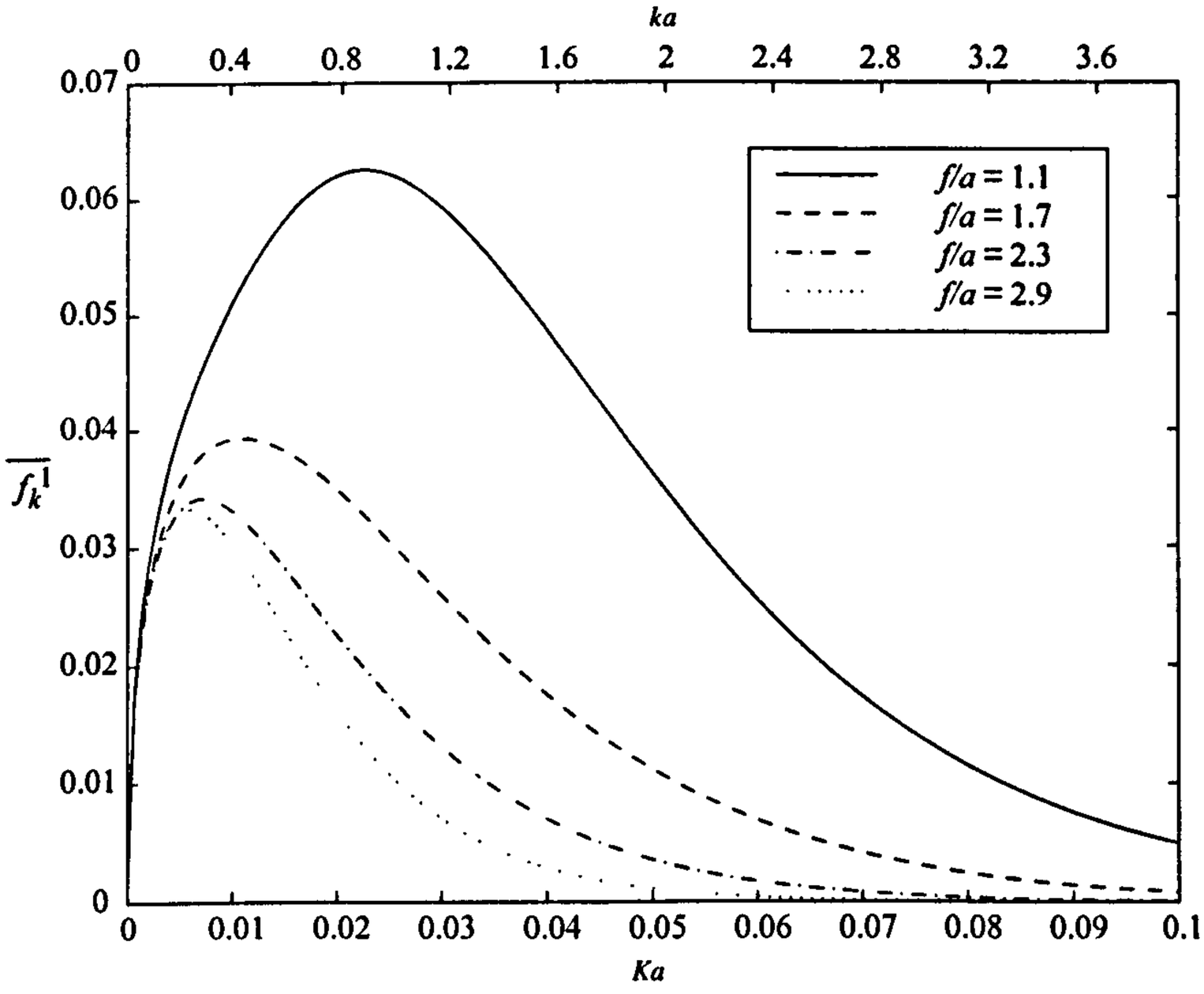

Figure 2.17: Non-dimensionalised horizontal force $\overline{f_k^1}$ by incident wave of wavenumber k on sphere plotted against Ka for different submersion depths in the upper fluid layer; $\rho = 0.95$ and $d/a = 4.0$.

Chapter 3

Finite depth of lower fluid

3.1 Introduction

We shall now consider the case when the lower fluid region has constant depth h, hence occupies the region $-h < z < 0$. As in chapter 2, we apply Green's theorem to the fluid domain to derive some hydrodynamic relations, in particular the classic result of symmetrical added-mass and damping matrices. Multipoles are then developed for a singularity in the lower and upper fluids and the heave and sway radiation problems are solved.

3.2 General theory

The velocity potentials must satisfy the conditions (2.2.2)–(2.2.5) in addition to having zero normal derivative on $z = -h$. The conditions in full are

$$\nabla^2\phi^I = \nabla^2\phi^{II} = 0 \qquad \text{everywhere in the fluid,} \tag{3.2.1}$$

$$\phi^I_z = \phi^{II}_z \qquad \text{on } z = 0, \tag{3.2.2}$$

$$\rho(\phi^I_z - K\phi^I) = \phi^{II}_z - K\phi^{II} \qquad \text{on } z = 0, \tag{3.2.3}$$

$$\phi^I_z = K\phi^I \qquad \text{on } z = d, \tag{3.2.4}$$

$$\phi^{II}_z = 0 \qquad \text{on } z = -h. \tag{3.2.5}$$

Solutions of Laplace's equation in polar coordinates, which are outgoing circular waves, are of the form

$$H^{(1)}_m(uR)\begin{Bmatrix}\cos m\alpha \\ \sin m\alpha\end{Bmatrix}\psi(z), \qquad m = 0, 1, 2, 3, \ldots \tag{3.2.6}$$

see Mei (1983) page 306. With hindsight we define the function $\psi(z)$ as

$$\psi^I = (u+K)e^{u(z-d)} + (u-K)e^{-u(z-d)}, \tag{3.2.7}$$

$$\psi^{II} = B\cosh u(z+h), \tag{3.2.8}$$

where B is some constant. Applying (3.2.3) we can find the constant B and hence ψ^{II}, which is

$$\psi^{II} = \frac{2\rho(K^2-u^2)\sinh ud}{u\sinh uh - K\cosh uh}\cosh u(z+h). \tag{3.2.9}$$

Using the remaining condition on $z=0$ we obtain the dispersion relation

$$\rho(u^2-K^2) = (u-K\coth ud)(u-K\coth uh). \tag{3.2.10}$$

By letting the depth of the lower region, h, tend to infinity this dispersion relation reduces to that of the infinite depth problem

$$(u-K)[K(\sigma+e^{-2ud}) - u(1-e^{-2ud})] = 0. \tag{3.2.11}$$

The dispersion relation for the finite depth case has two roots, both of which will require numerical methods to find. We will denote the two roots as k_1 and k_2, where $k_2 > k_1 > 0$. In the limit as $h \to \infty$ we find that $k_1 \to K$ and $k_2 \to k$, where k is the wavenumber described by (2.2.11), so we use K and k as estimates for the numerical evaluation k_1 and k_2 respectively. For the results presented below the Newton-Raphson method was used to calculate the wavenumbers k_1 and k_2.

With the asymptotic formula for $H_m^{(1)}$, the wave potential for an outgoing cylindrical wave of wavenumber u can be written

$$\phi \sim \sum_m H_m^{(1)}(uR)(\alpha'_m\cos m\alpha + \beta'_m\sin m\alpha)\psi(z) \tag{3.2.12}$$

$$\sim \left\{\sum_m(\alpha'_m\cos m\alpha + \beta'_m\sin m\alpha)e^{-im\pi/2}\right\}\left(\frac{2}{\pi uR}\right)^{1/2} e^{iuR-i\pi/4}\psi(z) \tag{3.2.13}$$

where α'_m and β'_m are some unknown coefficients. If we let the quantity inside { } be some function of α then two-layer outgoing cylindrical waves in finite depth have the form

$$\phi^I \sim \left[k_1^{-1/2}e^{ik_1R}g^I(z,k_1)A(\alpha) + k_2^{-1/2}e^{ik_2R}g^I(z,k_2)B(\alpha)\right]\left(\frac{2}{\pi R}\right)^{1/2} e^{-i\pi/4} \tag{3.2.14}$$

$$\phi^{II} \sim \left[k_1^{-1/2}e^{ik_1R}g^{II}(z,k_1)A(\alpha) + k_2^{-1/2}e^{ik_2R}g^{II}(z,k_2)B(\alpha)\right]\left(\frac{2}{\pi R}\right)^{1/2} e^{-i\pi/4} \tag{3.2.15}$$

as $KR \to \infty$, where $A(\alpha)$ and $B(\alpha)$ are the angular variations of the waves of wavenumbers k_1 and k_2 respectively and

$$g^I(z,u) = (u+K)e^{u(z-d)} + (u-K)e^{-u(z-d)}, \tag{3.2.16}$$

$$g^{II}(z,u) = [(u+K)e^{-ud} - (u-K)e^{ud}]\frac{\cosh u(z+h)}{\sinh uh}, \tag{3.2.17}$$

The functions $g^I(z,k_1)$, $g^I(z,k_2)$, $g^{II}(z,k_1)$ and $g^{II}(z,k_2)$ satisfy

$$g^I(z,k_1) \sim 2Ke^{K(z-d)}, \tag{3.2.18}$$

$$g^I(z,k_2) \sim e^{kd}[(k-K\sigma)e^{kz} + (k-K)e^{-kz}], \tag{3.2.19}$$

$$g^{II}(z,k_1) \sim 2Ke^{K(z-d)}, \tag{3.2.20}$$

$$g^{II}(z,k_2) \sim K(1-\sigma)e^{k(z+d)}, \tag{3.2.21}$$

as $h \to \infty$. We can relate these to the infinite depth case by

$$\frac{g^I(z,k_1)}{g^{II}(0,k_1)} \sim e^{Kz}, \tag{3.2.22}$$

$$\frac{g^I(z,k_2)}{g^{II}(0,k_2)} \sim g(z), \tag{3.2.23}$$

$$\frac{g^{II}(z,k_1)}{g^{II}(0,k_1)} \sim e^{Kz}, \tag{3.2.24}$$

$$\frac{g^{II}(z,k_2)}{g^{II}(0,k_2)} \sim e^{kz}, \tag{3.2.25}$$

as $h \to \infty$, where

$$g(z) = \frac{K\sigma - k}{K(\sigma-1)}e^{kz} + \frac{K-k}{K(\sigma-1)}e^{-kz}, \tag{3.2.26}$$

from (2.2.8). The function $g(z)$ is used in the infinite-depth case and is defined by (2.2.8).

3.3 Hydrodynamic relations

Applying Green's theorem to the problem of finite depth yields an equation very similar to that of infinite depth, see equation (2.2.20). The integral across the seabed vanishes so the only difference is the integral across S_∞^{II} where we now integrate from $z=-h$ to $z=0$. The equation we derive is

$$\rho\int_{B^I}\left(\phi^I\frac{\partial\psi^I}{\partial n} - \psi^I\frac{\partial\phi^I}{\partial n}\right)dS + \int_{B^{II}}\left(\phi^{II}\frac{\partial\psi^{II}}{\partial n} - \psi^{II}\frac{\partial\phi^{II}}{\partial n}\right)dS$$
$$= -\rho\int_{S_\infty^I}\left(\phi^I\frac{\partial\psi^I}{\partial R} - \psi^I\frac{\partial\phi^I}{\partial R}\right)dS - \int_{S_\infty^{II}}\left(\phi^{II}\frac{\partial\psi^{II}}{\partial R} - \psi^{II}\frac{\partial\phi^{II}}{\partial R}\right)dS. \tag{3.3.1}$$

3.4 Two radiation potentials

Let us consider two radiation potentials. Let $\phi = \phi_i$ and $\psi = \phi_j$, where ϕ_i, ϕ_j are two radiation potentials whose behaviour in the far field is described by (3.2.14) and (3.2.15). The first integral in the right-hand side of (3.3.1) after substituting in the forms for the potentials is

$$-\rho \lim_{R\to\infty} \int_{z=0}^{d}\int_{\alpha=0}^{2\pi} \left(\phi_i^I \frac{\partial \phi_j^I}{\partial R} - \phi_j^I \frac{\partial \phi_i^I}{\partial R}\right) R dz d\alpha = \frac{2ie^{-i\pi/2}\rho(k_1-k_2)}{\pi\sqrt{k_1 k_2}} e^{i(k_1+k_2)R} \times \int_{z=0}^{d} g^I(z,k_1) g^I(z,k_2) dz \int_{\alpha=0}^{2\pi} [A_i(\alpha)B_j(\alpha) - A_j(\alpha)B_i(\alpha)] d\alpha. \quad (3.4.1)$$

Now let us define I^I to be the integral with respect to z, such that

$$I^I = \int_0^d g^I(z,k_1) g^I(z,k_2) dz \quad (3.4.2)$$

$$= \int_0^d [(k_1+K)e^{k_1(z-d)} + (k_1-K)e^{-k_1(z-d)}] \times [(k_2+K)e^{k_2(z-d)} + (k_2-K)e^{-k_2(z-d)}] dz \quad (3.4.3)$$

$$= \frac{(k_1-K)(k_2-K)}{k_1+k_2} e^{(k_1+k_2)d} - \frac{(k_1+K)(k_2+K)}{k_1+k_2} e^{-(k_1+k_2)d} + \frac{(k_1-K)(k_2+K)}{k_1-k_2} e^{(k_1-k_2)d} - \frac{(k_1+K)(k_2-K)}{k_1-k_2} e^{-(k_1-k_2)d}. \quad (3.4.4)$$

The second integral in the right-hand side of (3.3.1) after substitution of the potentials gives

$$-\lim_{R\to\infty} \int_{z=-h}^{0}\int_{\alpha=0}^{2\pi} \left(\phi_i^{II} \frac{\partial \phi_j^{II}}{\partial R} - \phi_j^{II} \frac{\partial \phi_i^{II}}{\partial R}\right) R dz d\alpha = \frac{2ie^{-i\pi/2}(k_1-k_2)}{\pi\sqrt{k_1 k_2}} e^{i(k_1+k_2)R} \times \int_{z=-h}^{0} g^{II}(z,k_1) g^{II}(z,k_2) dz \int_{\alpha=0}^{2\pi} [A_i(\alpha)B_j(\alpha) - A_j(\alpha)B_i(\alpha)] d\alpha. \quad (3.4.5)$$

We define I^{II} to be the integral with respect to z and evaluating this gives

$$I^{II} = \int_{-h}^{0} g^{II}(z,k_1) g^{II}(z,k_2) dz \quad (3.4.6)$$

$$= \frac{4\rho^2(K^2-k_1^2)(K^2-k_2^2)\sinh k_1 d \sinh k_2 d}{(k_1 \sinh k_1 h - K\cosh k_1 h)(k_2 \sinh k_2 h - K\cosh k_2 h)} \times \int_{-h}^{0} \cosh k_1(z+h)\cosh k_2(z+h) dz \quad (3.4.7)$$

$$= \frac{4\rho^2(K^2-k_1^2)(K^2-k_2^2)\sinh k_1 d \sinh k_2 d}{(k_1 \sinh k_1 h - K\cosh k_1 h)(k_2 \sinh k_2 h - K\cosh k_2 h)} \times \left[\frac{\sinh(k_1+k_2)h}{k_1+k_2} + \frac{\sinh(k_1-k_2)h}{k_1-k_2}\right]. \quad (3.4.8)$$

We can rearrange the dispersion relation to give

$$\frac{\rho(K^2-u^2)\sinh ud}{u\sinh uh - K\cosh uh} = \frac{(u+K)e^{-ud} - (u-K)e^{ud}}{2\sinh uh}, \quad (3.4.9)$$

for $u = k_1, k_2$. Substituting this into I^{II} we obtain

$$\begin{aligned} I^{II} =& \frac{[(k_1+K)e^{-k_1 d} - (k_1-K)e^{k_1 d}][(k_2+K)e^{-k_2 d} - (k_2-K)e^{k_2 d}]}{2\sinh k_1 h \sinh k_2 h} \\ & \times \left[\frac{\sinh(k_1+k_2)h}{k_1+k_2} + \frac{\sinh(k_1-k_2)h}{k_1-k_2}\right] \qquad (3.4.10) \\ =& \frac{[(k_1+K)e^{-k_1 d} - (k_1-K)e^{k_1 d}][(k_2+K)e^{-k_2 d} - (k_2-K)e^{k_2 d}]}{k_1^2 - k_2^2} \\ & \times [k_1 \coth k_2 h - k_2 \coth k_1 h]. \qquad (3.4.11) \end{aligned}$$

By rearranging the dispersion relation in a different way we can write

$$\coth uh = \frac{u}{K} - \frac{\rho(K^2-u^2)[e^{ud} - e^{-ud}]}{K[(u+K)e^{-ud} - (u-K)e^{ud}]}, \qquad (3.4.12)$$

for $u = k_1, k_2$. Substituting this into I^{II} gives

$$\begin{aligned} I^{II} =& \frac{\rho}{K(k_1^2-k_2^2)}\Big[k_2(K^2-k_1^2)[(k_2+K)e^{-k_2 d} - (k_2-K)e^{k_2 d}](e^{k_1 d} - e^{-k_1 d}) \\ & - k_1(K^2-k_2^2)[(k_1+K)e^{-k_1 d} - (k_1-K)e^{k_1 d}](e^{k_2 d} - e^{-k_2 d})\Big] \qquad (3.4.13) \\ =& -\rho\Big[\frac{(k_1-K)(k_2-K)}{k_1+k_2}e^{(k_1+k_2)d} - \frac{(k_1+K)(k_2+K)}{k_1+k_2}e^{-(k_1+k_2)d} \\ & + \frac{(k_1-K)(k_2+K)}{k_1-k_2}e^{(k_1-k_2)d} - \frac{(k_1+K)(k_2-K)}{k_1-k_2}e^{-(k_1-k_2)d}\Big] \qquad (3.4.14) \\ =& -\rho I^I. \qquad (3.4.15) \end{aligned}$$

We can write this result as

$$\int_{-h}^{0} g^{II}(z,k_1)g^{II}(z,k_2)dz = -\rho\int_0^d g^I(z,k_1)g^I(z,k_2)dz. \qquad (3.4.16)$$

Using this we can evaluate the right-hand side of (3.3.1) to give

$$\frac{2ie^{-i\pi/2}(k_1-k_2)}{\pi\sqrt{k_1 k_2}}e^{i(k_1+k_2)R}(\rho I^I + I^{II})\int_{\alpha=0}^{2\pi}[A_i(\alpha)B_j(\alpha) - A_j(\alpha)B_i(\alpha)]d\alpha = 0. \qquad (3.4.17)$$

So equation (3.3.1) reduces to

$$\rho\int_{B^I}\left(\phi^I\frac{\partial\psi^I}{\partial n} - \psi^I\frac{\partial\phi^I}{\partial n}\right)dS + \int_{B^{II}}\left(\phi^{II}\frac{\partial\psi^{II}}{\partial n} - \psi^{II}\frac{\partial\phi^{II}}{\partial n}\right)dS = 0. \qquad (3.4.18)$$

Since $\frac{\partial\phi_i}{\partial n} = n_i$ on the body, where n_i is the inward normal to body in the ith direction, the above gives

$$\int_{S_B}\phi_i n_j dS = \int_{S_B}\phi_j n_i dS. \qquad (3.4.19)$$

This result is the same as (2.3.8) for infinite depth, and tells us that the added-mass and damping matrices are symmetric.

Suppose now we use $\psi = \overline{\phi_j}$. Thus, using the fact that the n_i are real, (3.3.1) becomes

$$\begin{aligned}
&\delta \int_{S_B} (\phi_i n_j - \overline{\phi_j} n_i) dS \\
&\qquad = \frac{4i}{\pi} \left(\rho \int_0^d \left[g^I(z,k_1) \right]^2 dz + \int_{-h}^0 \left[g^{II}(z,k_1) \right]^2 dz \right) \int_0^{2\pi} A_i(\alpha) \overline{A_j}(\alpha) d\alpha \\
&\qquad + \frac{k_1+k_2}{\sqrt{k_1 k_2}} \frac{2i}{\pi} \left(\rho \int_0^d g^I(z,k_1) g^I(z,k_2) dz + \int_{-h}^0 g^{II}(z,k_1) g^{II}(z,k_2) dz \right) \\
&\qquad\qquad \times \int_0^{2\pi} e^{i(k_1-k_2)R} A_i(\alpha) \overline{B_j}(\alpha) + e^{-i(k_1-k_2)R} B_i(\alpha) \overline{A_j}(\alpha) d\alpha \\
&\qquad + \frac{4i}{\pi} \left(\rho \int_0^d \left[g^I(z,k_2) \right]^2 dz + \int_{-h}^0 \left[g^{II}(z,k_2) \right]^2 dz \right) \int_0^{2\pi} B_i(\alpha) \overline{B_j}(\alpha) d\alpha, \quad (3.4.20)
\end{aligned}$$

where $\delta = \rho$ when the bodies are in region I or $\delta = 1$ when bodies are in region II. The second term in the right-hand side vanishes due to (3.4.16). Using the symmetry equation (3.4.19) we are left with

$$\delta \int_{S_B} (\phi_i n_j - \overline{\phi_j} n_i) dS = 2i\delta \Im \int_{S_B} \phi_i n_j dS \quad (3.4.21)$$

$$= \frac{2i}{\pi} \left(J_{k_1} \int_0^{2\pi} A_i(\alpha) \overline{A_j}(\alpha) d\alpha + J_{k_2} \int_0^{2\pi} B_i(\alpha) \overline{B_j}(\alpha) d\alpha \right) \quad (3.4.22)$$

where

$$J_u = 2\rho \int_0^d \left[g^I(z,u) \right]^2 dz + 2 \int_{-h}^0 \left[g^{II}(z,u) \right]^2 dz. \quad (3.4.23)$$

Thus the damping coefficient B_{ij} can be found in terms of the far-field behaviour

$$B_{ij} = -\Re i \rho^{II} \delta\omega \int_{S_B} \phi_i n_j dS \quad (3.4.24)$$

$$= \frac{\rho^{II}\omega}{\pi} \left[J_{k_1} \int_0^{2\pi} A_i(\alpha) \overline{A_j}(\alpha) d\alpha + J_{k_2} \int_0^{2\pi} B_i(\alpha) \overline{B_j}(\alpha) d\alpha \right]. \quad (3.4.25)$$

This result is very similar to (2.3.15) where J_K and J_k have been replaced with J_{k_1} and J_{k_2} respectively.

It is simple to show that all the reciprocity relations in chapter 2 can be used for finite depth by replacing J_K and J_k by J_{k_1} and J_{k_2} respectively.

3.5 Heave and sway radiation problems

We will now solve the heave and sway radiation problems for a sphere submerged in the upper and lower fluid layers where the lower layer has finite depth. The sphere has

radius a and its centre is positioned at $x = y = 0$, $z = f$. We will use the spherical polar coordinates (r, θ, α) centred on the sphere defined by (2.6.1) with $r = a$ being the sphere surface.

3.5.1 Sphere in lower fluid layer

Multipole expansions

We shall now construct multipoles for the case of a sphere in finite depth. As before these multipoles will satisfy the boundary conditions, except on the sphere, and behave as outgoing waves far from the singular point at the centre of the sphere. To find the form of such multipoles we use the solution to Laplace's equation in polar coordinates and its integral representations given in equations (2.6.2) and (2.6.39). Hence the multipoles will take the form of

$$\phi_n^{Im} = \frac{a^{n+2}\cos m\alpha}{(n-m)!}\int_0^\infty u^n \left[A_L(u)e^{uz} + B_L(u)e^{-uz}\right] J_m(uR)du, \tag{3.5.1}$$

$$\phi_n^{IIm} = a^{n+2}\cos m\alpha \left[\frac{P_n^m(\cos\theta)}{r^{n+1}} + \frac{1}{(n-m)!}\int_0^\infty u^n \left[C_L(u)e^{uz} + D_L(u)e^{-uz}\right] J_m(uR)du\right]. \tag{3.5.2}$$

We note that the difference between the form of these multipoles and those for the infinite-depth case, equations (2.6.3)–(2.6.4), is the function $D_L(u)$. This is due to the extra boundary condition on $z = -h$ which must be satisfied. To find the functions $A_L(u)$, $B_L(u)$, $C_L(u)$ and $D_L(u)$ we must apply the following boundary conditions to the multipole functions

$$\phi_z^{Im} = \phi_z^{IIm} \qquad \text{on } z = 0, \tag{3.5.3}$$

$$\rho(\phi_z^{Im} - K\phi^{Im}) = \phi_z^{IIm} - K\phi^{IIm} \qquad \text{on } z = 0, \tag{3.5.4}$$

$$\phi_z^{Im} = K\phi^{Im} \qquad \text{on } z = d, \tag{3.5.5}$$

$$\phi_z^{IIm} = 0 \qquad \text{on } z = -h. \tag{3.5.6}$$

After applying these conditions we obtain expressions involving $A_L(u)$, $B_L(u)$, $C_L(u)$ and $D_L(u)$ which are

$$\begin{aligned}
A_L(u) \quad & -B_L(u) \quad -C_L(u) \quad +D_L(u) = -e^{uf}, \\
\rho\frac{u-K}{u+K}A_L(u) \quad & -\rho B_L(u) - \frac{u-K}{u+K}C_L(u) \quad +D_L(u) = -e^{uf}, \\
A_L(u) - \frac{u+K}{u-K}e^{-2ud}B_L(u) \quad & =0, \\
C_L(u) - e^{2uh}D_L(u) &= -(-1)^{m+n}e^{-uf}.
\end{aligned} \tag{3.5.7}$$

The solutions to these equations are

$$A_L(u) = K(u+K)e^{-2ud}\left[(\coth uh+1)e^{uf} + (-1)^{m+n}(\coth uh-1)e^{-uf}\right]/H(u), \tag{3.5.8}$$

$$B_L(u) = K(u-K)\left[(\coth uh+1)e^{uf} + (-1)^{m+n}(\coth uh-1)e^{-uf}\right]/H(u), \tag{3.5.9}$$

$$\begin{aligned}
C_L(u) = e^{2uh}\Big[& K\left[u-K-(u+K)e^{-2ud}\right] \\
& \times \left[(\coth uh+1)e^{uf} + (-1)^{m+n}(\coth uh-1)e^{-uf}\right] \\
& - \left[e^{uf} + (-1)^{m+n}e^{-u(2h+f)}\right]H(u)\Big]/(1-e^{2uh})H(u),
\end{aligned} \tag{3.5.10}$$

$$\begin{aligned}
D_L(u) = \Big[& K\left[u-K-(u+K)e^{-2ud}\right] \\
& \times \left[(\coth uh+1)e^{uf} + (-1)^{m+n}(\coth uh-1)e^{-uf}\right] \\
& - \left[e^{uf} + (-1)^{m+n}e^{-uf}\right]H(u)\Big]/(1-e^{2uh})H(u),
\end{aligned} \tag{3.5.11}$$

where

$$H(u) = \left[(u+K)e^{-2ud} - u + K\right](u - K\coth uh) - \rho(K^2-u^2)(1-e^{-2ud}), \tag{3.5.12}$$

such that $H(k_1) = H(k_2) = 0$, from the dispersion relation. We now notice that these functions have poles so the multipoles must be written as

$$\phi_n^{Im} = \frac{a^{n+2}\cos m\alpha}{(n-m)!}\oint_0^\infty u^n\left[A_L(u)e^{uz} + B_L(u)e^{-uz}\right]J_m(uR)du, \tag{3.5.13}$$

$$\phi_n^{IIm} = a^{n+2}\cos m\alpha\left[\frac{P_n^m(\cos\theta)}{r^{n+1}} + \frac{1}{(n-m)!}\oint_0^\infty u^n\left[C_L(u)e^{uz} + D_L(u)e^{-uz}\right]J_m(uR)du\right], \tag{3.5.14}$$

where the path of integration is indented to pass beneath the poles of the integrand at $u = k_1$ and $u = k_2$. We indent beneath the poles so that the multipoles behave as outgoing waves far from the sphere.

The far-field form of ϕ_n^m, in the upper fluid, is

$$\phi_n^{Im} \sim -\frac{(-i)^{m+1}a^{n+2}\cos m\alpha}{(n-m)!}\left(\frac{2\pi}{R}\right)^{1/2} \times \left[k_1^{n-1/2}e^{ik_1R}\left(e^{k_1z}A_L^{k_1}+e^{-k_1z}B_L^{k_1}\right)+k_2^{n-1/2}e^{ik_2R}\left(e^{k_2z}A_L^{k_2}+e^{-k_2z}B_L^{k_2}\right)\right]e^{-i\pi/4} \tag{3.5.15}$$

as $KR \to \infty$, where $A_L^{k_1}$ ($B_L^{k_1}$) and $A_L^{k_2}$ ($B_L^{k_2}$) are the residues of $A_L(u)$ ($B_L(u)$) at $u = k_1$ and $u = k_2$ respectively. The forms of $A_L^{k_1}$ and $B_L^{k_1}$ are given by

$$A_L^{k_1} = K(k_1+K)e^{-2k_1d}\left[(\coth k_1h+1)e^{k_1f}+(-1)^{m+n}(\coth k_1h-1)e^{-k_1f}\right] /(1-e^{-2k_1d})\Big[(K\coth k_1h-k_1)(Kd\,\mathrm{cosech}^2k_1d+1) + (K\coth k_1d-k_1)(Kh\,\mathrm{cosech}^2k_1h+1)+2\rho k_1\Big] \tag{3.5.16}$$

and

$$B_L^{k_1} = K(k_1-K)\left[(\coth k_1h+1)e^{k_1f}+(-1)^{m+n}(\coth k_1h-1)e^{-k_1f}\right] /(1-e^{-2k_1d})\Big[(K\coth k_1h-k_1)(Kd\,\mathrm{cosech}^2k_1d+1) + (K\coth k_1d-k_1)(Kh\,\mathrm{cosech}^2k_1h+1)+2\rho k_1\Big]. \tag{3.5.17}$$

To obtain $A_L^{k_2}$ and $B_L^{k_2}$ we replace k_1 by k_2 in (3.5.16) and (3.5.17) respectively.

We can expand the multipoles around $r = 0$ in spherical polar coordinates by using (2.6.20) to give

$$\phi_n^{IIm} = a\cos m\alpha\left[\left(\frac{a}{r}\right)^{n+1}P_n^m(\cos\theta)+\sum_{s=m}^{\infty}\left(\frac{r}{a}\right)^s A_{ns}^m P_s^m(\cos\theta)\right], \tag{3.5.18}$$

where

$$A_{ns}^m = \frac{a}{(n-m)!(s+m)!}\oint_0^{\infty}(au)^{n+s}\left[e^{uf}C_L(u)+(-1)^{m+s}e^{-uf}D_L(u)\right]du. \tag{3.5.19}$$

Formulation of problem

We can now follow exactly the same method as for infinite depth to obtain expressions for the heave and sway damping and added-mass coefficients. The only difference is that the matrix A_{ns}^m is more complicated. First we expand the velocity potential in multipole potentials

$$\phi^m = U\sum_{n=1}^{\infty}b_n^m\phi_n^m \qquad m = 0,1. \tag{3.5.20}$$

After application of the body boundary condition and using the orthogonality of the Legendre Functions we obtain the familiar infinite system of linear equations for an infinite number of unknowns. Hence

$$b_s^m - \left[\frac{s}{s+1}\right] \sum_{n=1}^{\infty} A_{ns}^m b_n^m = -\delta_{1s}/2 \qquad s = 1, 2, \ldots \qquad m = 0, 1. \tag{3.5.21}$$

This system was solved numerically by truncating it to an $N \times N$ system and increasing N until the required degree of accuracy was attained. For the results presented in this chapter a value of $N = 4$ was used which gave results correct to 2 decimal places. Since (3.5.18) and (3.5.21) are the same as (2.6.21) and (2.6.30) respectively, but with different forms for A_{ns}^m, the non-dimensionalised added-mass and damping coefficients μ^m and ν^m respectively are given by (2.6.33). For convenience this result is

$$\mu^m + i\nu^m = -(1 + 3b_1^m) \qquad m = 0, 1. \tag{3.5.22}$$

The relation between the damping coefficient B_{ii} and the energy radiated to infinity, see equation (3.4.25), is given by

$$B_{ii} = \frac{4}{3}\pi\rho^{II}a^3\omega\nu^m = \frac{\rho^{II}\omega}{\pi}\left[J_{k_1}\int_0^{2\pi}|A^m(\alpha)|^2 d\alpha + J_{k_2}\int_0^{2\pi}|B^m(\alpha)|^2 d\alpha\right] \tag{3.5.23}$$

where $A^m(\alpha)$ and $B^m(\alpha)$ are the far-field coefficients of the waves of wavenumbers K and k respectively. The far-field form of ϕ^m, in the upper fluid region, can be written

$$\begin{aligned} U^{-1}\phi^{Im} \sim \left(\frac{2}{\pi R}\right)^{1/2} \Big\{ & k_1^{-1/2} e^{ik_1 R}\left[(k_1+K)e^{-k_1 d}e^{k_1 z} + (k_1-K)e^{k_1 d}e^{-k_1 z}\right] A^m(\alpha) \\ & + k_2^{-1/2} e^{ik_2 R}\left[(k_2+K)e^{-k_2 d}e^{k_2 z} + (k_2-K)e^{k_2 d}e^{-k_2 z}\right] B^m(\alpha)\Big\} e^{-i\pi/4}, \end{aligned} \tag{3.5.24}$$

as $KR \to \infty$. This form is used opposed to the lower region form as the functions $A^m(\alpha)$ and $B^m(\alpha)$ are simpler. The coefficients $A^m(\alpha)$ and $B^m(\alpha)$ can be extracted from (3.5.20) and (3.5.15). We obtain

$$|A^m(\alpha)|^2 = \left|\sum_{n=1}^{\infty} \frac{(k_1 a)^n b_n^m}{(n-m)!} A_L^{k_1}\right|^2 \left(\frac{a^2\pi\cos m\alpha\, e^{k_1 d}}{k_1 + K}\right)^2, \tag{3.5.25}$$

$$= \left|\sum_{n=1}^{\infty} \frac{(k_1 a)^n b_n^m}{(n-m)!} B_L^{k_1}\right|^2 \left(\frac{a^2\pi\cos m\alpha\, e^{-k_1 d}}{k_1 - K}\right)^2, \tag{3.5.26}$$

$$|B^m(\alpha)|^2 = \left|\sum_{n=1}^{\infty} \frac{(k_2 a)^n b_n^m}{(n-m)!} A_L^{k_2}\right|^2 \left(\frac{a^2\pi\cos m\alpha\, e^{k_2 d}}{k_2 + K}\right)^2, \tag{3.5.27}$$

$$= \left|\sum_{n=1}^{\infty} \frac{(k_2 a)^n b_n^m}{(n-m)!} B_L^{k_2}\right|^2 \left(\frac{a^2\pi\cos m\alpha\, e^{-k_2 d}}{k_2 - K}\right)^2. \tag{3.5.28}$$

Numerical results computed from (3.5.21) were checked using the following identity

$$\Im(b_1^m) = -\frac{\pi a}{2\epsilon_m}\left(\frac{J_{k_1}e^{2k_1d}}{(k_1+K)^2}\left|\sum_{n=1}^{\infty}\frac{(k_1a)^n b_n^m}{(n-m)!}A_L^{k_1}\right|^2 + \frac{J_{k_2}e^{2k_2d}}{(k_2+K)^2}\left|\sum_{n=1}^{\infty}\frac{(k_2a)^n b_n^m}{(n-m)!}A_L^{k_2}\right|^2\right) \quad (3.5.29)$$

which follows from (3.5.23) using (3.5.22) and (3.5.25)–(3.5.28). We can write this identity in three other ways using the alternative expressions of $|A^m(\alpha)|^2$ and $|B^m(\alpha)|^2$ from (3.5.25)–(3.5.28). There is no difference between these forms which are all algebraically the same.

Results

Curves of added-mass and damping coefficients for spheres in the lower fluid layer in both heave and sway are shown in figures 3.1–3.4. In all the curves $\rho = 0.95$, $d/a = 2$ and $f/a = -1.1$. Each plot shows the results obtained for four different depths, h/a, of the lower fluid, 2.2, 2.4, 3 and 4. The case of $h/a = 2.2$ represents a sphere with equal distance, $0.1a$, from the interface and the bottom, with h/a increasing as the bottom becomes further away from the sphere. As $h/a \to \infty$ the problem tends to infinite depth and so previous results will be recovered.

Figures 3.1 and 3.2 show the damping coefficients for heave and sway respectively. The two cases lead to similar results, but those for heave are greater than those for sway. As in the infinite depth case, there are two local maximums, one near $k_1a(\approx Ka) = 1$ which corresponds to waves being generated on the free surface and one near $k_2a(\approx ka) = 1$ which corresponds to waves on the interface. As one would expect we again see that the sphere's wave-making capabilities on the interface are much greater than those on the free surface. The effect of finite depth on the heave and sway damping coefficient for the chosen parameter values is relatively small. As the depth of the lower layer decreases we see that heave damping decreases whereas sway damping increases. The same effect was found to occur in the case of a sphere in a single-layer fluid of finite depth by Linton (1991).

Figures 3.3 and 3.4 show the added-mass coefficients for heave and sway respectively. We note that, as with the infinite-depth radiation problem, the deviation from 1/2 is greater in the case of heave. We can again see that there is an effect due to the interface near $k_2a = 1$ ($Ka \approx 0.025$) and a much smaller effect due to the free surface near $k_1a = 1$

($Ka \approx 1$). It can be seen that the closer the sphere is to the bottom the greater its added mass. This effect was also observed in Linton (1991) for the single-fluid case. In figures 3.1–3.4 we can see that the results for $h/a = 4$ are very close to the infinite-depth results shown in figures 2.2–2.5 for $f/a = -1.1$.

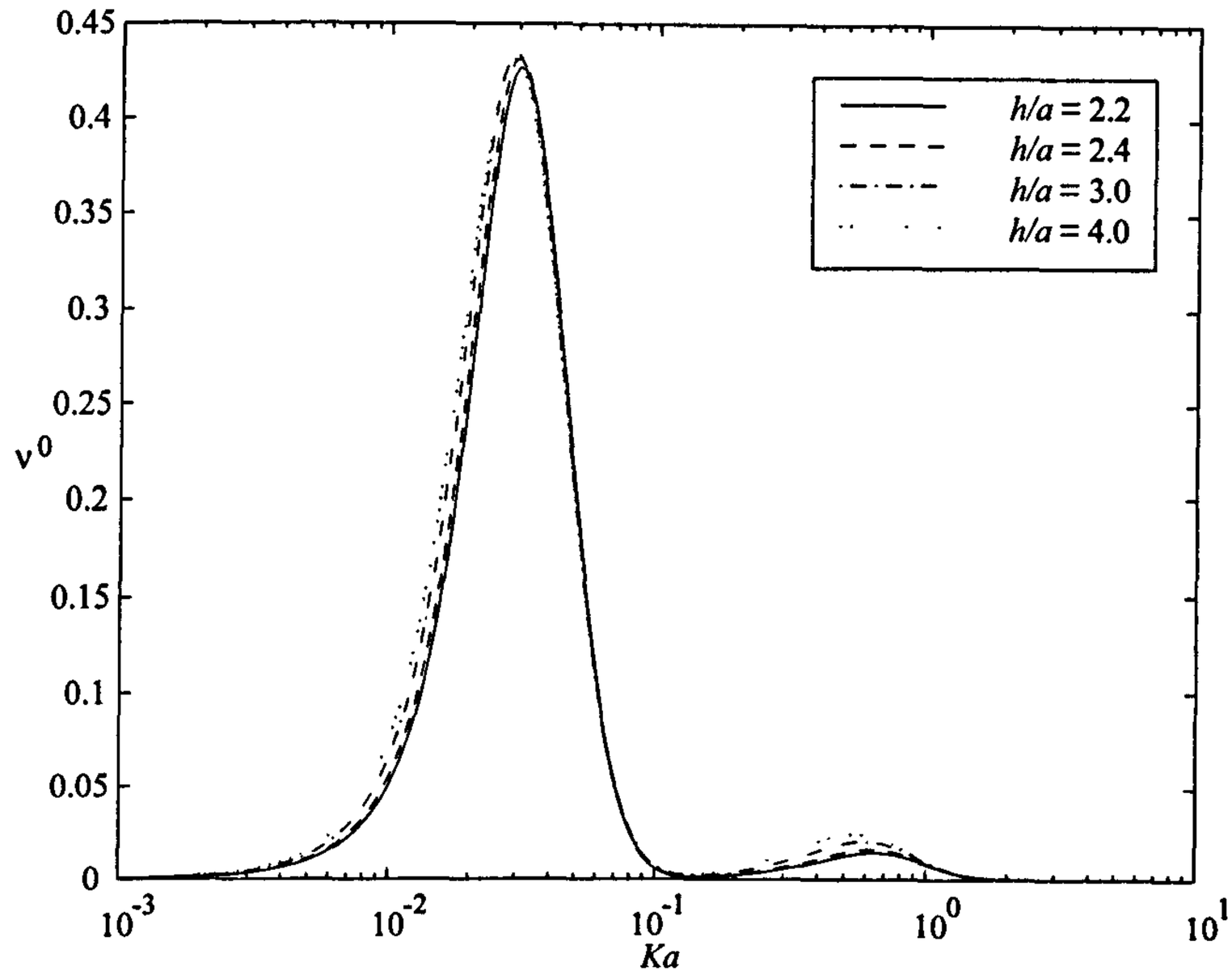

Figure 3.1: Damping coefficient ν^0 (heave) plotted against Ka for a submerged sphere in the lower fluid layer with varying depth of the lower fluid layer; $\rho = 0.95$, $d/a = 2.0$ and $f/a = -1.1$.

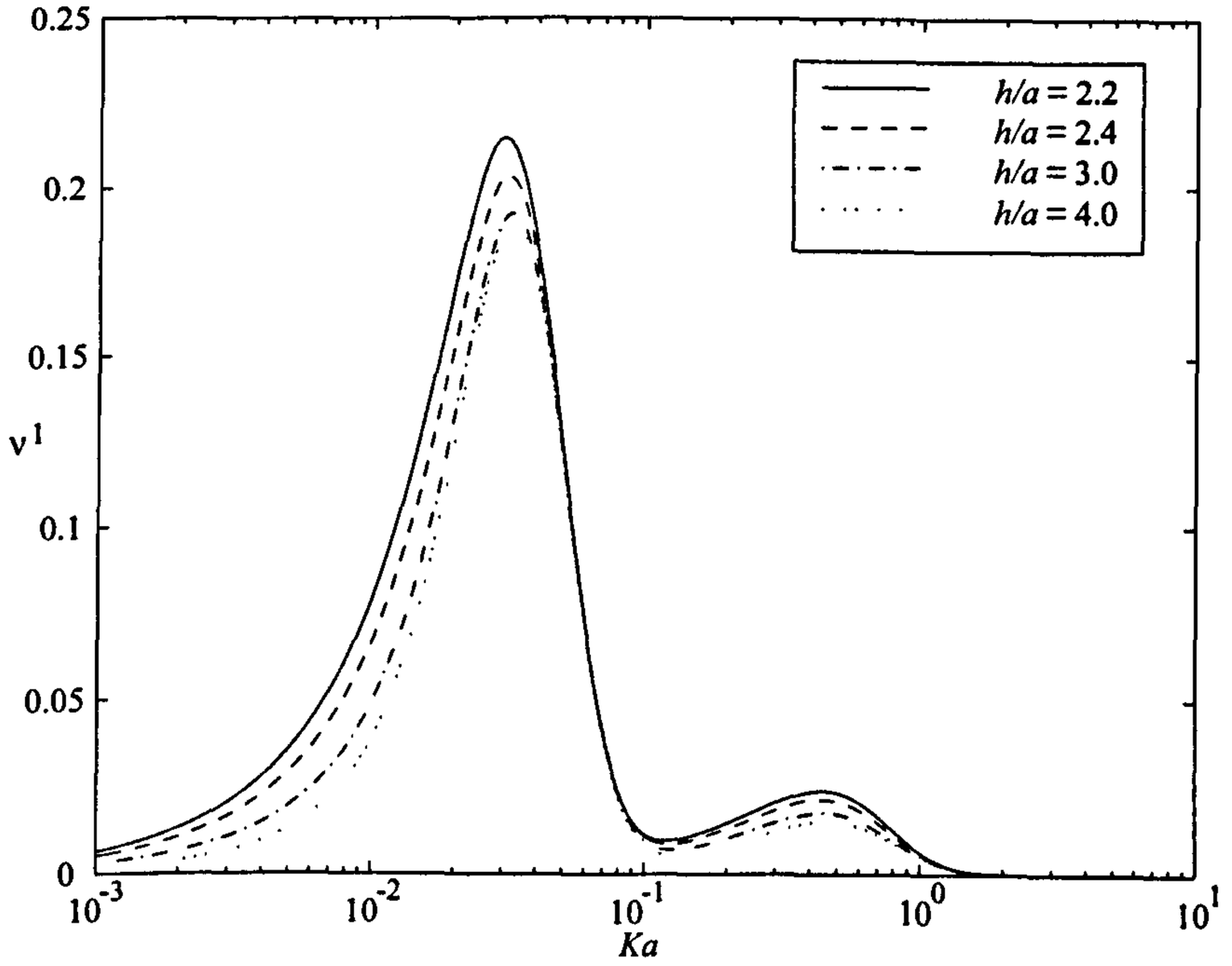

Figure 3.2: Damping coefficient ν^1 (sway) plotted against Ka for a submerged sphere in the lower fluid layer with varying depth of the lower fluid layer; $\rho = 0.95$, $d/a = 2.0$ and $f/a = -1.1$.

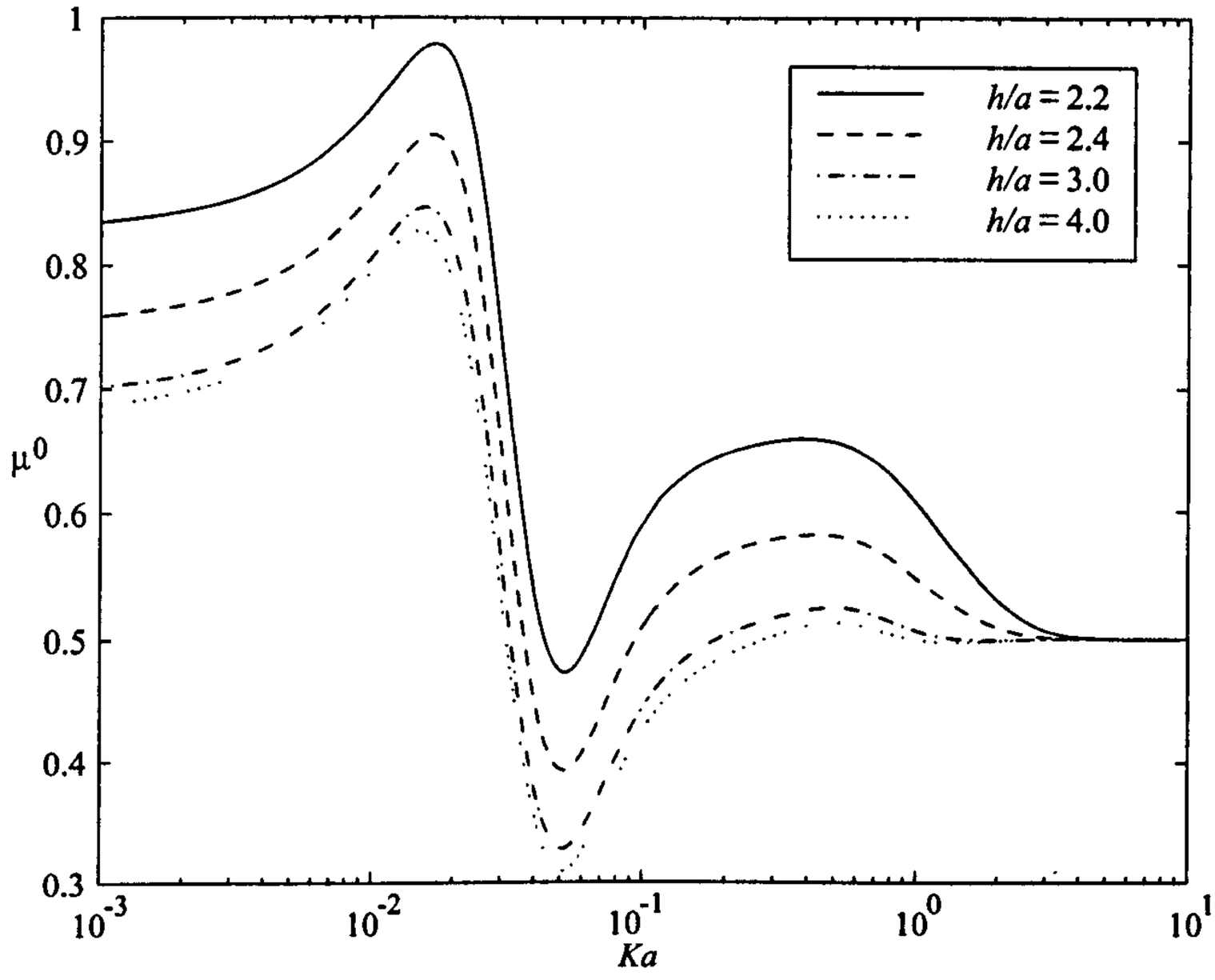

Figure 3.3: Added mass coefficient μ^0 (heave) plotted against Ka for a submerged sphere in the lower fluid layer with varying depth of the lower fluid layer; $\rho = 0.95$, $d/a = 2.0$ and $f/a = -1.1$.

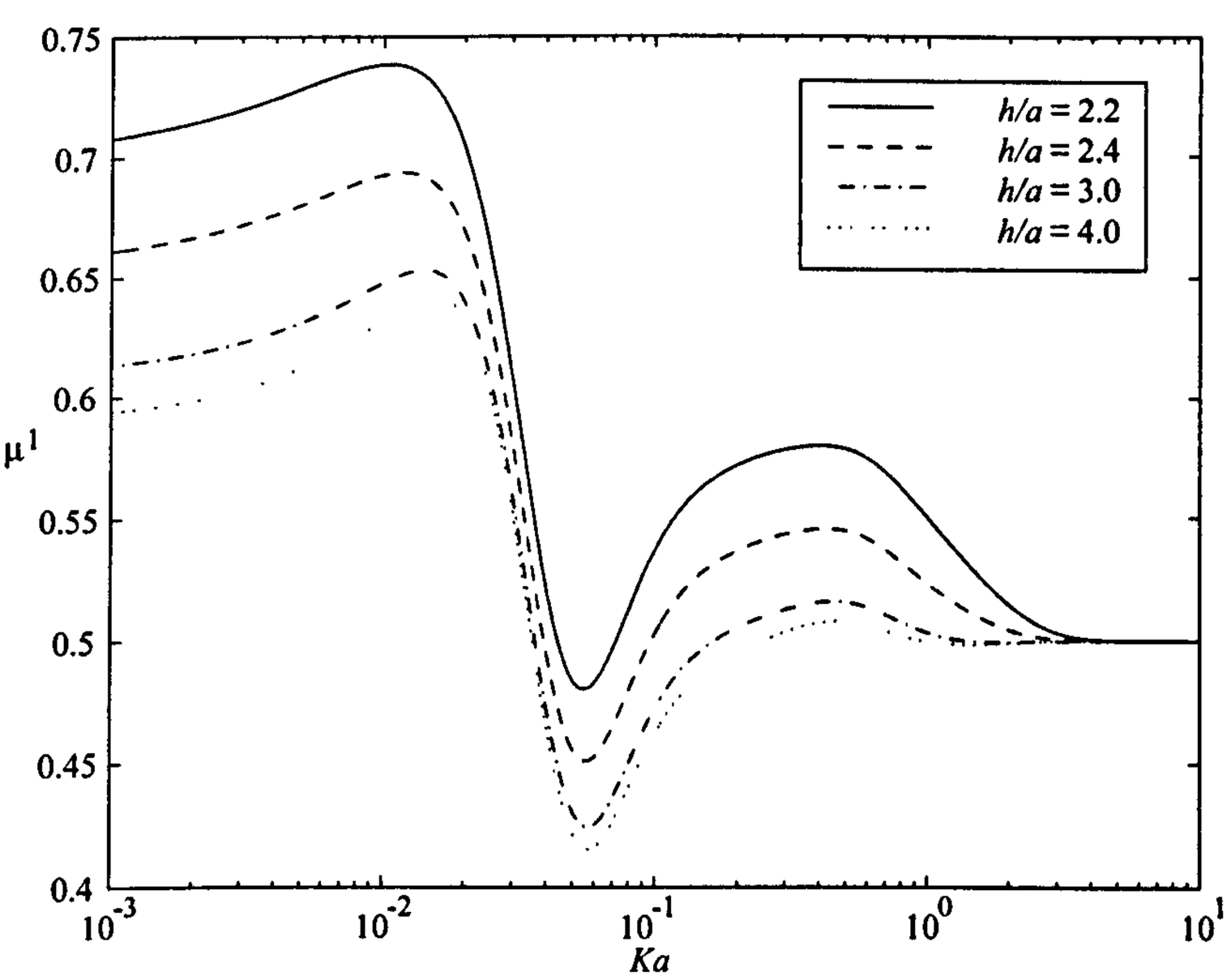

Figure 3.4: Added mass coefficient μ^1 (sway) plotted against Ka for a submerged sphere in the lower fluid layer with varying depth of the lower fluid layer; $\rho = 0.95$, $d/a = 2.0$ and $f/a = -1.1$.

3.5.2 Sphere in upper fluid layer

Multipole expansions

When the sphere is positioned in the upper region ($f > 0$) the multipoles will take the form

$$\phi_n^{Im} = a^{n+2}\cos m\alpha \left[\frac{P_n^m(\cos\theta)}{r^{n+1}} + \frac{1}{(n-m)!}\int_0^\infty u^n \left[A_U(u)e^{uz} + B_U(u)e^{-uz}\right] J_m(uR)du\right] \tag{3.5.30}$$

$$\phi_n^{IIm} = a^{n+2}\frac{\cos m\alpha}{(n-m)!}\int_0^\infty u^n \left[C_U(u)e^{uz} + D_U(u)e^{-uz}\right] J_m(uR)du. \tag{3.5.31}$$

We apply the boundary conditions (3.5.3)–(3.5.6) to these multipoles in order to find the functions $A_U(u)$, $B_U(u)$, $C_U(u)$ and $D_U(u)$. The seabed condition (3.5.6) yields the expression

$$C_U(u) = e^{2uh}D_U(u), \tag{3.5.32}$$

which is different to what we obtained when the singularity was in the lower fluid layer. This allows us to simplify the multipoles in the lower fluid layer by writing

$$\phi_n^{IIm} = \frac{a^{n+2}\cos m\alpha}{(n-m)!}\int_0^\infty u^n \cosh u(z+h)C_U(u)J_m(uR)du. \tag{3.5.33}$$

Applying the remaining conditions (3.5.3)–(3.5.5) to the multipole functions we obtain

$$\begin{aligned}
A_U(u) \qquad & -B_U(u) \qquad && -\sinh uh\, C_U(u) = -(-1)^{m+n}e^{-uf},\\
A_U(u) & -\frac{u+K}{u-K}B_U(u) && -\frac{u\sinh uh - K\cosh uh}{\rho(u-K)}C_U(u) = -(-1)^{m+n}e^{-uf},\\
\frac{u-K}{u+K}e^{2ud}A_U(u) \qquad & -B_U(u) && = e^{uf}.
\end{aligned} \tag{3.5.34}$$

Solutions to these expressions are

$$A_U(u) =(u+K)e^{-2ud}\Big[\Big[K\coth uh - u(1-\rho)\Big](e^{uf}+(-1)^{m+n}e^{-uf}) + K\rho(e^{uf}-(-1)^{m+n}e^{-uf})\Big]/H(u), \tag{3.5.35}$$

$$B_U(u) =(u-K)\Big[\Big[K\coth uh - u(1-\rho)\Big](e^{uf}+(-1)^{m+n}e^{-uf}) + K\rho(e^{uf}-(-1)^{m+n}e^{-uf})\Big]/H(u) - e^{uf}, \tag{3.5.36}$$

$$C_U(u) =\Big[(u+K)e^{-2ud}-u+K\Big]\Big[\Big[K\coth uh - u(1-\rho)+\frac{H(u)}{(u+K)e^{-2ud}-u+K}\Big] \times (e^{uf}+(-1)^{m+n}e^{-uf}) + K\rho(e^{uf}-(-1)^{m+n})e^{-uf}\Big]/(H(u)\sinh uh), \tag{3.5.37}$$

where $H(u)$ is given by (3.5.12). As in the previous problems these functions have poles so we write the multipoles as

$$\phi_n^{Im} = a^{n+2}\cos m\alpha\left[\frac{P_n^m(\cos\theta)}{r^{n+1}}+\frac{1}{(n-m)!}\oint_0^\infty u^n\left[A_U(u)e^{uz}+B_U(u)e^{-uz}\right]J_m(uR)du\right] \tag{3.5.38}$$

$$\phi_n^{IIm} = a^{n+2}\frac{\cos m\alpha}{(n-m)!}\oint_0^\infty u^n\cosh u(z+h)C_U(u)J_m(uR)du. \tag{3.5.39}$$

where the path of integration is indented to pass beneath the poles of the integrand at $u=k_1$ and $u=k_2$ such that the multipoles behave as outgoing waves as $KR\to\infty$.

The far-field form of the multipoles in the upper fluid layer is given by (3.5.15) with the residues of A_L and B_L replaced with the residues of A_U and B_U respectively.

We can expand the multipoles around $r=0$ in spherical polar coordinates using (2.6.20), to give

$$\phi_n^{Im} = a\cos m\alpha\left[\left(\frac{a}{r}\right)^{n+1}P_n^m(\cos\theta)+\sum_{s=m}^{\infty}\left(\frac{r}{a}\right)^s B_{ns}^m P_s^m(\cos\theta)\right], \tag{3.5.40}$$

where

$$B_{ns}^m = \frac{a}{(n-m)!(s+m)!}\oint_0^\infty (au)^{n+s}\left[e^{uf}A_U(u)+(-1)^{m+s}e^{-uf}B_U(u)\right]du. \tag{3.5.41}$$

To simplify the writing and computation of the expression for B_{ns}^m we define the following functions

$$c_1(u) =(u+K)\Big[K\coth uh - u+\rho(u+K)\Big], \tag{3.5.42}$$

$$c_2(u) =(u+K)\Big[(-1)^{m+n}+(-1)^{m+s}\Big]\Big[K\coth uh - u+\rho(u-K)\Big], \tag{3.5.43}$$

$$c_3(u) =(-1)^{n+s}(u-K)\Big[K\coth uh - u+\rho(u-K)\Big]. \tag{3.5.44}$$

Then

$$B_{ns}^m = \frac{a}{(n-m)!(s+m)!} \oint_0^\infty (au)^{n+s} \left[c_1(u) e^{2u(f-d)} + c_2(u) e^{-2ud} + c_3(u) e^{-2uf} \right] / H(u) du. \tag{3.5.45}$$

Formulation of problem

The velocity potential can be expanded in terms of the multipoles exactly as in (3.5.20) and then application of the body boundary condition leads to the infinite system of linear equations

$$b_s^m - \left[\frac{s}{s+1} \right] \sum_{n=1}^{\infty} B_{ns}^m b_n^m = -\delta_{1s}/2 \qquad s = 1, 2, \ldots \qquad m = 0, 1, \tag{3.5.46}$$

for the unknown coefficients b_n^m. The non-dimensionalised added-mass and damping coefficients μ^m and ν^m respectively are given by

$$\mu^m + i\nu^m = -(1 + 3b_1^m) \qquad m = 0, 1, \tag{3.5.47}$$

which is the same as (3.5.22), where ν^m can also be written as

$$\nu^m = \frac{3}{4\pi^2 \rho a^3} \left[J_{k_1} \int_0^{2\pi} |A^m(\alpha)|^2 d\alpha + J_{k_2} \int_0^{2\pi} |B^m(\alpha)|^2 d\alpha \right], \tag{3.5.48}$$

from (3.4.25). The coefficients $A^m(\alpha)$ and $B^m(\alpha)$ are found from the far-field form of ϕ^m and are

$$|A^m(\alpha)|^2 = \left| \sum_{n=1}^{\infty} \frac{(k_1 a)^n b_n^m}{(n-m)!} A_U^{k_1} \right|^2 \left(\frac{a^2 \pi \cos m\alpha \, e^{k_1 d}}{k_1 + K} \right)^2, \tag{3.5.49}$$

$$= \left| \sum_{n=1}^{\infty} \frac{(k_1 a)^n b_n^m}{(n-m)!} B_U^{k_1} \right|^2 \left(\frac{a^2 \pi \cos m\alpha \, e^{-k_1 d}}{k_1 - K} \right)^2, \tag{3.5.50}$$

$$|B^m(\alpha)|^2 = \left| \sum_{n=1}^{\infty} \frac{(k_2 a)^n b_n^m}{(n-m)!} A_U^{k_2} \right|^2 \left(\frac{a^2 \pi \cos m\alpha \, e^{k_2 d}}{k_2 + K} \right)^2, \tag{3.5.51}$$

$$= \left| \sum_{n=1}^{\infty} \frac{(k_2 a)^n b_n^m}{(n-m)!} B_U^{k_2} \right|^2 \left(\frac{a^2 \pi \cos m\alpha \, e^{-k_2 d}}{k_2 - K} \right)^2. \tag{3.5.52}$$

Results produced by solving (3.5.46) were checked using the following identity

$$\Im(b_1^m) = -\frac{\pi a}{2\epsilon_m \rho} \left(\frac{J_{k_1} e^{2k_1 d}}{(k_1 + K)^2} \left| \sum_{n=1}^{\infty} \frac{(k_1 a)^n b_n^m}{(n-m)!} A_U^{k_1} \right|^2 + \frac{J_{k_2} e^{2k_2 d}}{(k_2 + K)^2} \left| \sum_{n=1}^{\infty} \frac{(k_2 a)^n b_n^m}{(n-m)!} A_U^{k_2} \right|^2 \right), \tag{3.5.53}$$

which follows from (3.5.48) using (3.5.47) and (3.5.49)–(3.5.52).

Results

Curves of added-mass and damping coefficients for spheres in the upper fluid layer in both heave and sway are shown in figures 3.5–3.8. In all the curves ρ is 0.95, d/a is 4 and f/a is 2. Each plot shows the results obtained for four different depths, h/a, of the lower fluid, 0.5, 1, 2 and 3. When $h/a = 0.5$ the seabed is fairly close, half the sphere's radius, to the interface.

Figures 3.5 and 3.6 show the damping coefficients for heave and sway respectively. Again both cases lead to similar results with those for heave motion greater than those obtained for sway. As with the sphere in the lower fluid there are two local maximums near $k_1a = 1$ ($Ka \approx 1$) and $k_2a = 1$ ($Ka \approx 0.025$). We note that for this case the second local maximum is greatest as more waves are generated on the free surface. In both heave and sway motion we see that the first local maximum increases with the depth of the lower fluid, h/a, indicating that the sphere's wave-making capabilities on the interface is reduced with the presence of the bottom. The ability of the sphere to generate waves on the free surface is affected much less by the bottom as can be seen by the second local maximum. In the case of heave motion there is a slight decrease of the second maximum due to the presence of finite depth whereas for sway there is a slight increase.

The added-mass coefficients for heave and sway are shown in figures 3.7 and 3.8 respectively. As has been the case previously, the deviations from the infinite fluid value of 1/2 are greater for heave motion than for sway. The effect due to the free surface, near $k_1a = 1$, is much greater than that due to the interface. For both heave and sway motion the added mass near $k_1a = 1$ increases with the presence of finite depth whereas the added mass near $k_2a = 1$ decreases.

We can see in figures 3.5–3.8 that for when $Ka \gtrsim 0.06$ the effects of finite depth is the same as those discussed by Linton (1991). For $Ka \lesssim 0.06$ we find the effects due to the interface break these trends.

3.6 Conclusion

In this chapter we have considered three-dimensional radiation problems in a two-layer fluid where the upper fluid is bounded above by a free surface and the lower fluid is of finite depth. As in the infinite-depth case there are two different wavenumbers for a given

frequency at which waves can propagate. The added-mass and damping coefficients were calculated for heave and sway motion of a sphere situated entirely within either the upper or lower fluid layers. To solve these problems we expanded the velocity potential in terms of multipoles which are only applicable when the body geometry is simple. The multipoles are considerably more complicated than in the case of infinite depth but nevertheless provided accurate results for a small truncation parameter.

The effects of finite depth were found to be the same as those discussed in Linton (1991) except in some cases for low frequencies corresponding to waves being generated on the interface.

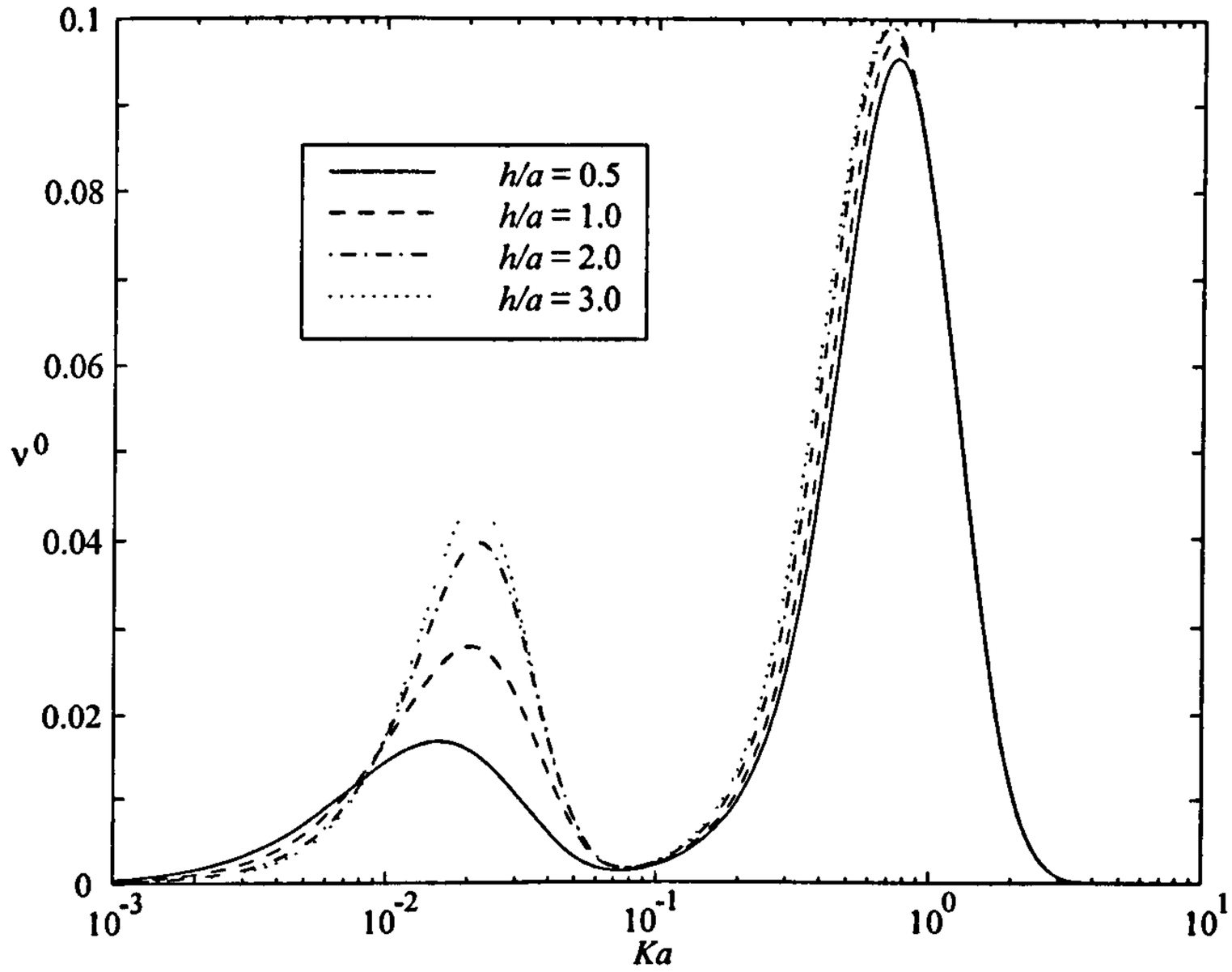

Figure 3.5: Damping coefficient ν^0 (heave) plotted against Ka for a submerged sphere in the upper fluid layer with varying depth of the lower fluid layer; $\rho = 0.95$, $d/a = 4.0$ and $f/a = 2.0$.

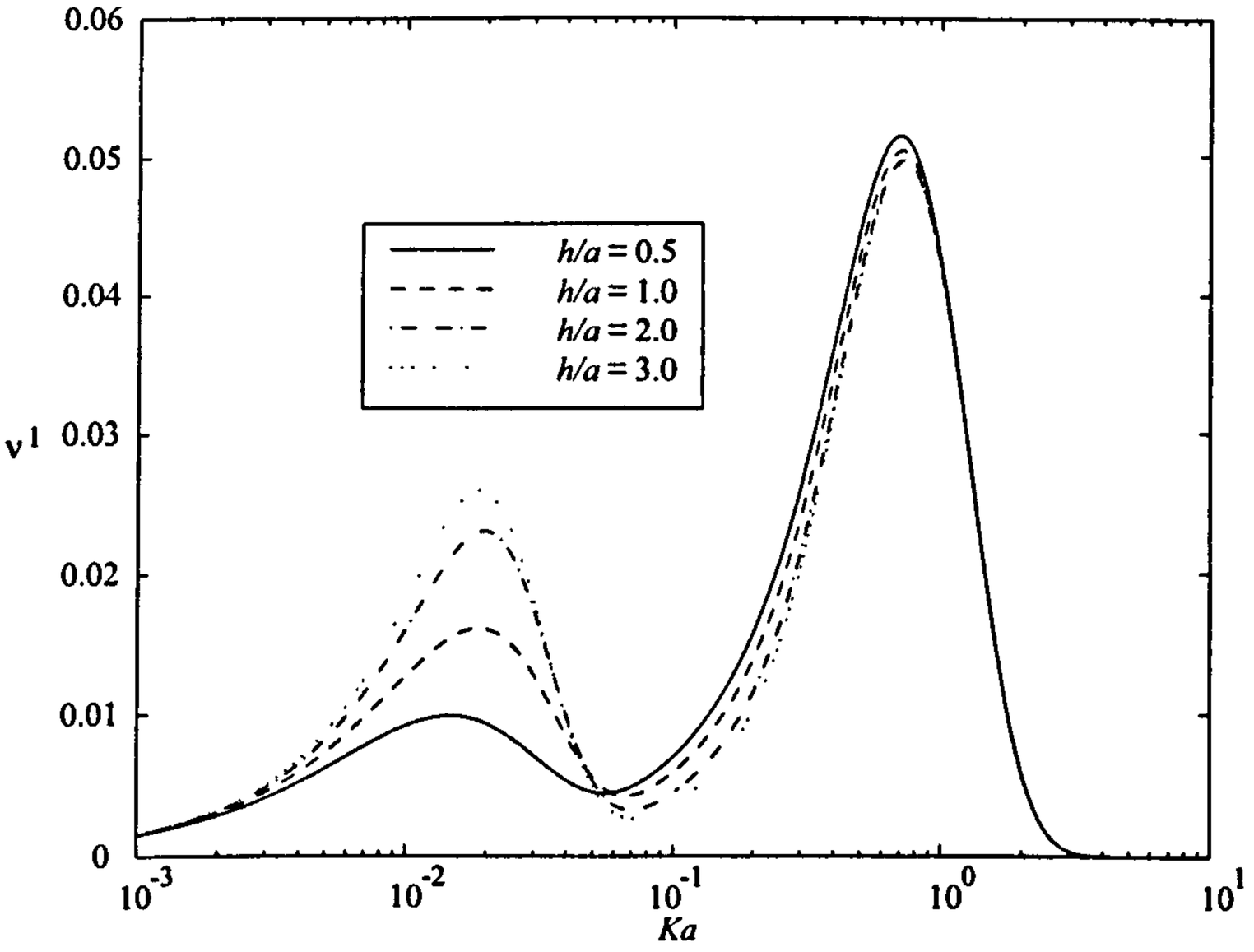

Figure 3.6: Damping coefficient ν^1 (sway) plotted against Ka for a submerged sphere in the upper fluid layer with varying depth of the lower fluid layer; $\rho = 0.95$, $d/a = 4.0$ and $f/a = 2.0$.

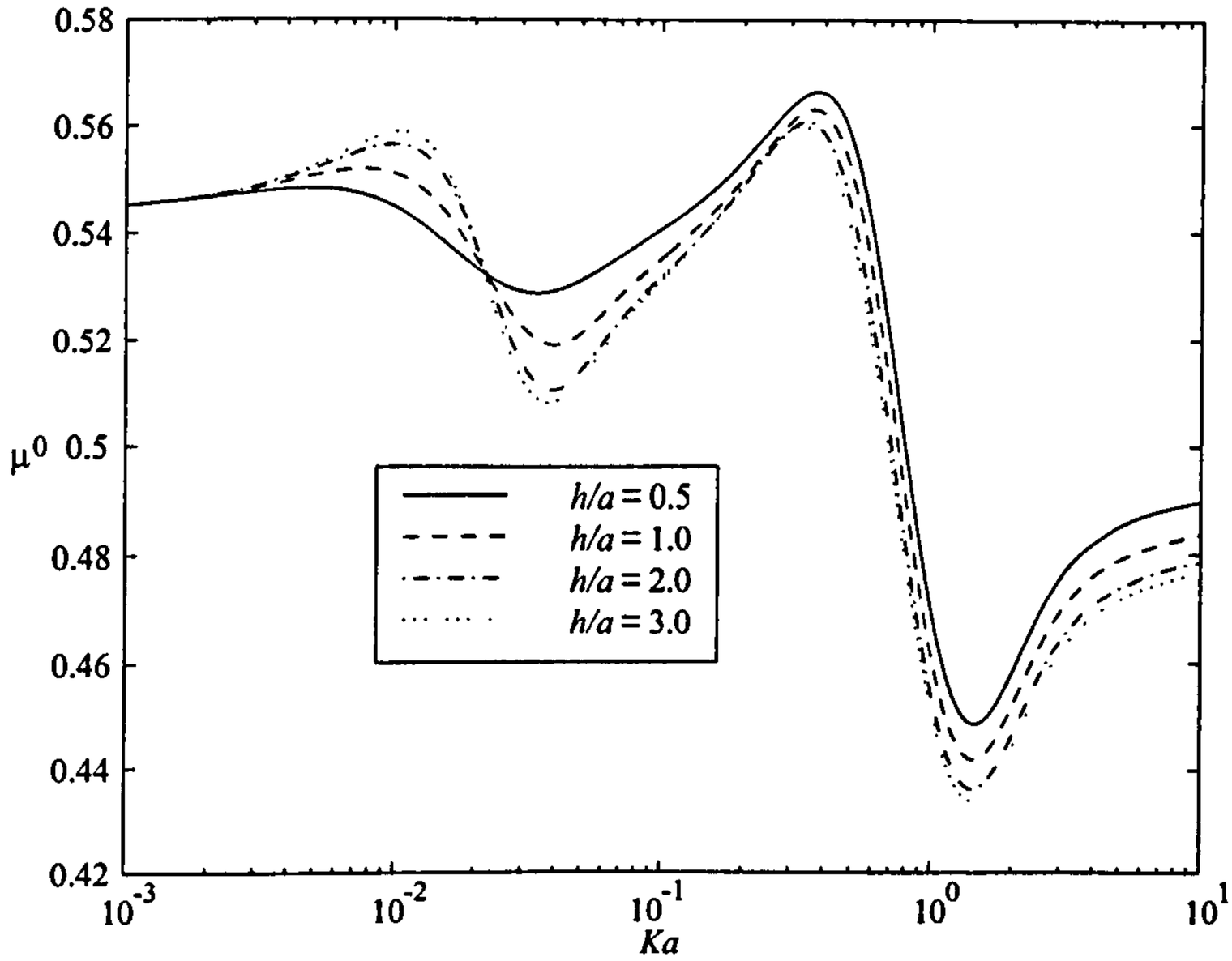

Figure 3.7: Added mass coefficient μ^0 (heave) plotted against Ka for a submerged sphere in the upper fluid layer with varying depth of the lower fluid layer; $\rho = 0.95$, $d/a = 4.0$ and $f/a = 2.0$.

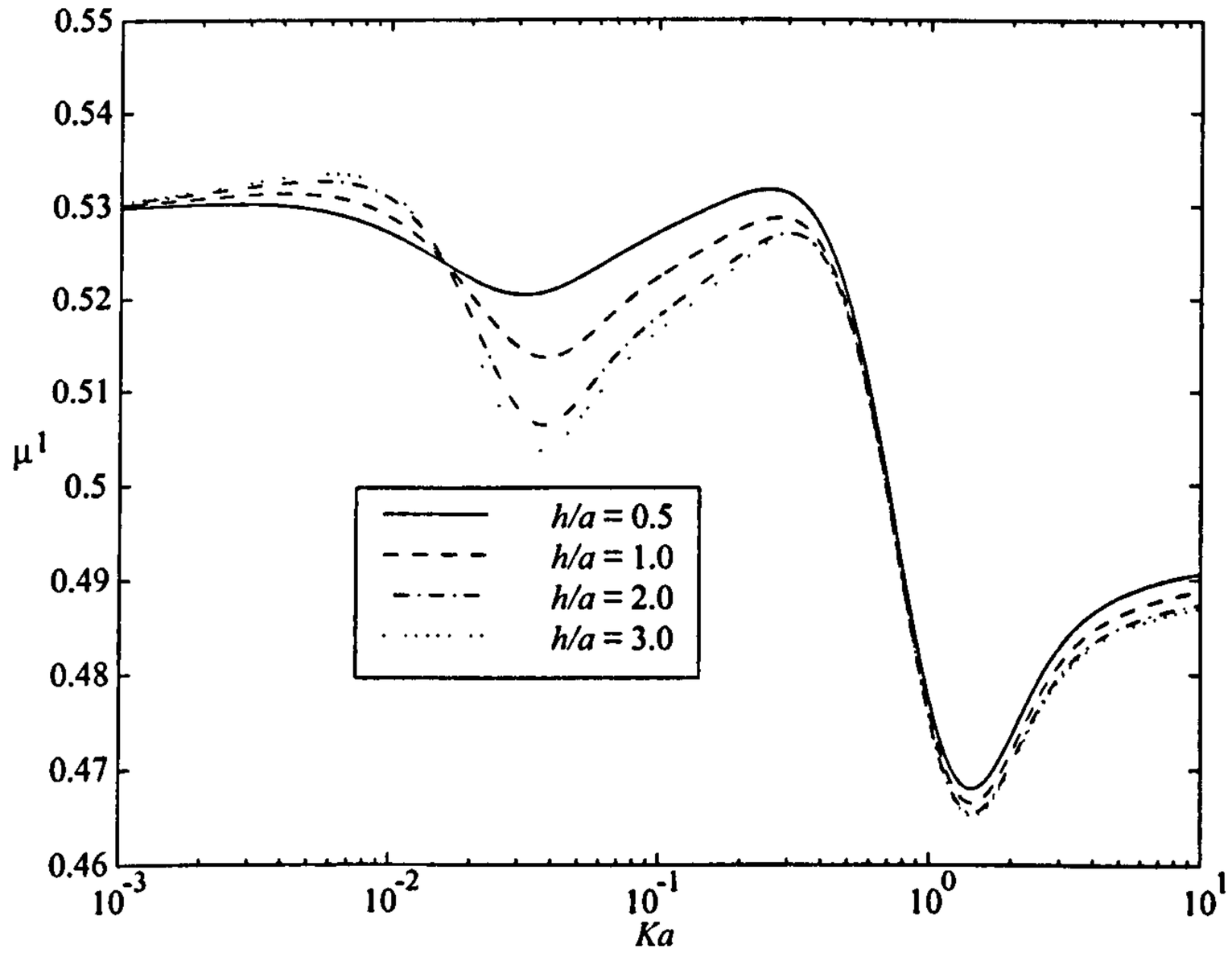

Figure 3.8: Added mass coefficient μ^1 (sway) plotted against Ka for a submerged sphere in the upper fluid layer with varying depth of the lower fluid layer; $\rho = 0.95$, $d/a = 4.0$ and $f/a = 2.0$.

Part II

Submerged Cylinders

Chapter 4

Finite depth of lower fluid

4.1 Introduction

In this second part of the thesis we are concerned with two-dimensional wave problems. Outgoing two-dimensional waves have the property that they have constant amplitude as they travel away from a wave source. This allows us to define reflection and transmission coefficients for the problems of waves incident on a body in two dimensions. They are the proportions of the incident waves which are reflected and transmitted. For a two-layer fluid there are two wavenumbers for a given frequency; one corresponding to waves on the free surface and the other to waves on the interface. When incident waves interact with an obstacle wave energy can be transferred from one mode to the other. Linton & McIver (1995) calculated the transmission and reflection coefficients, using multipole expansions, for the scattering of incident waves with a horizontal circular cylinder in a two-layer fluid where the lower fluid is infinite. Linton & McIver (1995) also derived all the first-order reciprocity relations for two-dimensional waves in a two-layer fluid of this type. In this chapter we will extend their work by letting the lower layer have constant depth h and investigate the effect of finite depth on the scattering of incident waves by a cylinder in the lower fluid layer. We will not treat the problem of a cylinder in the upper layer, the method being so similar to that given below.

4.2 Hydrodynamic relations

The velocity potentials must satisfy the conditions (3.2.1)–(3.2.5) as in the three-dimensional finite-depth case. Using separation of variables we find that two-layer

progressive waves take the form

$$\phi^I = Ae^{\pm iux}((u+K)e^{u(z-d)} + (u-K)e^{-u(z-d)}), \tag{4.2.1}$$

$$\phi^{II} = Ae^{\pm iux}\frac{(u+K)e^{-ud} - (u-K)e^{ud}}{\sinh uh}\cosh u(z+h), \tag{4.2.2}$$

where A is some constant. The dispersion relation is given by (3.2.10) and so waves of wavenumbers k_1 and k_2 exist and can propagate in either the positive or negative x direction. In any wave radiation or scattering problem therefore, the far field will take the form of incoming and outgoing waves of the wavenumbers k_1 and k_2. It can be shown that the correct form for the far field is in general given by

$$\phi^I \sim A^{\pm}e^{\pm ik_1x}g^I(z,k_1) + B^{\pm}e^{\pm ik_2x}g^I(z,k_2) + C^{\pm}e^{\mp ik_1x}g^I(z,k_1) + D^{\pm}e^{\mp ik_2x}g^I(z,k_2), \tag{4.2.3}$$

$$\phi^{II} \sim A^{\pm}e^{\pm ik_1x}g^{II}(z,k_1) + B^{\pm}e^{\pm ik_2x}g^{II}(z,k_2) + C^{\pm}e^{\mp ik_1x}g^{II}(z,k_1) + D^{\pm}e^{\mp ik_2x}g^{II}(z,k_2), \tag{4.2.4}$$

as $x \to \pm\infty$, where

$$g^I(z,u) = \frac{(u+K)e^{u(z-d)} + (u-K)e^{-u(z-d)}}{(u+K)e^{-ud} - (u-K)e^{ud}}\tanh uh, \tag{4.2.5}$$

$$g^{II}(z,u) = \frac{\cosh u(z+h)}{\cosh uh}, \tag{4.2.6}$$

and $A^{\pm}$ ($B^{\pm}$) and $C^{\pm}$ ($D^{\pm}$) are the respective far-field coefficients of outgoing and incoming waves of wavenumber k_1 (k_2). The functions $g^I(z,u)$ and $g^{II}(z,u)$ are chosen such that as $h \to \infty$ the far-field form tends to that given in Linton & McIver (1995) equations (2.8)–(2.9). A convenient shorthand for (4.2.3) and (4.2.4) is

$$\phi \sim \{A^-, B^-, C^-, D^-; A^+, B^+, C^+, D^+\}. \tag{4.2.7}$$

We now consider a situation in which there are a number of bodies within the fluid. The surfaces of those bodies in the upper fluid will be denoted by B^I and those in the lower fluid by B^{II}. We shall assume that the potentials ϕ_i and ϕ_j are solutions to two different problems, with $\partial\phi_i/\partial n$ and $\partial\phi_j/\partial n$ given on B^I and B^{II}, and the far-field forms given by

$$\phi_i \sim \{A_i^-, B_i^-, C_i^-, D_i^-; A_i^+, B_i^+, C_i^+, D_i^+\}, \tag{4.2.8}$$

$$\phi_j \sim \{A_j^-, B_j^-, C_j^-, D_j^-; A_j^+, B_j^+, C_j^+, D_j^+\}. \tag{4.2.9}$$

If we apply Green's theorem to the upper and lower fluid regions in the same way as Linton & McIver (1995) we obtain the following identity

$$\rho \int_{B^I} \left(\phi^I \frac{\partial \psi^I}{\partial n} - \psi^I \frac{\partial \phi^I}{\partial n} \right) ds$$
$$+ \int_{B^{II}} \left(\phi^{II} \frac{\partial \psi^{II}}{\partial n} - \psi^{II} \frac{\partial \phi^{II}}{\partial n} \right) ds = J_{k_1}(A_i^+ C_j^+ - C_i^+ A_j^+ + A_i^- C_j^- - C_i^- A_j^-)$$
$$+ J_{k_2}(B_i^+ D_j^+ - D_i^+ B_j^+ + B_i^- D_j^- - D_i^- B_j^-), \quad (4.2.10)$$

where

$$J_u = 2iu \left(\rho \int_0^d [g^I(z,u)]^2 dz + \int_{-h}^0 [g^{II}(z,u)]^2 dz \right). \quad (4.2.11)$$

Equation (4.2.10) is the finite-depth equivalent of equation (2.16) in Linton & McIver (1995), the only difference being J_K and J_k are replaced by J_{k_1} and J_{k_2} respectively. It is clear that all the relations in Linton & McIver (1995) for the infinite depth case can be used for the finite depth case simply by letting $J = J_{k_2}/J_{k_1}$.

4.3 Two radiation potentials

Several relations exist between two different radiation problems. Here we will briefly derive two standard results. Let us consider the case of two radiation potentials ϕ_i and ϕ_j due to a body oscillating in directions i and j respectively. These radiation potentials are defined to have the following body boundary condition

$$\frac{\partial \phi_i}{\partial n} = n_i \qquad \frac{\partial \phi_j}{\partial n} = n_j \qquad \text{on } S_B, \quad (4.3.1)$$

where n_i (n_j) is the component of the inward normal to the body in the direction i (j) and S_B is the body boundary, which for simplicity we will assume is entirely contained within region I or region II. Application of (4.2.10) to ϕ_i and ϕ_j yields

$$-B_{ij} + i\omega M_{ij} \equiv i\omega\delta\rho^{II} \int_{S_B} \phi_i n_j ds = i\omega\delta\rho^{II} \int_{S_B} \phi_j n_i ds = -B_{ji} + i\omega M_{ji}, \quad (4.3.2)$$

where B and M are the damping and added-mass coefficients respectively. Equation (4.3.2) states that the damping and added-mass matrices are symmetric. The same result is shown for the three-dimensional case by (2.3.8) and (3.4.19).

Application of (4.2.10) to ϕ_i and the complex conjugate of ϕ_j yields

$$B_{ij} = -\frac{i\rho^{II}\omega}{2} \left[J_{k_1}(A_i^+ \overline{A_j^+} + A_i^- \overline{A_j^-}) + J_{k_2}(B_i^+ \overline{B_j^+} + B_i^- \overline{B_j^-}) \right] \quad (4.3.3)$$

which relates the damping coefficient to the far-field amplitudes.

4.4 Two scattering potentials

We now consider the case of two scattering potentials having zero normal derivative on all the body boundaries hence the left-hand side of (4.2.10) will be zero. In general there are four problems to be considered. These are the scattering of an incident wave of wavenumber k_1 from $x = -\infty$, which we shall refer to as problem 1; the scattering of an incident wave of wavenumber k_1 from $x = +\infty$ (problem 2); the scattering of an incident wave of wavenumber k_2 from $x = -\infty$ (problem 3); and the scattering of an incident wave of wavenumber k_2 from $x = +\infty$ (problem 4). In each case there may be reflected and transmitted waves of wavenumber k_1 and k_2. We use R^{k_p} and T^{k_p} to represent the reflection and transmission coefficients corresponding to waves of wavenumber k_p, $p = 1, 2$. Applying (4.2.10) to the potential of each problem and its conjugate we obtain the following

$$E_j^{R_1} + E_j^{T_1} + E_j^{R_2} + E_j^{T_2} = 1, \qquad j = 1, 2, 3 \text{ or } 4. \tag{4.4.1}$$

where the energies are defined as follows

$$\left.\begin{aligned} E_j^{R_1} &= |R_j^{k_1}|^2, & E_j^{T_1} &= |T_j^{k_1}|^2, \\ E_j^{R_2} &= J|R_j^{k_2}|^2, & E_j^{T_2} &= J|T_j^{k_2}|^2, \end{aligned}\right\} j = 1, 2, \tag{4.4.2}$$

$$\left.\begin{aligned} E_j^{R_1} &= |R_j^{k_1}|^2/J, & E_j^{T_1} &= |T_j^{k_1}|^2/J, \\ E_j^{R_2} &= |R_j^{k_2}|^2, & E_j^{T_2} &= |T_j^{k_2}|^2, \end{aligned}\right\} j = 3, 4. \tag{4.4.3}$$

In words, $E_1^{R_2}$ is the reflected energy at wavenumber k_2 due to an incident wave of unit energy and wavenumber k_1 from $x = -\infty$ and so on. Equation (4.4.1) represents the conservation of energy and we will use it as a numerical check on results for the transmission and reflection coefficients. There are many more relations which can be derived from (4.2.10) using different combinations of the scattering potentials but are all equivalent to those given in Linton & McIver (1995) with an appropriate change in the definition of J.

4.5 Incident waves

Due to the symmetry of the body we will be using we only have to consider problems 1 and 3 described above. For problem 1 an incident wave of wavenumber k_1 on the free

surface from $x = -\infty$ has the form

$$\phi^I_{\text{inc}} = e^{ik_1 x} g^I(z, k_1), \tag{4.5.1}$$

$$\phi^{II}_{\text{inc}} = e^{ik_1 x} g^{II}(z, k_1). \tag{4.5.2}$$

Similarly for problem 3, an incident wave of wavenumber k_2 on the interface from $x = -\infty$ has the form

$$\phi^I_{\text{inc}} = e^{ik_2 x} g^I(z, k_2), \tag{4.5.3}$$

$$\phi^{II}_{\text{inc}} = e^{ik_2 x} g^{II}(z, k_2). \tag{4.5.4}$$

4.6 Scattering by a cylinder in the lower fluid layer

We will now solve the scattering problem of a horizontal circular cylinder in the lower fluid layer. For the case of a cylinder centred at $x = 0$, $z = f < 0$ of radius $a(< |f|)$ we need to construct multipoles singular at $z = f$, $f < 0$. It is convenient to distinguish those multipoles symmetric about $x = 0$ and those antisymmetric about this line. These will be denoted ϕ^s_n and ϕ^a_n respectively. We then write the velocity potential as the sum of the incident wave potential and the multipoles and solve for some unknown coefficients using the body boundary condition. The transmission and reflection coefficients can be extracted from the far-field form of the velocity potential and values of these are presented below.

4.6.1 Multipole expansions

Solutions of Laplace's equation singular at $z = f$ are $r^{-n}\cos n\theta$ and $r^{-n}\sin n\theta$, $n \geq 1$, where

$$x = r\sin\theta, \qquad z = f - r\cos\theta, \tag{4.6.1}$$

and these solutions have integral representations, valid for $z > f$

$$\frac{\cos n\theta}{r^n} = \frac{(-1)^n}{(n-1)!}\int_0^\infty u^{n-1} e^{-u(z-f)} \cos ux \, du, \tag{4.6.2}$$

$$\frac{\sin n\theta}{r^n} = \frac{(-1)^{n+1}}{(n-1)!}\int_0^\infty u^{n-1} e^{-u(z-f)} \sin ux \, du \tag{4.6.3}$$

and for $z < f$

$$\frac{\cos n\theta}{r^n} = \frac{1}{(n-1)!}\int_0^\infty u^{n-1}e^{u(z-f)}\cos ux\,du, \tag{4.6.4}$$

$$\frac{\sin n\theta}{r^n} = \frac{1}{(n-1)!}\int_0^\infty u^{n-1}e^{u(z-f)}\sin ux\,du \tag{4.6.5}$$

(Gradshteyn & Ryzhik (1980), equations 3.944(5) and (6)). The symmetric multipoles in the lower fluid layer take the form

$$\phi_n^{Is} = \frac{(-1)^n}{(n-1)!}\int_0^\infty u^{n-1}[A_L^s(u)e^{uz} + B_L^s(u)e^{-uz}]\cos ux\,du, \tag{4.6.6}$$

$$\phi_n^{IIs} = \frac{\cos n\theta}{r^n} + \frac{(-1)^n}{(n-1)!}\int_0^\infty u^{n-1}[C_L^s(u)e^{uz} + D_L^s(u)e^{-uz}]\cos ux\,du. \tag{4.6.7}$$

Applying the boundary conditions (3.2.2)–(3.2.5) to these multipoles we obtain expressions involving $A_L^s(u)$, $B_L^s(u)$, $C_L^s(u)$ and $D_L^s(u)$. These are

$$A_L^s(u) - B_L^s(u) - C_L^s(u) + D_L^s(u) = -e^{uf}\quad, \tag{4.6.8}$$

$$\rho\frac{u-K}{u+K}A_L^s(u) - \rho B_L^s(u) - \frac{u-K}{u+K}C_L^s(u) + D_L^s(u) = -e^{uf}\quad, \tag{4.6.9}$$

$$\frac{u-K}{u+K}e^{2ud}A_L^s(u) - B_L^s(u) = 0\quad, \tag{4.6.10}$$

$$C_L^s(u) - e^{2uh}D_L^s(u) = -(-1)^n e^{-uf}\,. \tag{4.6.11}$$

Solving the above equations we obtain the following functions

$$A_L^s(u) = K(u+K)e^{-2ud}[(\coth uh + 1)e^{uf} + (-1)^n(\coth uh - 1)e^{-uf}]/H(u), \tag{4.6.12}$$

$$B_L^s(u) = K(u-K)[(\coth uh + 1)e^{uf} + (-1)^n(\coth uh - 1)e^{-uf}]/H(u), \tag{4.6.13}$$

$$C_L^s(u) = e^{2uh}D_L^s(u) - (-1)^n e^{-uf}, \tag{4.6.14}$$

$$\begin{aligned} D_L^s(u) = (1-\rho)[&((u+K\sigma)e^{-2ud} - u + K)(u+K)e^{uf} \\ &+ (-1)^n((u+K)e^{-2ud} - u + K\sigma)(u-K)e^{-uf}]/(e^{2uh}-1)H(u), \end{aligned} \tag{4.6.15}$$

where $H(u)$ is given by (3.5.12).

The antisymmetric multipoles in the lower fluid layer take the form

$$\phi_n^{Ia} = \frac{(-1)^{n+1}}{(n-1)!}\int_0^\infty u^{n-1}[A_L^a(u)e^{uz} + B_L^a(u)e^{-uz}]\sin ux\,du, \tag{4.6.16}$$

$$\phi_n^{IIa} = \frac{\sin n\theta}{r^n} + \frac{(-1)^{n+1}}{(n-1)!}\int_0^\infty u^{n-1}[C_L^a(u)e^{uz} + D_L^a(u)e^{-uz}]\sin ux\,du. \tag{4.6.17}$$

Applying the boundary conditions (3.2.2)–(3.2.4) we obtain the expressions (4.6.8)–(4.6.10) for the functions $A_L^a(u)$, $B_L^a(u)$, $C_L^a(u)$ and $D_L^a(u)$. The seabed condition (3.2.5)

gives

$$C_L^a(u) - e^{2uh} D_L^a(u) = -(-1)^{n+1} e^{-uf}. \tag{4.6.18}$$

Hence the antisymmetric multipole functions will be the same as the symmetric functions but a $(-1)^{n+1}$ will replace any $(-1)^n$. We can now write the symmetric and antisymmetric multipoles as

$$\phi_n^{Is} = \frac{(-1)^n}{(n-1)!} \oint_0^\infty u^{n-1} [A_L^{(0)}(u) e^{uz} + B_L^{(0)}(u) e^{-uz}] \cos ux \, du, \tag{4.6.19}$$

$$\phi_n^{IIs} = \frac{\cos n\theta}{r^n} + \frac{(-1)^n}{(n-1)!} \oint_0^\infty u^{n-1} [C_L^{(0)}(u) e^{uz} + D_L^{(0)}(u) e^{-uz}] \cos ux \, du, \tag{4.6.20}$$

$$\phi_n^{Ia} = \frac{(-1)^{n+1}}{(n-1)!} \oint_0^\infty u^{n-1} [A_L^{(1)}(u) e^{uz} + B_L^{(1)}(u) e^{-uz}] \sin ux \, du, \tag{4.6.21}$$

$$\phi_n^{IIa} = \frac{\sin n\theta}{r^n} + \frac{(-1)^{n+1}}{(n-1)!} \oint_0^\infty u^{n-1} [C_L^{(1)}(u) e^{uz} + D_L^{(1)}(u) e^{-uz}] \sin ux \, du, \tag{4.6.22}$$

where the path of integration is indented below the poles at $u = k_1$ and $u = k_2$ so that the multipoles behave like outgoing waves as $|x| \to \infty$. The multipole functions are given by

$$A_L^{(q)}(u) = K(u+K) e^{-2ud} [(\coth uh + 1) e^{uf} + (-1)^{n+q} (\coth uh - 1) e^{-uf}] / H(u), \tag{4.6.23}$$

$$B_L^{(q)}(u) = K(u-K) [(\coth uh + 1) e^{uf} + (-1)^{n+q} (\coth uh - 1) e^{-uf}] / H(u), \tag{4.6.24}$$

$$C_L^{(q)}(u) = e^{2uh} D_L^{(q)}(u) - (-1)^{n+q} e^{-uf}, \tag{4.6.25}$$

$$\begin{aligned} D_L^{(q)}(u) = (1-\rho) [&((u+K\sigma) e^{-2ud} - u + K)(u+K) e^{uf} \\ &+ (-1)^{n+q} ((u+K) e^{-2ud} - u + K\sigma)(u-K) e^{-uf}] / (e^{2uh} - 1) H(u). \end{aligned} \tag{4.6.26}$$

The far-field form of the multipole potentials in the upper region are given by

$$\begin{aligned} \phi_n^{Is} \sim{}& \frac{(-1)^n \pi i}{(n-1)!} \\ &\times \left[k_1^{n-1} e^{\pm ik_1 x} (A_L^{(0)k_1} e^{k_1 z} + B_L^{(0)k_1} e^{-k_1 z}) + k_2^{n-1} e^{\pm ik_2 x} (A_L^{(0)k_2} e^{k_2 z} + B_L^{(0)k_2} e^{-k_2 z}) \right], \end{aligned} \tag{4.6.27}$$

$$\begin{aligned} \phi_n^{Ia} \sim{}& \mp \frac{(-1)^n \pi}{(n-1)!} \\ &\times \left[k_1^{n-1} e^{\pm ik_1 x} (A_L^{(1)k_1} e^{k_1 z} + B_L^{(1)k_1} e^{-k_1 z}) + k_2^{n-1} e^{\pm ik_2 x} (A_L^{(1)k_2} e^{k_2 z} + B_L^{(1)k_2} e^{-k_2 z}) \right], \end{aligned} \tag{4.6.28}$$

as $x \to \pm\infty$, where $A_L^{(q)k_p}$ and $B_L^{(q)k_p}$ are the residues of $A_L^{(q)}(u)$ and $A_L^{(q)}(u)$ respectively at $u = k_p$ for $q = 0, 1$ and $p = 1, 2$. We use the far-field form in the upper region as the functions are simpler than those in the lower region. The residues are given by

$$A_L^{(q)k_p} = K(k_p + K)e^{-2k_pd}\left[(\coth k_ph + 1)e^{k_pf} + (-1)^{n+q}(\coth k_ph - 1)e^{-k_pf}\right]$$
$$/(1 - e^{-2k_pd})\Big[(K\coth k_ph - k_p)(Kd\,\mathrm{cosech}^2 k_pd + 1)$$
$$+ (K\coth k_pd - k_p)(Kh\,\mathrm{cosech}^2 k_ph + 1) + 2\rho k_p\Big], \quad (4.6.29)$$

$$B_L^{(q)k_p} = K(k_p - K)\left[(\coth k_ph + 1)e^{k_pf} + (-1)^{n+q}(\coth k_ph - 1)e^{-k_pf}\right]$$
$$/(1 - e^{-2k_pd})\Big[(K\coth k_ph - k_p)(Kd\,\mathrm{cosech}^2 k_pd + 1)$$
$$+ (K\coth k_pd - k_p)(Kh\,\mathrm{cosech}^2 k_ph + 1) + 2\rho k_p\Big]. \quad (4.6.30)$$

The multipoles ϕ_m^s and ϕ_m^a can be expanded about $r = 0$ by using

$$e^{\pm u(z-f)}e^{iux} = \sum_{m=0}^{\infty} \frac{(\mp ur)^m}{m!} e^{\mp im\theta} \quad (4.6.31)$$

(Gradshteyn & Ryzhik (1980), equations 1.463(1) and (2)) which gives, valid for $r < |f|$,

$$\phi_n^s = \frac{\cos n\theta}{r^n} + \sum_{m=0}^{\infty} A_{nm}^s r^m \cos m\theta, \quad (4.6.32)$$

$$\phi_n^a = \frac{\sin n\theta}{r^n} + \sum_{m=0}^{\infty} A_{nm}^a r^m \sin m\theta, \quad (4.6.33)$$

where

$$A_{nm}^s = \frac{(-1)^n}{(n-1)!m!} \oint_0^{\infty} u^{n+m-1}[(-1)^m e^{uf} C_L^{(0)}(u) + e^{-uf} D_L^{(0)}(u)]du, \quad (4.6.34)$$

$$A_{nm}^a = \frac{(-1)^{n+1}}{(n-1)!m!} \oint_0^{\infty} u^{n+m-1}[(-1)^{m+1} e^{uf} C_L^{(1)}(u) + e^{-uf} D_L^{(1)}(u)]du. \quad (4.6.35)$$

To solve the scattering problem we write the velocity potential as the sum of the incident wave and the multipole potentials. Hence

$$\phi = \phi_{\text{inc}} + \sum_{n=1}^{\infty} a^n(\alpha_n\phi_n^a + \beta_n\phi_n^s) \quad (4.6.36)$$

where ϕ_{inc} is given by either (4.5.2) or (4.5.4) and α_n and β_n are unknowns. Since $\partial\phi/\partial r = 0$ on $r = a$ we have

$$\sum_{n=1}^{\infty} a^n \frac{\partial}{\partial r}(\alpha_n\phi_n^a + \beta_n\phi_n^s) = -\frac{\partial\phi_{\text{inc}}}{\partial r} \qquad \text{on } r = a. \quad (4.6.37)$$

4.6.2 Incident wavenumber k_1

We now consider problem 1 which is the scattering of a plane progressive wave of wavenumber k_1 from $x = -\infty$. First we expand the incident wave about $r = 0$ using (4.6.31) to give

$$\phi_{\text{inc}}^{II} = \frac{\cosh k_1(z+h)}{\cosh k_1 h} e^{ik_1 x} \tag{4.6.38}$$

$$= \frac{1}{2\cosh k_1 h} \sum_{m=0}^{\infty} \frac{(k_1 r)^m}{m!} [(-1)^m e^{k_1(h+f)} e^{-im\theta} + e^{-k_1(h+f)} e^{im\theta}]. \tag{4.6.39}$$

Substituting the polar expansions of the multipoles (4.6.32) and (4.6.33) and of the incident wave (4.6.39) into (4.6.37) and using the orthogonality of the trigonometric functions leads to uncoupled sets of equations for the unknowns α_n and β_n. These are

$$\alpha_m - \sum_{n=1}^{\infty} a^{n+m} A_{nm}^{a} \alpha_n = i \frac{(k_1 a)^m}{2(m!)\cosh k_1 h} [e^{-k_1(h+f)} - (-1)^m e^{k_1(h+f)}], \tag{4.6.40}$$

$$\beta_m - \sum_{n=1}^{\infty} a^{n+m} A_{nm}^{s} \beta_n = \frac{(k_1 a)^m}{2m!\cosh k_1 h} [e^{-k_1(h+f)} + (-1)^m e^{k_1(h+f)}], \tag{4.6.41}$$

$m = 1, 2, \ldots$. The equations decouple because of the symmetry of the geometry about the line $x = 0$.

The far-field form for ϕ_1, in the upper fluid, can be written as

$$\phi_1^I \sim \begin{cases} e^{ik_1 x} g^I(z, k_1) + R_1^{k_1} e^{-ik_1 x} g^I(z, k_1) + R_1^{k_2} e^{-ik_2 x} g^I(z, k_2) & x \to -\infty, \\ T_1^{k_1} e^{ik_1 x} g^I(z, k_1) + T_1^{k_2} e^{ik_2 x} g^I(z, k_2) & x \to +\infty. \end{cases} \tag{4.6.42}$$

The upper region multipoles are used as the functions are simpler. We can extract the transmission and reflection coefficients from (4.6.36) using (4.6.27), (4.6.28) and (4.6.38). They are

$$T_1^{k_1} = 1 - \frac{\pi[k_1 + K - (k_1 - K)e^{2k_1 d}]}{k_1(k_1 + K)\tanh k_1 h} \sum_{n=1}^{\infty} \frac{(-k_1 a)^n}{(n-1)!} [\alpha_n A_L^{(1)k_1} - i\beta_n A_L^{(0)k_1}], \tag{4.6.43}$$

$$T_1^{k_2} = -\frac{\pi[k_2 + K - (k_2 - K)e^{2k_2 d}]}{k_2(k_2 + K)\tanh k_2 h} \sum_{n=1}^{\infty} \frac{(-k_2 a)^n}{(n-1)!} [\alpha_n A_L^{(1)k_2} - i\beta_n A_L^{(0)k_2}], \tag{4.6.44}$$

$$R_1^{k_1} = \frac{\pi[k_1 + K - (k_1 - K)e^{2k_1 d}]}{k_1(k_1 + K)\tanh k_1 h} \sum_{n=1}^{\infty} \frac{(-k_1 a)^n}{(n-1)!} [\alpha_n A_L^{(1)k_1} + i\beta_n A_L^{(0)k_1}], \tag{4.6.45}$$

$$R_1^{k_2} = \frac{\pi[k_2 + K - (k_2 - K)e^{2k_2 d}]}{k_2(k_2 + K)\tanh k_2 h} \sum_{n=1}^{\infty} \frac{(-k_2 a)^n}{(n-1)!} [\alpha_n A_L^{(1)k_2} + i\beta_n A_L^{(0)k_2}]. \tag{4.6.46}$$

To compute values for the reflection and transmission coefficients we must first solve (4.6.40) and (4.6.41) using a truncation procedure. The systems were truncated to $N \times N$

systems and then the convergence of the results was observed as N increased. The results converged rapidly and a value of $N = 4$ gave the reflected and transmitted energies to 2 decimal places. The computed energies were then checked using the conservation of energy condition (4.4.1).

4.6.3 Incident wavenumber k_2

For problem 3, the scattering of an incident wave of wavenumber k_2 from $x = -\infty$, we simply replace k_1 with k_2 in equations (4.6.39)–(4.6.41). The reflection coefficients $R_2^{k_1}$ and $R_2^{k_2}$ are given by (4.6.45) and (4.6.46) respectively whereas the transmission coefficients are given by

$$T_3^{k_1} = -\frac{\pi[k_1 + K - (k_1 - K)e^{2k_1 d}]}{k_1(k_1 + K)\tanh k_1 h} \sum_{n=1}^{\infty} \frac{(-k_1 a)^n}{(n-1)!}[\alpha_n A_L^{(1)k_1} - i\beta_n A_L^{(0)k_1}], \qquad (4.6.47)$$

$$T_3^{k_2} = 1 - \frac{\pi[k_2 + K - (k_2 - K)e^{2k_2 d}]}{k_2(k_2 + K)\tanh k_2 h} \sum_{n=1}^{\infty} \frac{(-k_2 a)^n}{(n-1)!}[\alpha_n A_L^{(1)k_2} - i\beta_n A_L^{(0)k_2}]. \qquad (4.6.48)$$

4.7 Results

Figures 4.1–4.6 show the proportion of the incident energy that is transmitted and reflected at wavenumbers k_1 and k_2 due to waves of wavenumber k_1 and k_2 incident on a cylinder situated in the lower fluid. In all the curves $\rho = 0.95$, $d/a = 2.0$ and $f/a = -2$. Each plot shows the results obtained for four different depths, h/a, of the lower fluid which are 3.2, 4, 5 and 6. For the case when $h/a = 3.2$ the bottom is a distance $0.2a$ from the surface of the cylinder. As $h/a \to \infty$ the multipoles go over to those of the infinite-depth case and so results from Linton & McIver (1995) can be recovered.

Firstly we note that the finite depth equivalents of equations (2.48) and (2.49) from Linton & McIver (1995) are $R_3^{k_1} = JR_1^{k_2}$ and $T_3^{k_1} = JT_1^{k_2}$ respectively. In terms of the energies, defined by (4.4.2) and (4.4.3), these imply $E_3^{R_1} = E_1^{R_2}$ and $E_3^{T_1} = E_1^{T_2}$. Thus, figures 4.3 and 4.4 show the transmission and reflection energies at wavenumber k_2 due to an incident wave of wavenumber k_1 as well as the transmission and reflection energies at wavenumber k_1 due to an incident wave of wavenumber k_2.

Figures 4.1–4.4 show the reflected and transmitted energies due to an incident wave of wavenumber k_1 which corresponds to a free-surface wave. We can see that the transmitted energy at wavenumber k_1 in figure 4.1 has two local minimums. The first of these minimums, near $Ka = 0.014$, is the effect due to the interface whereas the second

local minimum, near $Ka = 0.17$ is due to the presence of finite depth. We deduce this from the range of frequencies over which the effects occur for infinite depth shown in Linton & McIver (1995) figure 2. The interface affects the transmission of the incident wave more than the seabed. The effect due to the interface however occurs for very long waves whereas the finite-depth effect is for more realistic frequencies. For the case of a cylinder in the lower layer of infinite depth it was found, by Linton & McIver (1995), that the incident wave was completely transmitted. Here we find that the incident wave is transmitted and reflected at both wavenumbers k_1 and k_2. The effect of finite depth therefore increases the cylinders ability to reflect the incident wave, albeit only by a small amount. As h/a increases the proportion of the incident energy which is reflected at wavenumbers k_1 and k_2 decreases to zero whereas the energy which is transmitted at wavenumbers k_1 and k_2 tends to the infinite depth values.

Figures 4.3–4.6 show the results obtained for an incident wave of wavenumber k_2 which corresponds to an interface wave. Here we have only one local minimum for the energy transmitted at the incident wavenumber as shown in figure 4.5. As with an incident wave of wavenumber k_1, we find that the cylinders reflective property is increased by the presence of finite depth. In the limit as $h/a \to \infty$ we find that the reflection energies $E_1^{R_1}$, $E_3^{R_1}(= E_1^{R_2})$ and $E_3^{R_2}$ tend to zero while $E_3^{T_2} \to E_1^{T_1}$ as in the infinite-depth case.

4.8 Conclusion

In this chapter we have examined the relationships that exist between the solutions of two-dimensional radiation and scattering problems in two-layer fluids where the upper fluid is bounded above by a free surface and the lower fluid is of finite depth. This is an extention of the work by Linton & McIver (1995) who considered infinite depth of the lower fluid. Using Green's theorem we found that all the reciprocity relations could be found using the infinite-depth relations by replacement of one function by another.

We then considered the scattering problem for a horizontal cylinder situated entirely within the lower fluid layer. This problem was solved using multipole expansions. In the infinite-depth case it has been shown that no energy is reflected by such a cylinder. For finite depth of the lower fluid layer we do not observe zero reflection. This is to be expected as non-zero reflection exists in the single-layer finite-depth scattering problem, see for example Evans & Linton (1989).

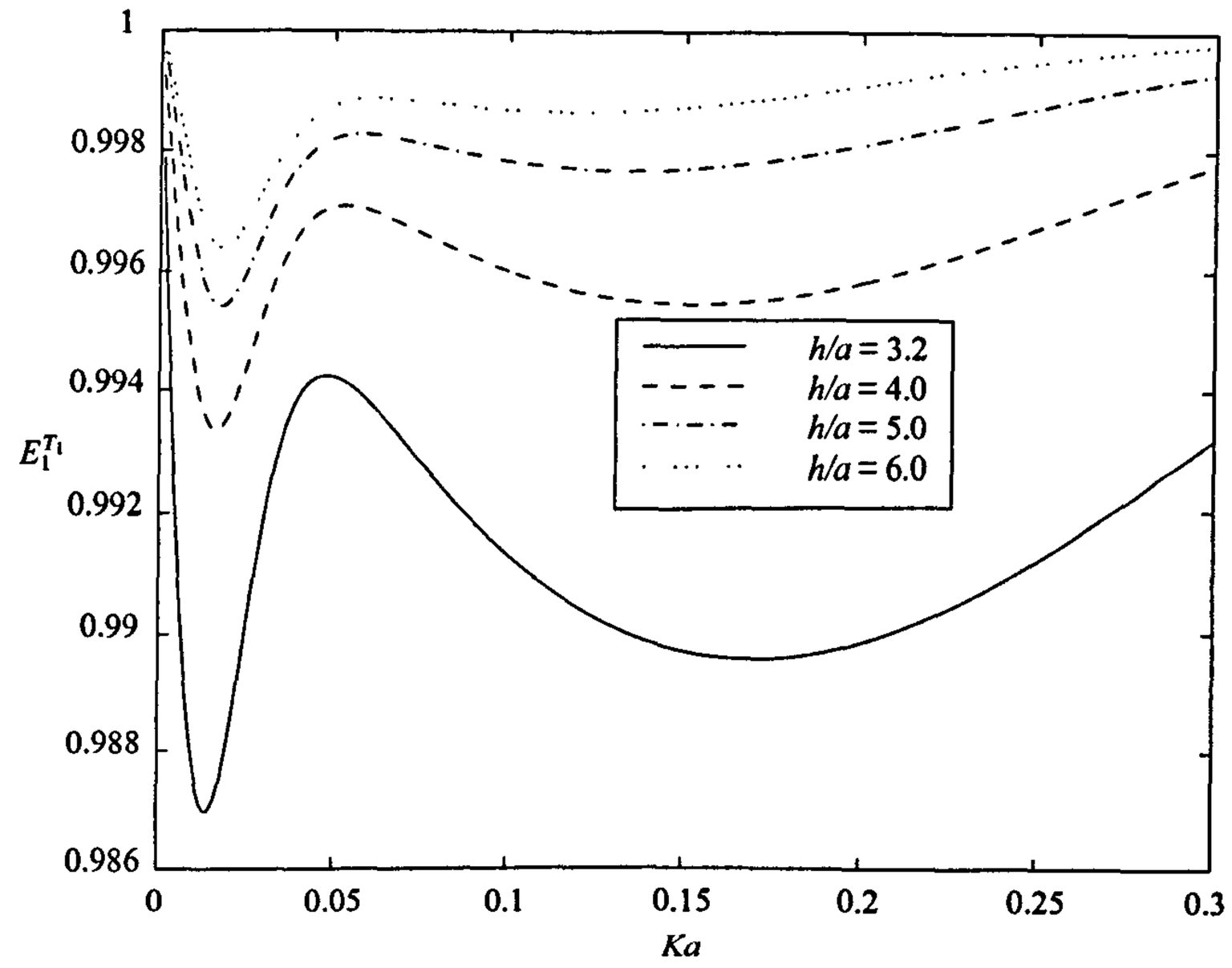

Figure 4.1: Transmitted energies due to a wave of wavenumber k_1 incident on a cylinder in the lower layer with varying depth; $\rho = 0.95$, $d/a = 2.0$ and $f/a = -2.0$.

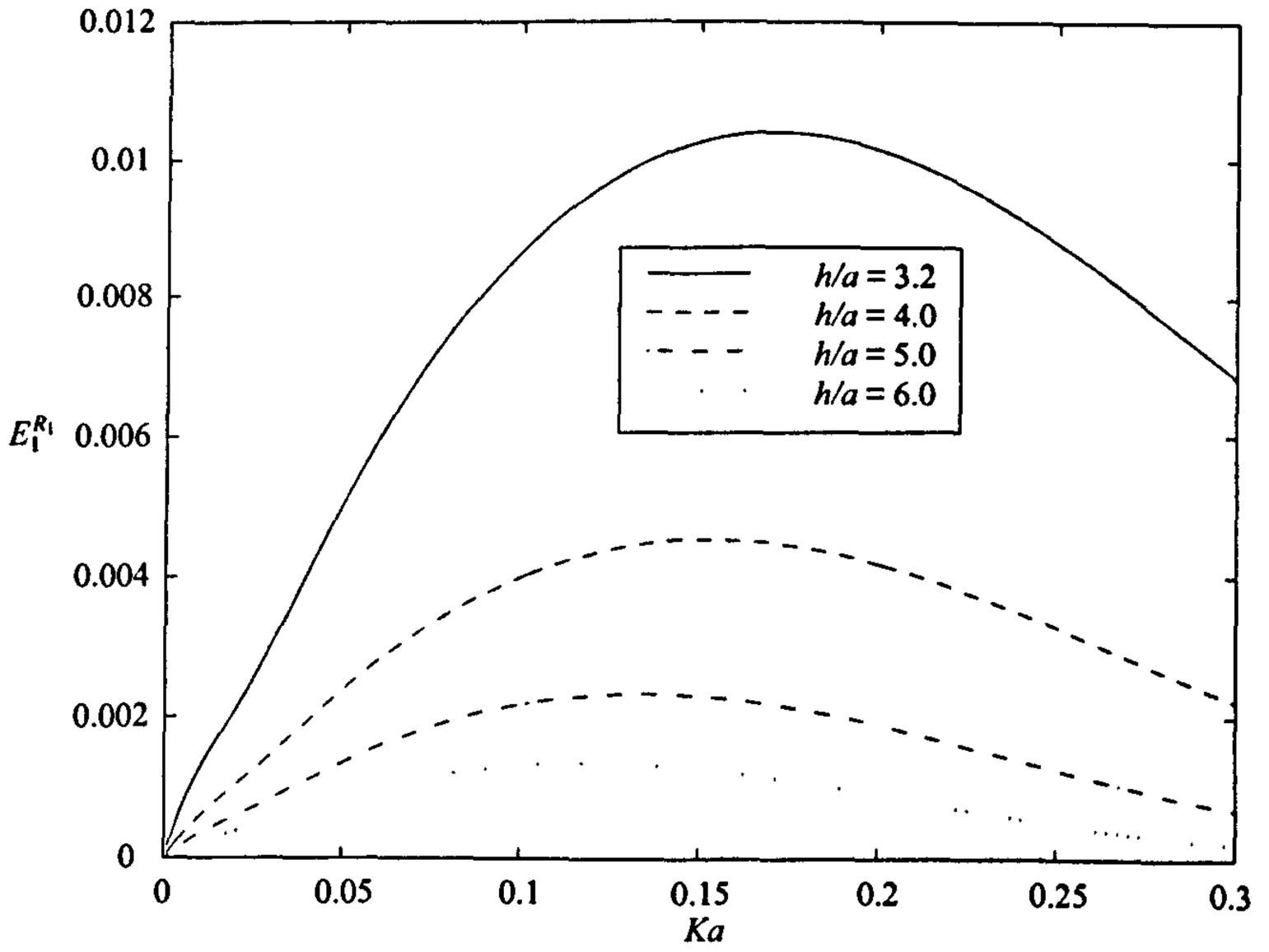

Figure 4.2: Reflected energies due to a wave of wavenumber k_1 incident on a cylinder in the lower layer with varying depth; $\rho = 0.95$, $d/a = 2.0$ and $f/a = -2.0$.

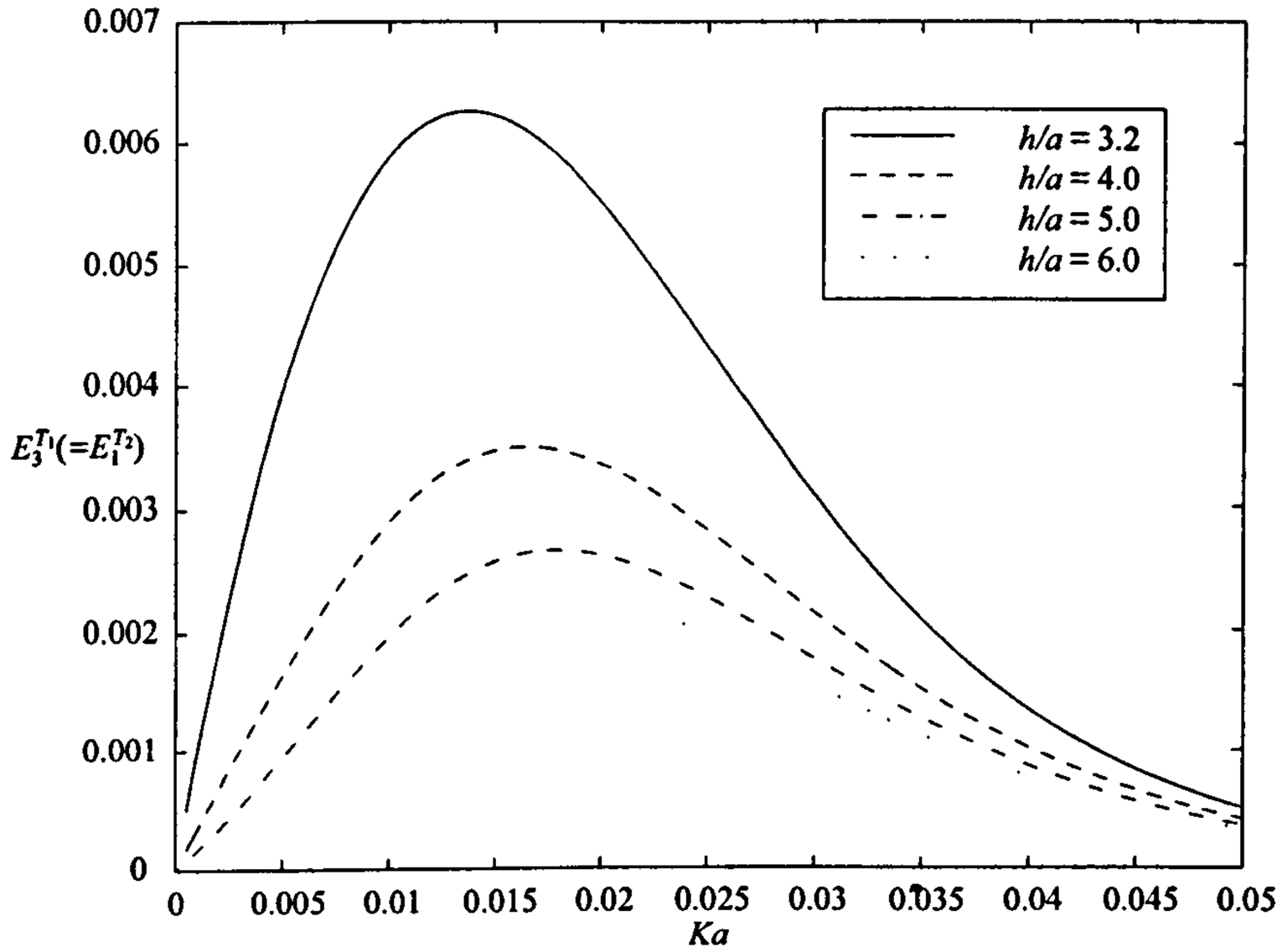

Figure 4.3: Transmitted energies due to a wave of wavenumber k_2 incident on a cylinder in the lower layer with varying depth; $\rho = 0.95$, $d/a = 2.0$ and $f/a = -2.0$.

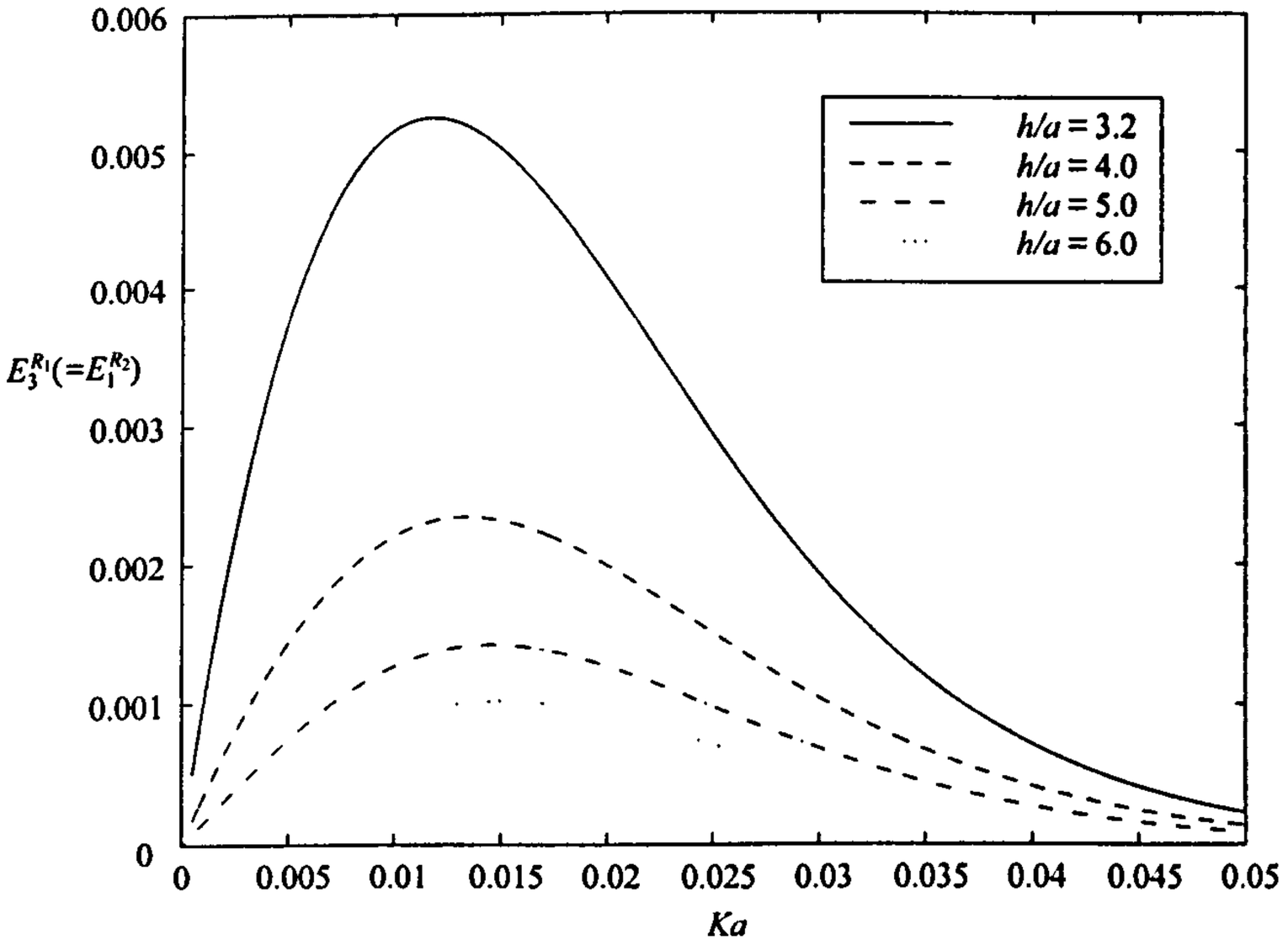

Figure 4.4: Reflected energies due to a wave of wavenumber k_2 incident on a cylinder in the lower layer with varying depth; $\rho = 0.95$, $d/a = 2.0$ and $f/a = -2.0$.

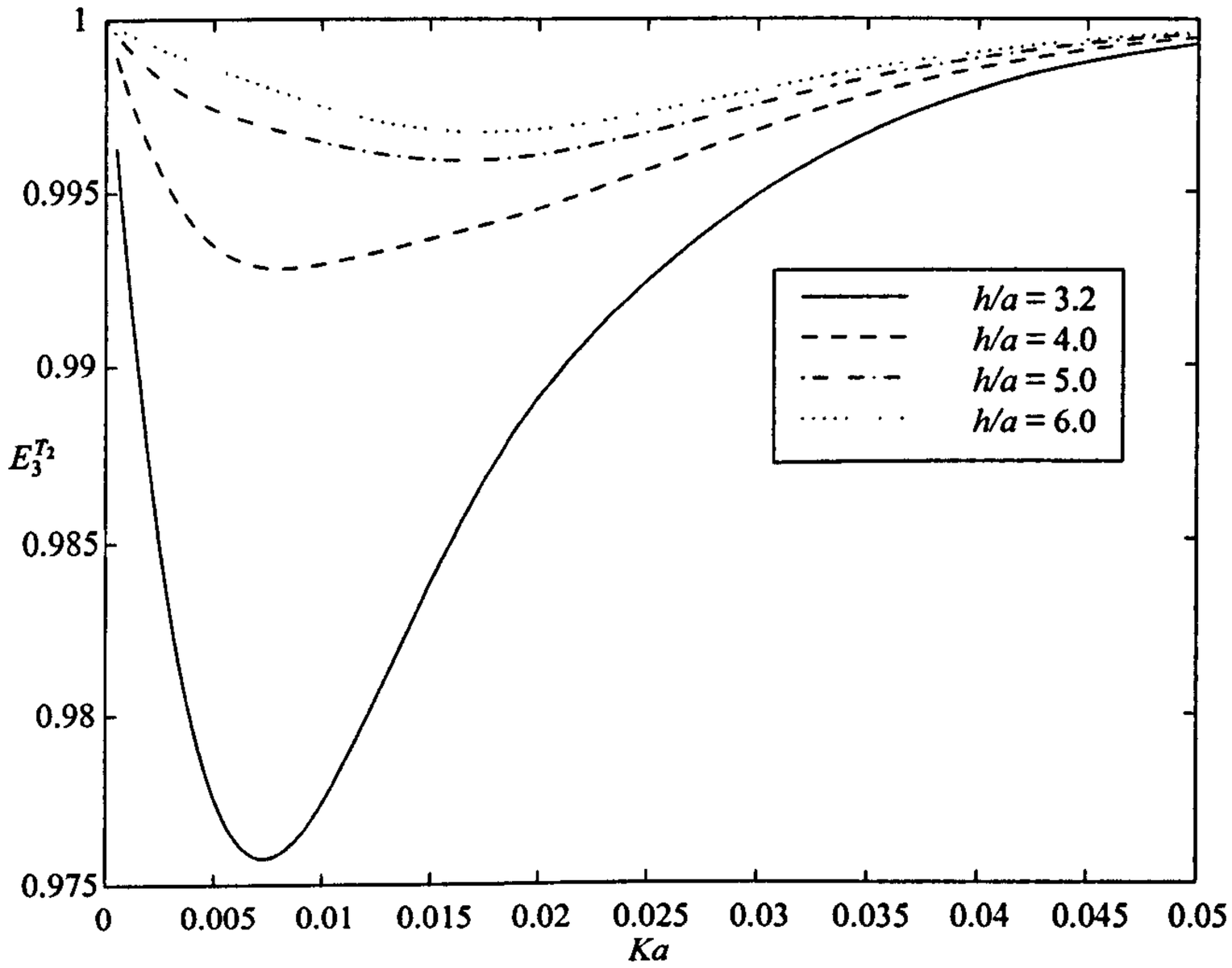

Figure 4.5: Transmitted energies due to a wave of wavenumber k_2 incident on a cylinder in the lower layer with varying depth; $\rho = 0.95$, $d/a = 2.0$ and $f/a = -2.0$.

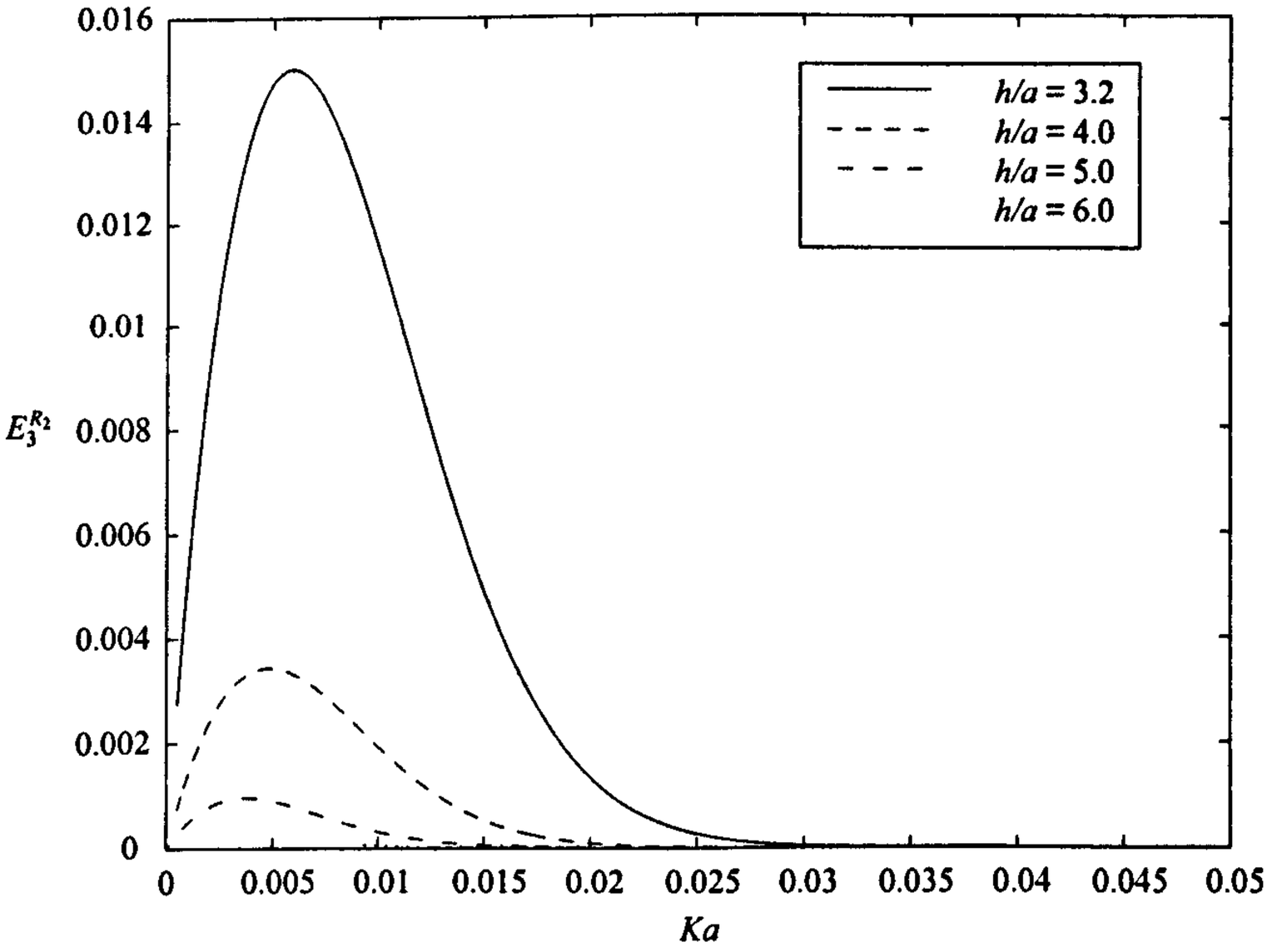

Figure 4.6: Reflected energies due to a wave of wavenumber k_2 incident on a cylinder in the lower layer with varying depth; $\rho = 0.95$, $d/a = 2.0$ and $f/a = -2.0$.

Chapter 5

Scattering of oblique waves with an infinite cylinder

5.1 Introduction

It can be shown using linear water wave theory that in infinitely deep water a submerged circular cylinder reflects no waves. This was arrived at originally by Dean (1948) and subsequently confirmed by Ursell (1950). Ogilvie (1963) further showed that a freely floating neutrally buoyant cylinder reflects no waves either. For the case of normal incidence in finite depth zero reflection does not occur, see Evans & Linton (1989).

Levine (1965) investigated whether the zero reflection result was true for obliquely incident waves and he found, using an integral equation technique, that it was not. Further, Garrison (1985) applied a Green's function procedure to compute the added-mass and damping coefficients as well as the forces on a semi-immersed circular cylinder.

In this chapter we shall solve the scattering problem of oblique waves on a circular cylinder; first in a single-layer finite-depth fluid and then in a two-layer fluid. For the single-layer fluid we will include a comparison to the results obtained by Levine (1965).

5.2 Single-layer fluid

Cartesian coordinates are chosen such that the (x, y)-plane coincides with the undisturbed free surface of the fluid and the z-axis points directly upwards. The fluid occupies the region $-h < z < 0$ and an infinite cylinder of radius a has its centre positioned at $z = f < 0$ and its generator runs parallel to the y-axis. Polar coordinates (r, θ) are

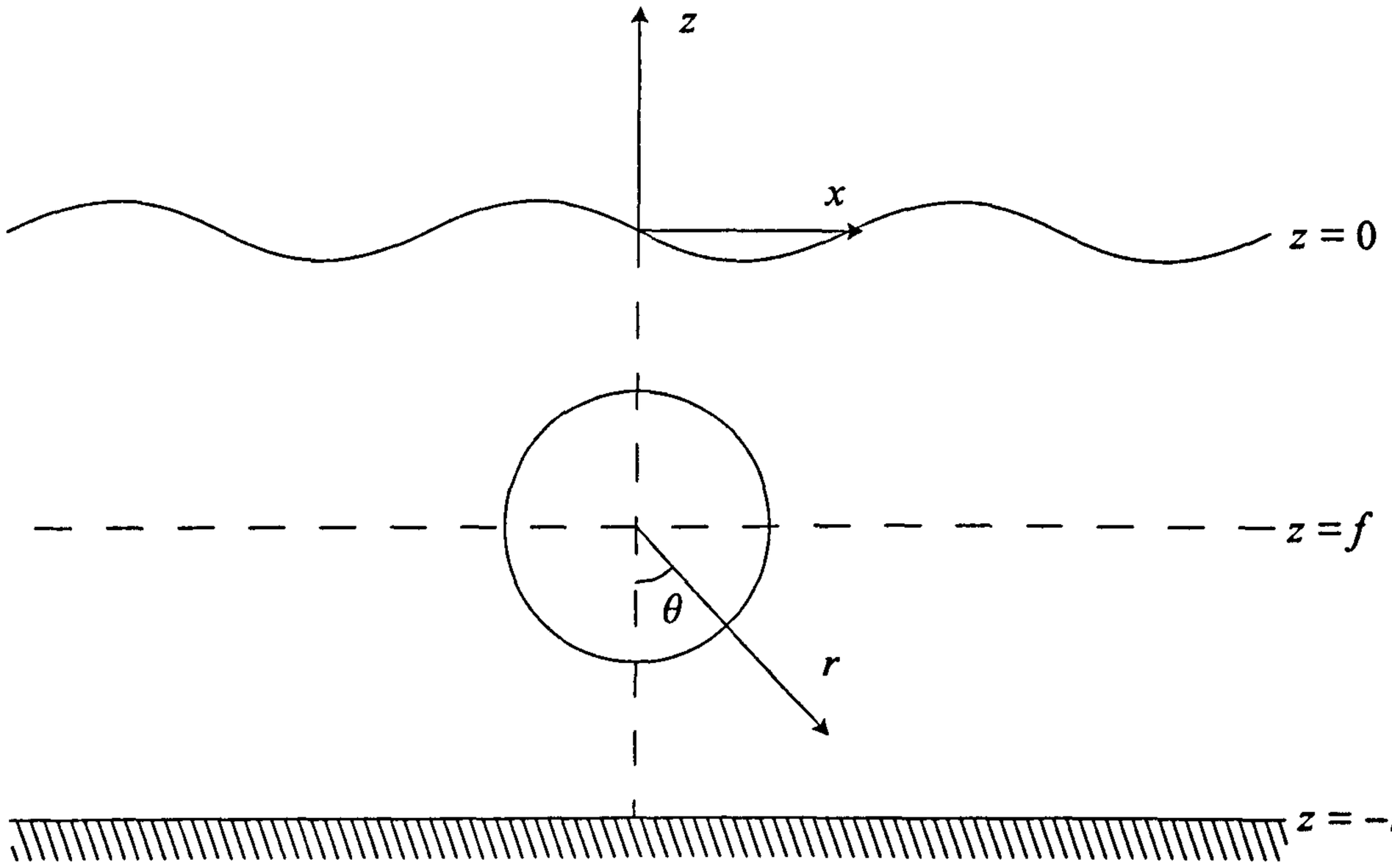

Figure 5.1: Definition sketch

defined in the (x, z)-plane where

$$x = r\sin\theta \quad \text{and} \quad z = f - r\cos\theta, \tag{5.2.1}$$

as illustrated in figure 5.1. The fluid is assumed to be inviscid and incompressible, and its motion to be irrotational. The velocity potential Φ can be written as

$$\Phi(x, y, z, t) = \Re\{\phi(x, y, z)e^{-i\omega t}\} \tag{5.2.2}$$

and must satisfy the following

$$\nabla^2\Phi = 0 \qquad \text{everywhere in the fluid,} \tag{5.2.3}$$

$$\frac{\partial\Phi}{\partial z} - K\Phi = 0 \qquad \text{on } z = 0, \tag{5.2.4}$$

$$\frac{\partial\Phi}{\partial z} = 0 \qquad \text{on } z = -h, \tag{5.2.5}$$

$$\frac{\partial\Phi}{\partial r} = 0 \qquad \text{on } r = a. \tag{5.2.6}$$

Solutions to these equations which represent horizontally travelling waves with wavenumber k can be found provided k is a solution of the dispersion relation, given by

$$K = k\tanh kh, \tag{5.2.7}$$

where $k = K$ for the infinite-depth case. The time independent potential $\phi_{\text{inc}}(x, y, z)$ of an obliquely incident plane wave Φ_{inc} with angle α_{inc} to the positive x-axis takes the

form

$$\phi_{\text{inc}} = e^{ik(x\cos\alpha_{\text{inc}}+y\sin\alpha_{\text{inc}})}\frac{\cosh k(z+h)}{\cosh kh} = e^{ikx\cos\alpha_{\text{inc}}}e^{ily}\frac{\cosh k(z+h)}{\cosh kh}, \tag{5.2.8}$$

where $l = k\sin\alpha_{\text{inc}}$. We can now redefine the potentials Φ_{inc} and ϕ_{inc} as

$$\Phi_{\text{inc}} = \Re\{\phi_{\text{inc}}(x,z)e^{ily}e^{-i\omega t}\} \tag{5.2.9}$$

$$\phi_{\text{inc}} = e^{iKx\cos\alpha_{\text{inc}}}\frac{\cosh k(z+h)}{\cosh kh}. \tag{5.2.10}$$

We shall now assume that the same can be done with the scattered field thus the problem is reduced to two dimensions. We now redefine the velocity potential as

$$\Phi = \Re\{\phi(x,z)e^{ily}e^{-i\omega t}\}. \tag{5.2.11}$$

All the conditions for Φ apply for ϕ except for Laplace's equation, which becomes

$$(\nabla^2 - l^2)\phi = 0 \tag{5.2.12}$$

everywhere in the fluid. This is known as the modified Helmholtz equation. A general scattered potential has far-field behaviour described by

$$\phi \sim (A^{\pm}e^{\pm i\beta x} + B^{\pm}e^{\mp i\beta x})\frac{\cosh k(z+h)}{\cosh kh} \tag{5.2.13}$$

as $x \to \pm\infty$, where $A^{\pm}$ and $B^{\pm}$ are the coefficients of outgoing and incoming waves respectively. To find β we apply the modified Helmholtz equation to the give

$$\beta = \sqrt{k^2 - l^2} = k\sqrt{1-\sin^2\alpha_{\text{inc}}} = k\cos\alpha_{\text{inc}}. \tag{5.2.14}$$

Hence all waves propagate at an angle α_{inc} to the x-axis, see figure 5.2. We can use the following shorthand to represent the potential

$$\phi \sim \{A^-, B^-; A^+, B^+\}. \tag{5.2.15}$$

5.2.1 Hydrodynamic relations

Let us consider two potentials ϕ and ψ which are solutions to two different problems involving submerged bodies. As both potentials satisfy the modified Helmholtz equation Green's theorem becomes

$$\int_s \left(\phi\frac{\partial\psi}{\partial n} - \psi\frac{\partial\phi}{\partial n}\right) ds = 0 \tag{5.2.16}$$

where S is the boundary around the entire fluid and $\mathbf{n}$ the outward normal. Due to the bottom condition, $\phi_z = 0$ on $z = -h$ and the free-surface condition, $\phi_z = K\phi$ on $z = 0$ equation (5.2.16) becomes

$$\int_{S_B} \left(\phi\frac{\partial\psi}{\partial n} - \psi\frac{\partial\phi}{\partial n}\right) ds = \lim_{M\to\infty} \int_{-h}^{0} \left(\phi\frac{\partial\psi}{\partial x} - \psi\frac{\partial\phi}{\partial x}\right)\Bigg|_{x=-M} dz - \lim_{L\to\infty} \int_{-h}^{0} \left(\phi\frac{\partial\psi}{\partial x} - \psi\frac{\partial\phi}{\partial x}\right)\Bigg|_{x=L} dz, \quad (5.2.17)$$

where S_B is the boundary of the bodies. Now if we let

$$\phi = \phi_i \sim \{A_i^-, B_i^-; A_i^+, B_i^+\}, \quad (5.2.18)$$

$$\psi = \phi_j \sim \{A_j^-, B_j^-; A_j^+, B_j^+\} \quad (5.2.19)$$

and use (5.2.17) we obtain

$$\int_{S_B} \left(\phi\frac{\partial\psi}{\partial n} - \psi\frac{\partial\phi}{\partial n}\right) ds = \frac{i\beta}{\cosh^2(kh)}\left(h + \frac{\sinh 2kh}{2k}\right)(A_i^- B_j^- + A_i^+ B_j^+ - B_i^+ A_j^+ - B_i^- A_j^-). \quad (5.2.20)$$

If we now let $\psi = \overline{\phi_i}$ then (5.2.17) gives

$$\int_{S_B} \left(\phi\frac{\partial\psi}{\partial n} - \psi\frac{\partial\phi}{\partial n}\right) ds = \frac{i\beta}{\cosh^2(kh)}\left(h + \frac{\sinh 2kh}{2k}\right)(|A_i^-|^2 + |A_i^+|^2 - |B_i^+|^2 - |B_i^-|^2). \quad (5.2.21)$$

We shall now consider the scattering problem as shown in figure 5.2, where the incident wave travels in the positive x- and y-direction. We can write the scattering potential as

$$\phi \sim \{R, 1; T, 0\}, \quad (5.2.22)$$

where R and T are the reflection and transmission coefficients respectively. Using (5.2.21) we obtain

$$|R|^2 + |T|^2 = 1, \quad (5.2.23)$$

which corresponds to conservation of energy.

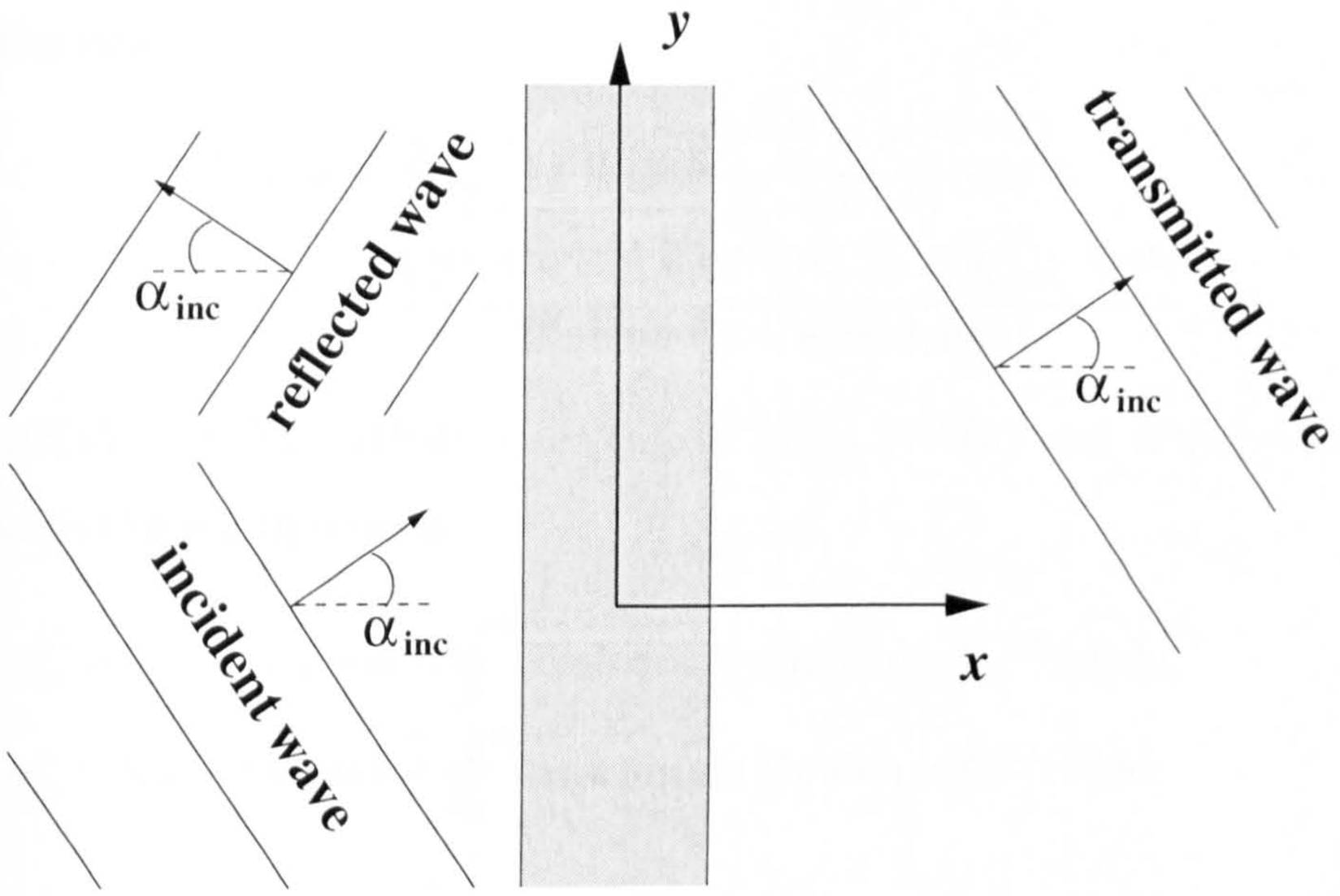

Figure 5.2: Scattering of an obliquely incident wave by a horizontal circular cylinder

5.2.2 Construction of multipoles

Symmetric and antisymmetric solutions to the modified Helmholtz equation, $(\nabla^2 - l^2)\phi(r,\theta) = 0$, which are singular at $r = 0$ are

$$K_m(lr)\cos m\theta \quad \text{and} \quad K_m(lr)\sin m\theta, \tag{5.2.24}$$

where K_m is the m^{th} order modified Bessel function. These solutions have the following integral representations

$$K_m(lr)\cos m\theta = \begin{cases} (-1)^m \int_0^\infty \cosh mu \cos(lx\sinh u) e^{-l(z-f)\cosh u} du, & z > f \\ \int_0^\infty \cosh mu \cos(lx\sinh u) e^{-l(f-z)\cosh u} du, & z < f \end{cases}, \tag{5.2.25}$$

$$K_m(lr)\sin m\theta = \begin{cases} (-1)^{m+1} \int_0^\infty \sinh mu \sin(lx\sinh u) e^{-l(z-f)\cosh u} du, & z > f \\ \int_0^\infty \sinh mu \sin(lx\sinh u) e^{-l(f-z)\cosh u} du, & z < f \end{cases}. \tag{5.2.26}$$

See appendix D for the derivation of these. Symmetric and antisymmetric multipoles ϕ_m^s and ϕ_m^a respectively will take the form

$$\phi_m^s = K_m(lr)\cos m\theta + \int_0^\infty \cosh mu \cos(lx\sinh u)[e^{vz}A^s(u) + e^{-vz}B^s(u)]du, \tag{5.2.27}$$

$$\phi_m^a = K_m(lr)\sin m\theta + \int_0^\infty \sinh mu \sin(lx\sinh u)[e^{vz}A^a(u) + e^{-vz}B^a(u)]du, \tag{5.2.28}$$

where $v = l\cosh u$. To find the functions $A^s(u)$, $A^a(u)$ and $B^s(u)$, $B^a(u)$ we need to apply the free-surface and bottom conditions and use (5.2.25) and (5.2.26). We obtain

the following functions

$$A^{(q)}(u) = \frac{(v+K)[(-1)^{m+q}e^{v(f+h)} + e^{-v(f+h)}]}{2(v\sinh vh - K\cosh vh)}, \tag{5.2.29}$$

$$B^{(q)}(u) = \frac{(-1)^{m+q}(v+K)e^{v(f-h)} + (v-K)e^{-v(f+h)}}{2(v\sinh vh - K\cosh vh)}, \tag{5.2.30}$$

such that $A^s(u) = A^{(0)}(u)$, $A^a(u) = A^{(1)}(u)$, $B^s(u) = B^{(0)}(u)$ and $B^a(u) = B^{(1)}(u)$. We will now write the multipoles as

$$\phi_m^s = K_m(lr)\cos m\theta + \int_0^\infty \cosh mu \cos(lx\sinh u)C^{(0)}(u)du, \tag{5.2.31}$$

$$\phi_m^a = K_m(lr)\sin m\theta + \int_0^\infty \sinh mu \sin(lx\sinh u)C^{(1)}(u)du, \tag{5.2.32}$$

where

$$C^{(q)}(u) = \frac{(-1)^{m+q}e^{vf}(v+K)\cosh v(z+h) + e^{-v(f+h)}(v\cosh vz + K\sinh vz)}{v\sinh vh - K\cosh vh}, \tag{5.2.33}$$

$$\to (-1)^{m+q}\frac{v+K}{v-K}e^{v(z+f)}, \qquad \text{as } h\to\infty, \tag{5.2.34}$$

and the path of integration is indented to pass beneath the pole at $u = \gamma$, such that

$$\cosh\gamma = \frac{1}{\sin\alpha_{\text{inc}}} \quad \text{and} \quad \sinh\gamma = \cot\alpha_{\text{inc}}. \tag{5.2.35}$$

The far-field form of the multipoles is given by

$$\phi_m^s \sim \pi i \cosh m\gamma e^{\pm i\beta x}C^{(0)\gamma}, \tag{5.2.36}$$

$$\phi_m^a \sim \pm\pi \sinh m\gamma e^{\pm i\beta x}C^{(1)\gamma}, \tag{5.2.37}$$

as $x \to \pm\infty$, where $C^{(q)\gamma}$ is the residue of $C^{(q)}(u)$ at $u = \gamma$ which is

$$C^{(q)\gamma} = \frac{(k\cosh kz + K\sinh kz)e^{-k(f+h)} + (-1)^{m+q}\cosh k(z+h)(k+K)e^{kf}}{\beta[(1-Kh)\sinh kh + kh\cosh kh]}. \tag{5.2.38}$$

The multipoles defined in (5.2.31) and (5.2.32) can be expanded about $r = 0$ in cylindrical polar coordinates, see figure 5.1, using the identities

$$e^{\pm l(f-z)\cosh u}\cos(lx\sinh u) = \sum_{n=0}^{\infty}(\pm 1)^n\epsilon_n\cosh nu\cos n\theta I_n(lr) \tag{5.2.39}$$

$$e^{\pm l(f-z)\cosh u}\sin(lx\sinh u) = 2\sum_{n=1}^{\infty}(\pm 1)^{n+1}\sinh nu\sin n\theta I_n(lr), \tag{5.2.40}$$

where $\epsilon_0 = 1$ and $\epsilon_n = 2$ for $n \neq 0$. These identities were derived from (D.8) by letting $r' = r$ and $\theta' = \theta$ and then $\theta' = \pi - \theta$. Using the above expansions with (5.2.31) and

(5.2.32) we obtain

$$\phi_m^s = K_m(lr)\cos m\theta + \sum_{n=0}^{\infty} A_{mn}^s I_n(lr)\cos n\theta, \tag{5.2.41}$$

$$\phi_m^a = K_m(lr)\sin m\theta + \sum_{n=1}^{\infty} A_{mn}^a I_n(lr)\sin n\theta, \tag{5.2.42}$$

where

$$A_{mn}^s = \frac{\epsilon_n}{2}\int_0^{\infty} \cosh mu \cosh nu\, D^{(0)}(u)du, \tag{5.2.43}$$

$$A_{mn}^a = \int_0^{\infty} \sinh mu \sinh nu\, D^{(1)}(u)du, \tag{5.2.44}$$

and

$$\begin{aligned} D^{(q)}(u) =& (((-1)^q(v+K)[(-1)^n+(-1)^m]+(v-K)e^{-2vf})e^{-vh} \\ &+ (-1)^{m+n}(v+K)e^{v(2f+h)})/(v\sinh vh - K\cosh vh), \end{aligned} \tag{5.2.45}$$

$$\rightarrow (-1)^{m+n}2e^{2vf}\frac{v+K}{v-K} \qquad \text{as } h\rightarrow\infty. \tag{5.2.46}$$

5.2.3 Formulation of problem

To solve the scattering problem for an incident plane wave from $x = -\infty$ we write

$$\phi = \phi_{\text{inc}} + \sum_{m=0}^{\infty}(\alpha_m\phi_m^a + \beta_m\phi_m^s), \tag{5.2.47}$$

where α_0 is included for convenience even though ϕ_0^a is zero. The incident wave potential ϕ_{inc} can be expanded in polar coordinates using (5.2.39) and (5.2.40) with $u = \gamma$, to give

$$\phi_{\text{inc}} = e^{i\beta x}\frac{\cosh k(z+h)}{\cosh kh}, \tag{5.2.48}$$

$$\begin{aligned} =& \frac{1}{2\cosh kh}\sum_{m=0}^{\infty}\epsilon_m I_m(lr)[((-1)^m e^{k(f+h)} + e^{-k(f+h)})\cos m\theta\cosh m\gamma \\ &+ i((-1)^{m+1}e^{k(f+h)} + e^{-k(f+h)})\sin m\theta\sinh m\gamma]. \end{aligned} \tag{5.2.49}$$

Applying the body boundary condition, $\partial\phi/\partial r = 0$ on $r = a$, to (5.2.47) and substituting in the forms of the multipoles (5.2.41)–(5.2.42) and of the incident wave (5.2.48) we

obtain

$$\sum_{m=1}^{\infty}\alpha_m\left(K'_m(la)\sin m\theta+\sum_{n=1}^{\infty}A^a_{mn}I'_n(la)\sin n\theta\right)$$
$$+\sum_{m=1}^{\infty}\beta_m\left(K'_m(la)\cos m\theta+\sum_{n=0}^{\infty}A^s_{mn}I'_n(la)\cos n\theta\right)$$
$$=-\frac{1}{2\cosh kh}\sum_{m=0}^{\infty}\epsilon_m I'_m(la)[((-1)^m e^{k(f+h)}+e^{-k(f+h)})\cos m\theta\cosh m\gamma$$
$$+i((-1)^{m+1}e^{k(f+h)}+e^{-k(f+h)})\sin m\theta\sinh m\gamma]. \quad (5.2.50)$$

Using the orthogonality of the trigonometric functions we find that the α_n and β_n satisfy the following infinite systems of equations

$$\alpha_n+\frac{I'_n(la)}{K'_n(la)}\sum_{m=1}^{\infty}\alpha_m A^a_{mn}=\frac{i\sinh n\gamma\, I'_n(la)}{\cosh kh\, K'_n(la)}((-1)^n e^{k(f+h)}-e^{-k(f+h)}) \qquad n\geq 1, \quad (5.2.51)$$

$$\beta_n+\frac{I'_n(la)}{K'_n(la)}\sum_{m=0}^{\infty}\beta_m A^s_{mn}=\frac{\epsilon_n\cosh n\gamma\, I'_n(la)}{2\cosh kh\, K'_n(la)}((-1)^{n+1}e^{k(f+h)}-e^{-k(f+h)}) \quad n\geq 0. \quad (5.2.52)$$

These systems can be solved as before using a truncation procedure. For most of the computations presented below two 4×4 systems were solved to obtain the coefficients α_m and β_m to three decimal places. For small $|f/a|$ some results required 16×16 systems to obtain the same accuracy.

We can extract the reflection and transmission coefficients from the asymptotic forms of the multipoles. Using (5.2.36)–(5.2.37) and (5.2.47)–(5.2.48) we obtain

$$T=1+\frac{\pi(k+K)}{\beta((1-Kh)\tanh kh+kh)}$$
$$\times\sum_{m=0}^{\infty}(\alpha_m\sinh m\gamma((-1)^{m+1}e^{kf}+e^{-k(f+2h)})+i\beta_m\cosh m\gamma((-1)^m e^{kf}+e^{-k(f+2h)})), \quad (5.2.53)$$

and

$$R=\frac{\pi(k+K)}{\beta((1-Kh)\tanh kh+kh)}$$
$$\times\sum_{m=0}^{\infty}(\alpha_m\sinh m\gamma((-1)^m e^{kf}-e^{-k(f+2h)})+i\beta_m\cosh m\gamma((-1)^m e^{kf}+e^{-k(f+2h)})). \quad (5.2.54)$$

Values of these can be checked using the conservation of energy equation (5.2.23).

For the case of infinite depth we can redo the analysis above or simply let $h \to \infty$ in the equations above. The systems of equations which must be solved are given by

$$\alpha_n + \frac{I_n'(la)}{K_n'(la)} \sum_{m=1}^{\infty} \alpha_m A_{mn}^a = (-1)^n 2i \frac{I_n'(la)}{K_n'(la)} e^{Kf} \sinh n\gamma, \qquad n = 1, 2, \ldots, \tag{5.2.55}$$

$$\beta_n + \frac{I_n'(la)}{K_n'(la)} \sum_{m=0}^{\infty} \beta_m A_{mn}^s = (-1)^{n+1} \epsilon_n \frac{I_n'(la)}{K_n'(la)} e^{Kf} \cosh n\gamma, \quad n = 0, 1, \ldots, \tag{5.2.56}$$

where

$$A_{mn}^s = (-1)^{m+n} \epsilon_n \int_0^{\infty} \cosh mu \cosh nu \, e^{2lf \cosh u} \frac{l \cosh u + K}{l \cosh u - K} du, \tag{5.2.57}$$

$$A_{mn}^a = (-1)^{m+n} 2 \int_0^{\infty} \sinh mu \sinh nu \, e^{2lf \cosh u} \frac{l \cosh u + K}{l \cosh u - K} du. \tag{5.2.58}$$

The transmission and reflection coefficients are given by

$$R = \frac{2\pi e^{Kf}}{\cos \alpha_{\text{inc}}} \sum_{m=0}^{\infty} (-1)^m \left[\alpha_m \sinh m\gamma + i\beta_m \cosh m\gamma \right], \tag{5.2.59}$$

$$T = 1 - \frac{2\pi e^{Kf}}{\cos \alpha_{\text{inc}}} \sum_{m=0}^{\infty} (-1)^m \left[\alpha_m \sinh m\gamma - i\beta_m \cosh m\gamma \right]. \tag{5.2.60}$$

Again values computed of these can be checked using the conservation of energy equation (5.2.23).

5.2.4 Results

Curves of the transmission energy $|T|^2$ for a cylinder in finite depth interacting with oblique waves are shown in figures 5.3–5.5. Graphs of the reflection energy have been omitted because they are easily obtainable from the conservation of energy equation, i.e. $|R|^2 = 1 - |T|^2$. To clearly illustrate the results they have been plotted on a log scale. The convergence of the results is much slower for small $|f/a|$ and high frequencies and so for some results 16×16 systems were solved to obtained 3 decimal place accuracy.

Figure 5.3 shows the transmission energy for different submersion depths, f/a, of the cylinder, -1.1, -1.2, -1.25 and -1.5. The angle of incidence, α_{inc}, is fixed at 1.1 ($\approx 63°$) and the depth of the fluid, h/a, is 3. For the case of the cylinder close to the free surface, $f/a = -1.1$, we see there are two local minimums and also at $Ka \approx 0.6$ there is a point of full transmission. For normal incidence waves in an infinite-depth fluid all the wave energy is transmitted so this is not a surprising result. As the cylinder is positioned deeper in the fluid we notice the frequency of full transmission increases as does that of the second minimum. For cylinders which are sufficiently deep the second

minimum vanishes altogether. Computations suggest that as the cylinder becomes closer to the free surface $f/a \to -1$ the number of frequencies at which $|T|^2 = 1$ will increase indefinitely.

Figure 5.4 shows the transmission energy for different angles, α_{inc}, of the incident wave, 0.9, 1.1, 1.3 and 1.4 covering the range between about 50° and 80°. The cylinder is submerged at $f/a = -1.2$ and the depth of the fluid is $h/a = 3$. We see there are three local minimums for this case. As the angle of incidence is increased we see the transmitted energy decreases.

Figure 5.5 shows transmission energies for different depths, h/a, of the fluid, 2.2, 2.5, 3 and 5. Here $f/a = -1.1$ and $\alpha_{\text{inc}} = 1.1$. For the case $h/a = 2.2$ we have the bottom and the free surface an equal distance, $0.1a$, from the surface of the cylinder. We notice there are two minimums and that as the depth of the fluid increases the second minimum decreases whereas the first decreases to begin with and then increases.

The behaviour is quite complicated but we can conclude from these graphs that for a cylinder sufficiently close to the free surface there will be a number of frequencies at which $|T|^2 = 1$. The greater the angle of incidence the less energy is transmitted.

Figure 5.6 shows transmission energies for infinite depth calculated by the multipole method (solid curves) and by the first approximation given by Levine (1965) (dashed curves). The two methods produce very similar results especially so for low frequencies $Ka \lesssim 0.4$ as convergence is quicker. For shallower submergence of the cylinder and incident angles closer to grazing the first approximation becomes less accurate.

5.2.5 Conclusion

In this chapter we have considered the scattering of oblique waves in a single-layer finite-depth fluid. We reduced the problem to two dimensions and then derived the classical expression of conservation of energy using Green's theorem. We then used the multipole method to solve the scattering problem for a horizontal circular cylinder. For normal incidence waves on a cylinder in deep water it is known that all the wave energy is transmitted. The presence of finite depth causes some of the wave energy to be reflected. Oblique incident waves are reflected more than normal incident waves and as the angle increases the reflection increases. For cylinders close to the free surface there are a number of frequencies at which full transmission occurs, the quantity of which increases as the submergence of the cylinder decreases.

The multipole method has again been shown to be an efficient way of solving such problems. However for small submergence and depth of the fluid quite large truncation parameters were required to attain the required accuracy. In Levine (1965) the infinite-depth case is considered and a first approximation of the solution described. By comparison to the results obtained by the multipole method we found the method in Levine (1965) to be a good estimation of the transmission and reflection coefficients when the cylinder is not close to the free surface.

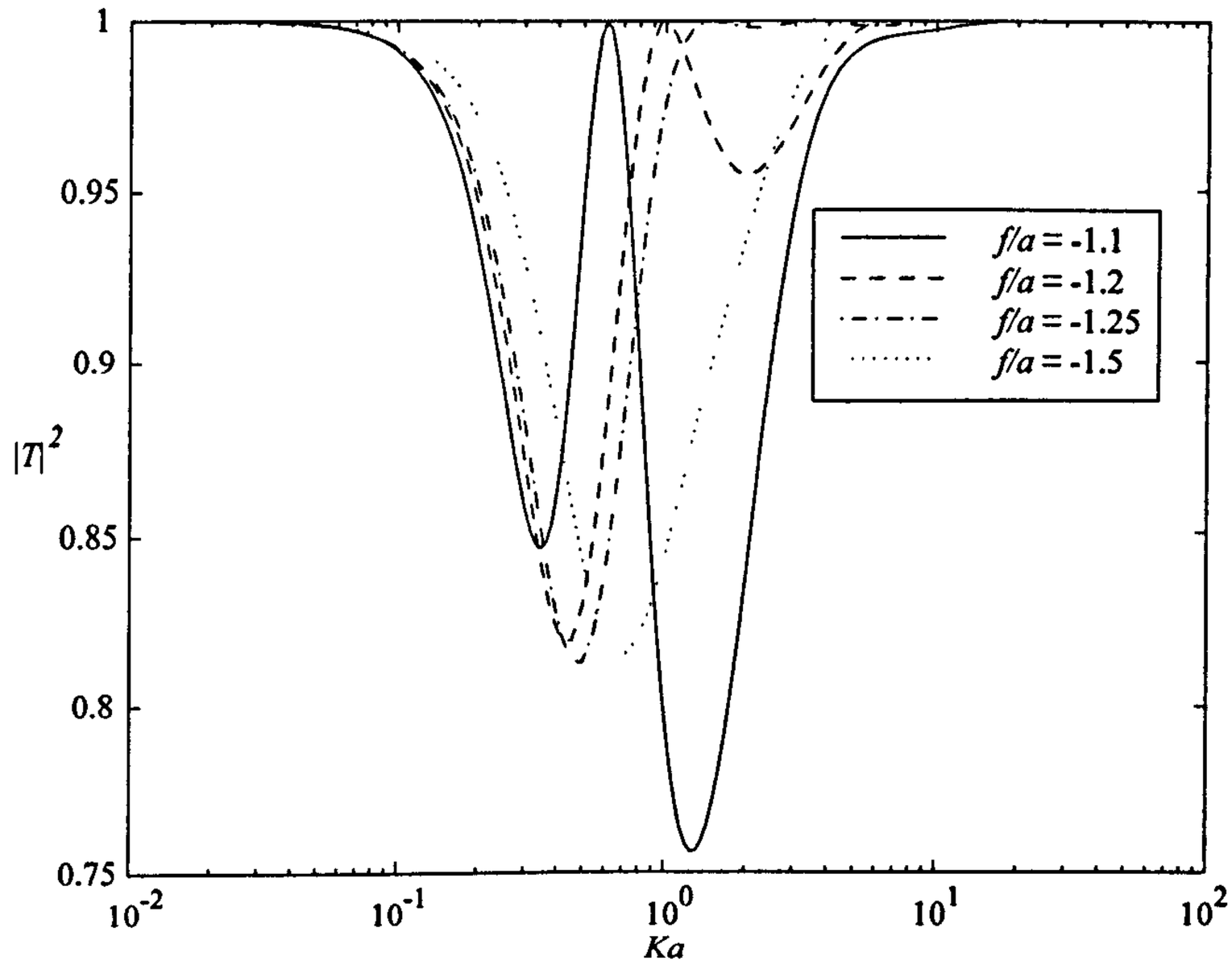

Figure 5.3: Transmission energies due to oblique plane waves incident on a cylinder with varying submergence; $h/a = 3$ and $\alpha_{\text{inc}} = 1.1$.

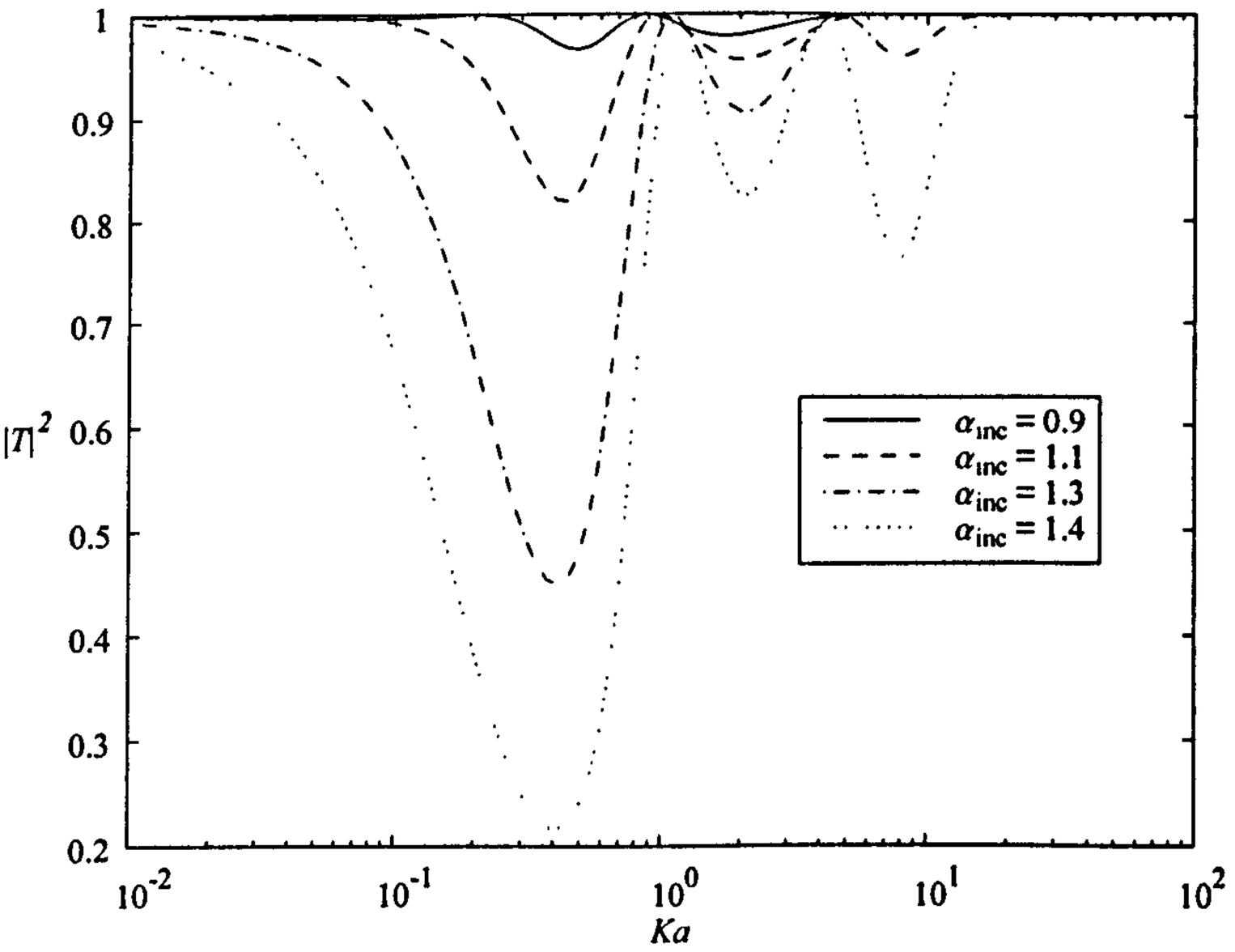

Figure 5.4: Transmission energies due to oblique plane waves with varying angle of incidence on a cylinder; $h/a = 3$ and $f/a = -1.2$.

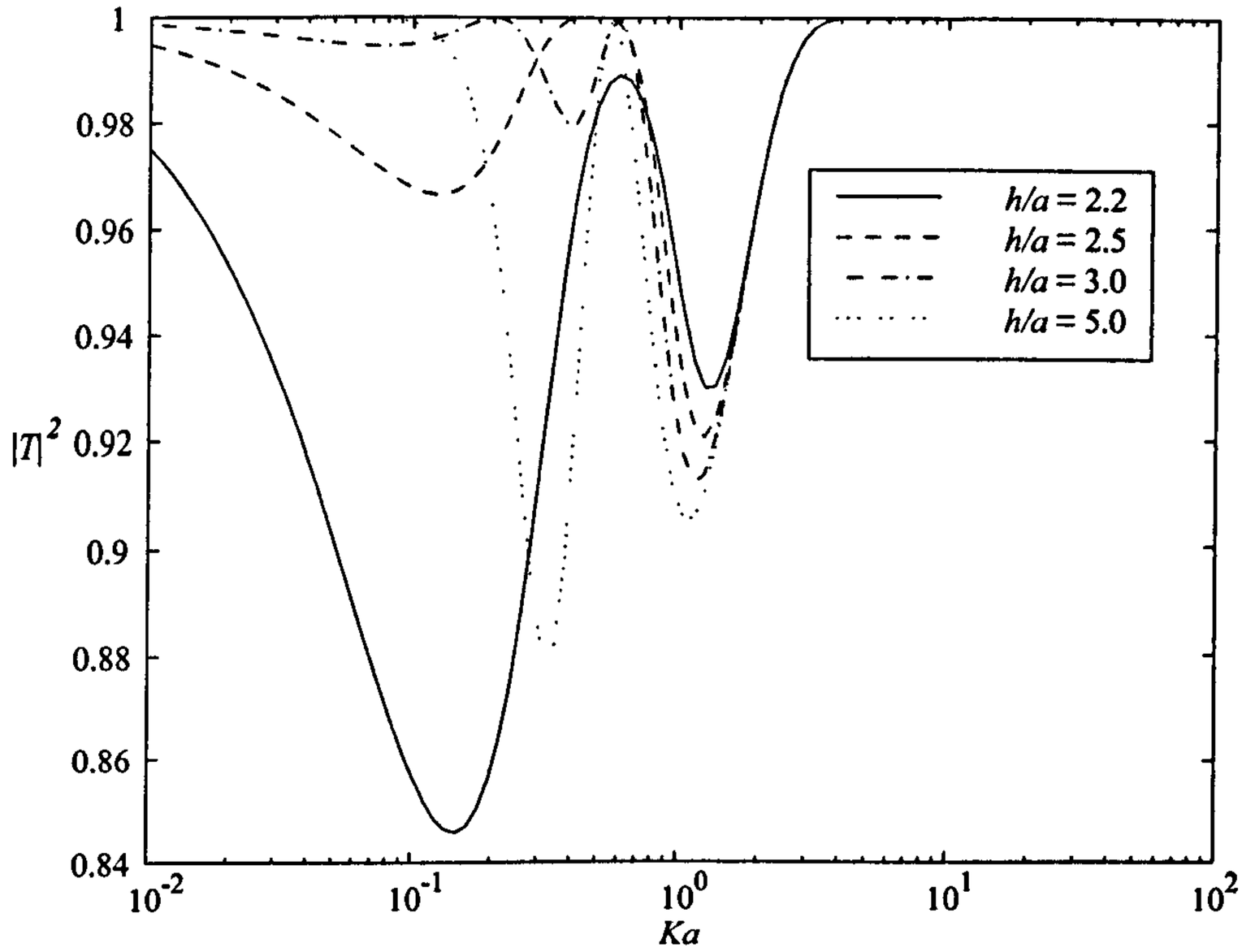

Figure 5.5: Transmission energies due to oblique plane waves incident on a cylinder with varying depth of the fluid; $f/a = -1.1$ and $\alpha_{\text{inc}} = 1.1$.

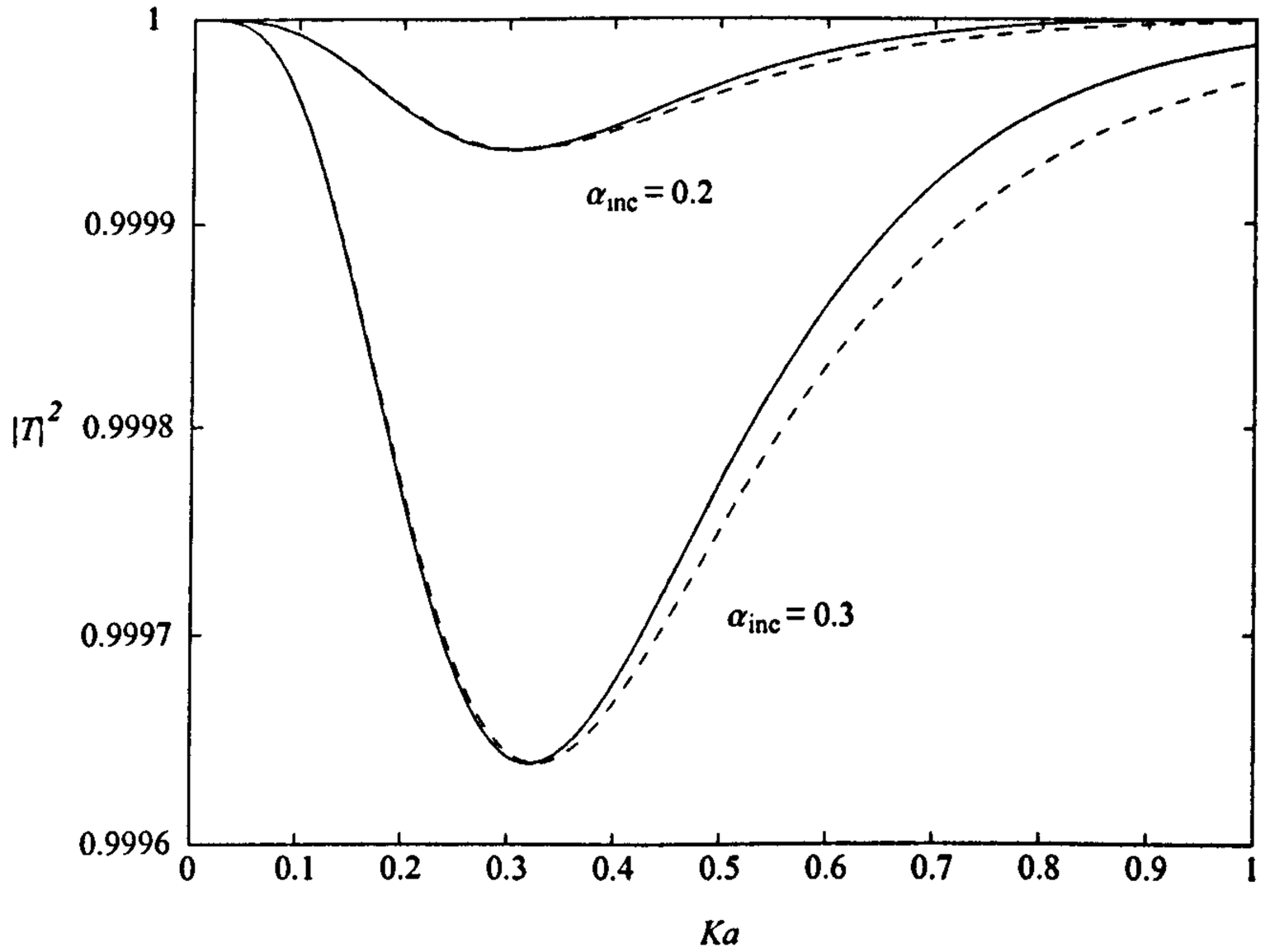

Figure 5.6: Transmission energies due to oblique plane waves with varying angle of incidence on a cylinder in infinite depth; $f/a = -2$. Multipole method (solid curves) and Levine's first approximation (dashed curves).

5.3 Two-layer fluid

We will now consider the case of oblique waves in a two-layer fluid where the lower fluid is infinitely deep. Cartesian coordinates are chosen such that the (x, y)-plane coincides with the undisturbed interface between the two fluids. The z-axis points directly upwards where $z = 0$ describes the interface and $z = d > 0$ describes the free surface. An infinite cylinder of radius a is positioned at $z = f$ and its generator runs parallel to the y-axis. Polar coordinates (r, θ) are defined in the (x, z)-plane where

$$x = r\sin\theta \quad \text{and} \quad z = f - r\cos\theta. \tag{5.3.1}$$

We shall assume that the velocity potentials are in the form

$$\Phi = \Re\{\phi(x, z)e^{ily}e^{-i\omega t}\} \tag{5.3.2}$$

where ϕ satisfies the conditions (2.2.3)–(2.2.5) and the modified Helmholtz equation (5.2.12). The dispersion relation has two solutions as before which are K and k where $k(> K)$ is given by (2.2.11).

An obliquely incident plane wave ϕ_{inc} of wavenumber K with angle α_{inc} to the positive x-axis has the form

$$\phi_{\text{inc}} = e^{iKx\cos\alpha_{\text{inc}}}e^{Kz}. \tag{5.3.3}$$

From the modified Helmholtz equation we find that $l = K\sin\alpha_{\text{inc}}$. A general scattered potential has the far-field behaviour described by

$$\phi^I \sim A^{\pm}e^{\pm i\beta x}e^{Kz} + B^{\pm}e^{\pm ibx}g(z) + C^{\pm}e^{\mp i\beta x}e^{Kz} + D^{\pm}e^{\mp ibx}g(z), \tag{5.3.4}$$

$$\phi^{II} \sim A^{\pm}e^{\pm i\beta x}e^{Kz} + B^{\pm}e^{\pm ibx}e^{kz} + C^{\pm}e^{\mp i\beta x}e^{Kz} + D^{\pm}e^{\mp ibx}e^{kz}, \tag{5.3.5}$$

as $x \to \pm\infty$. When written in the shorthand form this is

$$\phi \sim \{A^-, B^-, C^-, D^-; A^+, B^+, C^+, D^+\}. \tag{5.3.6}$$

To find β and b we apply the modified Helmholtz equation to the above potentials. Hence

$$\beta = \sqrt{K^2 - l^2} = K\cos\alpha_{\text{inc}}, \tag{5.3.7}$$

$$b = \sqrt{k^2 - l^2} = \sqrt{k^2 - K^2\sin^2\alpha_{\text{inc}}}. \tag{5.3.8}$$

From (5.3.7) we see that scattered waves of wavenumber K propagate at an angle α_{inc} to the positive or negative x-axis. We know that b is real since $k > K$ and so scattered waves of wavenumber k will exist for all frequencies and $0 \leq \alpha_{\text{inc}} \leq \pi/2$. The angle α_k of the scattered waves of wavenumber k is given by

$$\tan \alpha_k = \frac{l}{b} = \frac{K \sin \alpha_{\text{inc}}}{\sqrt{k^2 - K^2 \sin^2 \alpha_{\text{inc}}}}. \tag{5.3.9}$$

From this we know that $\tan \alpha_k < \tan \alpha_{\text{inc}}$ and hence $\alpha_k < \alpha_{\text{inc}}$.

The form of an incident wave of wavenumber k with angle α_{inc} to the positive x-axis is given by

$$\phi^I_{\text{inc}} = e^{ikx \cos \alpha_{\text{inc}}} g(z), \tag{5.3.10}$$

$$\phi^{II}_{\text{inc}} = e^{ikx \cos \alpha_{\text{inc}}} e^{kz}. \tag{5.3.11}$$

For the scattering of this wave we find

$$l = k \sin \alpha_{\text{inc}}, \tag{5.3.12}$$

$$\beta = \sqrt{K^2 - k^2 \sin^2 \alpha_{\text{inc}}}, \tag{5.3.13}$$

$$b = k \cos \alpha_{\text{inc}}, \tag{5.3.14}$$

and so waves of wavenumber k travel at an angle α_{inc} to the x-axis. From (5.3.13) we see that for a given angle α_{inc} there maybe a value of K for which $K = k \sin \alpha_{\text{inc}}$ and so $\beta = 0$. We will call this the cut-off frequency and denote it K_c. For $K > K_c$ we have real β and so waves of wavenumber K will propagate in the fluid. When $K < K_c$ the value of β will be complex corresponding to an evanescent mode which is only of local importance hence we have no propagating waves of wavenumber K. An expression for K_c in terms of the incident angle can be found using (5.3.13) and the dispersion relation to give

$$K_c d = \frac{\sin \alpha_{\text{inc}}}{2} \ln \left[\frac{1 + \sin \alpha_{\text{inc}}}{1 - \sigma \sin \alpha_{\text{inc}}} \right]. \tag{5.3.15}$$

Figure 5.7 shows a plot of the cut-off frequency $K_c d$ for a density ratio of $\rho = 0.5$. There is a critical angle α_{crit}, given by $\sin^{-1}(1/\sigma)$, such that as $\alpha_{\text{inc}} \to \alpha_{\text{crit}}$ we have $K_c d \to \infty$ and for $\alpha_{\text{inc}} > \alpha_{\text{crit}}$ we have no propagating waves of wavenumber K for any frequencies. The scattering angle α_K of the waves of wavenumber K is given by

$$\tan \alpha_K = \frac{k \sin \alpha_{\text{inc}}}{\sqrt{K^2 - k^2 \sin^2 \alpha_{\text{inc}}}}, \tag{5.3.16}$$

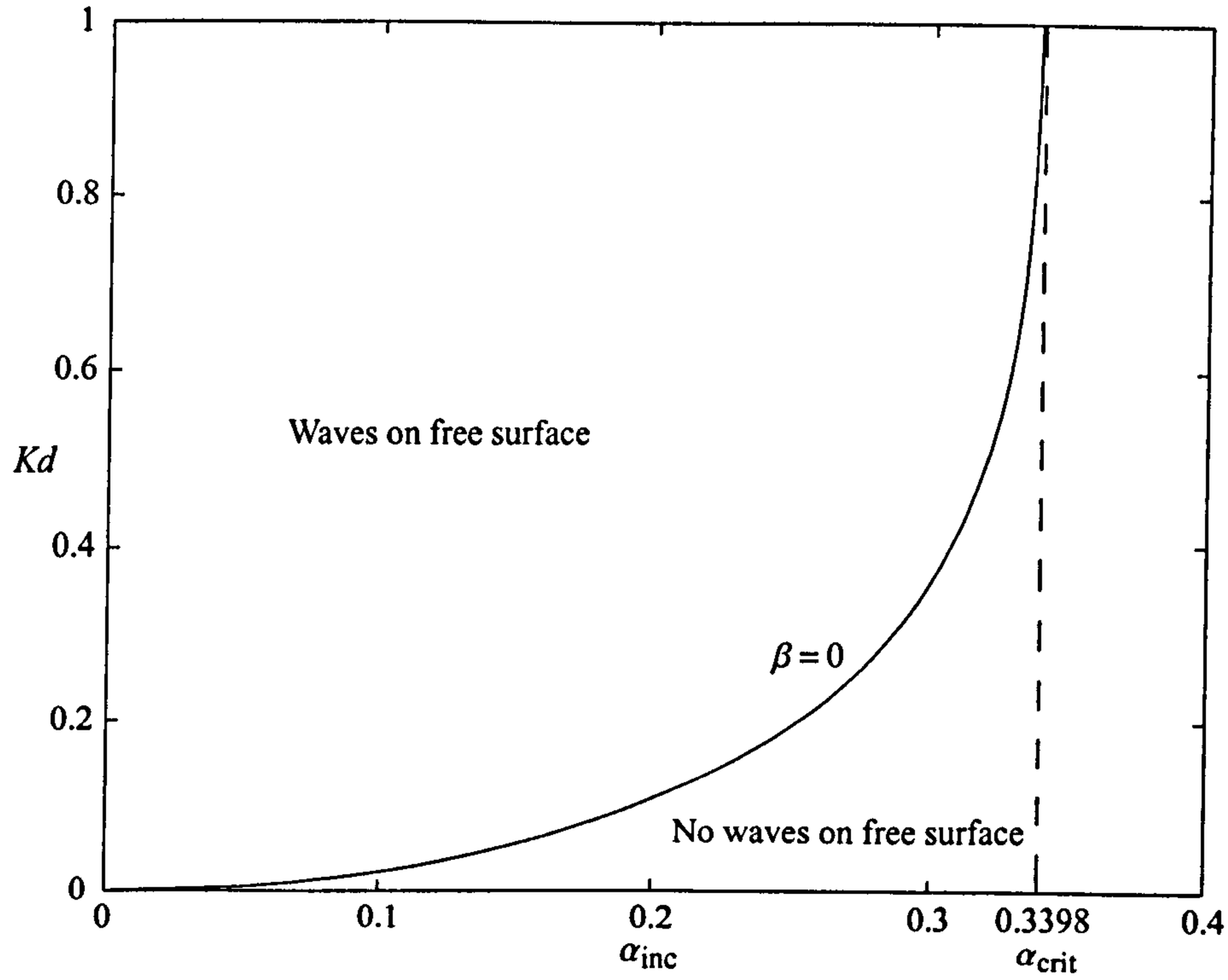

Figure 5.7: Cut-off frequency $K_c d$ due to an incident wave of wavenumber k; $\rho = 0.5$.

and hence $\alpha_K > \alpha_{\text{inc}}$.

We conclude that waves of the incident wavenumber propagate at an angle α_{inc} to the x-axis and waves of wavenumber k always scatter at an angle less than waves of wavenumber K.

5.3.1 Hydrodynamic relations

Let us consider a situation where there are a number of bodies entirely submerged in either the upper or lower fluid layer. From Green's theorem we have

$$\begin{aligned}
&\delta \int_{S_B} \left(\phi \frac{\partial \psi}{\partial n} - \psi \frac{\partial \phi}{\partial n} \right) ds \\
&= \lim_{M \to \infty} \left\{ \rho \int_0^d \left(\phi^I \frac{\partial \psi^I}{\partial x} - \psi^I \frac{\partial \phi^I}{\partial x} \right) \Big|_{x=-M} dz + \int_{-\infty}^0 \left(\phi^{II} \frac{\partial \psi^{II}}{\partial x} - \psi^{II} \frac{\partial \phi^{II}}{\partial x} \right) \Big|_{x=-M} dz \right\} \\
&\quad - \lim_{L \to \infty} \left\{ \rho \int_0^d \left(\phi^I \frac{\partial \psi^I}{\partial x} - \psi^I \frac{\partial \phi^I}{\partial x} \right) \Big|_{x=L} dz + \int_{-\infty}^0 \left(\phi^{II} \frac{\partial \psi^{II}}{\partial x} - \psi^{II} \frac{\partial \phi^{II}}{\partial x} \right) \Big|_{x=L} dz \right\},
\end{aligned} \tag{5.3.17}$$

where S_B is the boundary of the bodies. We now let $\phi = \phi_i$ and $\psi = \phi_j$ where ϕ_i, ϕ_j are two scattering potentials whose behaviour in the far field is described by (5.3.4) and

(5.3.5). Applying (5.3.17) we obtain

$$\delta \int_{S_B} \left(\phi \frac{\partial \psi}{\partial n} - \psi \frac{\partial \phi}{\partial n} \right) ds = J_K (A_i^+ C_j^+ - C_i^+ A_j^+ + A_i^- C_j^- - C_i^- A_j^-) + J_k (B_i^+ D_j^+ - D_i^+ B_j^+ + B_i^- D_j^- - D_i^- B_j^-), \quad (5.3.18)$$

where

$$J_K = i\beta \left[\frac{1}{K} + 2\rho \int_0^d e^{2Kz} dz \right], \quad (5.3.19)$$

$$J_k = ib \left[\frac{1}{k} + 2\rho \int_0^d [g(z)]^2 dz \right]. \quad (5.3.20)$$

In particular, if ϕ and ψ are both scattering potentials having zero normal derivative on all body boundaries then the left-hand side of (5.3.18) is zero.

Now let's consider the scattering of an incident wave of wavenumber K propagating at an angle α_{inc} to the positive x-axis. We can write the velocity potential for this problem as

$$\phi_1 \sim \{R_1, r_1, 1, 0; T_1, t_1, 0, 0\} \quad (5.3.21)$$

where R_1 and r_1 are the reflection coefficients and T_1 and t_1 are the transmission coefficients of wavenumbers K and k respectively. If we let $\phi = \phi_1$ and $\psi = \overline{\phi_1}$ in (5.3.18) we obtain

$$|R_1|^2 + |T_1|^2 + J(|t_1|^2 + |r_1|^2) = 1, \quad (5.3.22)$$

where $J = J_k / J_K$. For an incident wave of wavenumber k we define the velocity potential to be

$$\phi_3 \sim \{R_3, r_3, 0, 1; T_3, t_3, 0, 0\}, \quad (5.3.23)$$

and after application of (5.3.18) with $\phi = \phi_3$ and $\psi = \overline{\phi_3}$ we obtain

$$|R_3|^2 + |T_3|^2 + J(|t_3|^2 + |r_3|^2) = J. \quad (5.3.24)$$

It is convenient to define energies as follows

$$E_1^R = |R_1|^2 \quad , \quad E_1^T = |T_1|^2 \quad , \quad E_1^r = J|r_1|^2, \quad E_1^t = J|t_1|^2, \quad (5.3.25)$$

$$E_3^R = |R_3|^2/J, \quad E_3^T = |T_3|^2/J, \quad E_3^r = |r_3|^2 \quad , \quad E_3^t = |t_3|^2 \quad . \quad (5.3.26)$$

The energy relations (5.3.22) and (5.3.24) then become

$$E_j^R + E_j^T + E_j^r + E_j^t = 1, \qquad j = 1, 3. \tag{5.3.27}$$

Equation (5.3.27) serves as a numerical check on results obtained for the reflection and transmission coefficients.

Equations (5.3.18)–(5.3.20) are the oblique equivalents of (2.16)–(2.18) in Linton & McIver (1995). Since (5.3.18) and (2.16) are similar we can use the relations (2.44)–(2.51) derived in Linton & McIver (1995) for the oblique incident case simply by using the alternative forms for J_K and J_k given by (5.3.19)–(5.3.20). However, these relations can only be used when the value of l is the same for both problems. Say we wish to relate a scattering problem with potential ϕ_1 and angle of incidence α_1 to a problem with potential ϕ_3 and angle α_3. If we assign a value to α_1 then the angle α_3 is given by

$$\alpha_3 = \sin^{-1}\left(\frac{K}{k}\sin\alpha_1\right) \tag{5.3.28}$$

and since $k > K$ there will always be an angle α_3. Unlike the normal incidence relations, we can only relate the results between the two problems at one certain frequency. If we assign α_3 a value then

$$\alpha_1 = \sin^{-1}\left(\frac{k}{K}\sin\alpha_3\right). \tag{5.3.29}$$

Here it will not always be possible to relate the problems because $k > K$. When the frequency is less than the cut-off frequency or when α_3 is greater than the critical angle we will not be able to use the relations.

5.3.2 Cylinder in the lower fluid layer

Multipoles

Symmetric and antisymmetric multipoles ϕ_m^s and ϕ_m^a respectively for a cylinder in the lower fluid layer are

$$\phi_m^{Is} = (-1)^m \oint_0^\infty \cosh mu \cos(lx\sinh u)[A_L(u)e^{vz} + B_L(u)e^{-vz}]du, \tag{5.3.30}$$

$$\phi_m^{IIs} = K_m(lr)\cos m\theta + (-1)^m \oint_0^\infty \cosh mu \cos(lx\sinh u)e^{vz}C_L(u)du, \tag{5.3.31}$$

$$\phi_m^{Ia} = (-1)^{m+1} \oint_0^\infty \sinh mu \sin(lx\sinh u)[A_L(u)e^{vz} + B_L(u)e^{-vz}]du, \tag{5.3.32}$$

$$\phi_m^{IIa} = K_m(lr)\sin m\theta + (-1)^{m+1} \oint_0^\infty \sinh mu \sin(lx\sinh u)e^{vz}C_L(u)du, \tag{5.3.33}$$

where $v = l\cosh u$,

$$A_L(u) = K(1+\sigma)(v+K)e^{v(f-2d)}/(v-K)h(v), \tag{5.3.34}$$

$$B_L(u) = K(1+\sigma)e^{vf}/h(v), \tag{5.3.35}$$

$$C_L(u) = (v+K)[(v+K\sigma)e^{-2vd} - v + K]e^{vf}/(v-K)h(v), \tag{5.3.36}$$

and
$$h(u) = (u+K)e^{-2ud} - u + K\sigma. \tag{5.3.37}$$

We note that the functions (5.3.34)–(5.3.36) are the same as (3.7)–(3.9) in Linton & McIver (1995) with u replaced by $v(= l\cosh u)$. From the dispersion relation $h(k) = 0$ hence the multipoles have poles at $u = \gamma_1$ and $u = \gamma_2$ which are defined by

$$\cosh\gamma_1 = K/l \qquad \text{and} \qquad \cosh\gamma_2 = k/l. \tag{5.3.38}$$

For $l > K$ we note there is only one pole at $u = \gamma_2$.

Using the following

$$l\sinh\gamma_1 = l\sqrt{\cosh^2\gamma_1 - 1} = \quad K\sqrt{1-\sin^2\alpha_{\text{inc}}} = K\cos\alpha_{\text{inc}} = \beta, \tag{5.3.39}$$

$$l\sinh\gamma_2 = l\sqrt{\cosh^2\gamma_2 - 1} = \sqrt{k^2 - K^2\sin^2\alpha_{\text{inc}}} = b, \tag{5.3.40}$$

we find that the far-field form of the multipoles, in the lower fluid, is given by

$$\phi_m^{IIs} \sim (-1)^m\pi i[\cosh m\gamma_1 C_L^{\gamma_1} e^{\pm i\beta x}e^{Kz} + \cosh m\gamma_2 C_L^{\gamma_2} e^{\pm ibx}e^{kz}], \tag{5.3.41}$$

$$\phi_m^{IIa} \sim \mp(-1)^m\pi[\sinh m\gamma_1 C_L^{\gamma_1} e^{\pm i\beta x}e^{Kz} + \sinh m\gamma_2 C_L^{\gamma_2} e^{\pm ibx}e^{kz}], \tag{5.3.42}$$

as $x \to \pm\infty$. Where $C_L^{\gamma_1}$ and $C_L^{\gamma_2}$ are the residues of $C_L(u)$ at $u = \gamma_1$ and $u = \gamma_2$ given by

$$C_L^{\gamma_1} = \frac{2K(1+\sigma)e^{K(f-2d)}}{\beta(2e^{-2Kd} - 1 + \sigma)} \tag{5.3.43}$$

and
$$C_L^{\gamma_2} = \frac{(k+K)e^{kf}\left[(k+K\sigma)e^{-2kd} - k + K\right]}{b(k-K)\left[(1-2d(k+K))e^{-2kd} - 1\right]}. \tag{5.3.44}$$

The multipoles can be expanded in cylindrical polar coordinates about $r = 0$ using (5.2.39) and (5.2.40) to give

$$\phi_m^{IIs} = K_m(lr)\cos m\theta + \sum_{n=0}^{\infty} A_{mn}^s I_n(lr)\cos n\theta, \tag{5.3.45}$$

$$\phi_m^{IIa} = K_m(lr)\sin m\theta + \sum_{n=1}^{\infty} A_{mn}^a I_n(lr)\sin n\theta, \tag{5.3.46}$$

where

$$A_{mn}^s = (-1)^{m+n}\epsilon_n \int_0^{\infty} \cosh mu\cosh nu\, e^{vf} C_L(u)du, \tag{5.3.47}$$

$$A_{mn}^a = (-1)^{m+n}2 \int_0^{\infty} \sinh mu\sinh nu\, e^{vf} C_L(u)du. \tag{5.3.48}$$

Incident wavenumber K

Let us consider the case of an incident plane wave of wavenumber K with angle α_{inc} to the positive x-axis, hence $l = K\sin\alpha_{\text{inc}}$. The incident wave potential when expanded about $r = 0$ using (5.2.39) and (5.2.40) has the form

$$\phi_{\text{inc}} = e^{i\beta x}e^{Kz} = e^{Kf}\sum_{m=0}^{\infty}\epsilon_m(-1)^m I_m(lr)[\cosh m\gamma\cos m\theta - i\sinh m\gamma\sin\theta], \quad (5.3.49)$$

where $\cosh\gamma = 1/\sin\alpha_{\text{inc}}$. For the scattering problem we write the velocity potential as

$$\phi_1 = \phi_{\text{inc}} + \sum_{m=0}^{\infty}(\alpha_m\phi_m^a + \beta_m\phi_m^s), \quad (5.3.50)$$

where α_m and β_m are unknowns and α_0 is included for convenience. To solve for α_m and β_m we substitute the polar expansions of the multipoles and of the incident wave into (5.3.50) and apply the body boundary condition $\partial\phi_1/\partial r = 0$ on $r = a$. We then use the orthogonality of the trigonometric functions to obtain infinite systems of equations for the unknowns α_m and β_m which are

$$\alpha_n + \frac{I_n'(la)}{K_n'(la)}\sum_{m=1}^{\infty}\alpha_m A_{mn}^a = (-1)^n 2i\frac{I_n'(la)}{K_n'(la)}e^{Kf}\sinh n\gamma, \qquad n = 1,2,\ldots, \quad (5.3.51)$$

$$\beta_n + \frac{I_n'(la)}{K_n'(la)}\sum_{m=0}^{\infty}\beta_m A_{mn}^s = (-1)^{n+1}\epsilon_n\frac{I_n'(la)}{K_n'(la)}e^{Kf}\cosh n\gamma, \quad n = 0,1,\ldots. \quad (5.3.52)$$

These systems can be solved by truncation as before and in the computations presented below 5×5 systems were solved. When the cylinder has submergence $f/a = -2$ we obtain five decimal place accuracy whereas for $f/a = -1.1$ we have three decimal place accuracy.

The far-field form for ϕ_1, in the lower fluid layer, can be written as

$$\phi_1^{II} \sim \begin{cases} e^{i\beta x}e^{Kz} + R_1 e^{-i\beta x}e^{Kz} + r_1 e^{-ibx}e^{kz} & x\to-\infty, \\ T_1 e^{i\beta x}e^{Kz} + t_1 e^{ibx}e^{kz} & x\to+\infty. \end{cases} \quad (5.3.53)$$

Using (5.3.50), (5.3.41) and (5.3.42) we can extract the reflection and transmission coefficients to obtain

$$T_1 = 1 - \pi C_L^{\gamma_1}\sum_{m=0}^{\infty}(-1)^m[\alpha_m\sinh m\gamma_1 - i\beta_m\cosh m\gamma_1], \quad (5.3.54)$$

$$R_1 = \pi C_L^{\gamma_1}\sum_{m=0}^{\infty}(-1)^m[\alpha_m\sinh m\gamma_1 + i\beta_m\cosh m\gamma_1], \quad (5.3.55)$$

$$t_1 = \pi C_L^{\gamma_2}\sum_{m=0}^{\infty}(-1)^m[-\alpha_m\sinh m\gamma_2 + i\beta_m\cosh m\gamma_2], \quad (5.3.56)$$

$$r_1 = \pi C_L^{\gamma_2}\sum_{m=0}^{\infty}(-1)^m[\alpha_m\sinh m\gamma_2 + i\beta_m\cosh m\gamma_2]. \quad (5.3.57)$$

Computed values of these reflection and transmission coefficients were checked against the conservation of energy relation (5.3.27).

Incident wavenumber k

The velocity potential ϕ_3 for this problem can be expanded using (5.3.50). For an incident wave of wavenumber k and angle α_{inc} to the positive x-axis we have $l = k\sin\alpha_{\text{inc}}$ and the incident potential when expanded about $r = 0$ is given by

$$\phi_{\text{inc}} = e^{ibx}e^{kz} = e^{kf}\sum_{m=0}^{\infty}\epsilon_m(-1)^m I_m(lr)[\cosh m\gamma\cos m\theta - i\sinh m\gamma\sin\theta]. \quad (5.3.58)$$

We note the only difference between this expansion and (5.3.49) is the wavenumber so the equations for α_m and β_m are given by (5.3.51) and (5.3.52) where $\exp(Kf)$ is replaced by $\exp(kf)$.

The far-field form for ϕ_3, in the lower fluid layer, can be written as

$$\phi_3^{II} \sim \begin{cases} e^{ibx}e^{kz} + R_3e^{-i\beta x}e^{Kz} + r_3e^{-ibx}e^{kz} & x \to -\infty, \\ T_3e^{i\beta x}e^{Kz} + t_3e^{ibx}e^{kz} & x \to +\infty. \end{cases} \quad (5.3.59)$$

Using the far-field forms of the multipoles (5.3.41) and (5.3.42) with the expansion of ϕ_3 we find that the expressions for R_3 and r_3 are the same as those for R_1 and r_1 given by (5.3.55) and (5.3.57). For the transmission coefficients we have

$$T_3 = \pi C_L^{\gamma_1}\sum_{m=0}^{\infty}(-1)^m[-\alpha_m\sinh m\gamma_1 + i\beta_m\cosh m\gamma_1], \quad (5.3.60)$$

$$t_3 = 1 - \pi C_L^{\gamma_2}\sum_{m=0}^{\infty}(-1)^m[\alpha_m\sinh m\gamma_2 - i\beta_m\cosh m\gamma_2]. \quad (5.3.61)$$

For K less than the cut-off frequency K_c there are no waves of wavenumber K propagating to infinity so we will have $T_3 = R_3 = 0$.

Results

In figures 5.8–5.11 the reflection and transmission energies are shown for the case of a wave of wavenumber K incident on a cylinder in the lower fluid layer. In all these plots the immersion depth f/a is -2, the depth of the upper fluid layer d/a is 2 and the density ratio ρ is 0.5. The value of ρ used here is not a realistic ratio of fresh water and salt water density (around 0.97) but has been chosen such that the various characteristics, which do occur for such realistic values, are easily recognised. The different curves correspond to different angles of incidence, α_{inc}, which are 1.35, 1.4, 1.53 and 1.56 covering the

range between about 75° to 89°. These values were chosen to illustrate the scattering behaviour when the angle of the incident wave approaches that of grazing ($\pi/2$). From figures 5.8 and 5.9 we see that as the angle of incidence increases E_1^T decreases whereas E_1^R increases. This effect is similar to the oblique scattering problem in a single-layer fluid. The transmission and reflection energies of the waves of wavenumber k, shown in figures 5.10 and 5.11, are small in comparison to those of wavenumber K but show there is some conversion of energy from one mode to the other. As $\alpha_{\text{inc}} \to \pi/2$ it appears from the results that E_1^t, E_1^r and E_1^T tend to zero while E_1^R tends to unity. A similar result for the single-layer problem has been shown by Levine (1965). As $\alpha_{\text{inc}} \to 0$ we find that the energies tend to the normal incidence results where there is zero reflection as shown by Linton & McIver (1995). We can neither put $\alpha_{\text{inc}} = 0$ or $\alpha_{\text{inc}} = \pi/2$ directly into the above analysis.

Figures 5.12–5.15 show the transmission and reflection energies for the scattering of an incident wave of wavenumber k. Here the immersion depth of the cylinder is $f/a = -1.1$ and we have the values $d/a = 2$ and $\rho = 0.5$, as before. Each plot shows the results obtained for four different angles, α_{inc}, of the incident wave, 0.3, 0.32, 0.33 and 0.34. When $\alpha_{\text{inc}} = 0.34$, which is greater than the critical angle $\alpha_{\text{crit}} = 0.3398$ for the given parameter values, we have no waves of wavenumber K propagating through the fluid. For the remaining angles of incidence we have the following cut-off frequencies $K_c a \approx 0.180$, 0.248 and 0.313. Only for frequencies greater than the cut-off will there be conversion of energy from one mode to the other. The transmission and reflection energies for the incident wavenumber are shown in figures 5.14 and 5.15. For a frequency just less than the cut-off there is zero transmission and full reflection of the incident wave. As α_{inc} increases the frequency of this zero of transmission increases and the spike from which it comes widens. When $\alpha_{\text{inc}} = 0.34$ there are in fact two zeros of transmission and full reflection, the second occuring at a higher frequency than those shown on the plot.

Examples of oscillation where there are two frequencies of full reflection are shown in figures 5.16 and 5.17. Both these plots show the reflected energy of an incident wave of wavenumber k where the values $\rho = 0.5$ and $\alpha_{\text{inc}} = 0.34$ ($> \alpha_{\text{crit}}$) have been used. In figure 5.16 the submergence of the cylinder is fixed at -1.95 and each curve corresponds to four different depths of the upper fluid layer, d/a =2.7, 2.5, 2.2 and 2. When $d/a \approx 2.5$ we see there is just one frequency of full reflection. As the depth of the

upper fluid layer decreases this splits and gives two frequencies at which total reflection exists. A similar effect is observed when fixing the depth of the upper fluid and varying the submergence of the cylinder as in figure 5.17. This is somewhat surprising as normal incident waves on a cylinder in the lower fluid are completely transmitted as shown by Linton & McIver (1995).

For the scattering of an incident wave k as $\alpha_{\text{inc}} \to \pi/2$ we find that $E_3^r \to 1$ while all the other energies tend to zero. As $\alpha_{\text{inc}} \to 0$ we again find the energies tend to those of the normal incident case.

If we let $\rho \to 0$ in this problem then it is easy to show that the multipoles defined by (5.3.31) and (5.3.33) go over to the single-layer multipoles for infinite depth defined by (5.2.31) and (5.2.32). Thus by letting $\rho \to 0$ in the above analysis we recover the results for the scattering of oblique waves by a horizontal cylinder in deep water.

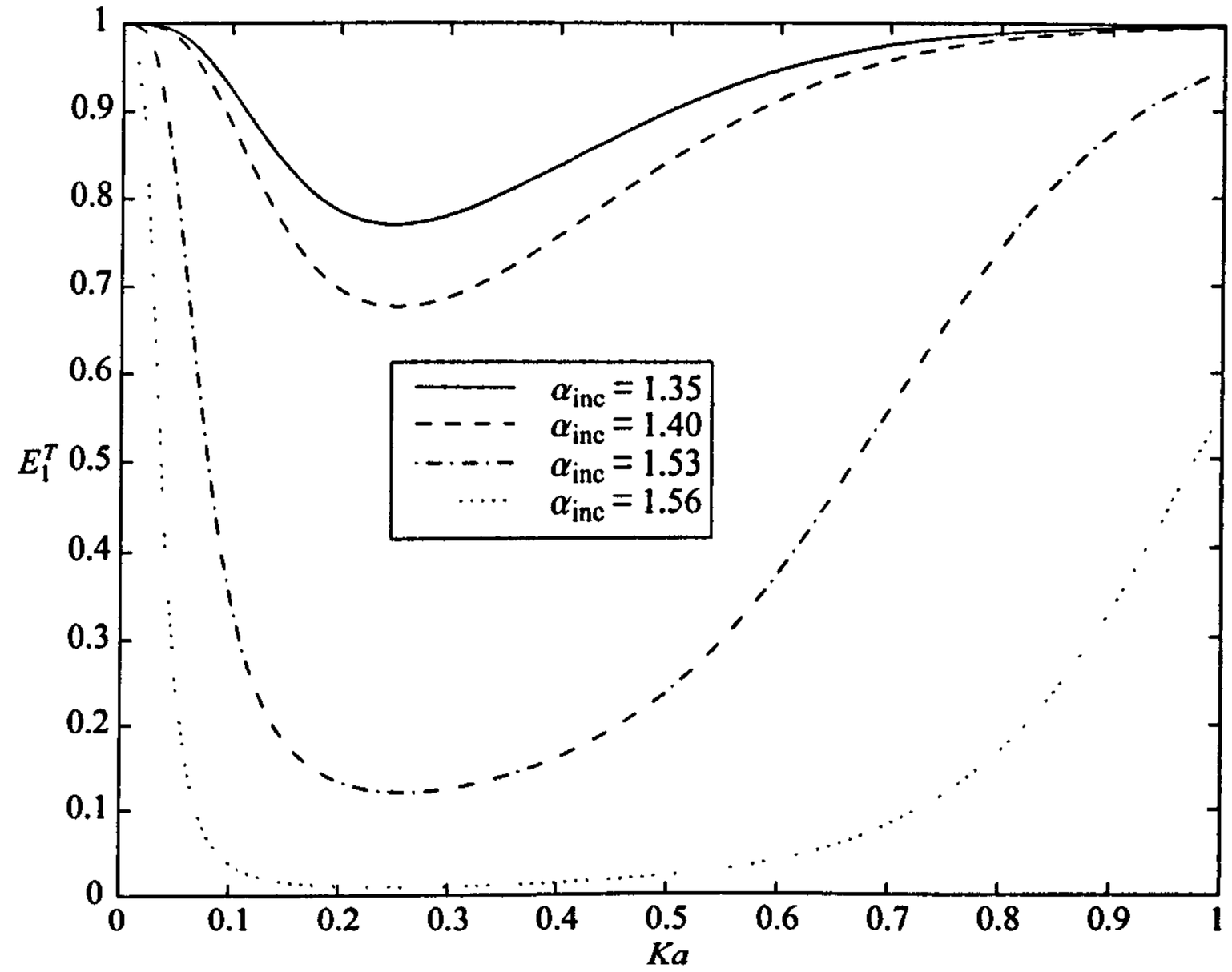

Figure 5.8: Transmission energies due to a wave of wavenumber K incident on a cylinder in the lower layer; $\rho = 0.5$, $d/a = 2.0$ and $f/a = -2.0$.

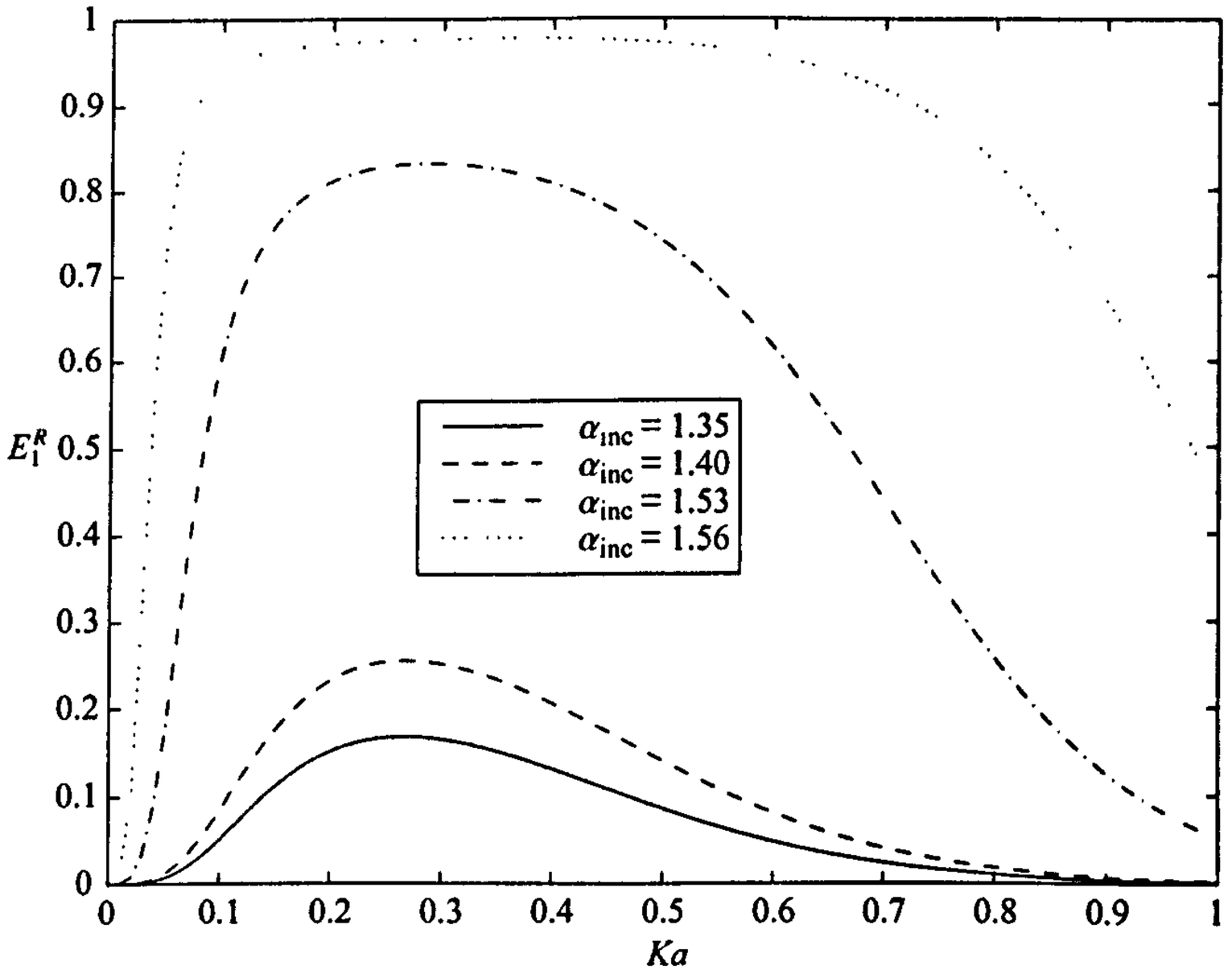

Figure 5.9: Reflection energies due to a wave of wavenumber K incident on a cylinder in the lower layer; $\rho = 0.5$, $d/a = 2.0$ and $f/a = -2.0$.

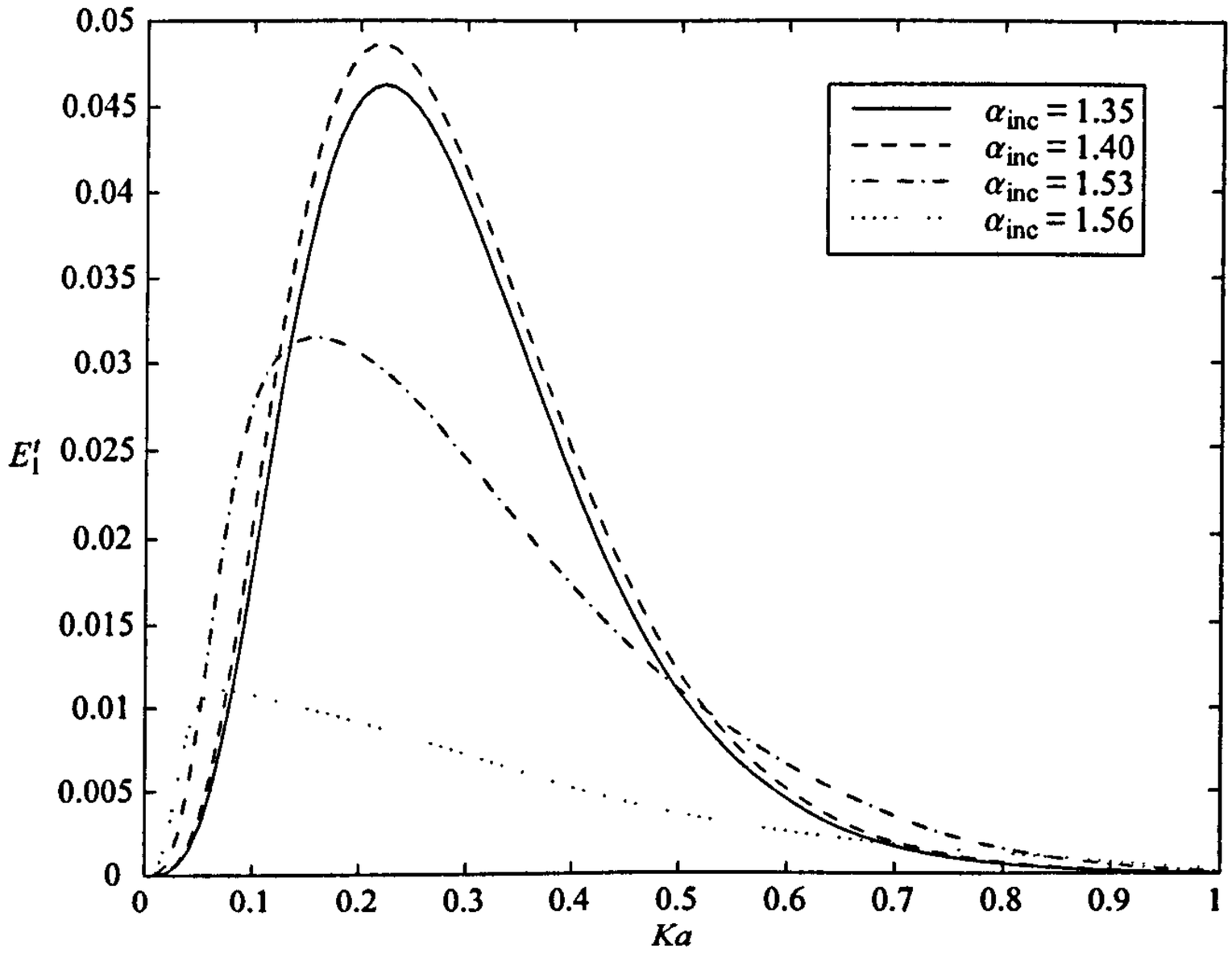

Figure 5.10: Transmission energies due to a wave of wavenumber K incident on a cylinder in the lower layer; $\rho = 0.5$, $d/a = 2.0$ and $f/a = -2.0$.

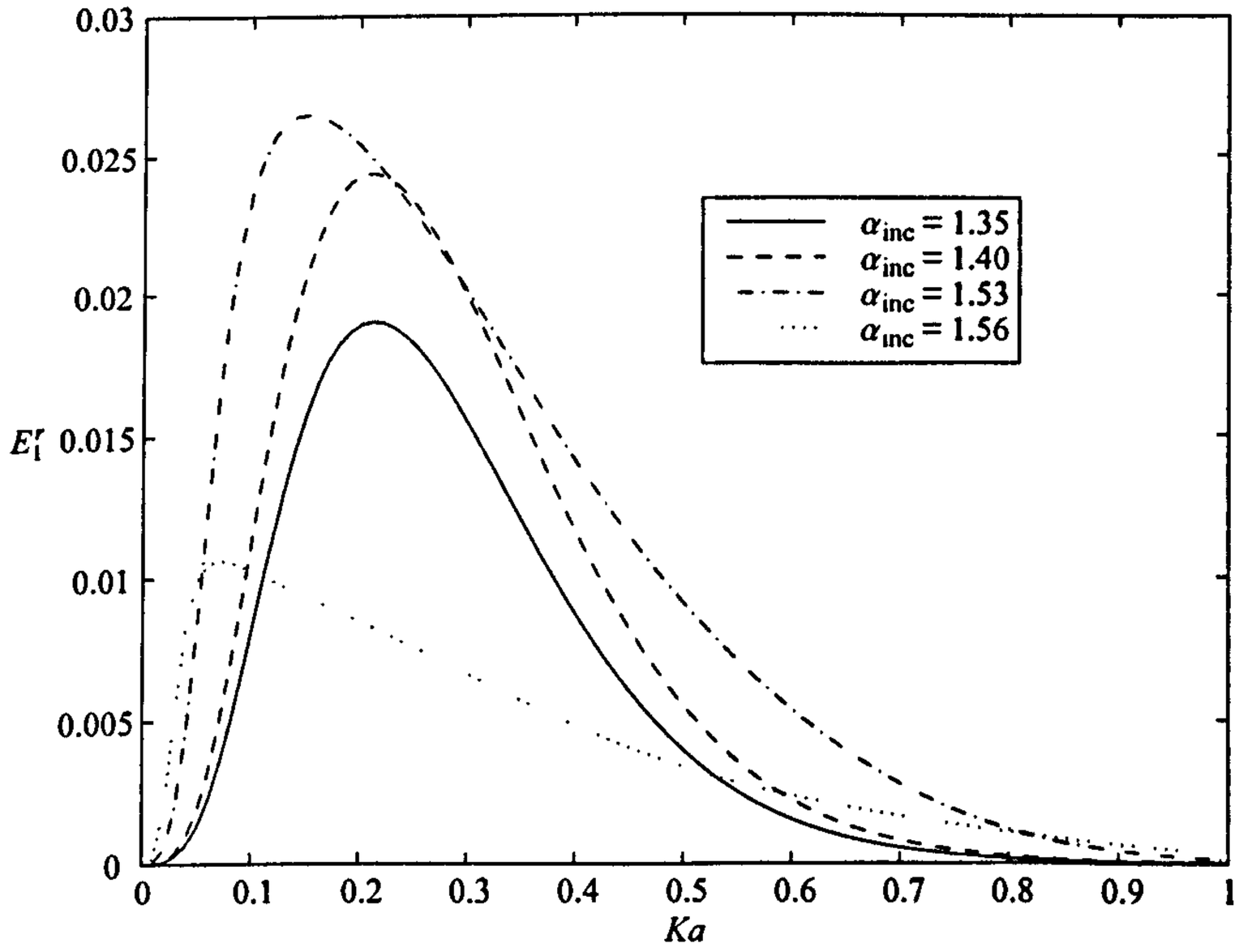

Figure 5.11: Reflection energies due to a wave of wavenumber K incident on a cylinder in the lower layer; $\rho = 0.5$, $d/a = 2.0$ and $f/a = -2.0$.

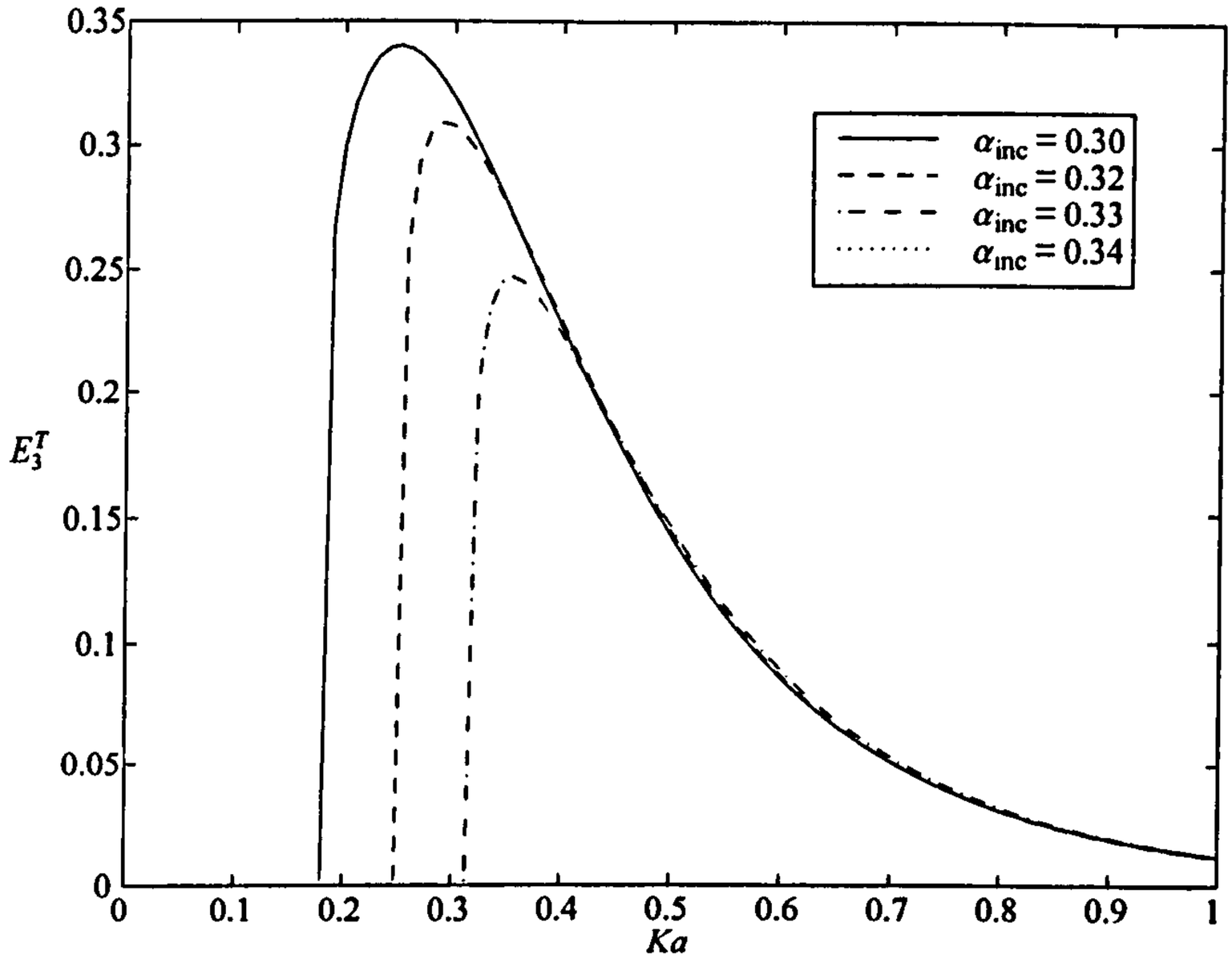

Figure 5.12: Transmission energies due to a wave of wavenumber k incident on a cylinder in the lower layer; $\rho = 0.5$, $d/a = 2.0$ and $f/a = -1.1$.

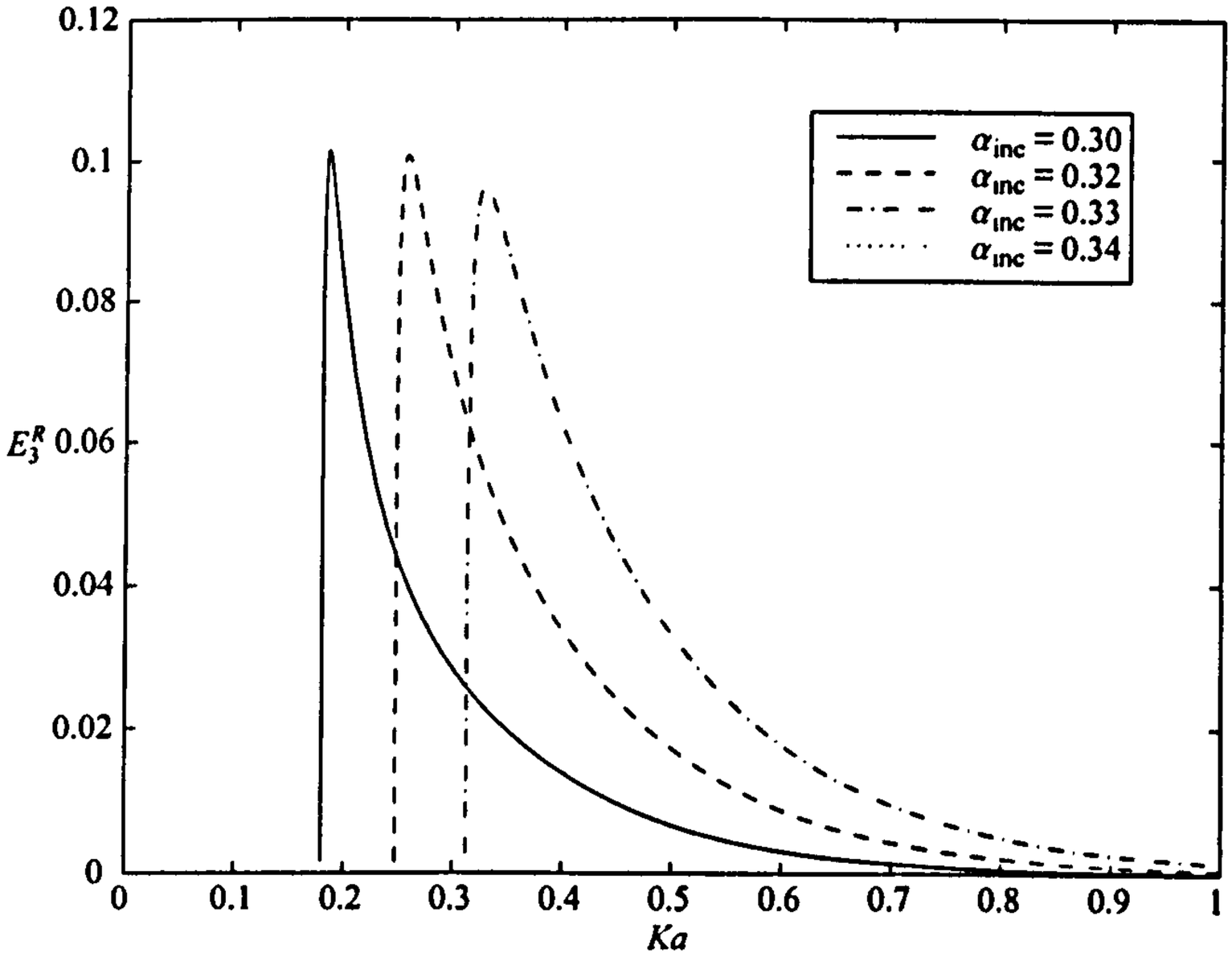

Figure 5.13: Reflection energies due to a wave of wavenumber k incident on a cylinder in the lower layer; $\rho = 0.5$, $d/a = 2.0$ and $f/a = -1.1$.

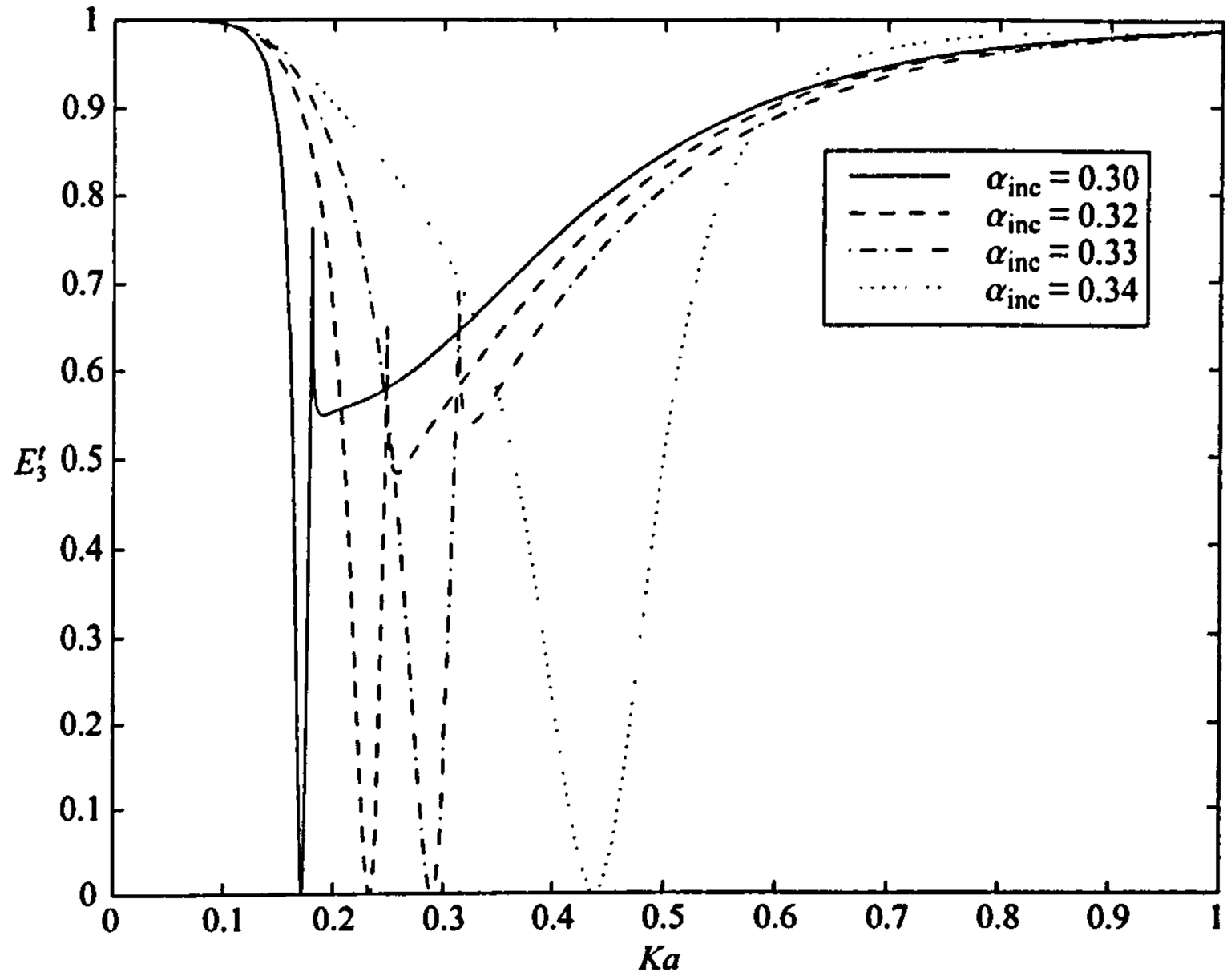

Figure 5.14: Transmission energies due to a wave of wavenumber k incident on a cylinder in the lower layer; $\rho = 0.5$, $d/a = 2.0$ and $f/a = -1.1$.

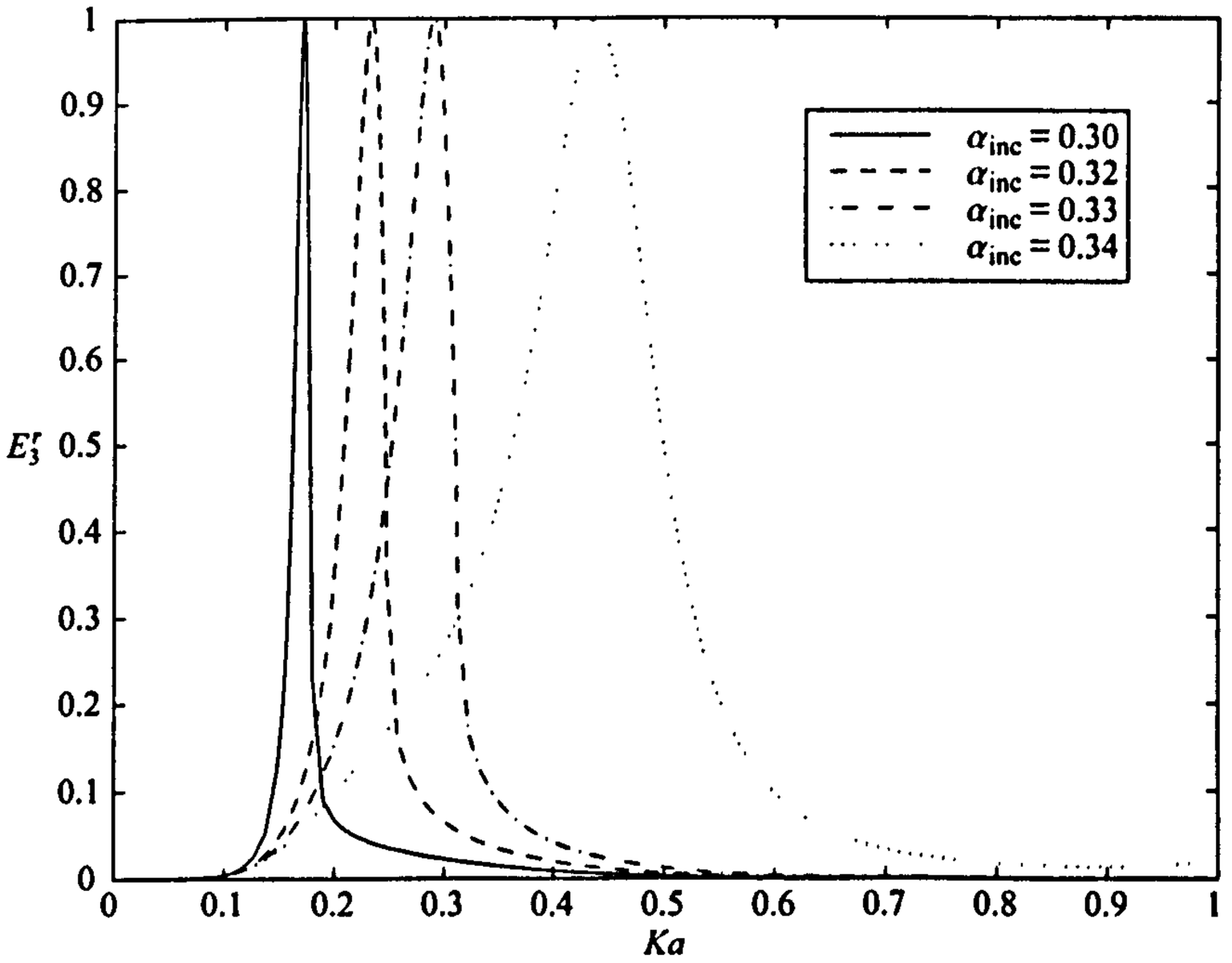

Figure 5.15: Reflection energies due to a wave of wavenumber k incident on a cylinder in the lower layer; $\rho = 0.5$, $d/a = 2.0$ and $f/a = -1.1$.

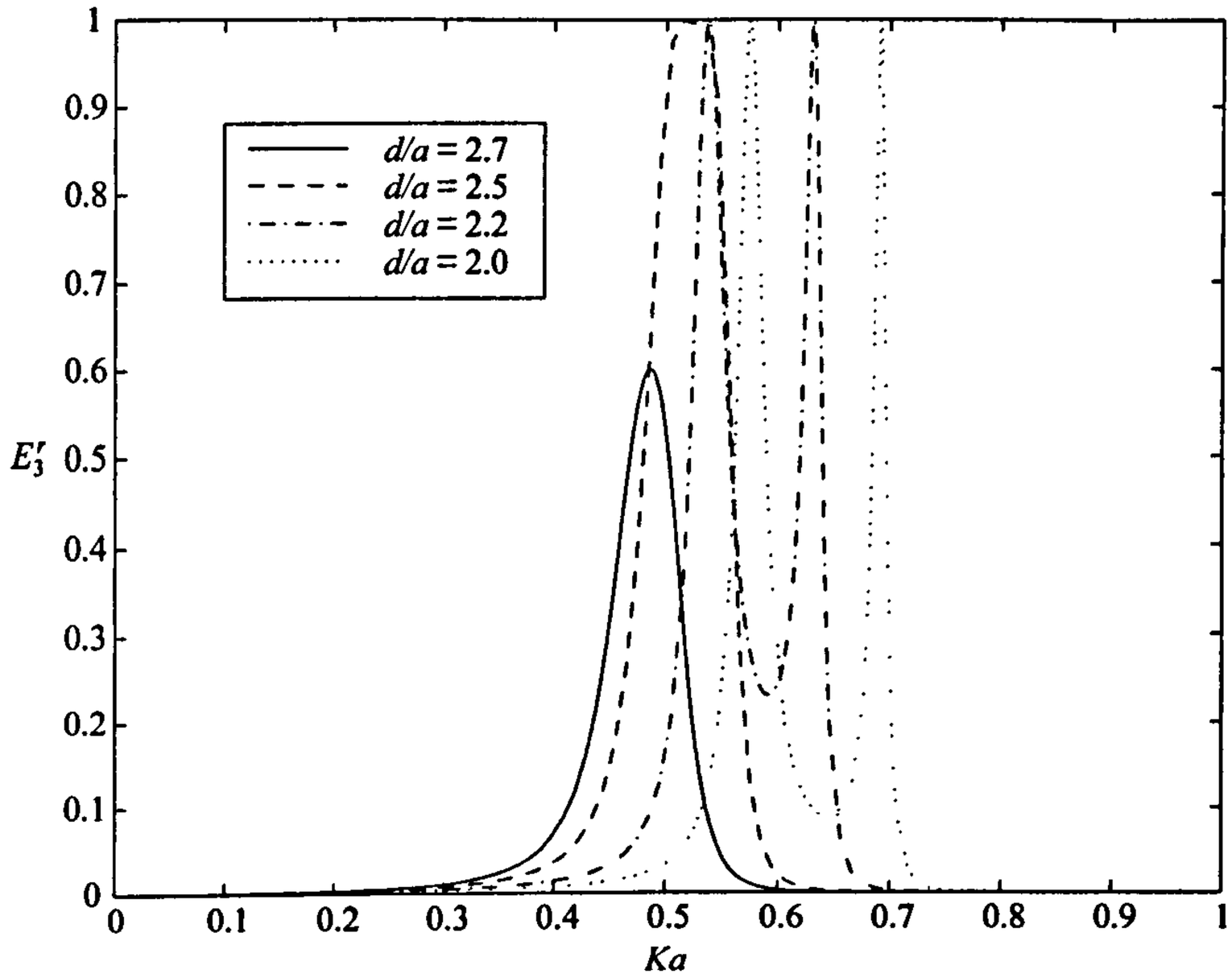

Figure 5.16: Reflection energies due to a wave of wavenumber k incident on a cylinder in the lower layer; $\rho = 0.5$, $f/a = -1.95$ and $\alpha_{\text{inc}} = 0.34$.

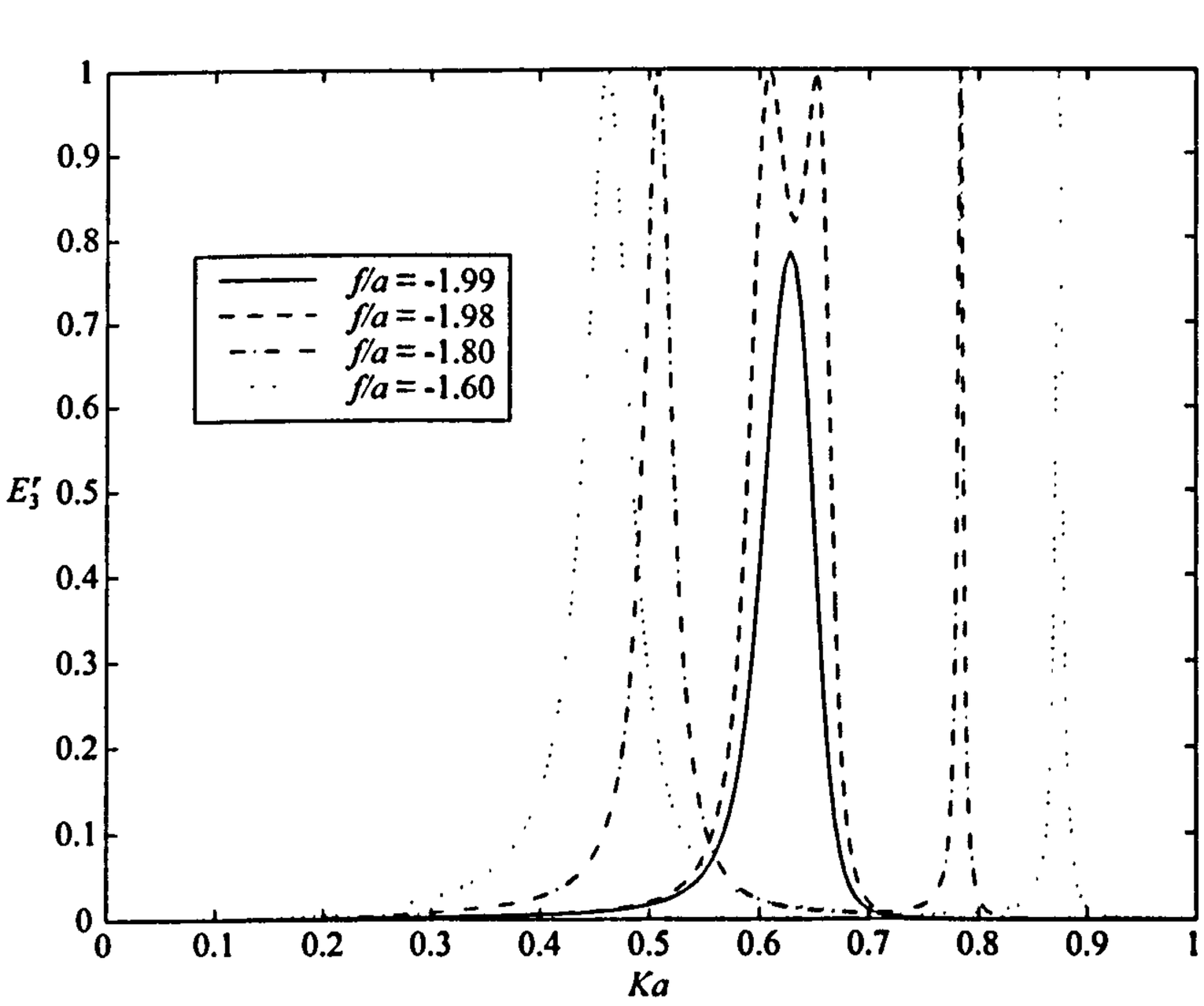

Figure 5.17: Reflection energies due to a wave of wavenumber k incident on a cylinder in the lower layer; $\rho = 0.5$, $d/a = 2.0$ and $\alpha_{\text{inc}} = 0.34$.

5.3.3 Cylinder in the upper fluid layer

Multipoles

We now consider the case of a cylinder positioned in the upper fluid layer, $f/a > 1$. Suitable multipoles take the form

$$\phi_m^{Is} = K_m(lr)\cos m\theta + \oint_0^\infty \cosh mu \cos(lx\sinh u)[A_U^{(0)}(u)e^{vz} + B_U^{(0)}(u)e^{-vz}]du, \tag{5.3.62}$$

$$\phi_m^{IIs} = \oint_0^\infty \cosh mu \cos(lx\sinh u)e^{vz}C_U^{(0)}(u)du, \tag{5.3.63}$$

$$\phi_m^{Ia} = K_m(lr)\sin m\theta + \oint_0^\infty \sinh mu \sin(lx\sinh u)[A_U^{(1)}(u)e^{vz} + B_U^{(1)}(u)e^{-vz}]du, \tag{5.3.64}$$

$$\phi_m^{IIa} = \oint_0^\infty \sinh mu \sin(lx\sinh u)e^{vz}C_U^{(1)}(u)du, \tag{5.3.65}$$

where

$$A_U^{(q)}(u) = (v+K)e^{-2vd}[(-1)^{m+q+1}(v-K\sigma)e^{vf} - (v-K)e^{-vf}]/(v-K)h(v), \tag{5.3.66}$$

$$B_U^{(q)}(u) = [(-1)^{m+q+1}(v+K)e^{v(f-2d)} - (v-K)e^{-vf}]/h(v), \tag{5.3.67}$$

$$C_U^{(q)}(u) = K(1-\sigma)B_U^{(q)}(u)/(v-K). \tag{5.3.68}$$

We note that the multipole functions (5.3.66)–(5.3.68) are the same as (4.7)–(4.9) in Linton & McIver (1995) with u replaced by v.

The far-field form of the multipoles, in the lower fluid layer, is given by

$$\phi_m^{IIs} \sim \pi i[\cosh m\gamma_1 C_U^{(0)\gamma_1}e^{\pm i\beta x}e^{Kz} + \cosh m\gamma_2 C_U^{(0)\gamma_2}e^{\pm ibx}e^{kz}], \tag{5.3.69}$$

$$\phi_m^{IIa} \sim \pm\pi[\sinh m\gamma_1 C_U^{(1)\gamma_1}e^{\pm i\beta x}e^{Kz} + \sinh m\gamma_2 C_U^{(1)\gamma_2}e^{\pm ibx}e^{kz}], \tag{5.3.70}$$

as $x \to \pm\infty$, where

$$C_U^{(q)\gamma_1} = \frac{(-1)^{m+q+1}2K(1-\sigma)e^{K(f-2d)}}{\beta(2e^{-2Kd} - 1 + \sigma)} \tag{5.3.71}$$

and

$$C_U^{(q)\gamma_2} = \frac{K(1-\sigma)\left[(-1)^{m+q+1}(k+K)e^{k(f-2d)} - (k-K)e^{-kf}\right]}{b(k-K)\left[(1-2d(k+K))e^{-2kd} - 1\right]}. \tag{5.3.72}$$

We can expand the multipoles about $r = 0$ using (5.2.39) and (5.2.40) to give

$$\phi_m^{Is} = K_m(lr)\cos m\theta + \sum_{n=0}^{\infty} B_{mn}^s \cos n\theta I_n(lr), \tag{5.3.73}$$

$$\phi_m^{Ia} = K_m(lr)\sin m\theta + \sum_{n=1}^{\infty} B_{mn}^a \sin n\theta I_n(lr), \tag{5.3.74}$$

where

$$B^s_{mn} = \epsilon_n \int_0^\infty \cosh mu \cosh nu[(-1)^n A^{(0)}_U(u)e^{vf} + B^{(0)}_U(u)e^{-vf}]du, \tag{5.3.75}$$

$$B^a_{mn} = 2\int_0^\infty \sinh mu \sinh nu[(-1)^{n+1} A^{(1)}_U(u)e^{vf} + B^{(1)}_U(u)e^{-vf}]du. \tag{5.3.76}$$

Incident wavenumber K

The potential ϕ_1 can again be expanded using (5.3.50), but we now use the multipole expansions developed for the upper fluid layer, (5.3.62)–(5.3.65). The form of ϕ_{inc} is given by (5.3.49) and after applying the body boundary condition, $\partial\phi_1/\partial r = 0$ on $r = 0$, we obtain systems of equations for the unknowns α_m and β_m, which are

$$\alpha_n + \frac{I'_n(la)}{K'_n(la)} \sum_{m=1}^{\infty} \alpha_m B^a_{mn} = (-1)^n 2i \frac{I'_n(la)}{K'_n(la)} e^{Kf} \sinh n\gamma, \tag{5.3.77}$$

$$\beta_n + \frac{I'_n(la)}{K'_n(la)} \sum_{m=0}^{\infty} \beta_m B^s_{mn} = (-1)^{n+1} \epsilon_n \frac{I'_n(la)}{K'_n(la)} e^{Kf} \cosh n\gamma. \tag{5.3.78}$$

The systems (5.3.77) and (5.3.78) were solved by truncating to 4×4 systems to produce the results presented below. The accuracy achieved with this truncation parameter was to three decimal places.

The transmission and reflection coefficients are extracted from the far-field form of the potential ϕ_1. Using (5.3.50), (5.3.69) and (5.3.70) with (5.3.53) we obtain

$$T_1 = 1 + \pi \sum_{m=0}^{\infty} [\alpha_m \sinh m\gamma_1 C^{(1)\gamma_1}_U + i\beta_m \cosh m\gamma_1 C^{(0)\gamma_1}_U], \tag{5.3.79}$$

$$R_1 = \pi \sum_{m=0}^{\infty} [-\alpha_m \sinh m\gamma_1 C^{(1)\gamma_1}_U + i\beta_m \cosh m\gamma_1 C^{(0)\gamma_1}_U], \tag{5.3.80}$$

$$t_1 = \pi \sum_{m=0}^{\infty} [\alpha_m \sinh m\gamma_2 C^{(1)\gamma_2}_U + i\beta_m \cosh m\gamma_2 C^{(0)\gamma_2}_U], \tag{5.3.81}$$

$$r_1 = \pi \sum_{m=0}^{\infty} [-\alpha_m \sinh m\gamma_2 C^{(1)\gamma_2}_U + i\beta_m \cosh m\gamma_2 C^{(0)\gamma_2}_U]. \tag{5.3.82}$$

Again, calculations of the reflection and transmission coefficients were checked using the conservation of energy relation (5.3.27).

Incident wavenumber k

For this problem ϕ_{inc}, when expanded about $r = 0$ using (5.2.39) and (5.2.40) with $u = \gamma_2 = \gamma$, is described by

$$\phi^I_{\text{inc}} = e^{ibx} g(z) \tag{5.3.83}$$

$$= e^{ibx} \frac{1}{K(\sigma-1)} [(K\sigma - k)e^{kz} + (K-k)e^{-kz}] \tag{5.3.84}$$

$$= \frac{1}{K(\sigma-1)} \sum_{m=0}^{\infty} \epsilon_m I_m(lr) \Big[((-1)^m e^{kf}(K\sigma - k) + e^{-kf}(K-k)) \cos m\theta \cosh m\gamma$$

$$+ i((-1)^{m+1} e^{kf}(K\sigma - k) + e^{-kf}(K-k)) \sin m\theta \sinh m\gamma \Big]. \tag{5.3.85}$$

The velocity potential ϕ_3 is expanded in the same way as (5.3.50), where ϕ^s_m and ϕ^a_m are the symmetrical and antisymetrical multipoles developed for the upper fluid. After application of the body boundary condition we obtain the following systems of equations for the unknowns α_n and β_n

$$\alpha_n + \frac{I'_n(la)}{K'_n(la)} \sum_{m=1}^{\infty} \alpha_m B^a_{mn} = \frac{2i}{K(\sigma-1)} \frac{I'_n(la)}{K'_n(la)} [(-1)^n e^{kf}(K\sigma - k)$$

$$- e^{-kf}(K-k)] \sinh n\gamma \tag{5.3.86}$$

$$\beta_n + \frac{I'_n(la)}{K'_n(la)} \sum_{m=0}^{\infty} \beta_m B^s_{mn} = \frac{\epsilon_n}{K(\sigma-1)} \frac{I'_n(la)}{K'_n(la)} [(-1)^{n+1} e^{kf}(K\sigma - k)$$

$$- e^{-kf}(K-k)] \cosh n\gamma. \tag{5.3.87}$$

$$\tag{5.3.88}$$

The reflection and transmission coefficients are given by

$$T_3 = \pi \sum_{m=0}^{\infty} [\alpha_m \sinh m\gamma_1 C_U^{(1)\gamma_1} + i\beta_m \cosh m\gamma_1 C_U^{(0)\gamma_1}], \tag{5.3.89}$$

$$R_3 = \pi \sum_{m=0}^{\infty} [-\alpha_m \sinh m\gamma_1 C_U^{(1)\gamma_1} + i\beta_m \cosh m\gamma_1 C_U^{(0)\gamma_1}], \tag{5.3.90}$$

$$t_3 = 1 + \pi \sum_{m=0}^{\infty} [\alpha_m \sinh m\gamma_2 C_U^{(1)\gamma_2} + i\beta_m \cosh m\gamma_2 C_U^{(0)\gamma_2}], \tag{5.3.91}$$

$$r_3 = \pi \sum_{m=0}^{\infty} [-\alpha_m \sinh m\gamma_2 C_U^{(1)\gamma_2} + i\beta_m \cosh m\gamma_2 C_U^{(0)\gamma_2}]. \tag{5.3.92}$$

Results

Figures 5.18–5.21 show the reflection and transmission energies for an incident wave of wavenumber K on a cylinder submerged in the upper fluid layer. The submergence of the cylinder, f/a, is fixed at 1.25, the depth, d/a, of the upper fluid layer is 2.5 and

the density ratio, ρ, is 0.5. The different curves correspond to four different angles of incidence, $\alpha_{\text{inc}} = 1.35$, 1.4, 1.53 and 1.56. These angles are same as those used in figures 5.8–5.11. The results are very similar to those for the scattering of an incident wave of wavenumber K in the lower fluid layer and display the same trends.

Figures 5.22–5.25 show reflection and transmission energies of an incident wave of wavenumber k on a cylinder submerged in the upper fluid layer. Here we have the same parameter settings as in the case of an incident wavenumber K and the different curves correspond to $\alpha_{\text{inc}} = 0.3$, 0.32, 0.33 and 0.34. The critical angle, α_{crit}, is 0.3398 and the cut-off frequencies for the first three angles are $K_c a \approx 0.144$, 0.198 and 0.250 respectively. We find these results show similar trends to the corresponding case of the cylinder in the lower fluid. Again we only have mode swapping for frequencies greater than the cut-off frequency as shown in figures 5.22 and 5.23. Figures 5.24 and 5.25 show the transmitted and reflected energies of the incident wave. There is a zero of transmission occuring before the cut-off frequency, however we have a point of full transmission preceeding this. As the angle of incidence is increased the frequencies of these pairs of zero and total transmission increase and also separate.

Figure 5.26 shows the transmission energies E_3^t for an incident wave of wavenumber k with angle $\alpha_{\text{inc}} = 0.35$, which is greater than the critical angle. The ratio of the depth of the upper fluid layer to the submergence of the cylinder is fixed at $d/f = 2$ so that the cylinder is always halfway between the interface and the free surface. The different curves correspond to the values $d/a = 2.24$, 2.238, 2.234 and 2.23. For all the curves there is a frequency of total transmission at $Ka \approx 0.213$ followed shortly by a zero of transmission at $Ka \approx 0.227$. When $d/a = 2.24$ we have a local minimum at $Ka \approx 1.825$ and as the depth of the upper fluid layer is decreased, bringing the free surface and interface closer to the surface of the cylinder, we obtain another zero of transmission. As the depth is decreased further this splits and we obtain a total of three zeros of transmission.

As α_{inc} tends to $\pi/2$ in either problem the reflected energy at the incident wavenumber tends to 1 while the other energies tend to zero. If we let $\rho \to 0$ in this problem then the multipoles defined by (5.3.62) and (5.3.64) go over to the single-layer multipoles for finite depth defined by (5.2.31) and (5.2.32). Thus by letting $\rho \to 0$ we can recover the results for the scattering of oblique waves by a horizontal circular cylinder in finite water depth.

5.3.4 Conclusion

In this section we have solved the scattering problem of oblique waves with a horizontal circular cylinder submerged in a two-layer fluid. The problem was reduced to two dimensions and the energy conservation relation was derived using Green's theorem. It was found that for waves incident along the interface there was a cut-off frequency for the scattered waves on the free surface. Only for frequencies greater than the cut-off frequency would there be conversion of energy from one mode to another. There is a critical angle of incidence such that for angles greater than it there is no cut-off frequency and so all the wave energy propagates on the interface for all frequencies.

For normal incidence when the cylinder is positioned in the lower fluid layer it was shown by Linton & McIver (1995) that all the energy is transmitted. We have shown that this is not true for oblique waves. We have found that for oblique incident waves along the interface when a cylinder is in either fluid layer there are frequencies at which all the incident energy is reflected. The occurrence of these zeros of transmission leads us to consider embedded trapped modes between a pair of cylinders.

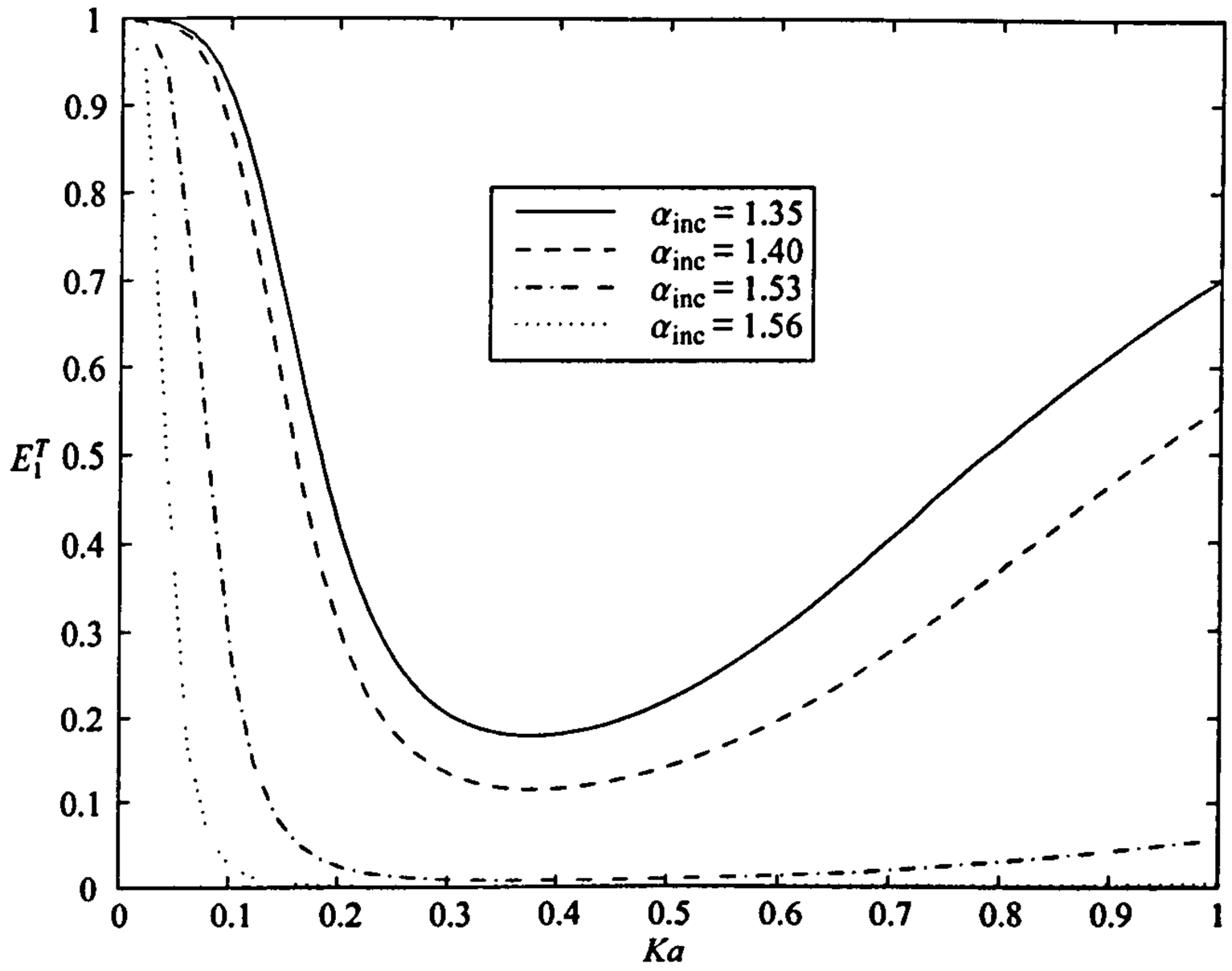

Figure 5.18: Transmission energies due to a wave of wavenumber K incident on a cylinder in the upper layer; $\rho = 0.5$, $d/a = 2.5$ and $f/a = 1.25$.

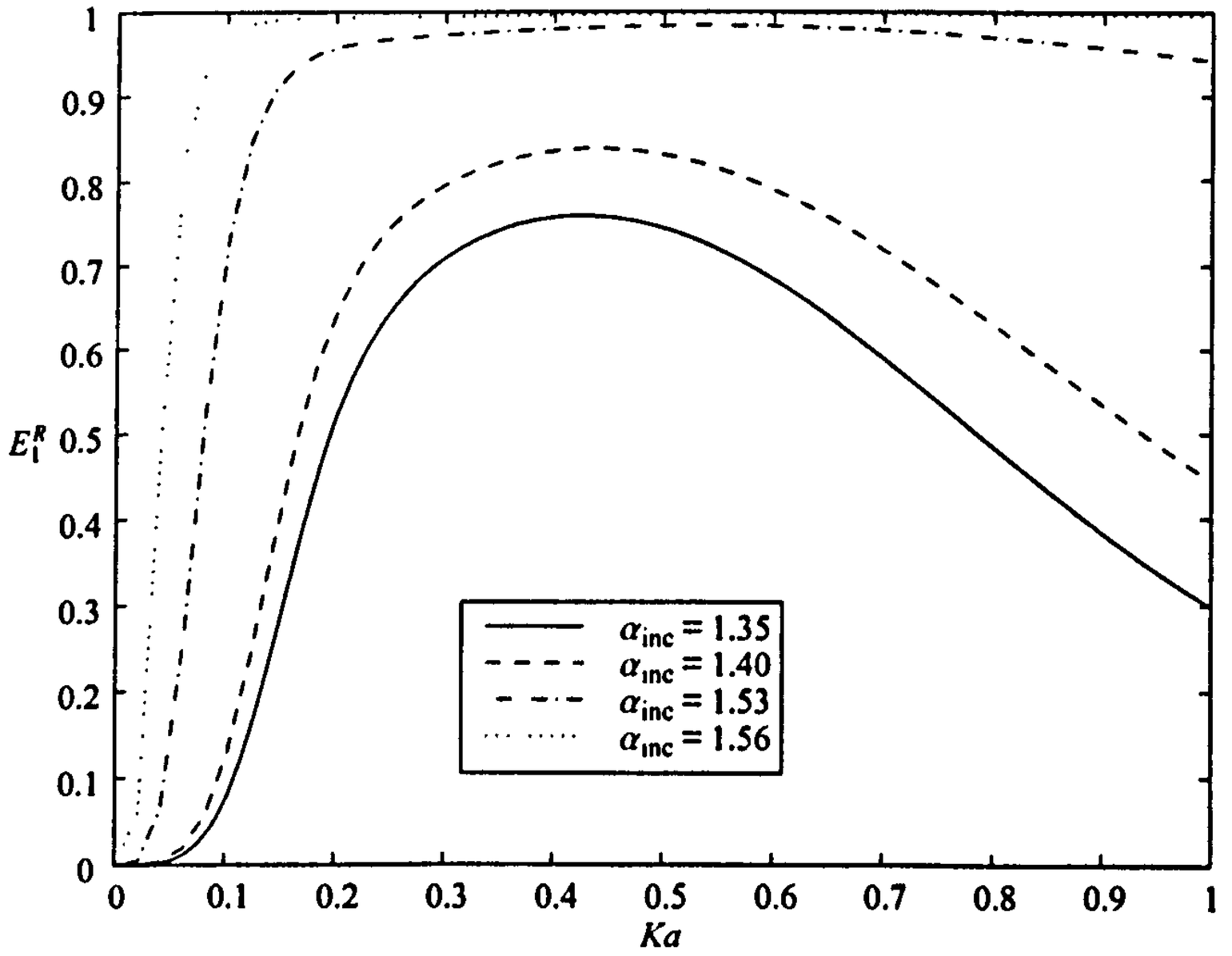

Figure 5.19: Reflection energies due to a wave of wavenumber K incident on a cylinder in the upper layer; $\rho = 0.5$, $d/a = 2.5$ and $f/a = 1.25$.

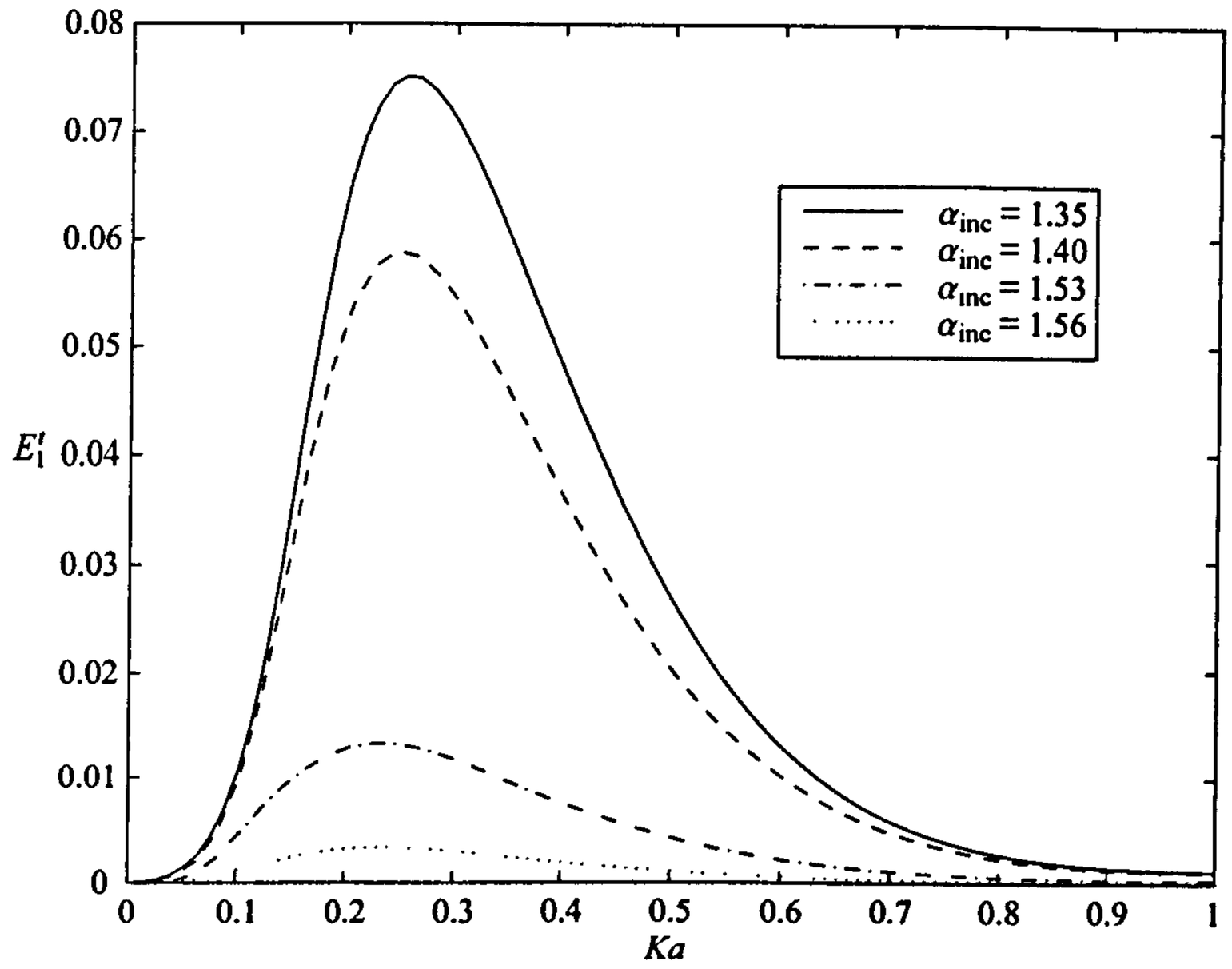

Figure 5.20: Transmission energies due to a wave of wavenumber K incident on a cylinder in the upper layer; $\rho = 0.5$, $d/a = 2.5$ and $f/a = 1.25$.

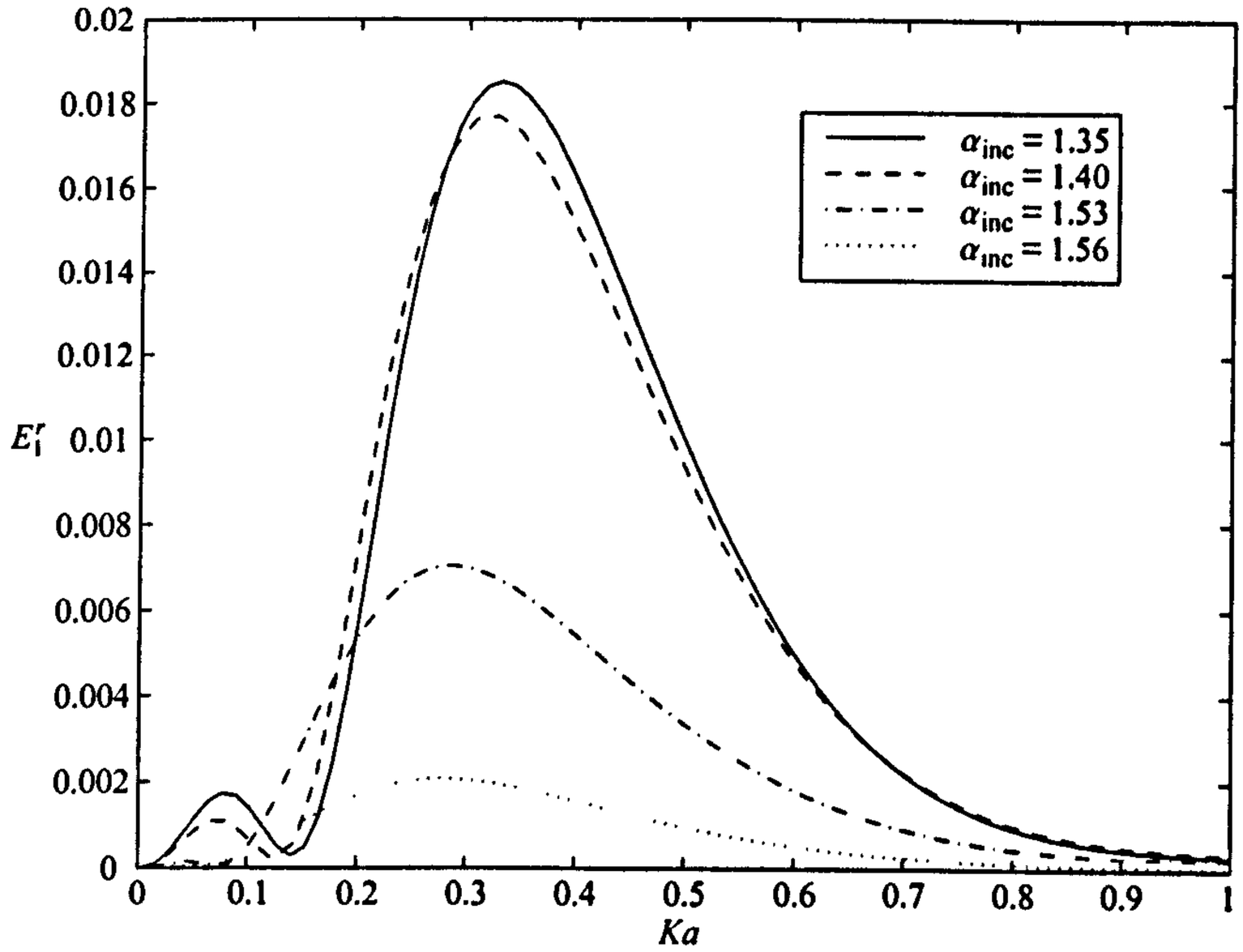

Figure 5.21: Reflection energies due to a wave of wavenumber K incident on a cylinder in the upper layer; $\rho = 0.5$, $d/a = 2.5$ and $f/a = 1.25$.

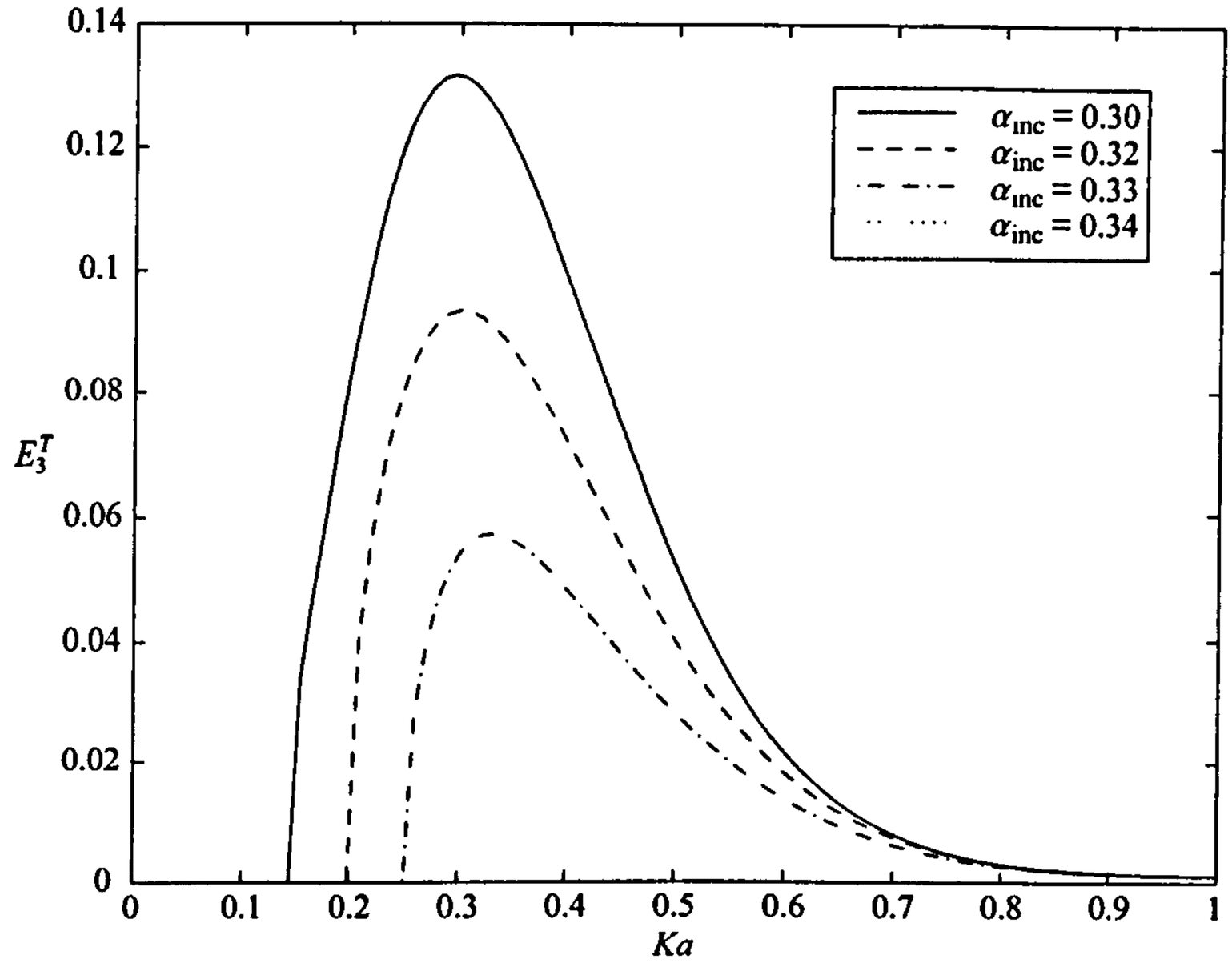

Figure 5.22: Transmission energies due to a wave of wavenumber k incident on a cylinder in the upper layer; $\rho = 0.5$, $d/a = 2.5$ and $f/a = 1.25$.

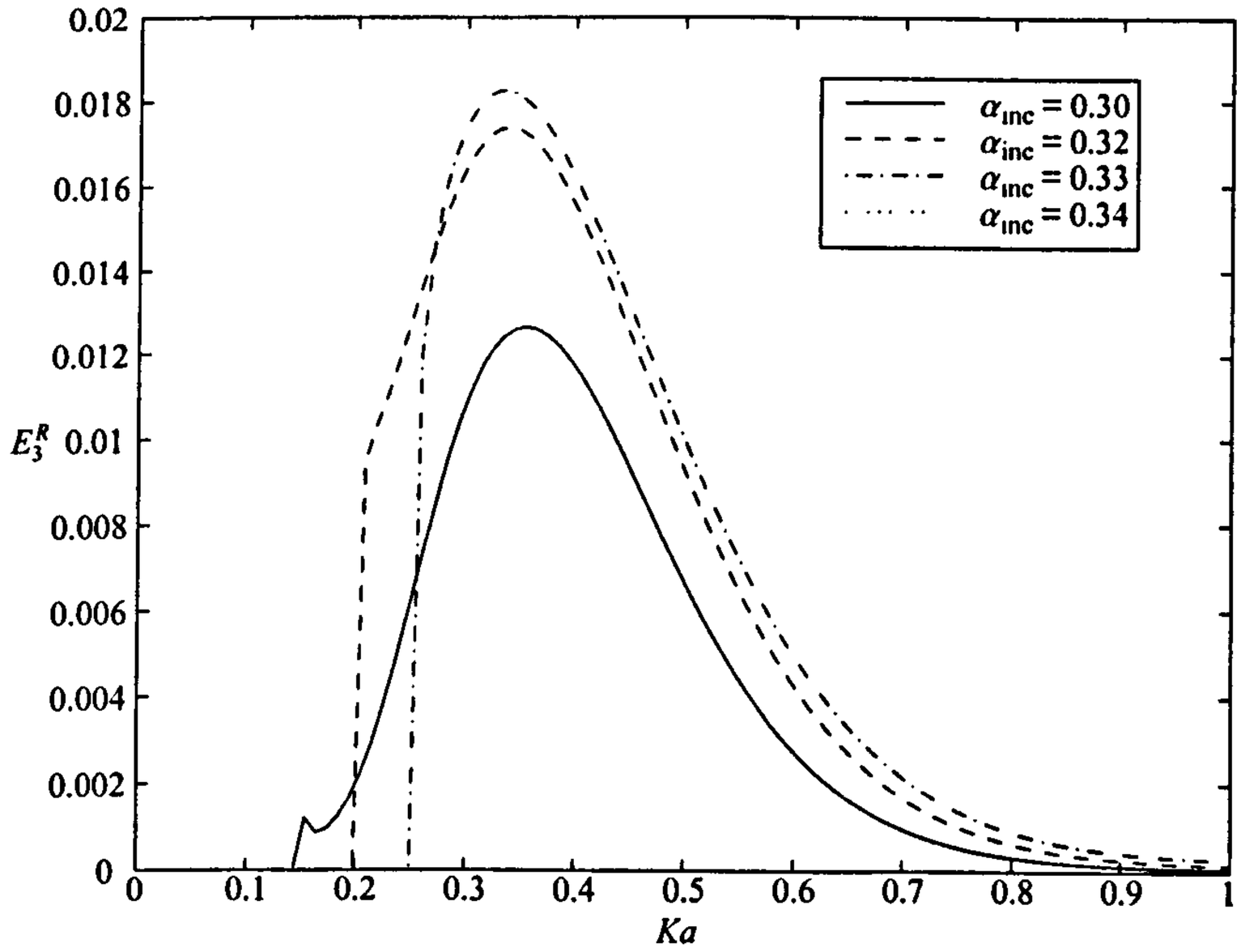

Figure 5.23: Reflection energies due to a wave of wavenumber k incident on a cylinder in the upper layer; $\rho = 0.5$, $d/a = 2.5$ and $f/a = 1.25$.

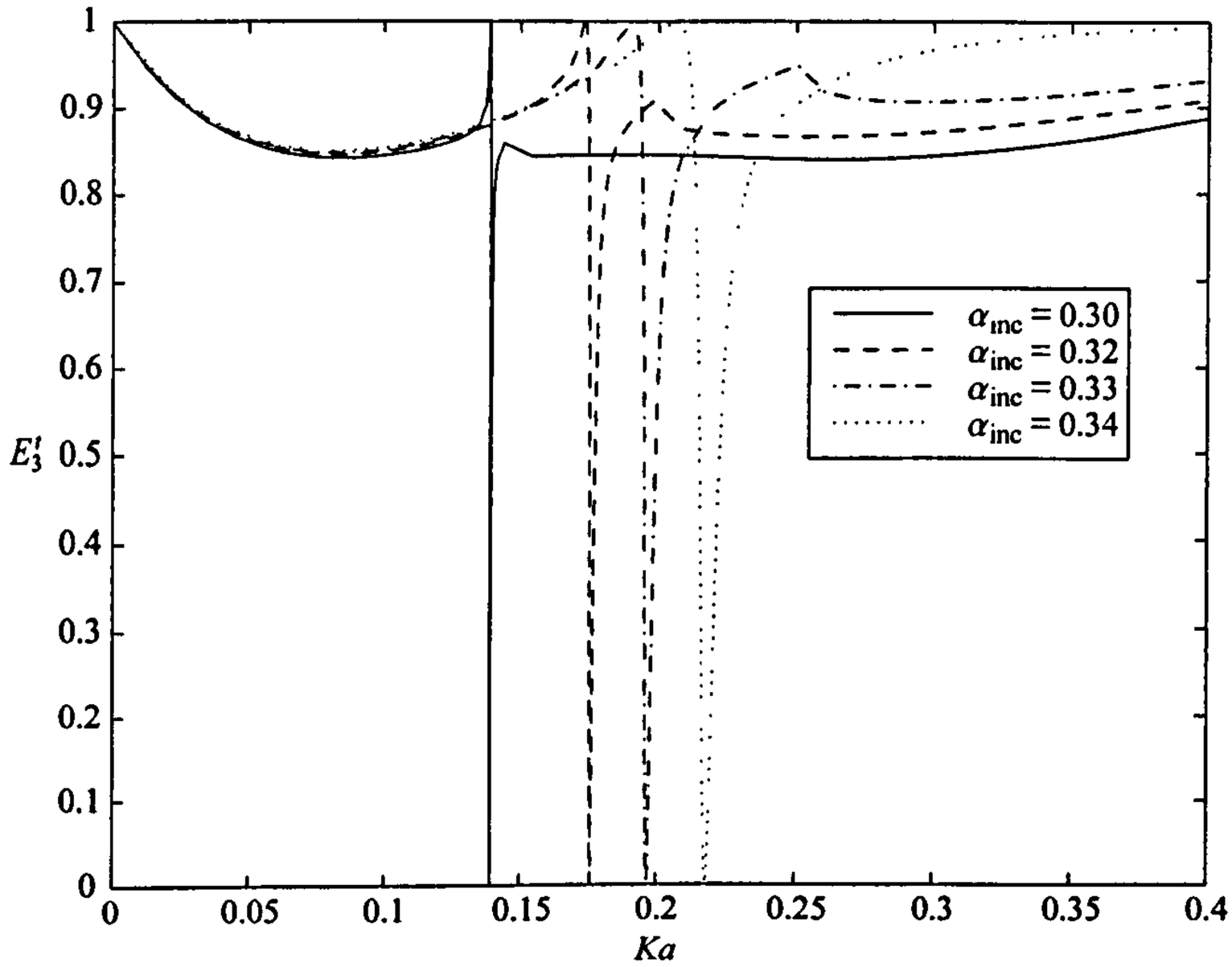

Figure 5.24: Transmission energies due to a wave of wavenumber k incident on a cylinder in the upper layer; $\rho = 0.5$, $d/a = 2.5$ and $f/a = 1.25$.

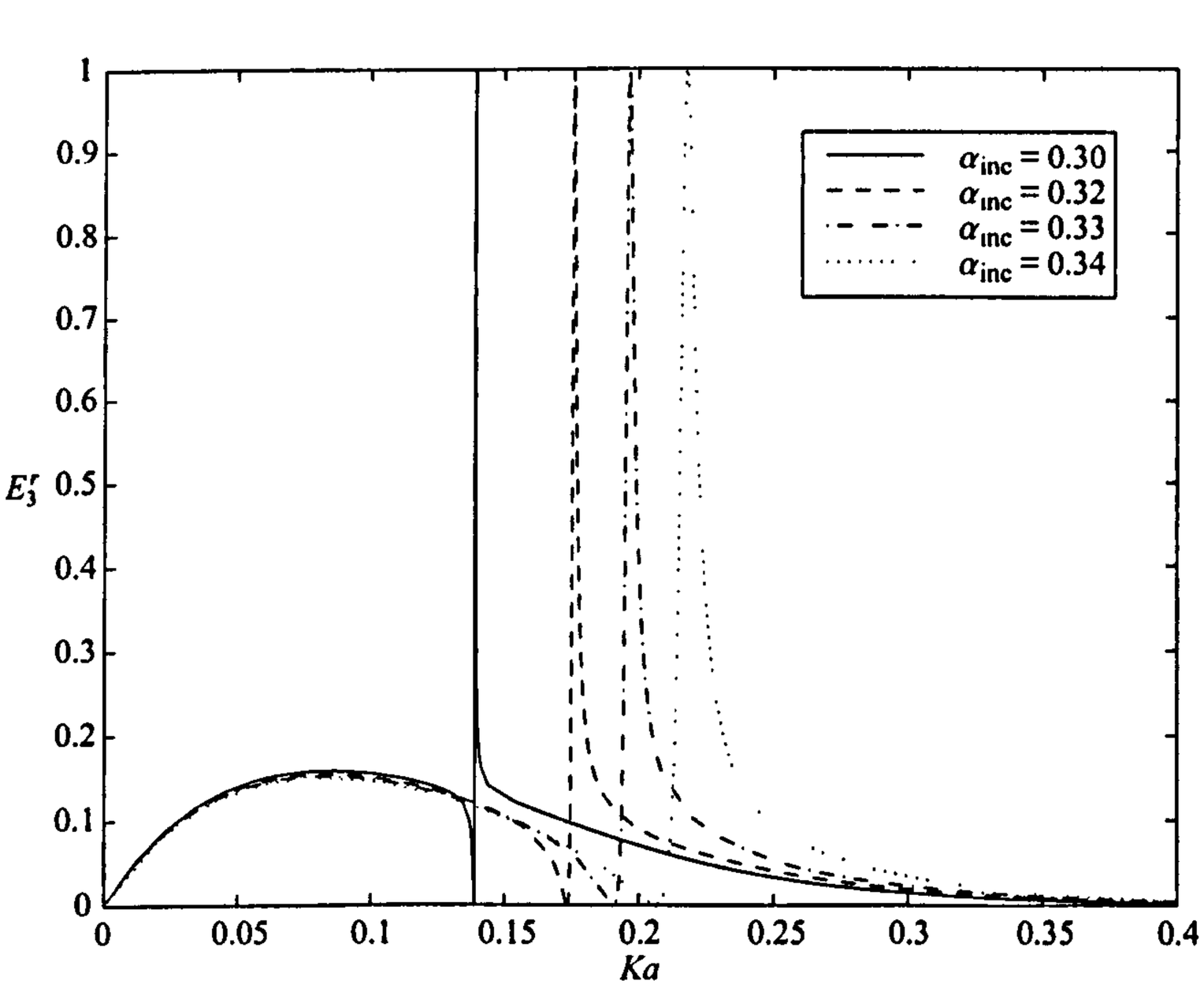

Figure 5.25: Reflection energies due to a wave of wavenumber k incident on a cylinder in the upper layer; $\rho = 0.5$, $d/a = 2.5$ and $f/a = 1.25$.

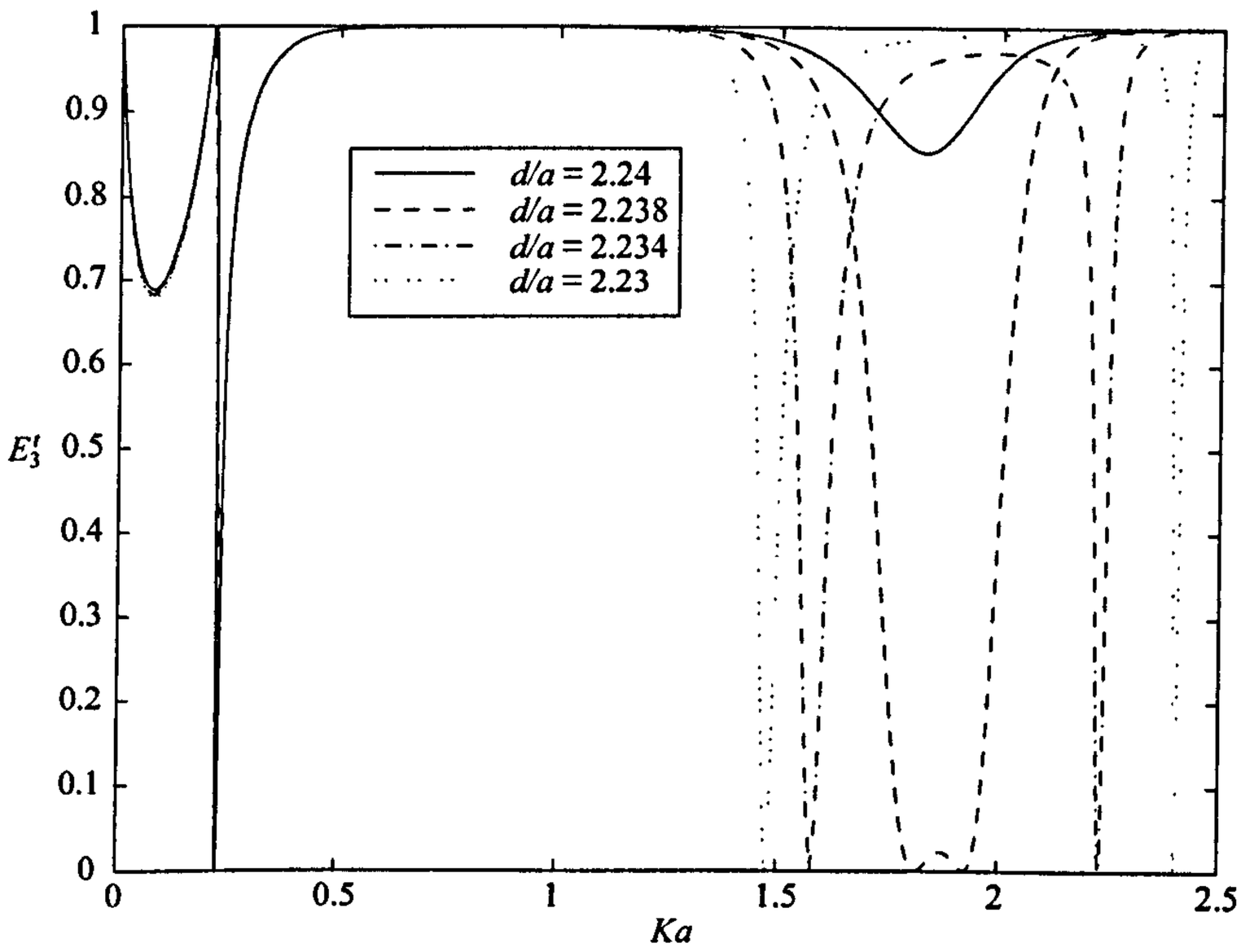

Figure 5.26: Transmission energies due to a wave of wavenumber k incident on a cylinder in the upper layer; $\rho = 0.5$, $d/f = 2$ and $\alpha_{\text{inc}} = 0.35$.

Chapter 6

Trapped modes above a cylinder

6.1 Introduction

A mass of fluid bounded by fixed surfaces and by a free surface of infinite extent is capable of vibrating under gravity in a mode, called a trapped mode, containing finite energy. The existence of a trapped mode above a submerged, horizontal, circular cylinder was first proved by Ursell (1951). On the basis of full linear theory of water waves he showed that the vanishing of a certain infinite determinant was required for the existence of the trapped waves. He went on to show that zeros of the determinant exist if the radius of the cylinder was small compared to the length of the waves. Further work by McIver & Evans (1985) found the dispersion curves by evaluating the determinant numerically and compared the results to those obtained using the mild slope equation.

Trapped modes in a two-layer fluid have received very little attention. Kuznetsov (1993) studied trapped modes in a channel occupied by a two-layer fluid spanned by a cylinder. Using a perturbation method Kuznetsov claimed to show there are two sets of frequencies of trapped modes; one set corresponding to trapped modes on the free surface which are close to the single-layer fluid case, and the other set corresponding to trapped modes on the interface. Only the set of interfacial modes exist, the frequencies at which the free-surface modes would exist are such that waves would propagate on the interface thus cannot be trapped modes.

In this chapter we will extend the work to the case of a submerged, horizontal, circular cylinder firstly in finite depth and then in a two-layer fluid.

6.2 Finite-depth single-layer fluid

We choose Cartesian coordinates such that the (x, y)-plane coincides with the undisturbed free surface of the fluid and the z-axis points directly upwards. The fluid occupies the region $-h < z < 0$ and an infinite cylinder of radius a has its centre positioned at $z = f < 0$ and its generator runs parallel to the y-axis. As in section 5.2, we write the velocity potential as

$$\Phi = \Re\{\phi(x, z)e^{ily}e^{-i\omega t}\}, \tag{6.2.1}$$

where ϕ satisfies the following conditions

$$(\nabla^2 - l^2)\phi = 0 \qquad \text{everywhere in the fluid,} \tag{6.2.2}$$

$$\phi_z - K\phi = 0 \qquad \text{on } z = 0, \tag{6.2.3}$$

$$\phi_z = 0 \qquad \text{on } z = -h, \tag{6.2.4}$$

$$\frac{\partial \phi}{\partial r} = 0 \qquad \text{on } r = a, \tag{6.2.5}$$

from (5.2.3)–(5.2.6).

Propagating waves have wavenumber k which satisfies the dispersion relation $K = k \tanh kh$. A general scattering potential, which satisfies the above conditions, is described by (5.2.13) in the far field. For trapped mode solutions the motion must decay away from the cylinder, which implies

$$\phi, |\nabla\phi| \to 0 \text{ as } |x| \to \infty. \tag{6.2.6}$$

To satisfy (6.2.6) we set $l > k$ and so the far-field behaviour is described by

$$\phi \sim A^{\pm}e^{\mp\sqrt{l^2-k^2}x}\frac{\cosh k(z+h)}{\cosh kh}, \tag{6.2.7}$$

as $x \to \pm\infty$, from (5.2.13). The term involving $B^{\pm}$ is removed as it grows exponentially away from the cylinder which is not physically feasible. We can represent the velocity potential in terms of the multipoles described by (5.2.31) and (5.2.32). Here we shall only consider trapped modes symmetric about the line $x = 0$ because we know they exist for the infinite-depth case as shown by McIver & Evans (1985). Some calculations of antisymmetric modes have been made by Martin (1989). We write the velocity potential as

$$\phi = \sum_{m=0}^{\infty} \alpha_m \phi_m^s, \tag{6.2.8}$$

where

$$\phi_m^s = K_m(lr)\cos m\theta + \sum_{n=0}^{\infty} A_{mn}^s I_n(lr)\cos n\theta, \tag{6.2.9}$$

$$A_{mn}^s = \frac{\epsilon_n}{2}\int_0^\infty \cosh mu \cosh nu\, D^{(0)}(u)du, \tag{6.2.10}$$

$$\begin{aligned} D^{(0)}(u) =& (((v+K)[(-1)^n + (-1)^m] + (v-K)e^{-2vf})e^{-vh} \\ &+ (-1)^{m+n}(v+K)e^{v(2f+h)})/(v\sinh vh - K\cosh vh), \end{aligned} \tag{6.2.11}$$

and $v = l\cosh u$, from (5.2.41), (5.2.43) and (5.2.45). We note that the multipole function $D^{(0)}$ no longer has a pole because v cannot satisfy the dispersion relation since $v = l\cosh u > k$. This means that A_{mn}^s, $m \geq 0$, $n \geq 0$ and hence all the multipoles ϕ_m^s, $m \geq 0$ will be real. To solve for the unknowns α_m, $m \geq 0$ we apply the body boundary condition (6.2.5) to obtain

$$\alpha_n + \frac{I_n'(la)}{K_n'(la)}\sum_{m=0}^{\infty}\alpha_m A_{mn}^s = 0. \tag{6.2.12}$$

We can write the above in matrix form

$$\mathbf{A}\underline{\alpha} = 0, \tag{6.2.13}$$

$$\text{where} \qquad \mathbf{A} = [\delta_{mn} + I_n'(la)A_{mn}^s/K_n'(la)], \tag{6.2.14}$$

$$\underline{\alpha} = [\alpha_m], \tag{6.2.15}$$

and for non-trivial solutions we require the determinant of the real matrix $\mathbf{A}$ to be zero. The solution procedure used was to fix la and systematically vary ka, looking for zeros of a suitably truncated determinant. Convergence checks were made and convergence was worst with the cylinder close to the free surface. The results presented below were computed to three decimal places for which in some cases a 40×40 system was required. Generally, higher frequencies required more terms than lower frequencies.

6.2.1 Results

Figures 6.1 and 6.2 show the trapped mode frequencies for a circular cylinder submerged in a finite-depth single-layer fluid. In both graphs we have plotted the values of ka against la for when the determinant of the matrix $\mathbf{A}$ vanishes. The existence of the trapped modes requires $k < l$ so the line $k = l$ (thin dashed line) is included as an upper bound for the dispersion curves.

In figure 6.1 the different curves correspond to different submergence depths, f/a, of the cylinder which are -1.01, -1.05, -1.1 and -1.5, where the depth, h/a, of the fluid is 3. For the submergence $f/a = -1.5$ we see there is just a single mode and that the curve lies close to the upper bound. As the cylinder approaches the free surface, $|f/a| \to 1$, the frequency of the first mode decreases and as we come closer still a second mode appears. For $f/a = -1.05$ a second mode exists for $2.1 \leq la \leq 19.4$. When $f/a = -1.01$ there is a third mode appearing at $ka \approx 6$. These results are very similar to those found in McIver & Evans (1985), and it would seem likely that the number of possible modes increases without bound as the top of the cylinder approaches the free surface.

In Figure 6.2 the curves correspond to different depths, h/a, of the fluid which are 2.03, 2.5, 3 and 15, where the submergence of the cylinder has the value $f/a = -1.01$. We can see that the frequencies of the trapped modes are increased by the presence of the finite depth. The first mode being affected more that the second.

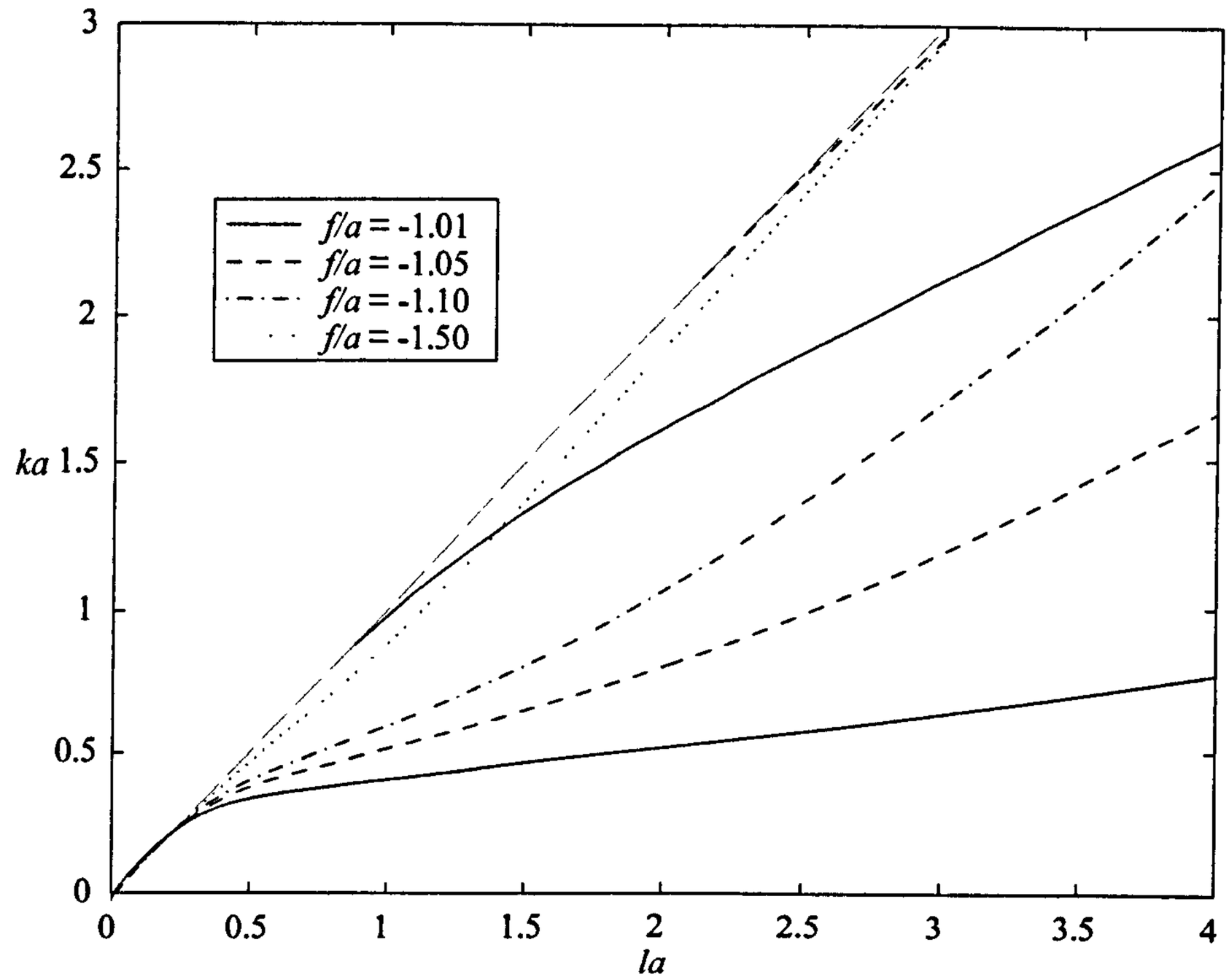

Figure 6.1: Trapped mode frequencies in a finite depth single layer fluid; $h/a = 3$.

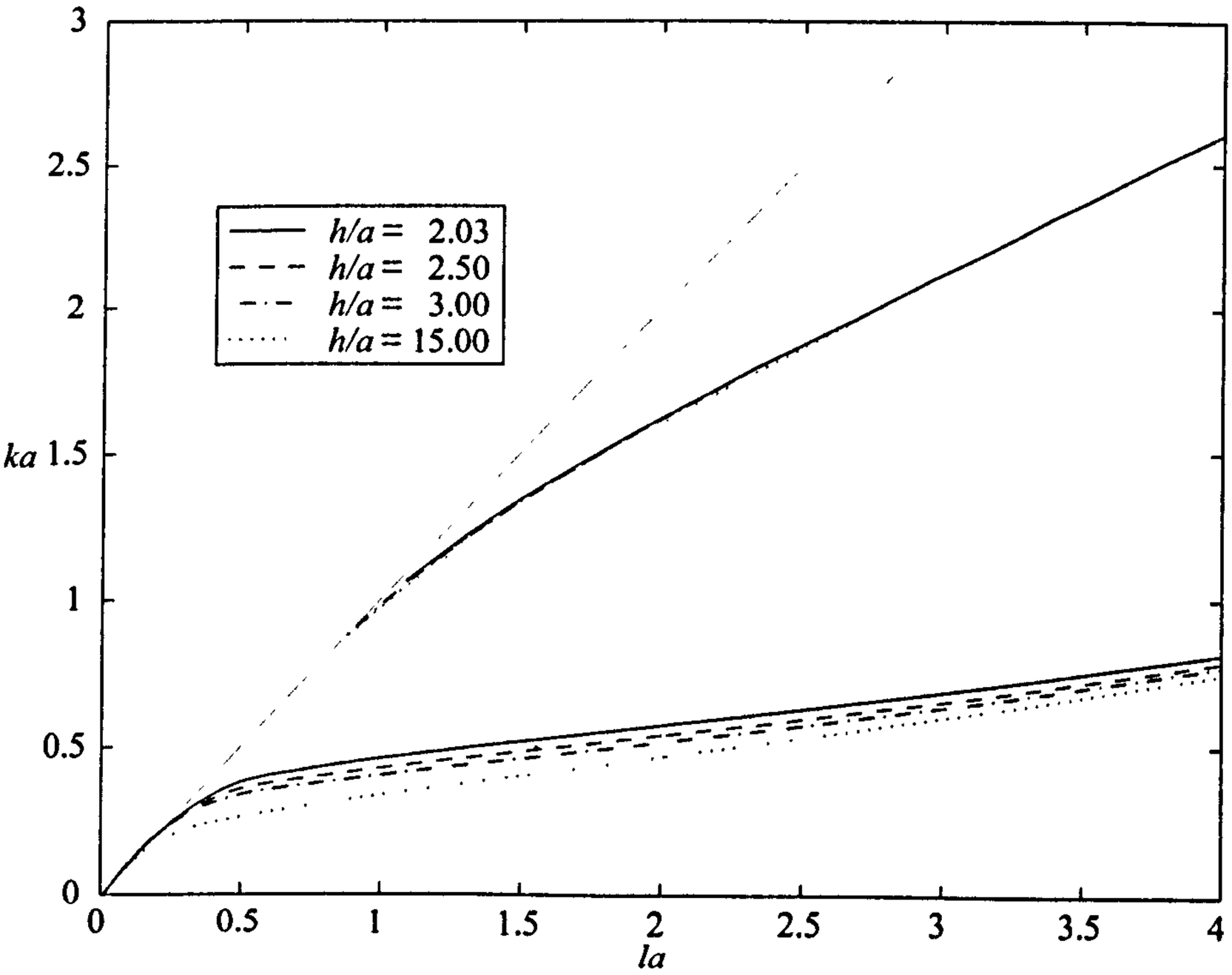

Figure 6.2: Trapped mode frequencies in a finite depth single layer fluid; $f/a = -1.01$.

6.3 Two-layer fluid

We now consider the case of trapped modes above a horizontal cylinder in a two-layer fluid. The velocity potential is written as in (5.3.2) where the time independent potential $\phi(x,z)$, satisfies the boundary conditions (2.2.3)–(2.2.5) and the modified Helmholtz equation (5.2.12). For trapped modes we restrict l to be in the range $l > k > K$ so that there are no waves propagating on either the free surface or the interface. The far-field behaviour, from (5.3.4)-(5.3.5), becomes

$$\phi^I \sim A^{\pm} e^{\mp \beta x} e^{Kz} + B^{\pm} e^{\mp bx} g(z), \tag{6.3.1}$$

$$\phi^{II} \sim A^{\pm} e^{\mp \beta x} e^{Kz} + B^{\pm} e^{\mp bx} e^{kz}, \tag{6.3.2}$$

as $x \to \pm\infty$, where $\beta = \sqrt{l^2 - K^2}$ and $b = \sqrt{l^2 - k^2}$. This corresponds to waves progressing along the length of the cylinder in the y-axis direction with the motion decaying exponentially in the positive and negative x-direction. The terms involving $C^{\pm}$ and $D^{\pm}$ are removed as they tend to infinity as $|x| \to \infty$.

6.3.1 Cylinder in the lower fluid layer

We seek trapped modes symmetric about the line $x = 0$ as they are known to exist for the single-fluid problem. For symmetric modes we write the velocity potential as

$$\phi = \sum_{m=0}^{\infty} \alpha_m \phi_m^s, \tag{6.3.3}$$

where ϕ_m^s are the symmetric multipoles described by (5.3.30)–(5.3.31), and when expanded about $z = f(< 0)$ are

$$\phi_m^s = K_m(lr)\cos m\theta + \sum_{n=0}^{\infty} A_{mn}^s I_n(lr)\cos n\theta, \tag{6.3.4}$$

$$\text{where } A_{mn}^s = (-1)^{m+n}\epsilon_n \int_0^{\infty} \cosh mu \cosh nu \; e^{vf} C_L(v)du, \tag{6.3.5}$$

$$C_L(v) = \frac{(v+K)[(v+K\sigma)e^{-2vd} - v + K]e^{vf}}{(v-K)[(v+K)e^{-2vd} - v + K\sigma]}, \tag{6.3.6}$$

and $v = l\cosh u$, from (5.3.45), (5.3.47) and (5.3.36). We note that since $l > k > K$ there will be no real poles of the function $C_L(u)$ because

$$\cosh\gamma_1 \neq K/l < 1, \tag{6.3.7}$$

$$\cosh\gamma_2 \neq k/l < 1, \tag{6.3.8}$$

and so the multipoles, ϕ_m^s, will be real. Applying the body boundary condition, $\partial\phi/\partial r = 0$ on $r = a$, we obtain an infinite system of linear equations for the unknowns α_m, which is

$$\alpha_n + \frac{I_n'(la)}{K_n'(la)} \sum_{m=0}^{\infty} \alpha_m A_{mn}^s = 0. \tag{6.3.9}$$

Truncation allows us to write this in matrix form

$$\mathbf{A}\underline{\alpha} = 0, \tag{6.3.10}$$

$$\text{where} \quad \mathbf{A} = [\delta_{mn} + I_n'(la)A_{mn}^s/K_n'(la)], \tag{6.3.11}$$

$$\underline{\alpha} = [\alpha_m], \tag{6.3.12}$$

and for non-trivial solutions we require the determinant of the real matrix **A** to vanish. As before, we fix one parameter, say la, and vary another, say ka, to find the zeros of the truncated determinant of **A**. The results presented below were obtained to two decimal places and for some values a 32×32 system was required.

Free-surface and interfacial elevations

In order to appreciate the nature of the trapped modes in two-layer fluids it will be helpful to look at the profiles of the free-surface and interface. The free-surface and interfacial elevations, denoted by H_d and H_0 respectively, can be written in the form $H = \Re\{\eta(x)e^{ily}e^{-i\omega t}\}$. These elevations are related to the velocity potentials by

$$\frac{\partial H_d}{\partial t} = \frac{\partial \Phi^I}{\partial z} \qquad z = d, \tag{6.3.13}$$

$$\frac{\partial H_0}{\partial t} = \frac{\partial \Phi^{II}}{\partial z} = \frac{\partial \Phi^I}{\partial z} \qquad z = 0. \tag{6.3.14}$$

Using the form of the velocity potentials given by (5.3.2) with (6.3.13) and (6.3.14) we obtain

$$\begin{aligned} H_d(x) &= \Re\left\{\frac{i}{\omega}\phi_z^I(x,d)e^{i(ly-\omega t)}\right\} \\ &= -\frac{1}{\omega}\phi_z^I(x,d)\sin(ly-\omega t), \end{aligned} \tag{6.3.15}$$

$$H_0(x) = -\frac{1}{\omega}\phi_z^I(x,0)\sin(ly-\omega t), \tag{6.3.16}$$

where

$$\phi_z^I(x,d) = \sum_{m=0}^{\infty}(-1)^m 2(1+\sigma)K^2\alpha_m \int_0^{\infty} v\cosh mu\cos(lx\sinh u)\frac{e^{v(f-d)}}{(v-K)h(v)}du, \tag{6.3.17}$$

$$\phi_z^I(x,0) = \sum_{m=0}^{\infty}(-1)^m(1+\sigma)K\alpha_m \times \int_0^{\infty} v\cosh mu\cos(lx\sinh u)e^{vf}\frac{[(v+K)e^{-2vd}-v+K]}{(v-K)h(v)}du, \tag{6.3.18}$$

from (6.3.3), (5.3.30) and (5.3.34)–(5.3.35). The coefficients α_m are the components of the eigenvector of the matrix **A** corresponding to the eigenvalue zero. The non-dimensionalised normalised maximum displacements of the free surface and interface from their mean positions, denoted Y_d and Y_0, are written

$$Y_d(X) = \phi_z^I(X,d/a)/\overline{H}, \tag{6.3.19}$$

$$Y_0(X) = \phi_z^I(X,0)/\overline{H}, \tag{6.3.20}$$

where $\overline{H} = \max(|\phi_z^I(0,d/a)|, |\phi_z^I(0,0)|)$ and $X = x/a$. Hence, for each pair of profiles the amplitudes will be scaled such that the maximum deviation at $X = 0$ is 1.

Results

Figures 6.3–6.5 show the results obtained for trapped modes above a circular horizontal cylinder situated in the lower fluid of a two-layer fluid. In all the figures the submergence, f/a, of the cylinder is -1.01 which is very close to the interface.

Figure 6.3 shows the trapped mode frequencies for a density ratio of $\rho = 0.5$. The different curves correspond to four different depths of the upper fluid layer; $d/a = 0.5$, 1, 1.5 and 2. For each value of d/a there are two curves; the lower curve will be referred to as the first mode and the upper curve will be referred to as the second mode. The existence of trapped modes requires $l > k$ so that $l = k$ (thin dashed line) is an upper bound for these curves. The curves are similar to those obtained for a single-layer fluid. We notice that as we increase the depth of the upper fluid layer these trapped mode frequencies decrease. By fixing d/a and ρ and varying the submergence we can find different numbers of modes. As f/a approaches -1 we see a 'fanning out' of the curves as higher modes appear just like in the single-layer case.

Figure 6.4 shows the trapped mode frequencies against ρ when $la = 2$. There are four sets of results corresponding to different depths of the upper fluid layer. These are

$d/a = 0.8$, 1.0, 1.2 and 2.0 and for each of these values there are two curves showing the first and second modes. We recover the results for the infinite-depth single-layer fluid problem when $\rho = 0$. As $\rho \to 1$ we see that the frequency Ka of the trapped modes, in the lower plot, tends to 0 while the wavenumber ka, in the upper plot, tends to some limit for each mode. One would expect that as $\rho \to 1$ we would recover the single-layer fluid results where the submergence of the cylinder is $f/a - d/a$. This is not the case however and further discussion is given in section 6.3.3 below.

In Figure 6.5 we have the free-surface and interfacial profiles, Y_d and Y_0 respectively, of the trapped modes when $la = 2$ and $d/a = 1$. The different curves correspond to six different values of the density ratio; $\rho = 0$, 0.2, 0.4, 0.6, 0.8 and 0.999. The frequencies for these profiles are given by the dashed line in figure 6.4. The left-hand plots are for the first mode, no crossings of $Y_0 = 0$ or $Y_d = 0$, corresponding to the lower frequencies in figure 6.4 whilst the right-hand plots are for the second mode, one zero crossing on the interface, corresponding to the higher frequencies. Note that for each density ratio the profiles for each mode are scaled such that the maximum deviation at $X = 0$ is 1. For both modes the motion is concentrated about the interface as shown in the lower plots. The free-surface and interface are out of phase for the first mode whereas they are in phase for the second. We can see that the amplitude of the free surface becomes very small as $\rho \to 1$ for both modes. The shape of the interface profile for the first mode barely changes over the range of values of ρ. For the second mode however the disturbance on the interface projects further into the fluid as $\rho \to 1$. This is explained by the value of the wavenumber k in the limit $\rho \to 1$. In the far-field form of the potential we have an $\exp(-\sqrt{l^2 - k^2}|x|)$ term. We see as $\rho \to 1$ in figure 6.4 that the second mode $ka \to 2 = la$. This is not a trapped mode in the limit as the exponential term will not decay away from the body.

If we let $\rho \to 0$ in this problem (corresponding to $\sigma \to 1$) then we must have $\rho^I \to 0$. The continuity of pressure condition (2.2.4) at the interface reduces to a free-surface condition and the multipoles go over to those for a single-layer infinite-depth fluid. Thus by letting $\rho \to 0$ in the above analysis we recover the results for trapped modes above a horizontal circular cylinder in deep water, as in McIver & Evans (1985).

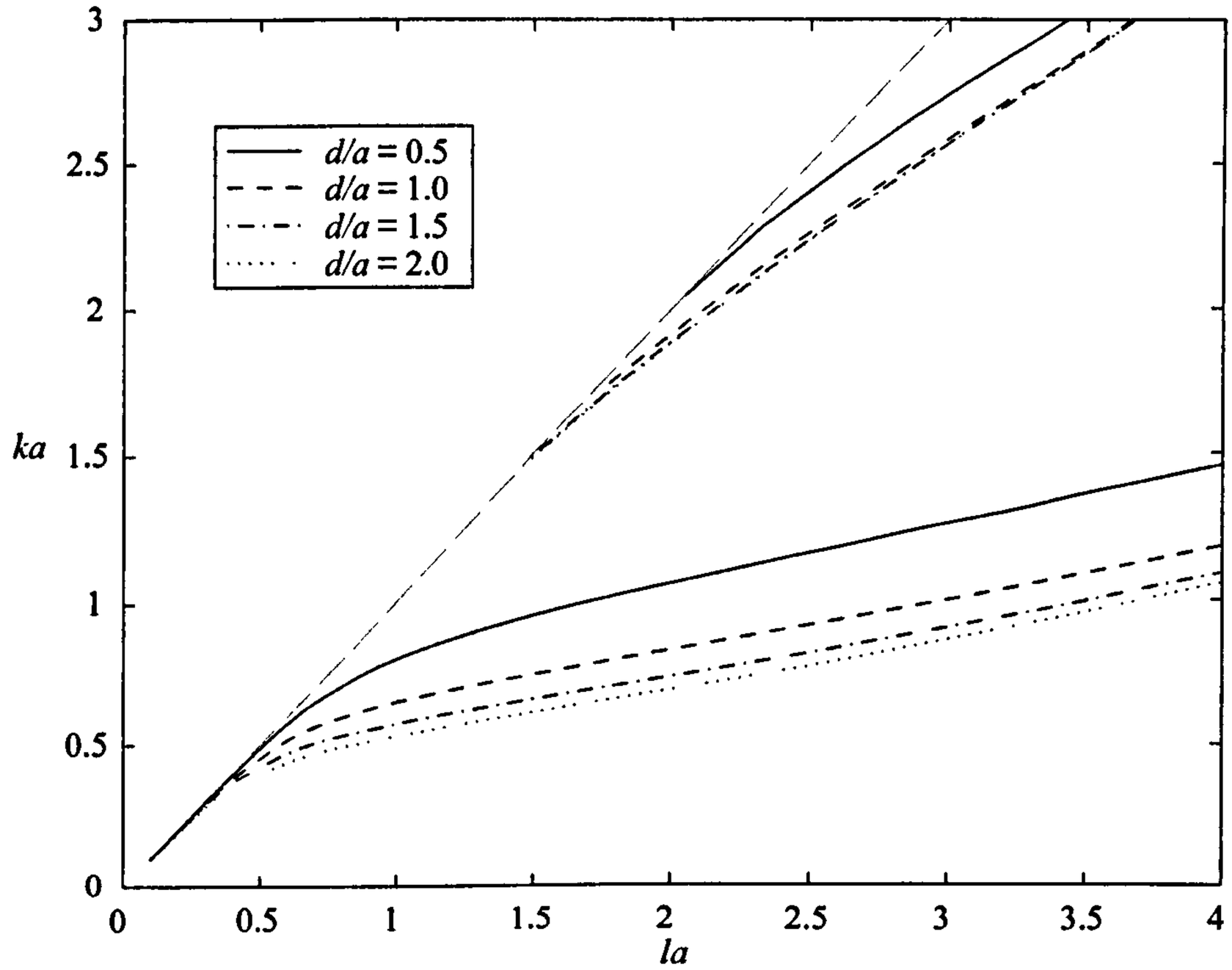

Figure 6.3: Trapped mode frequencies for a cylinder in the lower fluid layer; $\rho = 0.5$ and $f/a = -1.01$.

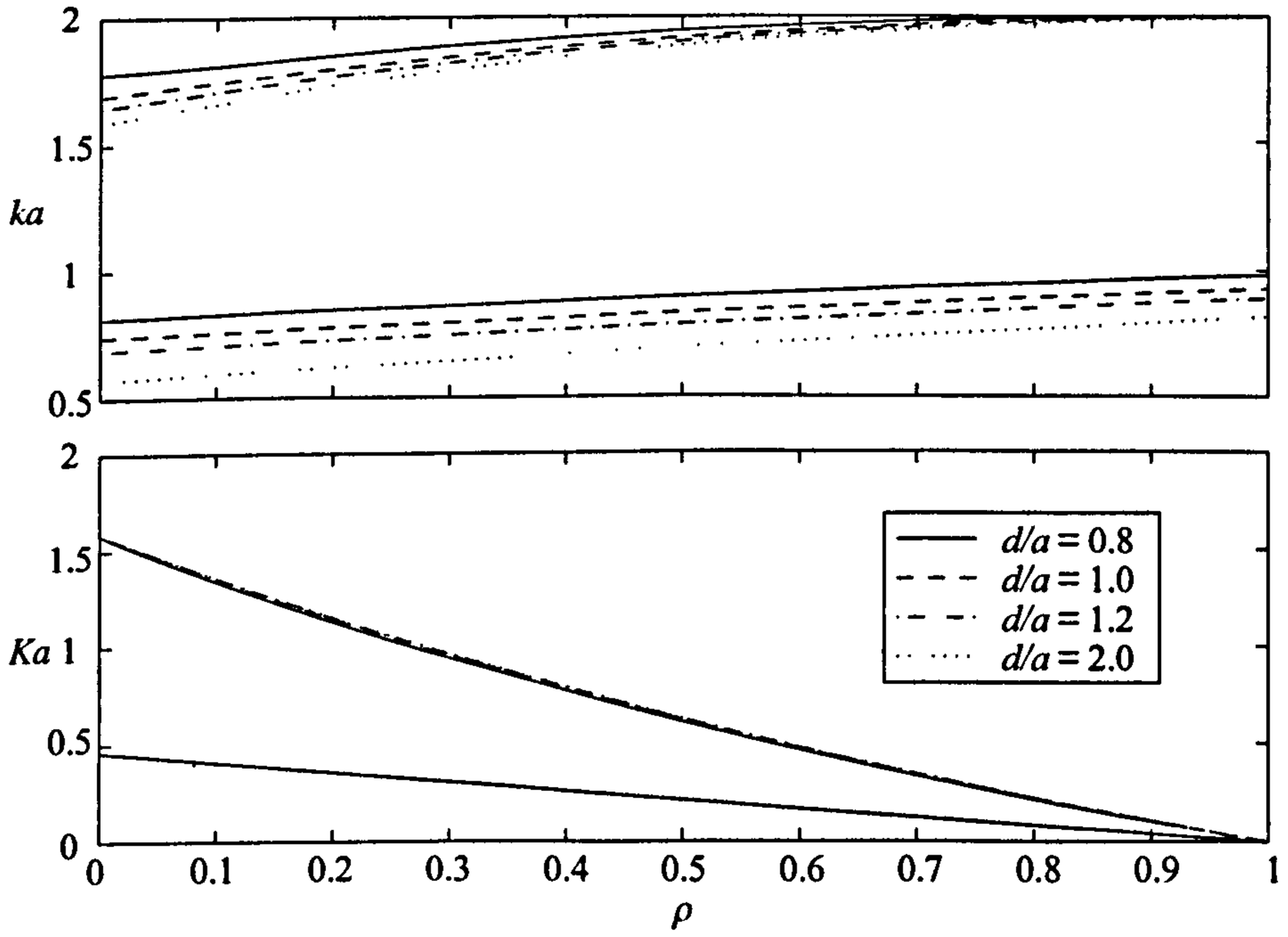

Figure 6.4: Trapped mode frequencies for a cylinder in the lower fluid layer; $la = 2$ and $f/a = -1.01$.

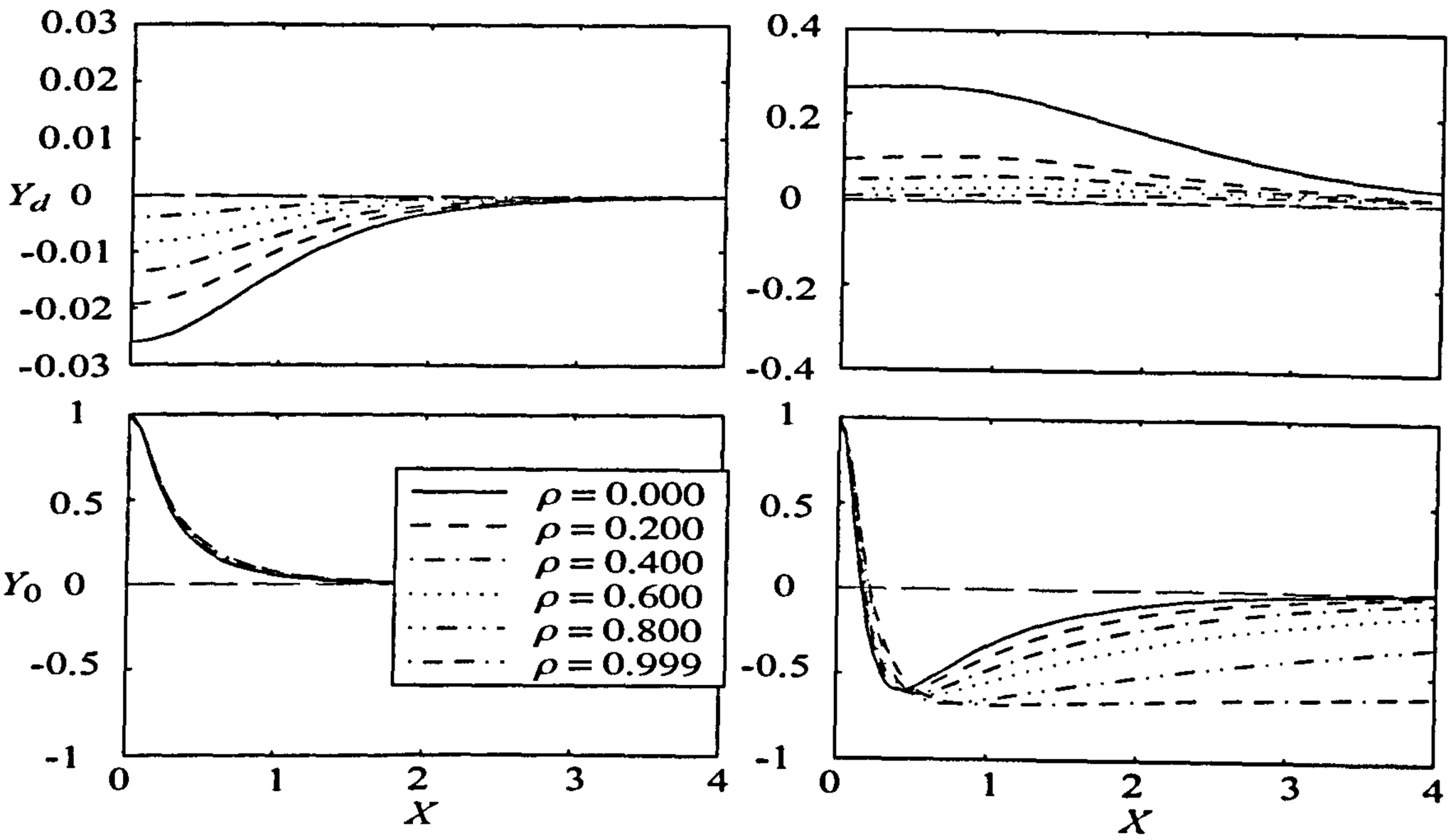

Figure 6.5: The free-surface and interfacial profiles of trapped modes for a cylinder in the lower fluid layer; $la = 2$, $f/a = -1.01$ and $d/a = 1.0$.

6.3.2 Cylinder in upper layer

For the case of a cylinder in the upper fluid layer the velocity potential can be expanded using (6.3.3), but we now use the symmetric multipole expansions for the upper fluid layer. Hence, from (5.3.73), (5.3.75), (5.3.66) and (5.3.67) the multipole potentials when expanded about $r = 0$ are

$$\phi_m^s = K_m(lr)\cos m\theta + \sum_{n=0}^{\infty} B_{mn}^s I_n(lr)\cos n\theta, \tag{6.3.21}$$

$$\text{where } B_{mn}^s = \epsilon_n \int_0^{\infty} \cosh mu \cosh nu[(-1)^n A_U^{(0)}(v)e^{vf} + B_U^{(0)}(v)e^{-vf}]du, \tag{6.3.22}$$

$$A_U^{(0)}(v) = \frac{(v+K)\ e^{-2vd}[(-1)^{m+1}(v-K\sigma)e^{vf} - (v-K)\ e^{-vf}]}{(v-K)((v+K)e^{-2vd} - v + K\sigma)}, \tag{6.3.23}$$

$$B_U^{(0)}(v) = \frac{(-1)^{m+1}(v+K)e^{v(f-2d)} - (v-K)\ e^{-vf}}{(v+K)e^{-2vd} - v + K\sigma}, \tag{6.3.24}$$

and $v = l\cosh u$. There are no poles of the functions $A_U^{(0)}$ and $B_U^{(0)}$ so the multipoles will again be real. By applying the body boundary condition, $\partial\phi/\partial r = 0$ on $r = a$, we obtain the same system of equations for α_m as (6.3.9) except A_{mn}^s is replaced by B_{mn}^s. We now need to find the zeros of the determinant of the real matrix described by

$$\mathbf{B} = [\delta_{mn} + I_n'(la)B_{mn}^s/K_n'(la)]. \tag{6.3.25}$$

The free-surface and interfacial elevations are given by (6.3.19) and (6.3.20), but we use the following forms for ϕ_z^I

$$\phi_z^I(x,d) = \sum_{m=0}^{\infty} 2K\alpha_m \times \int_0^{\infty} v\cosh mu\cos(lx\sinh u)\frac{e^{-vd}[(-1)^m(K\sigma - v)e^{vf} + (v-K)e^{-vf}]}{(v-K)h(v)}du, \tag{6.3.26}$$

$$\phi_z^I(x,0) = \sum_{m=0}^{\infty} (\sigma-1)K\alpha_m \times \int_0^{\infty} v\cosh mu\cos(lx\sinh u)\frac{(-1)^m(v+K)e^{v(f-2d)} + (v-K)e^{-vf}}{(v-K)h(v)}du, \tag{6.3.27}$$

from (6.3.3), (5.3.62), (5.3.66)–(5.3.67) and (5.2.25).

Results

Figures 6.6–6.13 show the results obtained for trapped modes in a two-layer fluid with a horizontal circular cylinder situated in the upper fluid.

Figure 6.6 shows the trapped mode frequencies where the depth of the upper region is $d/a = 2.0$ and the density ratio is fixed at $\rho = 0.5$. There are four curves corresponding to different submergence depths of the cylinder. These submergence depths are $f/a =$ 1.01, 1.09, 1.17 and 1.34. The upper bound for trapped modes $k = l$ is included, shown by the thin dashed line. We can see that as the surface of the cylinder approaches the interface, $f/a \to 1$, the curves fold out from the upper bound $k = l$. A similar effect is observed when the cylinder surface approaches the free surface as shown in figure 6.7. It is noted that in figure 6.7 there is a curve for each value of f/a which lies roughly on $k = l$.

In figure 6.8 we have the trapped mode frequencies plotted against the density ratio when $la = 2$ and $d/a = 2.1$. The results presented are for four values of submergence: $f/a = 1.05$, 1.06, 1.07 and 1.08. For each value of submergence there are two curves. When $\rho = 0$ we recover the single-layer finite-depth fluid results for depth d/a and cylinder submergence $f/a - d/a$. The first modes, the lower of each pair of curves, correspond to lines of constant Ka which are solutions to the single-layer fluid problem. These first modes appear to cross the second modes, the higher curves, but with closer inspection at these points, see figure 6.9, we observe near crossing. These near crossings, or diabolical points as described by Berry & Wilkinson (1984), of the trapped mode curves occur for other problems, see for example Linton & McIver (1998). Thus, for increasing ρ the first and second modes come very close to each other at some point after which the second mode terminates at $ka = 2(= la)$ and the first tends to some value as $\rho \to 1$. The limit of the first mode as $\rho \to 1$ does not correspond to a solution of the single-layer fluid problem since $Ka \to 0$ and discussion of its meaning is given in section 6.3.3. For $f/a = 1.08$ (the dotted curves) there is in fact a third mode for small ρ. This third mode has a near crossing with the second mode at around $\rho \approx 0.045$ and then terminates when it reaches $ka = 2$. For cylinders closer to the free surface more modes will appear and there will be more near crossings.

Figures 6.10–6.13 show the free-surface and interfacial profiles for $f/a = 1.05$, $d/a =$ 2.1 and $la = 2$. The left-hand plots in figures 6.10–6.12 are the profiles corresponding to the lower frequencies of the solid curve shown in figure 6.8, whereas the right-hand plots are the profiles corresponding to the higher frequencies. The upper graphs are the free-surface profiles while the lower graphs are the interfacial profiles. For all values of ρ used, the free-surface and interfacial profiles are in phase for the second modes

and out of phase for the first modes. For low density ratios, shown in figure 6.10, the motion for the first mode is concentrated about the free surface and for the second mode the motion is concentrated about the interface. As the density ratio is increased the motion for the first mode (left-hand graphs) is transferred from the free surface to the interface. At a density ratio of $\rho \approx 0.3275$ the free-surface and interfacial amplitudes for the first mode at $X = 0$ are equal. For the second mode we have a similar effect where the motion transfers from the interface to the free surface at $\rho \approx 0.326$. We note that both these changes take place in the region of the near crossing of the modes shown by the solid curves in figure 6.9. If we follow the first (second) mode with increasing ρ we begin with a free-surface (interface) trapped mode which later becomes an interface (free-surface) trapped mode. About the near-crossing point trapped modes can exist on both the free-surface and interface for both modes. It seems likely that if there were more modes with near-crossing points then these points would have similar properties. The second mode stops at $\rho \approx 0.435$ and approaching this value the motion remains on the free surface with very little happening at the interface. As $\rho \to 1$ the motion of the first mode is confined to the interface as the free-surface elevation becomes very small, as shown in figure 6.13.

When a submerged floating tunnel enters the fjord it does so at a gradual slope. At some point the tunnel would be completely within the upper fluid layer and typical parameter values would be $f/a = 1.05$, $d/a = 2.1$ and $\rho = 0.97$. In such a situation trapped modes may exist on the interface with little motion on the free surface as illustrated in figure 6.13.

If we let $\rho \to 0$ in this case then we now must have $\rho^{II} \to \infty$. The dispersion relation reduces to $K = k\tanh(kd)$ and the multipoles go over to those for a single-layer finite-depth fluid. Thus by letting $\rho \to 0$ we can recover the results for single-layer trapped modes above a cylinder in finite depth.

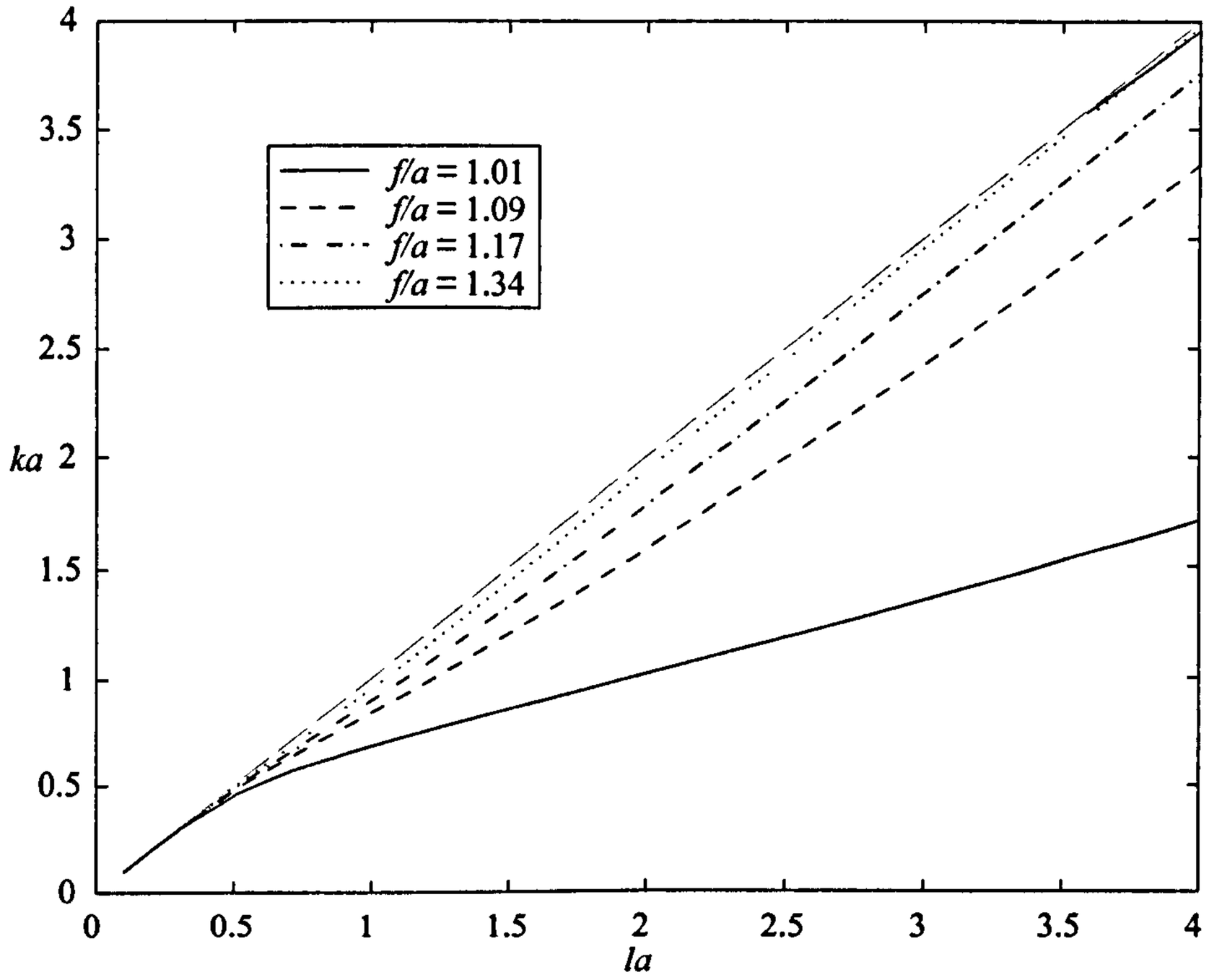

Figure 6.6: Trapped mode frequencies for a cylinder in the upper fluid layer; $d/a = 2$ and $\rho = 0.5$.

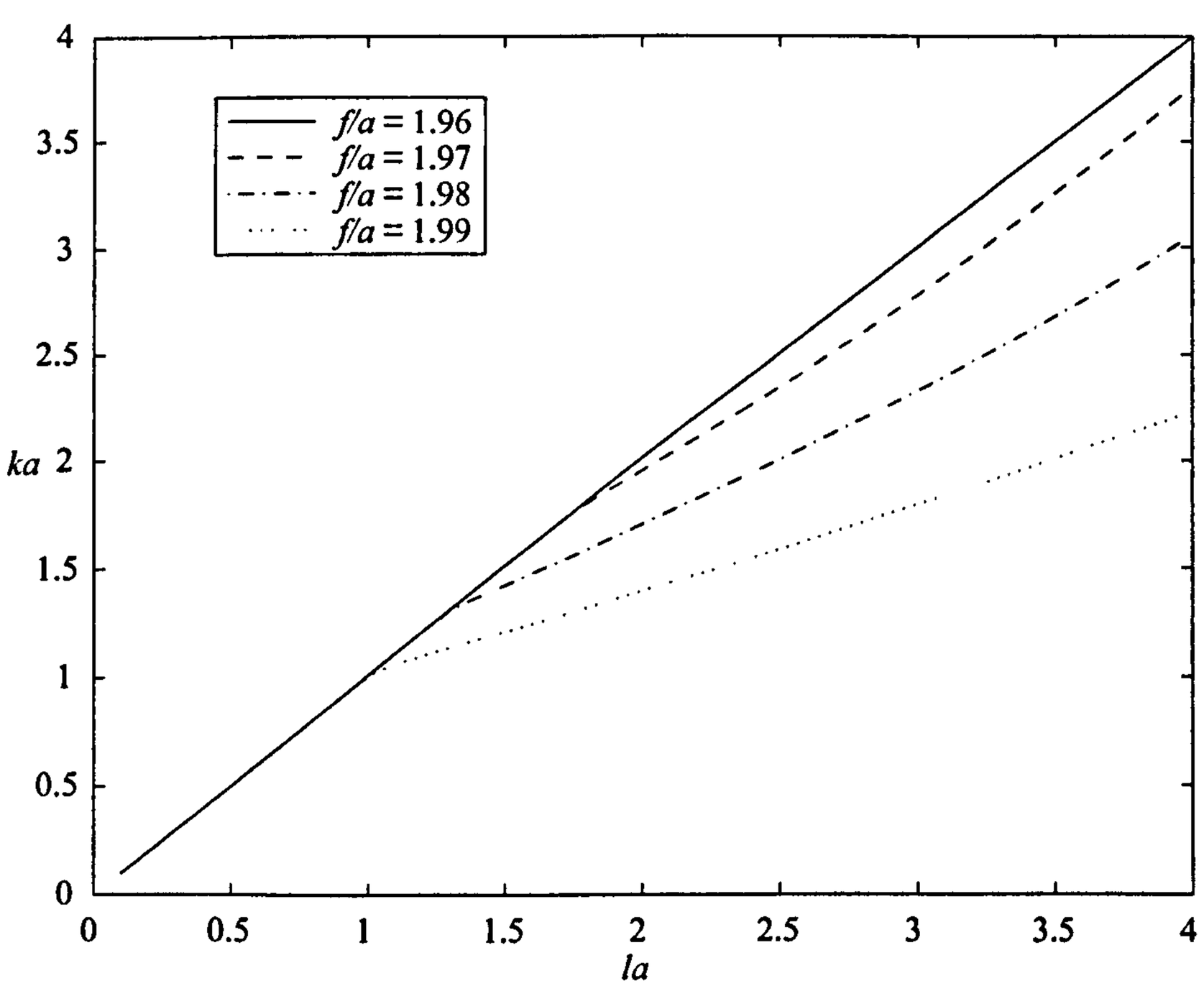

Figure 6.7: Trapped mode frequencies for a cylinder in the upper fluid layer; $d/a = 2$ and $\rho = 0.5$.

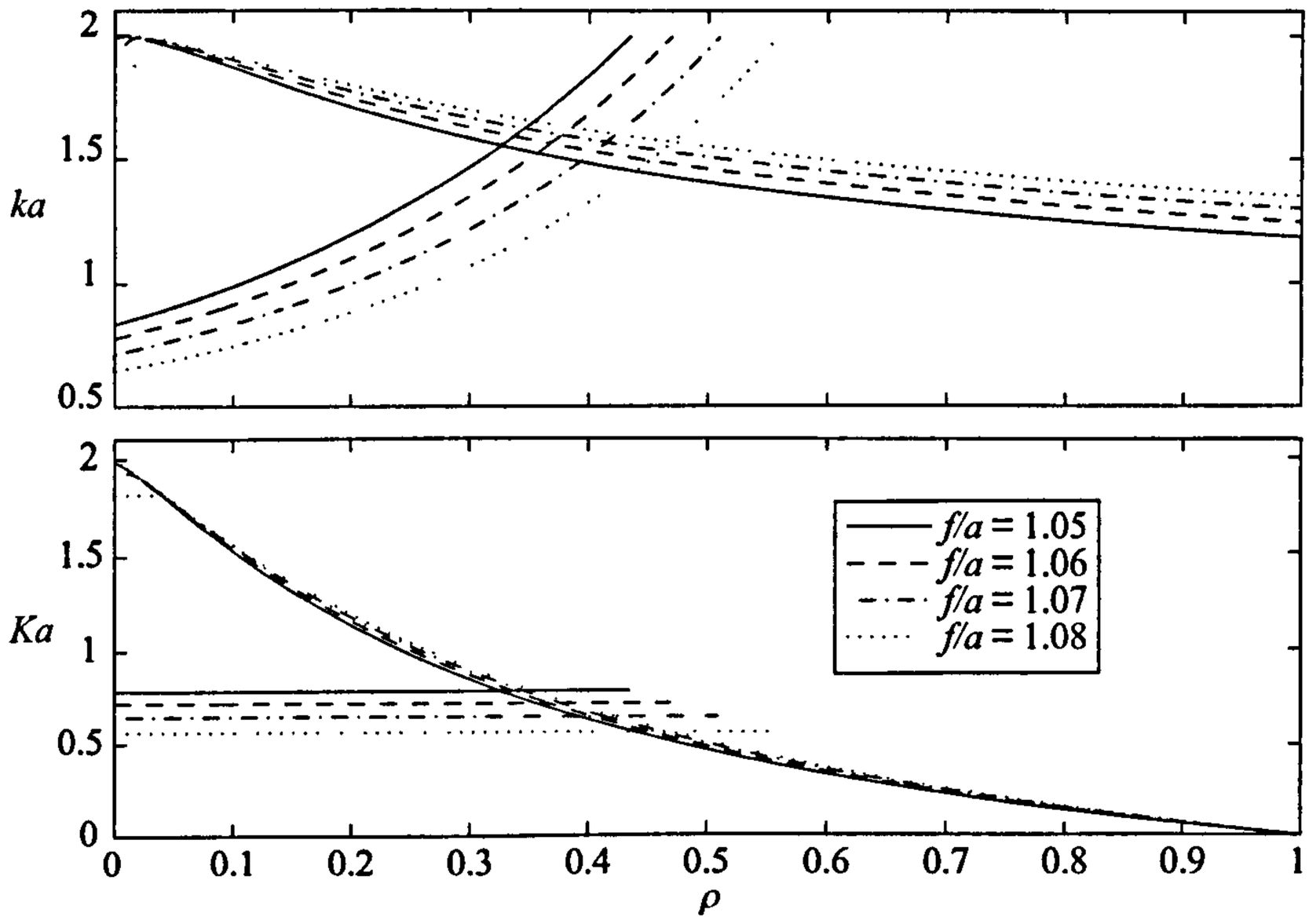

Figure 6.8: Trapped mode frequencies for a cylinder in the upper fluid layer; $la = 2$ and $d/a = 2.1$.

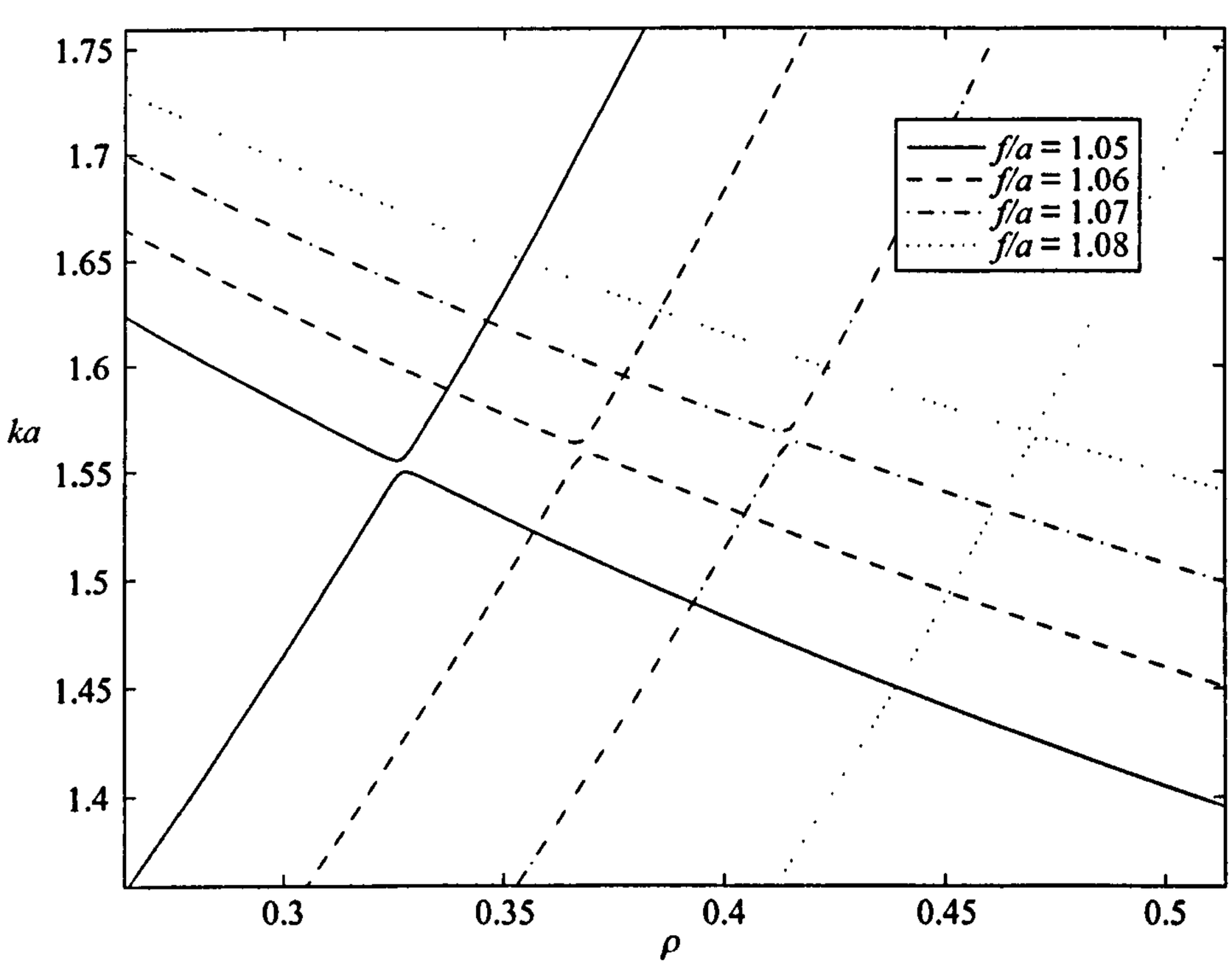

Figure 6.9: Trapped mode frequencies for a cylinder in the upper fluid layer, close up of near crossing; $la = 2$ and $d/a = 2.1$.

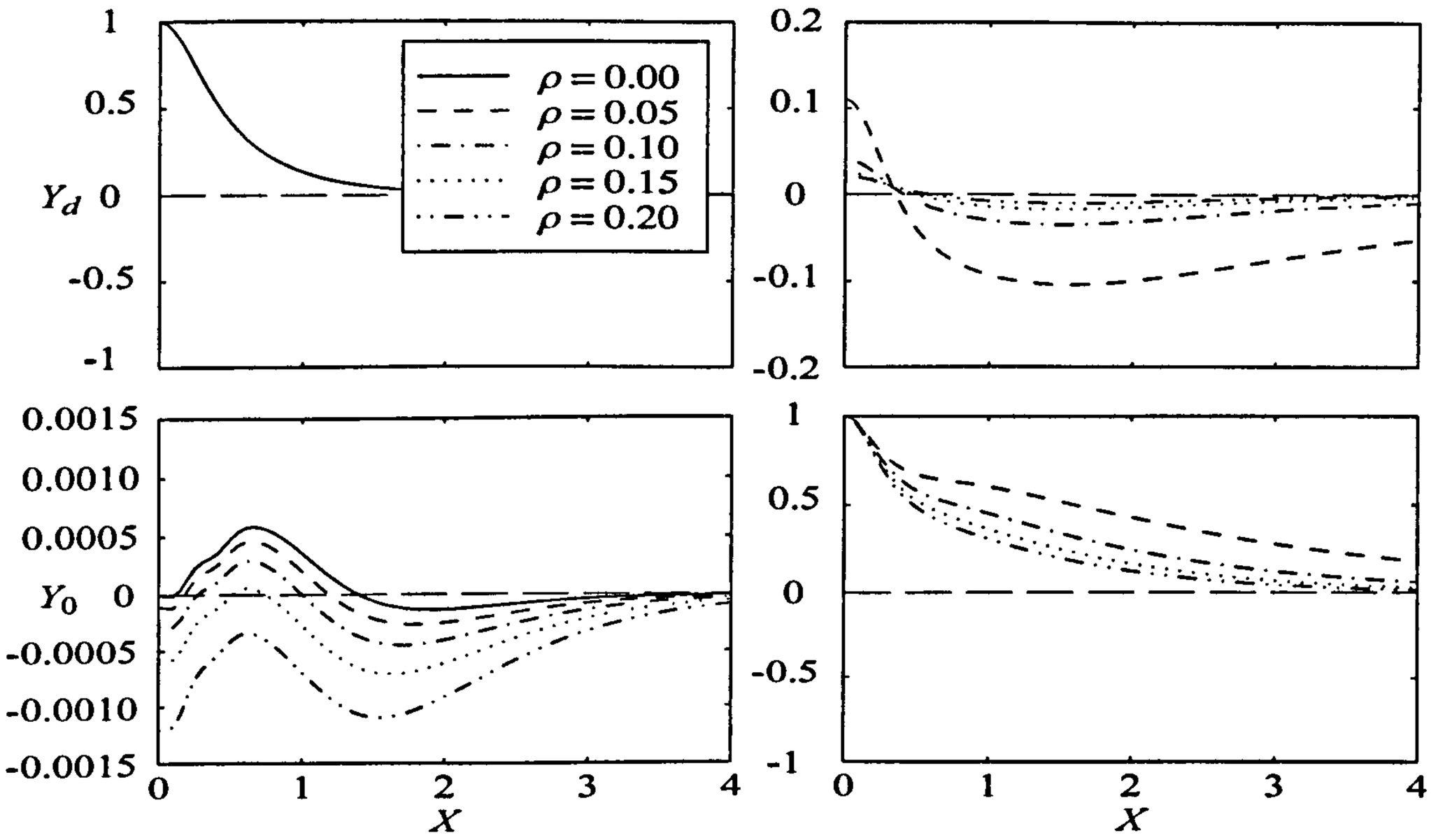

Figure 6.10: Free-surface and interfacial profiles for a cylinder in the upper fluid layer; $f/a = 1.05$, $d/a = 2.1$ and $la = 2$.

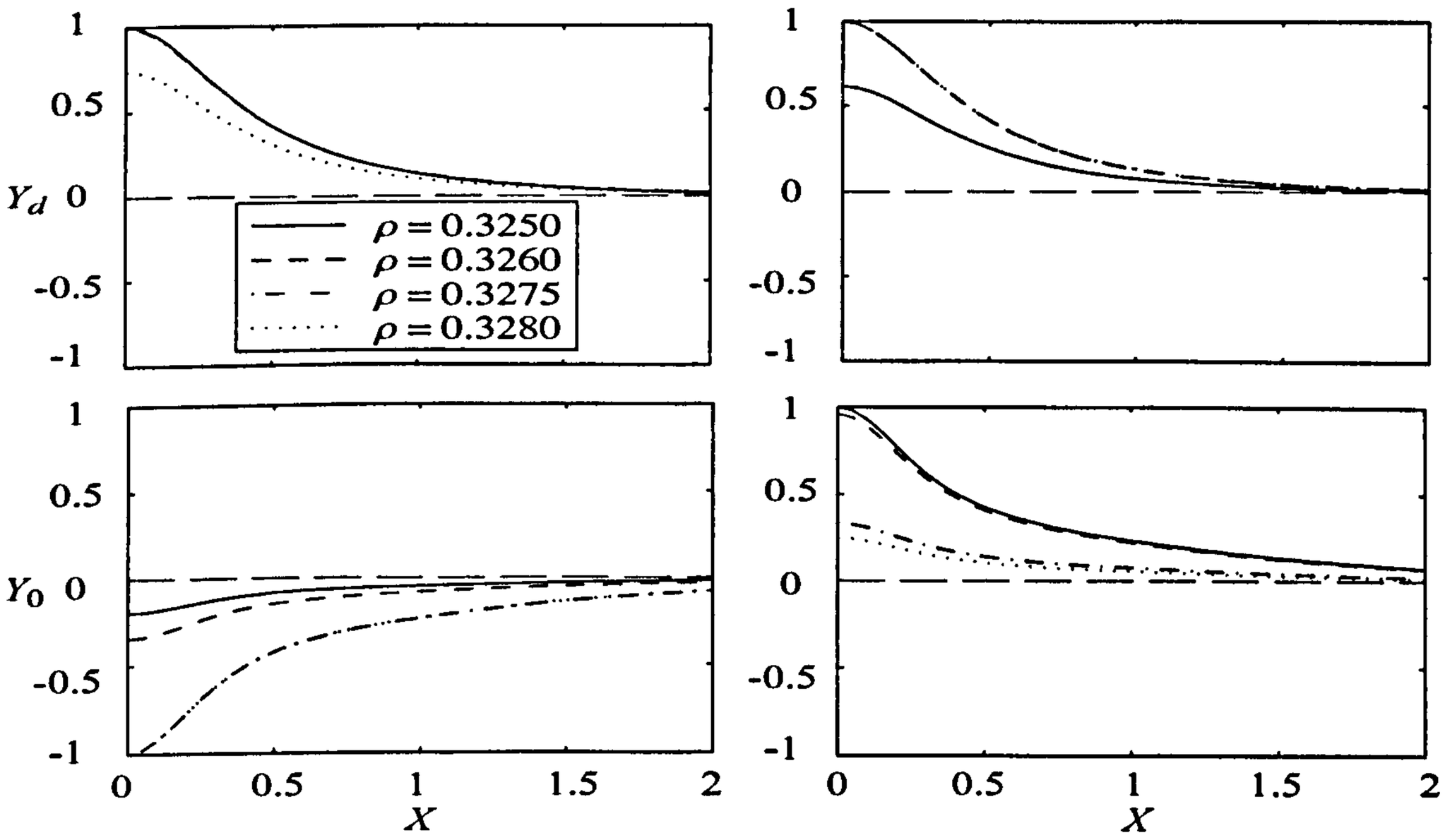

Figure 6.11: Free-surface and interfacial profiles for a cylinder in the upper fluid layer; $f/a = 1.05$, $d/a = 2.1$, $la = 2$.

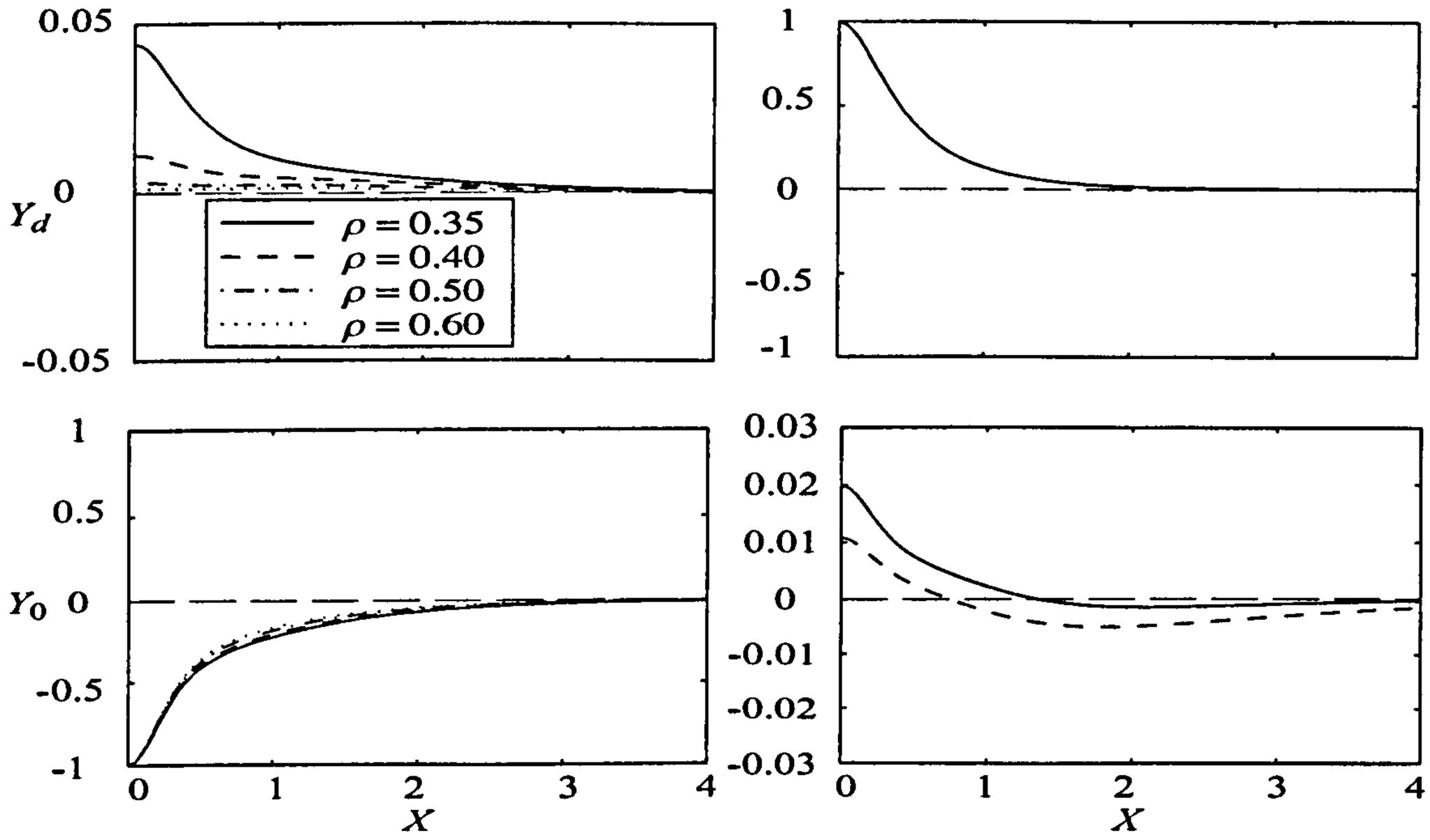

Figure 6.12: Free-surface and interfacial profiles for a cylinder in the upper fluid layer; $f/a = 1.05$, $d/a = 2.1$ and $la = 2$.

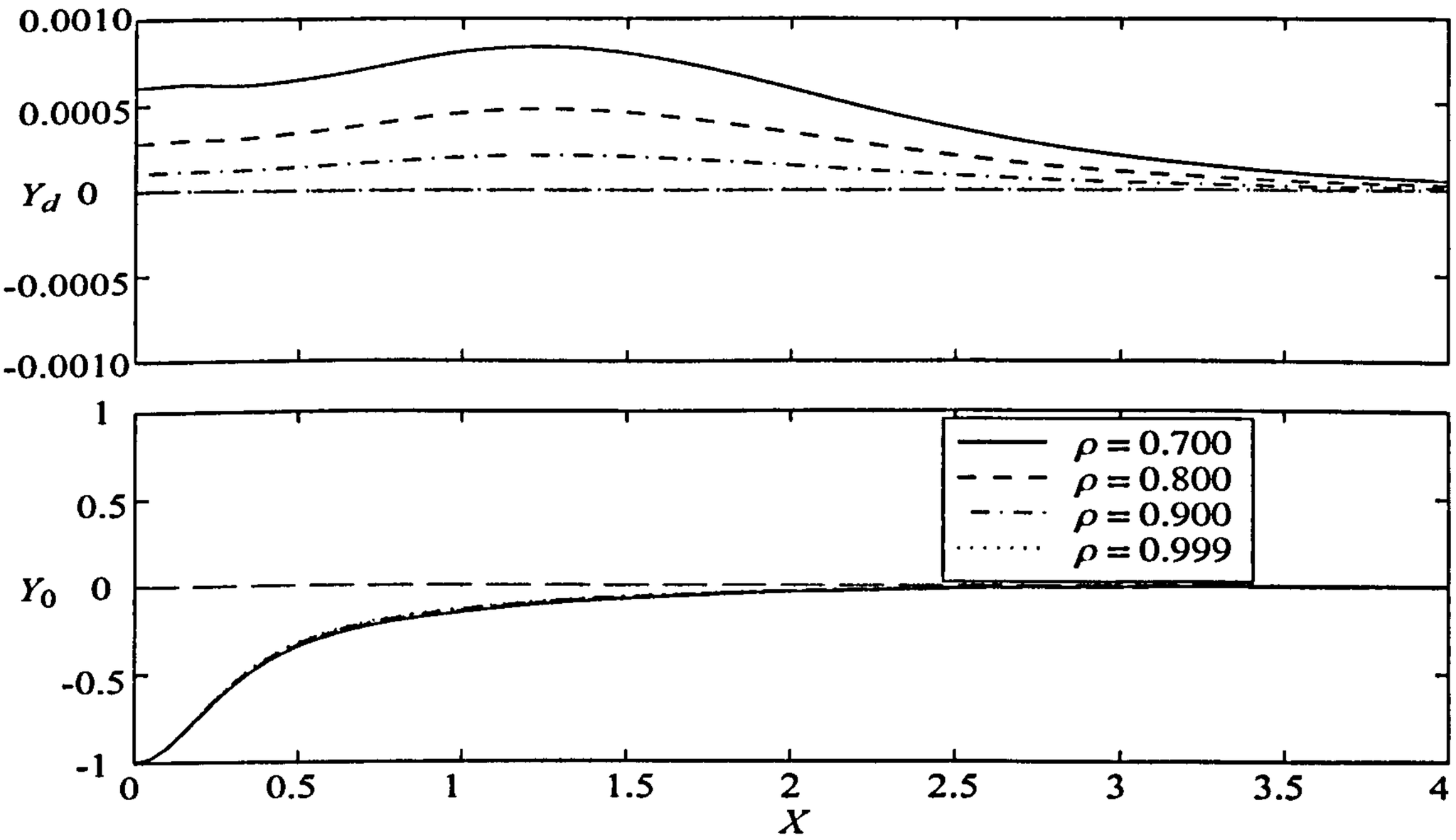

Figure 6.13: Free-surface and interfacial profiles for a cylinder in the upper fluid layer; $f/a = 1.05$, $d/a = 2.1$ and $la = 2$.

6.3.3 Limit as $\rho \to 1$

We would expect to recover the infinite-depth single-layer fluid trapped mode results from the two-layer analysis by letting $\rho \to 1$ (corresponding to $\sigma \to \infty$). This is not the case as illustrated in the results presented above.

In the limit $\rho \to 1$, we find that $K/k \to 0$, from the dispersion relation (2.2.11), and so if $l(> k)$ is fixed then K must tend to zero. Figures 6.4 and 6.8 show the trapped mode frequencies verses the density ratio for a cylinder in the lower and upper fluid respectively. For each set of parameter values there are two curves corresponding to two modes which are displayed in the graphs. We have already discussed the behaviour of the second mode as $\rho \to 1$ in the results above. $la \exp(-\sqrt{l^2 - k^2}|x|)$ term from the trapped mode. For a cylinder in either fluid layers, the lower mode tends to some value which is a trapped mode but certainly does not correspond to one of a single-layer fluid because $Ka \to 0$. To explain what is happening we shall consider the boundary conditions in the limit as $\rho \to 1$ and $K \to 0$ simultaneously.

First let us define the following

$$K = \varepsilon \qquad \ll 1, \tag{6.3.28}$$

$$\rho = 1 - \delta, \qquad \delta \ll 1, \tag{6.3.29}$$

$$K' = \frac{K}{1-\rho} = \frac{\varepsilon}{\delta} = O(1), \tag{6.3.30}$$

(the δ used here is different to those used previously) such that when $\rho \to 1$ along one of the lower curves in figure 6.4 or 6.8, which is for fixed l, we have $\varepsilon \to 0$ and $\delta \to 0$. The potentials satisfy the modified Helmholtz equation $(\nabla^2 - l^2)\phi = 0$ everywhere in the fluid. The free-surface condition becomes

$$\phi_z^I = K\phi^I = \varepsilon\phi^I \to 0, \qquad \text{on } z = d, \tag{6.3.31}$$

which represents a rigid lid upon the fluid. The continuity of vertical velocity at the interface remains the same, $\phi_z^I = \phi_z^{II}$, on $z = 0$. We can write the continuity of pressure

on the interface as

$$\rho(\phi_z^I - K\phi^I) = \phi_z^{II} - K\phi^{II}, \tag{6.3.32}$$

$$(1-\delta)(\phi_z^{II} - \varepsilon\phi^I) = \phi_z^{II} - \varepsilon\phi^{II}, \tag{6.3.33}$$

$$\varepsilon\phi^{II} - \delta\phi_z^{II} = \varepsilon(1-\delta)\phi^I, \tag{6.3.34}$$

$$K'\phi^{II} - \phi_z^{II} = K'(1-\delta)\phi^I,$$

$$\to K'\phi^I \qquad \text{as } \rho \to 1. \tag{6.3.35}$$

The dispersion relation will have only one solution, k, which must satisfy

$$2K' = k(1 - e^{-2kd}). \tag{6.3.36}$$

In the absence of any bodies, oblique waves propagating in the fluid take the form

$$\phi^I = Ae^{\pm ibx}\cosh k(z-d), \tag{6.3.37}$$

$$\phi^{II} = -Ae^{\pm ibx}\sinh kd\, e^{kz}, \tag{6.3.38}$$

where $b = \sqrt{k^2 - l^2}$. For trapped modes we require $l > k$ so that the motion decays as $|x| \to \infty$. Thus, in the limit $\rho \to 1$ for fixed l we obtain a boundary-value problem in terms of the new spectral parameter K'. It is simple to find the forms of the multipoles for this problem and compute the trapped mode frequencies. The results match those found in the limit of figures 6.4 and 6.8 and so we have related the limits of the trapped mode curves in figures 6.4 and 6.8 to the trapped modes for the limiting problem defined above.

For trapped modes in a single-layer fluid we have the condition $K < l$ and for a two-layer fluid we have $K < k < l$. In the limit as $\rho \to 1$ we have $K/k \to 0$ by the dispersion relation. As we have shown above, in the limit $\rho \to 1$ when l is fixed we have $K \to 0$. If we fix K and let $\rho \to 1$ then we have $k \to \infty$ and hence $l \to \infty$. It is thus not possible to recover the single-layer fluid results in the limit $\rho \to 1$.

6.4 Conclusion

In this chapter we have investigated trapped modes above a horizontal cylinder, first in a single-layer finite-depth fluid and then in a two-layer fluid. The existence of trapped modes for these problems required the vanishing of a certain infinite determinant. This

was first shown by Ursell (1951) for the case of a horizontal circular cylinder spanning a channel.

For the single-layer case we have extended the work by McIver & Evans (1985) to finite depth and computed the trapped mode frequencies. Very similar results were found and the presence of finite depth has a small effect on the trapped mode frequencies. The main result being that the number of modes increases as the cylinder becomes closer to the free surface.

We evaluated the trapped mode frequencies for a cylinder in the upper and lower layers of a two-layer fluid. For a cylinder in the lower fluid layer we found that the motion of the trapped modes was confined to the interface. When the cylinder is submerged entirely within the upper layer the trapped modes can be on either the free surface or the interface. By varying the density ratio of the fluid layers we found that a mode on the free surface can transfer to the interface and vice versa. These transfers take place when the trapped mode has a near crossing with another mode. For points close to the near crossing it is possible to have trapped waves on the free surface and interface simultaneously with the same amplitude.

We related the two-layer problems to the single-layer problems by letting the density ratio tend to zero. In this limit the two-layer problem reduces to a single-layer fluid of infinite or finite depth when the cylinder is in the lower or upper layers respectively. We also investigated the trapped modes as the density ratio tends to 1. In this limit the two-layer problem reduces to some boundary-value problem and the results show that trapped modes do exist for this problem.

Chapter 7

Embedded trapped modes between a wall and a cylinder in a two-layer fluid

7.1 Introduction

In section 5.3 frequencies were found for oblique incident waves such that all the wave energy was reflected by a submerged horizontal cylinder in a two-layer fluid. Here we shall consider the case of a pair of identical horizontal cylinders arranged symmetrically about a vertical line in a two-layer fluid. Only oscillations symmetric about this line are considered so that the geometry is equivalent to a horizontal cylinder next to a vertical wall. We then look for embedded trapped modes, modes for which l is not greater than k, such that the wave motion is confined to the area between the wall and cylinder and decays far away. The frequencies at which the zeros of transmission occur provide a clue as to where one might start searching for eigenvalues. Physically, if the cylinders in our geometry are far enough apart it is reasonable to suggest that the presence of one cylinder will not influence what goes on at the other. Thus a wave, at a frequency for which zero transmission occurs, which exists between the cylinders might be totally reflected by one cylinder and then this reflected wave might travel to the other cylinder and be totally reflected and so on, thus leading to a trapped oscillation. A similar problem involving a pair of surface piercing barriers in a single-layer fluid was investigated by Linton & Kuznetsov (1997). The problem will be formulated as

in Linton & Kuznetsov (1997) leading to the need to calculate the zeros of a complex determinant. Complications arise from this method which we will overcome by using the alternative formulation given by Evans & Porter (1998).

7.2 Formulation of problem

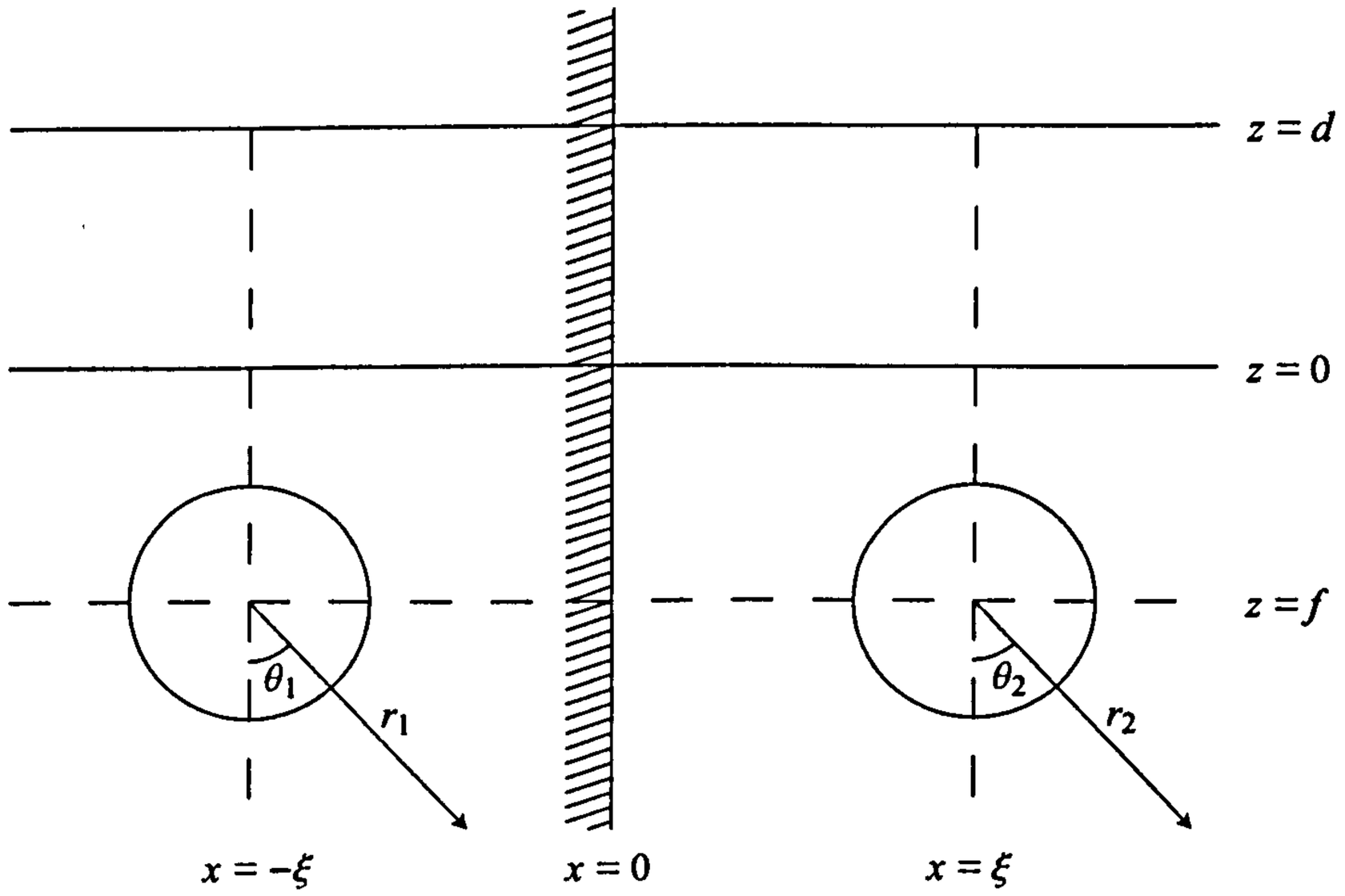

Figure 7.1: Definition sketch.

Two circular horizontal cylinders of radius a are centred on $(x, z) = (-\xi, f)$ and (ξ, f) and the problem considered will be equivalent to that of a cylinder next to a wall on $x = 0$, see figure 7.1. In other words the solutions will satisfy

$$\frac{\partial \phi}{\partial x} = 0 \qquad \text{on } x = 0, \tag{7.2.1}$$

along with the conditions (2.2.3)–(2.2.5), (5.2.12) and zero normal velocity on the cylinders, where the velocity potential is defined by $\Phi = \Re\{\phi(x, z)e^{ily}e^{-i\omega t}\}$. Here we shall only consider the case of a cylinder in the lower fluid layer, such that $f < 0$, and so the superscripts I and II shall be omitted for notational convenience. We choose the problem of a cylinder in the lower fluid layer purely for simplicity, and the case of a cylinder in the upper fluid layer could also be solved. We use polar coordinates (r_1, θ_1)

and (r_2, θ_2) centred about $(-\xi, f)$ and (ξ, f) respectively such that

$$x = -\xi + r_1 \sin\theta_1 = \xi + r_2 \sin\theta_2, \tag{7.2.2}$$

$$z = \quad f - r_1 \cos\theta_1 = f - r_2 \cos\theta_2. \tag{7.2.3}$$

To satisfy the wall condition we write the velocity potential, expanded in polar coordinates, as

$$\phi = \sum_{m=0}^{\infty} [\alpha_m(\phi_m^{a(1)} - \phi_m^{a(2)}) + \beta_m(\phi_m^{s(1)} + \phi_m^{s(2)})] \tag{7.2.4}$$

where $\phi_m^{s(q)}$ and $\phi_m^{a(q)}$ are the respective symmetric and antisymmetric multipoles described by equations (5.3.31) and (5.3.33) centred on $r_q = 0$. The zeros of transmission in the oblique wave scattering problem were found just below the cut-off frequency so we restrict attention to $K < l < k$ to obtain embedded trapped modes. In this region waves propagating to $x = \infty$ can exist with wavenumber k (associated with the interface) but not with wavenumber K (associated with the free surface). We let $l = k \sin\alpha_{\text{inc}}$, as in the oblique scattering problem, and restrict K to be below the cut-off frequency, defined by (5.3.15). To apply the body boundary condition, and hence solve for α_m, β_m, $m \geq 0$, we require all the multipoles to be expanded in the polar coordinates (r_2, θ_2). The multipoles centred about (ξ, f) are easily expanded in these coordinates and are given by

$$\phi_m^{s(2)} = K_m(lr_2)\cos m\theta_2 + \sum_{n=0}^{\infty} A_{mn}^s I_n(lr_2)\cos n\theta_2, \tag{7.2.5}$$

$$\phi_m^{a(2)} = K_m(lr_2)\sin m\theta_2 + \sum_{n=0}^{\infty} A_{mn}^a I_n(lr_2)\sin n\theta_2, \tag{7.2.6}$$

where A_{mn}^s and A_{mn}^a are given by equations (5.3.47) and (5.3.48). We write the multipoles which are centred about $(-\xi, f)$ as

$$\phi_m^{s(1)} = K_m(lr_1)\cos m\theta_1 + \psi_m^{s(1)}, \tag{7.2.7}$$

$$\phi_m^{a(1)} = K_m(lr_1)\sin m\theta_1 + \psi_m^{a(1)}, \tag{7.2.8}$$

where

$$\psi_m^{s(1)} = (-1)^m \int_0^{\infty} \cosh mu \cos[l(x+\xi)\sinh u] e^{l(z+f)\cosh u} C_L(u)du, \tag{7.2.9}$$

$$\psi_m^{a(1)} = (-1)^{m+1} \int_0^{\infty} \sinh mu \sin[l(x+\xi)\sinh u] e^{l(z+f)\cosh u} C_L(u)du, \tag{7.2.10}$$

$$\text{and } C_L(u) = \frac{(v+K)[(v+K\sigma)e^{-2vd} - v + K]}{(v-K)H(v)}. \tag{7.2.11}$$

We can expand $\psi_m^{s(1)}$ and $\psi_m^{a(1)}$ in the polar coordinates (r_2, θ_2) by using the following identities

$$e^{l(z+f)\cosh u}\cos\left[l(x+\xi)\sinh u\right]$$
$$= e^{2lf\cosh u}\sum_{m=0}^{\infty}(-1)^m\epsilon_m(\cosh mu\cos m\theta_2\cos(2l\xi\sinh u)$$
$$+\sinh mu\sin m\theta_2\sin(2l\xi\sinh u))I_m(lr_2), \quad (7.2.12)$$

and

$$e^{l(z+f)\cosh u}\sin\left[l(x+\xi)\sinh u\right]$$
$$= e^{2lf\cosh u}\sum_{m=0}^{\infty}(-1)^m\epsilon_m(\cosh mu\cos m\theta_2\sin(2l\xi\sinh u)$$
$$-\sinh mu\sin m\theta_2\cos(2l\xi\sinh u))I_m(lr_2). \quad (7.2.13)$$

These are obtained from equation (D.8) by letting $r' = r_2$, $\theta' = \theta_2$, multiplying both sides by $\exp(2lf\cosh u)\exp(-2il\xi\sinh u)$ and then taking the real and imaginary parts. Applying (7.2.12) and (7.2.13) to $\psi_m^{s(1)}$ and $\psi_m^{a(1)}$ we obtain

$$\psi_m^{s(1)} = \sum_{n=0}^{\infty}(A_{mn}^{s(1)}\cos n\theta_2 + B_{mn}^{s(1)}\sin n\theta_2)I_n(lr_2), \quad (7.2.14)$$

$$\psi_m^{a(1)} = \sum_{n=0}^{\infty}(A_{mn}^{a(1)}\cos n\theta_2 - B_{mn}^{a(1)}\sin n\theta_2)I_n(lr_2), \quad (7.2.15)$$

where

$$A_{mn}^{s(1)} = (-1)^{m+n}\epsilon_n\oint_0^{\infty}\cosh mu\cosh nu\, e^{2lf\cosh u}\cos(2l\xi\sinh u)C_L(u)du, \quad (7.2.16)$$

$$B_{mn}^{s(1)} = (-1)^{m+n}\epsilon_n\oint_0^{\infty}\cosh mu\sinh nu\, e^{2lf\cosh u}\sin(2l\xi\sinh u)C_L(u)du, \quad (7.2.17)$$

$$A_{mn}^{a(1)} = (-1)^{m+n+1}\epsilon_n\oint_0^{\infty}\sinh mu\cosh nu\, e^{2lf\cosh u}\sin(2l\xi\sinh u)C_L(u)du,$$
$$= -B_{nm}^{s(1)} \quad (7.2.18)$$

$$B_{mn}^{a(1)} = (-1)^{m+n+1}\epsilon_n\oint_0^{\infty}\sinh mu\sinh nu\, e^{2lf\cosh u}\cos(2l\xi\sinh u)C_L(u)du. \quad (7.2.19)$$

We now need to expand $K_m(lr_1)\cos m\theta_1$ and $K_m(lr_1)\sin m\theta_1$ in the polar coordinates (r_2, θ_2). This is done in appendix E and we obtain

$$K_m(lr_1)\cos m\theta_1 = \sum_{n=0}^{\infty}\frac{\epsilon_n}{2}I_n(lr_2)(K_{m-n}(2l\xi) + (-1)^m K_{m+n}(2l\xi))$$
$$\times\left[\cos(m+n)\frac{\pi}{2}\cos n\theta_2 - \sin(m+n)\frac{\pi}{2}\sin n\theta_2\right], \quad (7.2.20)$$

$$K_m(lr_1)\sin m\theta_1 = \sum_{n=0}^{\infty}\frac{\epsilon_n}{2}I_n(lr_2)(K_{m-n}(2l\xi) + (-1)^{m+1}K_{m+n}(2l\xi))$$
$$\times\left[\sin(m+n)\frac{\pi}{2}\cos n\theta_2 + \cos(m+n)\frac{\pi}{2}\sin n\theta_2\right]. \quad (7.2.21)$$

If we now apply the body boundary condition on the cylinder, $\partial\phi/\partial r_2 = 0$ on $r_2 = a$, and use the orthogonality of the trigonometric functions we obtain two coupled infinite systems of equations for the unknowns α_m and β_m, $m \geq 0$. These are

$$\alpha_s - \frac{I_s'(la)}{K_s'(la)} \sum_{m=0}^{\infty} \left(P_{ms}\alpha_m + Q_{ms}\beta_m \right) = 0, \tag{7.2.22}$$

$$\beta_s + \frac{I_s'(la)}{K_s'(la)} \sum_{m=0}^{\infty} \left(R_{ms}\alpha_m + T_{ms}\beta_m \right) = 0, \tag{7.2.23}$$

$s \geq 0$, where

$$\begin{aligned} P_{ms} =& \frac{\epsilon_s}{2}(K_{m-s}(2l\xi) + (-1)^{m+1}K_{m+s}(2l\xi))\cos(m+s)\frac{\pi}{2} \\ &+ (-1)^{m+s}\epsilon_s \int_0^{\infty} \sinh mu \sinh su\, e^{2lf\cosh u}(\cos(2l\xi\sinh u) - 1)C_L(u)du, \end{aligned} \tag{7.2.24}$$

$$\begin{aligned} Q_{ms} =& -\frac{\epsilon_s}{2}(K_{m-s}(2l\xi) + (-1)^{m}K_{m+s}(2l\xi))\sin(m+s)\frac{\pi}{2} \\ &+ (-1)^{m+s}\epsilon_s \int_0^{\infty} \cosh mu \sinh su\, e^{2lf\cosh u}\sin(2l\xi\sinh u)C_L(u)du, \end{aligned} \tag{7.2.25}$$

$$\begin{aligned} R_{ms} =& \frac{\epsilon_s}{2}(K_{m-s}(2l\xi) + (-1)^{m+1}K_{m+s}(2l\xi))\sin(m+s)\frac{\pi}{2} \\ &+ (-1)^{m+s+1}\epsilon_s \int_0^{\infty} \sinh mu \cosh su\, e^{2lf\cosh u}\sin(2l\xi\sinh u)C_L(u)du, \end{aligned} \tag{7.2.26}$$

$$\begin{aligned} T_{ms} =& \frac{\epsilon_s}{2}(K_{m-s}(2l\xi) + (-1)^{m}K_{m+s}(2l\xi))\cos(m+s)\frac{\pi}{2} \\ &+ (-1)^{m+s}\epsilon_s \int_0^{\infty} \cosh mu \cosh su\, e^{2lf\cosh u}(\cos(2l\xi\sinh u) + 1)C_L(u)du. \end{aligned} \tag{7.2.27}$$

We can write these systems of equations in matrix form as follows

$$\mathbf{A}\underline{x} = \begin{pmatrix} \mathbf{P} - \mathbf{I} & \mathbf{Q} \\ \mathbf{R} & \mathbf{T} + \mathbf{I} \end{pmatrix} \begin{bmatrix} \underline{\alpha} \\ \underline{\beta} \end{bmatrix} = 0, \tag{7.2.28}$$

where

$$\mathbf{P} = [I_s'(la)P_{ms}/K_s'(la)], \qquad \mathbf{Q} = [I_s'(la)Q_{ms}/K_s'(la)], \tag{7.2.29}$$

$$\mathbf{R} = [I_s'(la)R_{ms}/K_s'(la)], \qquad \mathbf{T} = [I_s'(la)T_{ms}/K_s'(la)], \tag{7.2.30}$$

$$\underline{\alpha} = [\alpha_s], \qquad \underline{\beta} = [\beta_s], \tag{7.2.31}$$

for $s \geq 0$ and $m \geq 0$. For non-trivial solutions we require the determinant of the complex matrix $\mathbf{A}$ to be zero. To find these points we truncate the matrix $\mathbf{A}$ to a $2N \times 2N$ system and calculate the determinant. By fixing, say, ξ and varying K we can find where the real and imaginary parts vanish. We use a wide-spacing approximation to aid locating the points at which both the real and imaginary parts vanish.

7.3 A wide-spacing approximation

The wide-spacing approximation has been used many times before to provide both good evidence for the existence of trapped-mode phenomena and also accurate and efficient methods for the computation of the frequencies at which they occur (see, for example, Linton & Kuznetsov (1997)). Consider a wave of wavenumber k with angle α_{inc} to the positive x-axis of the form $\exp[ib(x-\xi)]$ incident upon the right-hand cylinder in figure 7.1 from $x = -\infty$ and assume that the wall at $x = 0$ does not affect the interaction between the wave and the cylinder. Then, as shown in section 5.3, there are certain values of Ka at which zeros of transmission occur and the wave is totally reflected. At such a frequency the reflection coefficient can be written as $r_3 = \exp\{i\chi\}$ for some $\chi \in \mathbb{R}$. In order for this solution to be consistent with the presence of the wall we must have (note that because of the phase shift the r_3 discussed above is for a cylinder whose centre is at $(0,f)$)

$$e^{ib(x-\xi)} + r_3 e^{-ib(x-\xi)} = A\cos bx \tag{7.3.1}$$

where $b = \sqrt{k^2 - l^2} = k\cos\alpha_{\text{inc}}$ and A is some complex constant. By substituting the form for r_3 we find this is equivalent to the condition

$$e^{i(\chi+2b\xi)} = 1. \tag{7.3.2}$$

It follows that the distance of the cylinder from the wall must be related to the frequency at which total reflection occurs through the equation

$$\frac{\xi}{a} = \frac{n\pi}{ba} - \frac{\chi}{2ba} \tag{7.3.3}$$

for some integer n.

7.4 Results

The values of Ka at which zeros of the real and imaginary parts of the determinant occur are plotted in figure 7.2 for a range of values of ξ/a using $N = 8$. In the curves ρ is 0.5, d/a is 2, f/a is -1.1 and α_{inc} is 0.34. Note that α_{inc} is greater than the critical angle for the given parameter values so there is no cut-off frequency. This means that there are no propagating free-surface waves for all Ka and hence the range of values for Ka in which we seek embedded trapped modes is unbounded. The solid lines represent

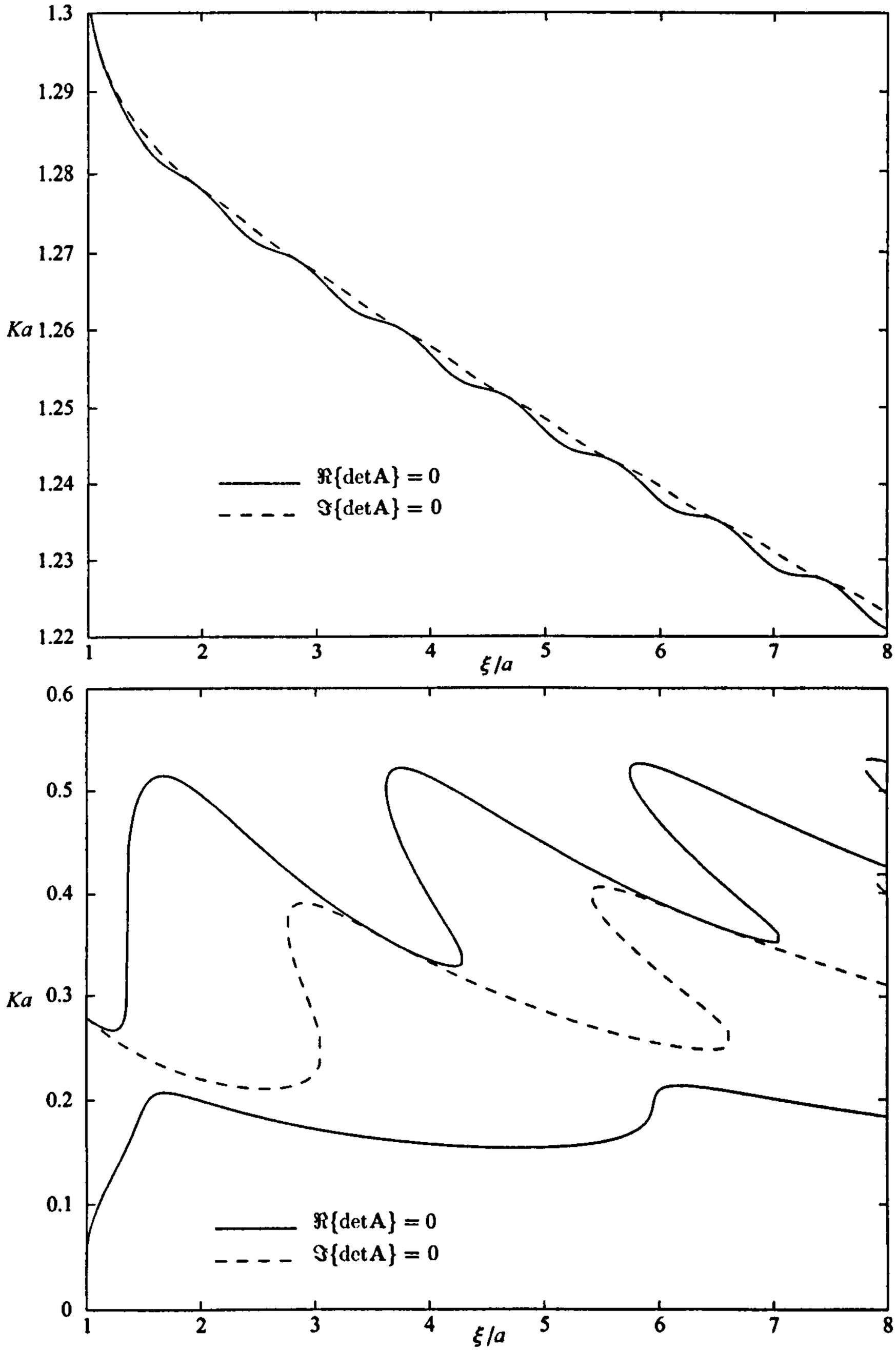

Figure 7.2: Values of Ka at which the real part (solid lines) and the imaginary part (dashed lines) of the determinant vanish; $d/a = 2$, $f/a = -1.1$, $\rho = 0.5$ and $\alpha_{\text{inc}} = 0.34$.

zeros of the real part and the dashed lines represent zeros of the imaginary part. The two sets of curves appear to touch and the numbers computed strongly suggest that this is the case but because of the nature of the contact (the lines do not cross) one cannot be sure. An embedded trapped mode will exist if the solid lines and dashed lines do actually touch.

For the values of the parameters used here we find two frequencies, $Ka \approx 0.4481$ (as shown in figure 5.15) and $Ka \approx 1.0825$, at which zeros of transmission occur for the scattering of oblique waves. Using a wide-spacing approximation we obtain estimations for the separation variable ξ/a as shown in table 7.1. The left-hand column in table 7.1

n	ξ/a, $Ka = 0.4481$	ξ/a, $Ka = 1.0825$
1	2.8186	1.2254
2	5.2826	2.2515
3	7.7466	3.2776
4	10.2107	4.3037
5	12.6747	5.3298
6	15.1387	6.3559
7	17.6028	7.3820

Table 7.1: A wide-spacing approximation; $\rho = 0.5$, $d/a = 2$, $f/a = -1.1$ and $\alpha_{\text{inc}} = 0.34$.

corresponds to predicted values of ξ/a in the lower plot of figure 7.2 whereas the right-hand column corresponds to the upper plot. It would appear that for $Ka \approx 0.4481$ these are poor estimates of where the curves possibly touch but for greater values of ξ/a we find them more satisfactory.

It is clear from figure 7.2 that if we vary ξ/a an arbitrarily small amount from the point of contact then the embedded trapped mode will cease to exist. These modes are unstable in the sense that a small change in the geometry results in the loss of the trapped mode. We now need to consider a different method which will tell us if indeed the curves touch.

7.5 Reformulation of problem

We now consider the results if the multipoles in (7.2.4) are replaced by real-valued multipoles in which the indented integrals are replaced with principal-value integrals.

These integrals differ from the ones used previously by their forms in the far field. If we follow the above analysis with these real-valued multipoles the matrix $\mathbf{A}$ defined by (7.2.28) will be real and we will denote this real matrix by $\tilde{\mathbf{A}}$. The solutions of the reformulated problem, when $\det(\tilde{\mathbf{A}}) = 0$, will correspond to either trapped modes or standing waves in the entire fluid. This method was used by Evans & Porter (1998) for the case of a rigid vertical circular cylinder placed on the centre-plane of a channel. To find the trapped mode frequencies we must calculate the potential in the far field for each solution and find when it vanishes, i.e. $\phi \to 0$ as $x \to +\infty$. The far-field form of the multipoles is given by

$$\phi_m^{s(1)} \sim \mp (-1)^m \pi \cosh m\gamma_2 C_L^{\gamma_2} \sin b(x+\xi) e^{k(z+f)}, \tag{7.5.1}$$

$$\phi_m^{a(1)} \sim \mp (-1)^m \pi \sinh m\gamma_2 C_L^{\gamma_2} \cos b(x+\xi) e^{k(z+f)}, \tag{7.5.2}$$

$$\phi_m^{s(2)} \sim \mp (-1)^m \pi \cosh m\gamma_2 C_L^{\gamma_2} \sin b(x-\xi) e^{k(z+f)}, \tag{7.5.3}$$

$$\phi_m^{a(2)} \sim \mp (-1)^m \pi \sinh m\gamma_2 C_L^{\gamma_2} \cos b(x-\xi) e^{k(z+f)}, \tag{7.5.4}$$

as $x \to \pm\infty$, where $C_L^{\gamma_2}$ is given by (5.3.44). To satisfy the far-field condition for embedded trapped modes we require

$$\sum_{m=0}^{\infty} [\alpha_m(\phi_m^{a(1)} - \phi_m^{a(2)}) + \beta(\phi_m^{s(1)} + \phi_m^{s(2)})] \to 0 \qquad \text{as } x \to \infty. \tag{7.5.5}$$

After substitution of the far-field form of the multipoles we obtain the following condition

$$2\pi C_L^{\gamma_2} e^{k(z+f)} \sin bx \sum_{m=0}^{\infty} (-1)^m [\alpha_m \sinh m\gamma_2 \sin b\xi - \beta_m \cosh m\gamma_2 \cos b\xi] = 0. \tag{7.5.6}$$

Thus we need to find the frequencies at which both the determinant of the new matrix $\tilde{\mathbf{A}}$ and also the summation in (7.5.6) vanishes. We will denote the sum as S such that

$$S = \sum_{m=0}^{\infty} (-1)^m [\alpha_m \sinh m\gamma_2 \sin b\xi - \beta_m \cosh m\gamma_2 \cos b\xi]. \tag{7.5.7}$$

The coefficients α_m and β_m in the sum are the eigenvectors of the matrix $\tilde{\mathbf{A}}$ corresponding to the eigenvalue zero.

7.6 Results

Figure 7.3 shows results obtained from using the real-valued multipoles where the same values for the parameters have been used as before, $f/a = -1.1$, $d/a = 2$, $\rho = 0.5$, $\alpha_{\text{inc}} = 0.34$ and $N = 8$. The top plot in figure 7.3 shows the values of Ka at which

the determinant of the real matrix $\tilde{\mathbf{A}}$ vanishes as a function of ξ/a. Each curve has been given a different line style so that it can be recognised in the other plots. We note that these values are exactly the same as those found for where the real part of the complex matrix $\mathbf{A}$ determinant is zero. An explanation of why this is so is given below. The middle plot shows the corresponding far-field sums, S, and when they cross zero we have an embedded trapped mode. The points where the dashed curve crosses zero correspond to the approximations in the left-hand column of table 7.1, while those for the dot-dashed curve correspond to the numbers in the right-hand column. The solid curve has no $S = 0$ crossings and so never describes an embedded trapped mode. The lower plot shows the modulus of the complex matrix $\mathbf{A}$ determinant where the frequency, Ka, and separation, ξ/a, of the cylinder are given by the top graph. We can see that where there are zero crossings of the far-field sum the modulus of the complex matrix determinant touches zero. These figures provide confirmation that the curves in figure 7.2 do indeed touch and thus that embedded trapped modes do exist for the geometry.

We now explain why the real part of the determinant of the complex matrix $\mathbf{A}$ and the determinant of the real matrix $\tilde{\mathbf{A}}$ vanish at the same values of Ka. Using (7.2.24)–(7.2.31) we can write the truncated complex matrix $\mathbf{A}$ in the form

$$\mathbf{A} = \begin{pmatrix} b_{11} + ic_1d_1 & b_{12} + ic_1d_2 & \dots & b_{1M} + ic_1d_M \\ b_{21} + ic_2d_1 & b_{22} + ic_2d_2 & \dots & b_{2M} + ic_2d_M \\ \vdots & \vdots & \ddots & \vdots \\ b_{M1} + ic_Md_1 & b_{M2} + ic_Md_2 & \dots & b_{MM} + ic_Md_M \end{pmatrix} \tag{7.6.1}$$

where $M = 2 \times N$. It is the special forms of the imaginary parts of the elements that is significant. If we consider $N = 1$ we can write the determinant of such a matrix as

$$\det \mathbf{A} = \begin{vmatrix} b_{11} + ic_1d_1 & b_{12} + ic_1d_2 \\ b_{21} + ic_2d_1 & b_{22} + ic_2d_2 \end{vmatrix} \tag{7.6.2}$$

$$= \begin{vmatrix} b_{11} & b_{12} \\ b_{21} + ic_2d_1 & b_{22} + ic_2d_2 \end{vmatrix} + \begin{vmatrix} ic_1d_1 & ic_1d_2 \\ b_{21} + ic_2d_1 & b_{22} + ic_2d_2 \end{vmatrix}. \tag{7.6.3}$$

Using the elementary row operation Row 2 = Row 2 $- c_2 \times$ Row $1/c_1$ on the second determinant of (7.6.3), which does not change its value, we get

$$\det \mathbf{A} = \begin{vmatrix} b_{11} & b_{12} \\ b_{21} + ic_2d_1 & b_{22} + ic_2d_2 \end{vmatrix} + i \begin{vmatrix} c_1d_1 & c_1d_2 \\ b_{21} & b_{22} \end{vmatrix}. \tag{7.6.4}$$

If we now expand the first determinant in the above equation about the second row we obtain

$$\det \mathbf{A} = \begin{vmatrix} b_{11} & b_{12} \\ b_{21} & b_{22} \end{vmatrix} + i \begin{vmatrix} b_{11} & b_{12} \\ c_2 d_1 & c_2 d_2 \end{vmatrix} + i \begin{vmatrix} c_1 d_1 & c_1 d_2 \\ b_{21} & b_{22} \end{vmatrix} \tag{7.6.5}$$

where the second and third determinants are purely imaginary. Hence the real part of $\det \mathbf{A}$ is given by the first determinant which is clearly $\det \tilde{\mathbf{A}}$. The above procedure can be applied to larger matrices where the algebra is more lengthy to give the same result.

7.7 Conclusion

In this chapter we have considered the case of embedded trapped modes for the case of a pair of horizontal circular cylinders in a two-layer fluid. Only symmetric oscillations were considered such that the geometry was equivalent to a cylinder next to a wall. The existence of the embedded trapped modes depended upon the vanishing of a certain complex matrix. Due to the grazing nature of the real and imaginary zeros the problem was reformulated using the real-valued multipoles. Solutions to the problem then required the determinant of the matrix and the potential in the far field to vanish.

We have shown that embedded trapped modes do exist for a cylinder situated in the lower fluid of a two-layer fluid next to a wall. For the parameter values chosen, nine trapped modes embedded in the continuous spectrum have been found for nine separation values.

The wide-spacing equation we used suggests there are an infinite number of embedded trapped modes. For higher separations of the cylinder the wide-spacing approximation becomes more accurate, which provides strong evidence that there are indeed an infinite number of embedded trapped modes.

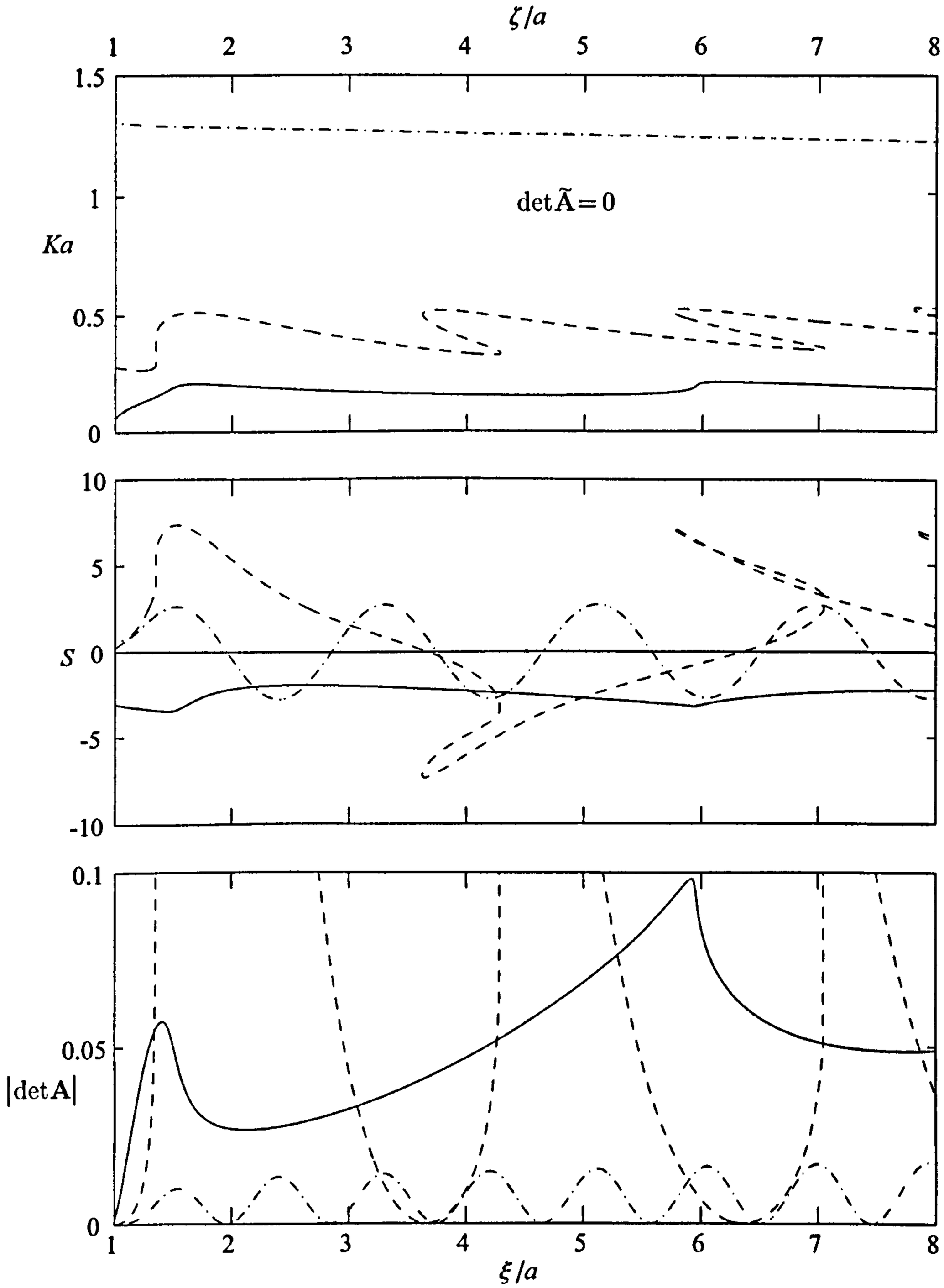

Figure 7.3: Values of Ka at which the determinant of the real matrix vanish with corresponding far-field sum and modulus of the determinant of the complex matrix; $d/a = 2$, $f/a = -1.1$, $\rho = 0.5$ and $\alpha_{\text{inc}} = 0.34$.

Appendix A

The Method of Stationary Phase

The stationary phase method was originally developed by Lord Kelvin for the ship-wave system. It is used to find an asymptotic approximation to the following general integral

$$I = \int F(\alpha) e^{iRG(\alpha)} d\alpha, \tag{A.1}$$

where $F(\alpha)$ and $G(\alpha)$ are arbitrary regular functions and R is a large parameter such as the polar radius. The function F may be complex, but G will be assumed real. For large values of R, the phase RG will vary rapidly, and the integrand (A.1) will be a highly oscillatory function. The resulting oscillations of the integrand will tend to cancel out over the range of the integration, except locally at points of stationary phase where the derivative $G'(\alpha)$ vanishes.

Thus the principal contribution(s) to the integrand (A.1) will come from the point(s) of stationary phase, assuming that such points exist in the range of integration. If a stationary phase point occurs at $\alpha = \alpha_0$ then the asymptotic approximation of (A.1) is given by

$$I \simeq F(\alpha_0) \left(\frac{2\pi}{|RG''(\alpha_0)|} \right)^{1/2} \exp[i(RG(\alpha_0) \pm \pi/4)]. \tag{A.2}$$

The $\pm$ sign is the same as the sign of the second derivative $G''(\alpha_0)$. This expression is valid, for sufficiently large values of R, unless $G''(\alpha_0) = 0$. If there are multiple points of stationary phase in the domain integration, the contribution from each may be treated separately, according to (A.2), and added together to give the total contribution from all relevant points. The singular case $G''(\alpha_0) = 0$ occurs if two points of stationary phase coalesce. This case will not be considered here as it does not occur in the integrals appearing in this thesis.

With this stationary phase approximation the integral (2.4.2) can be evaluated. So

$$I = \delta \int_{S_B} \phi n_i ds \tag{A.3}$$

$$= iJ_K \left(\frac{KR}{2\pi}\right)^{1/2} e^{-i\pi/4} \int_0^{2\pi} [\cos(\alpha - \alpha_{\text{inc}}) - 1] e^{iKR[\cos(\alpha-\alpha_{\text{inc}})+1]} A_i(\alpha) d\alpha \tag{A.4}$$

$$= iJ_K \left(\frac{KR}{2\pi}\right)^{1/2} e^{-i\pi/4} \int_0^{2\pi} F(\alpha) e^{iRG(\alpha)} d\alpha \tag{A.5}$$

where

$$F(\alpha) = [\cos(\alpha - \alpha_{\text{inc}}) - 1] A_i(\alpha) \tag{A.6}$$

$$\text{and} \qquad G(\alpha) = K[\cos(\alpha - \alpha_{\text{inc}}) + 1]. \tag{A.7}$$

Stationary phase points are found when $G'(\alpha) = 0$ and are $\alpha_0 = \alpha_{\text{inc}}$ and $\alpha_1 = \alpha_{\text{inc}} + \pi$. The contributions from these two points, given by (A.2), are added and so the asymptotic approximation to (2.4.2) is given by

$$I = iJ_K \left(\frac{KR}{2\pi}\right)^{1/2} e^{-i\pi/4} \left\{ F(\alpha_0) \left(\frac{2\pi}{|RG''(\alpha_0)|}\right)^{1/2} \exp[i(RG(\alpha_0) + \pi/4)] \right.$$

$$\left. + F(\alpha_1) \left(\frac{2\pi}{|RG''(\alpha_1)|}\right)^{1/2} \exp[i(RG(\alpha_1) + \pi/4)] \right\} \tag{A.8}$$

$$= iJ_K \left(\frac{KR}{2\pi}\right)^{1/2} e^{-i\pi/4} \left\{ 0 - 2A_i(\alpha_{\text{inc}} + \pi) \left(\frac{2\pi}{KR}\right)^{1/2} e^{i\pi/4} \right\} \tag{A.9}$$

$$= -2iJ_K A_i(\alpha_{\text{inc}} + \pi). \tag{A.10}$$

If $\alpha_{\text{inc}} = 0$ or $\alpha_{\text{inc}} = \pi$ then one of the stationary points would lie at the limits of integration. This would not cause a problem as we can easily shift the limits, since the integrand is periodic with period 2π, and arrive at the same result given above.

Appendix B

Far-field form of multipoles

For many of the problems discussed in this thesis we are required to find the far-field form of the multipole expansions. In this appendix we will find the far-field form of the multipoles for the case of a point singularity situated below the interface in a two-layer fluid. From (2.6.4), these multipoles take the form in the lower fluid as

$$\phi_n^{IIm} = a^{n+2}\cos m\alpha \left[\frac{P_n^m(\cos\theta)}{r^{n+1}} + \frac{1}{(n-m)!}\oint_0^\infty u^n C_L(u) e^{uz} J_m(uR)du\right], \qquad \text{(B.1)}$$

where $C_L(u)$ is given by (2.6.13). The first term in the expression for ϕ_n^{IIm} clearly makes no contribution as $R \to \infty$. The second term is defined as the principal-value integral plus contributions from the residues of the integrand at the poles $u = K$ and $u = k$. Using the asymptotic form for $J_m(uR)$, from Abramowitz & Stegun (1965) equation (9.2.1), we can write the integral as

$$\begin{aligned}\oint_0^\infty u^n C_L(u) e^{uz} J_m(uR)du &= \int_0^\infty u^n C_L(u) e^{uz} J_m(uR)du \\ &\quad + i\pi K^n C_L^K e^{Kz} J_m(KR) + i\pi k^n C_L^k e^{kz} J_m(kR) \qquad \text{(B.2)} \\ &\sim \left(\frac{2}{\pi R}\right)^{1/2} \int_0^\infty u^{n-1/2} C_L(u) e^{uz} \cos(uR - \frac{m\pi}{2} - \frac{\pi}{4})du \\ &\quad + i\left(\frac{2\pi}{R}\right)^{1/2} \left(K^{n-1/2} C_L^K e^{Kz} \cos(KR - \frac{m\pi}{2} - \frac{\pi}{4})\right. \\ &\quad \left. + k^{n-1/2} C_L^k e^{kz} \cos(kR - \frac{m\pi}{2} - \frac{\pi}{4})\right) \qquad \text{(B.3)}\end{aligned}$$

as $KR \to \infty$. We can write the principal-value integral as follows

$$\int_0^\infty u^{n-1/2} C_L(u) e^{uz} \cos(uR - \frac{m\pi}{2} - \frac{\pi}{4})du = \Re\left\{(-i)^m e^{-i\pi/4} \int_0^\infty u^{n-1/2} C_L(u) e^{uz} e^{iuR} du\right\} \qquad \text{(B.4)}$$

and to examine the behaviour of this as $R \to \infty$ we look at

$$I = \lim_{U\to\infty}(-i)^m e^{-i\pi/4}\int_\Gamma u^{n-1/2}C_L(u)e^{uz}e^{iuR}du \tag{B.5}$$

where Γ is the contour in the complex u-plane comprising of Γ_1, Γ_2 and Γ_3 as described in figure B.1. Since there are no singularities inside the Γ contour Cauchy's theorem implies that $I = 0$. We denote the integral along contour Γ_1 as I_1 and if we let $u = Ue^{i\theta}$

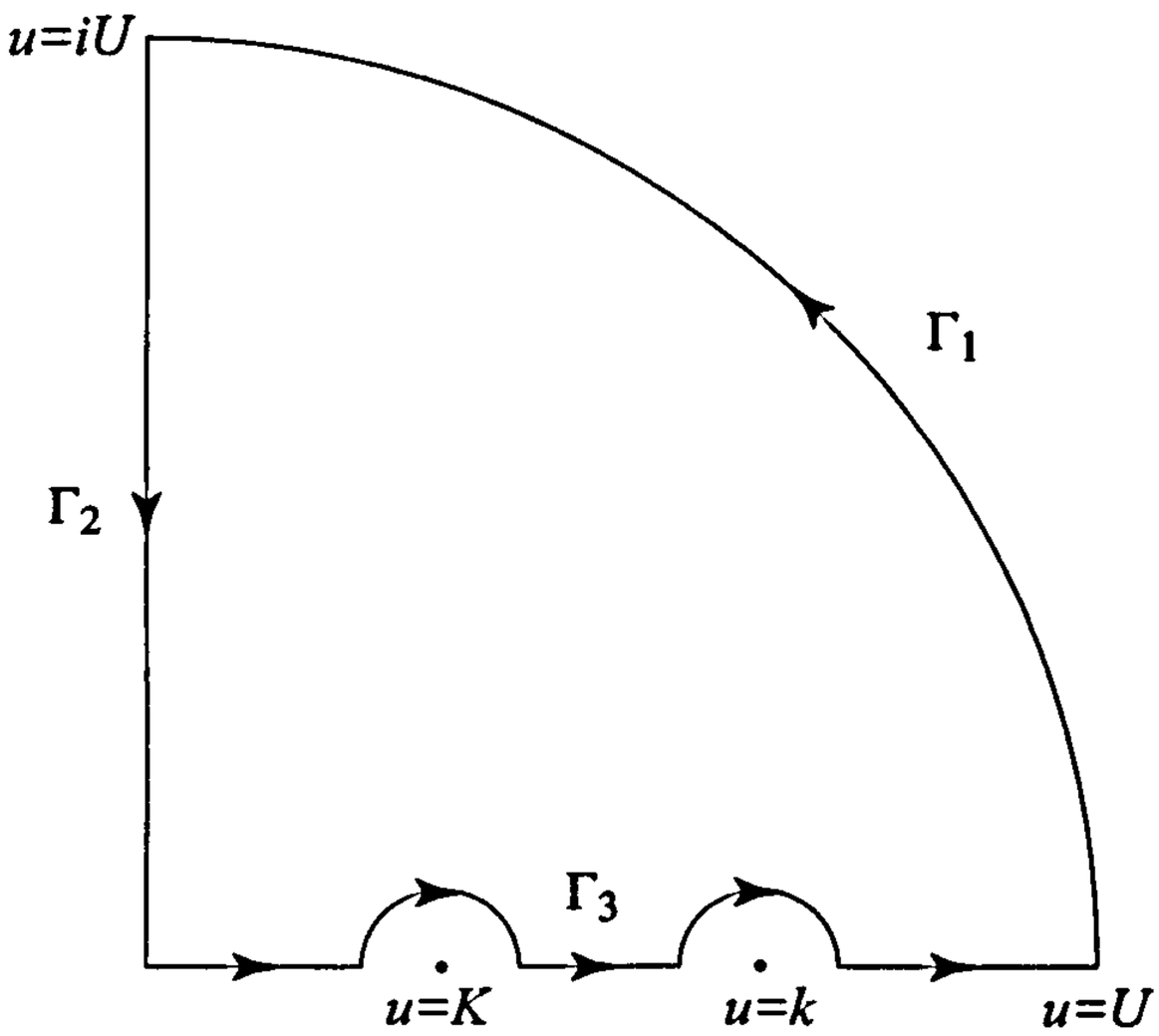

Figure B.1: Definition sketch.

this becomes

$$I_1 = -\lim_{U\to\infty}(-i)^{m+1}e^{-i\pi/4}U^{n+1/2}\int_0^{\pi/2} e^{i(n+1/2)\theta}C_L(Ue^{i\theta})e^{Uze^{i\theta}}e^{iURe^{i\theta}}d\theta. \tag{B.6}$$

It is simple to show that the integrand in (B.6) has an exponential factor of $\exp[U((z+f)\cos\theta - R\sin\theta)]$. Thus, for sufficiently large R the integral I_1 will be zero.

For the integral along Γ_2, denoted I_2, we let $u = it$ to give

$$I_2 = \lim_{U\to\infty}(-1)^m i^{m+n+1/2}e^{-i\pi/4}\int_U^0 t^{n-1/2}C_L(it)e^{itz}e^{-tR}dt. \tag{B.7}$$

It is clear that as $R \to \infty$ the integral $I_2 \to 0$ due to the e^{-tR} term. We are now left with the integral along Γ_3 which is

$$I_3 = \lim_{U\to\infty}(-i)^m e^{-i\pi/4}\int_0^U u^{n-1/2}C_L(u)e^{uz}e^{iuR}du \tag{B.8}$$

$$=(-i)^m e^{-i\pi/4} \times\left(\int_0^\infty u^{n-1/2}C_L(u)e^{uz}e^{iuR}du - \pi i K^{n-1/2}C_L^K e^{Kz}e^{iKR} - \pi i k^{n-1/2}C_L^k e^{kz}e^{ikR}\right). \tag{B.9}$$

Since $I = 0$ we can write this as

$$(-i)^m e^{-i\pi/4} \oint_0^\infty u^{n-1/2} C_L(u) e^{uz} e^{iuR} du$$
$$= -(-i)^{m+1} \pi \left(K^{n-1/2} C_L^K e^{Kz} e^{iKR} + k^{n-1/2} C_L^k e^{kz} e^{ikR} \right) e^{-i\pi/4}. \quad \text{(B.10)}$$

If we take the real part of both sides then we obtain a form for the principal-value integral in (B.3). We can now write the far-field form of the multipole (B.1) as

$$\phi_n^{IIm} \sim -\frac{(-i)^{m+1} a^{n+2} \cos(m\alpha)}{(n-m)!} \left(\frac{2\pi}{R}\right)^{1/2} \left(K^{n-1/2} C_L^K e^{Kz} e^{iKR} + k^{n-1/2} C_L^k e^{kz} e^{ikR} \right) e^{-i\pi/4} \quad \text{(B.11)}$$

as $KR \to \infty$. A similar approach can be taken to find the far-field forms of the multipole functions for the other problems presented in this thesis.

Appendix C

Numerical evaluation of principal-value integrals

In order to solve the various problems shown in this thesis we are required to numerically evaluate principal-value integrals. There are two methods shown in this appendix for such a task. The first technique was employed by the author for the calculation of the results shown and the second technique came to the author's attention after all calculations were completed.

A principal-value integral with two singularities can be represented by

$$I = \fint_0^\infty \frac{F(u)}{G(u)} du \tag{C.1}$$

where $G(K) = G(k) = 0$, $G'(K) \neq 0$, $G'(k) \neq 0$ and $0 < K < k$. This implies by definition, that

$$I = \lim_{\epsilon \to 0} \left\{ \int_0^{K-\epsilon} + \int_{K+\epsilon}^{k-\epsilon} + \int_{k+\epsilon}^{\infty} \right\} \frac{F(u)}{G(u)} du. \tag{C.2}$$

The problem arises from the fact that the integrals in (C.2) are divergent and so cannot be evaluated independently. If we subtract the behaviour of the integrand near the singularity and then add it back on we can write I as

$$I = \int_{2k}^\infty \frac{F(u)}{G(u)} du + \fint_0^{2k} \left[\frac{F(u)}{G(u)} - \frac{F(K)}{G'(K)(u-K)} - \frac{F(k)}{G'(k)(u-k)} \right] du + \frac{F(K)}{G'(K)} \fint_0^{2k} \frac{du}{u-K} + \frac{F(k)}{G'(k)} \fint_0^{2k} \frac{du}{u-k}. \tag{C.3}$$

Evaluating the last two principal-value integrals gives

$$\begin{aligned} \fint_0^{2k} \frac{du}{u-k} &= \lim_{\epsilon\to 0}\left\{\int_0^{k-\epsilon} + \int_{k+\epsilon}^{2k}\right\}\frac{du}{u-k} \\ &= \lim_{\epsilon\to 0}\left\{[\ln(k-u)]_0^{k-\epsilon} + [\ln(u-k)]_{k+\epsilon}^{2k}\right\} \\ &= 0 \end{aligned} \tag{C.4}$$

and

$$\begin{aligned} \fint_0^{2k} \frac{du}{u-K} &= \lim_{\epsilon\to 0}\left\{\int_0^{K-\epsilon} + \int_{K+\epsilon}^{2k}\right\}\frac{du}{u-K} \\ &= \lim_{\epsilon\to 0}\left\{[\ln(K-u)]_0^{K-\epsilon} + [\ln(u-K)]_{K+\epsilon}^{2k}\right\} \\ &= \lim_{\epsilon\to 0}\{\ln(\epsilon) - \ln(K) + \ln(2k-K) - \ln(\epsilon)\} \\ &= \ln\left(\frac{2k}{K}-1\right). \end{aligned} \tag{C.5}$$

So now I becomes

$$I = \int_{2k}^{\infty}\frac{F(u)}{G(u)}du + \fint_0^{2k}\left[\frac{F(u)}{G(u)} - \frac{F(K)}{G'(K)(u-K)} - \frac{F(k)}{G'(k)(u-k)}\right]du + \frac{F(K)}{G'(K)}\ln\left(\frac{2k}{K}-1\right). \tag{C.6}$$

This form of I ensures that the principal-value integrand is well behaved near $u = K$ and $u = k$. This is because $G(u) \sim (u-k)G'(u)$ near $u = k$ and $G(u) \sim (u-K)G'(u)$ near $u = K$. Hence the integrand will involve the subtraction of large numbers. For the case of a principal-value integral, I, with one singularity at $u = k$ we obtain

$$I = \fint_0^{\infty}\frac{F(u)}{G(u)}du = \int_{2k}^{\infty}\frac{F(u)}{G(u)}du + \fint_0^{2k}\left[\frac{F(u)}{G(u)} - \frac{F(k)}{G'(k)(u-k)}\right]du. \tag{C.7}$$

In a lot of cases we can write the principal-value integrals as

$$I = \fint_0^{\infty} e^{uf}\frac{F(u)}{G(u)}du \tag{C.8}$$

where $f < 0$, $G(K) = G(k) = 0$, $G'(K) \neq 0$, $G'(k) \neq 0$ and $0 < K < k$. If we subtract the behaviour of the integrand near the poles and then add it back on we obtain

$$I = \fint_0^{\infty} e^{uf}\left[\frac{F(u)}{G(u)} - \frac{F(K)}{G'(K)(u-K)} - \frac{F(k)}{G'(k)(u-k)}\right]du + \frac{F(K)}{G'(K)}\fint_0^{\infty}\frac{e^{uf}}{u-K}du + \frac{F(k)}{G'(k)}\fint_0^{\infty}\frac{e^{uf}}{u-k}du. \tag{C.9}$$

We now evaluate the last two integrals as follows

$$\int_0^\infty \frac{e^{uf}}{u-c}du = \int_f^\infty \frac{e^{cf}e^{-ct}}{-ct/f}.\frac{-c}{f}dt = e^{cf}\int_f^\infty \frac{e^{-ct}}{t}dt = -e^{cf}\mathrm{Ei}(-cf) \tag{C.10}$$

where $c = K$ or k and the exponential integral $\mathrm{Ei}(x)$ is described by Abramowitz & Stegun (1965), equation (5.1.12). The principal-value integral can now be written as

$$I = \int_0^\infty e^{uf}\left[\frac{F(u)}{G(u)} - \frac{F(K)}{G'(K)(u-K)} - \frac{F(k)}{G'(k)(u-k)}\right]du - e^{Kf}\mathrm{Ei}(-Kf) - e^{kf}\mathrm{Ei}(-kf). \tag{C.11}$$

This second method can be found in Endo (1987).

Appendix D

Integral representations of $K_n(lr)\cos n\theta$ and $K_n(lr)\sin n\theta$

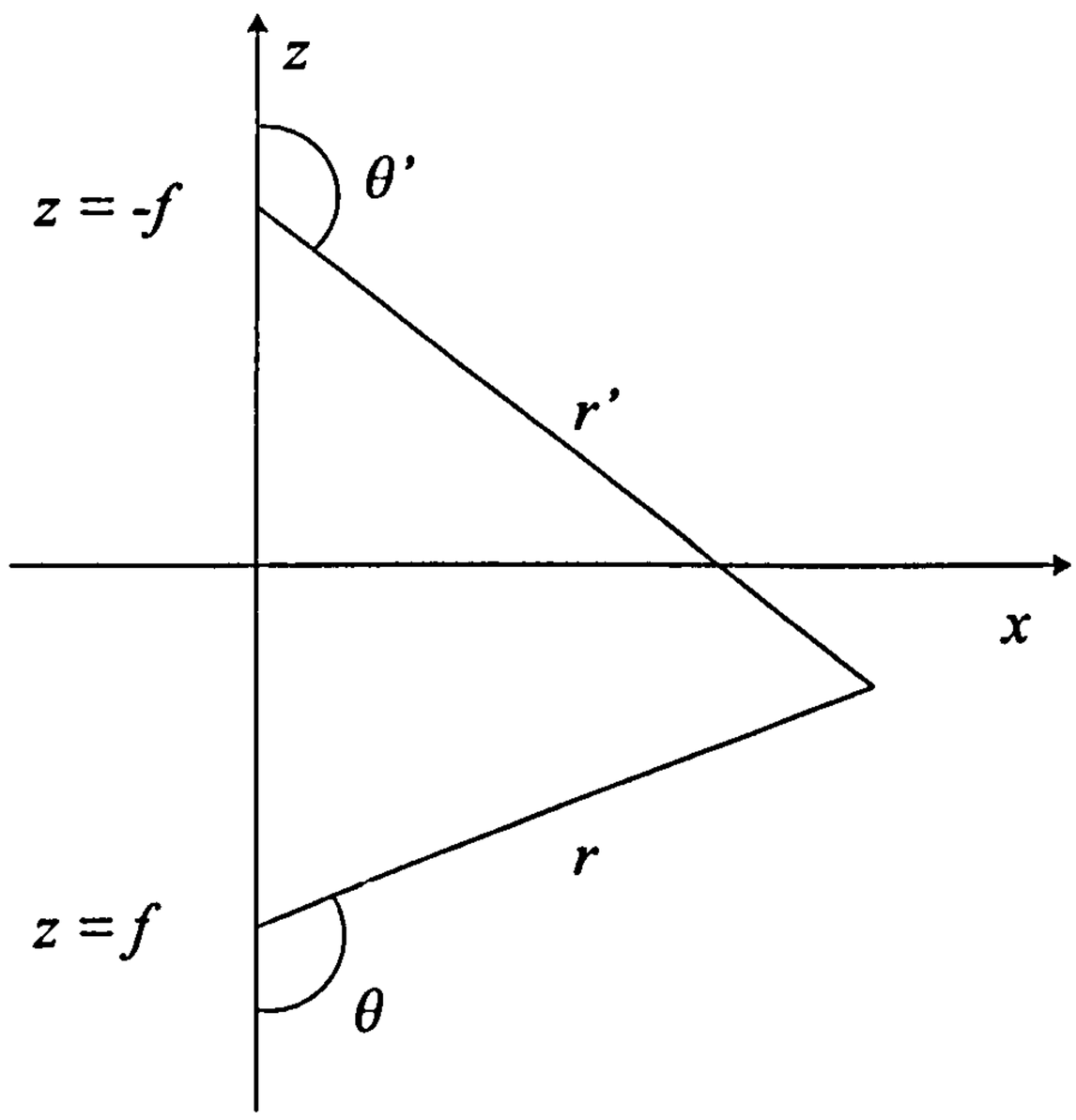

Figure D.1: Definition sketch

In this appendix we will develop integral representations of the functions $K_n(lr)\cos n\theta$ and $K_n(lr)\sin n\theta$. We will use cylindrical polar coordinates (r,θ) and (r',θ') centred on $z=f$ and $z=-f$ respectively defined by

$$x = r\sin\theta = r'\sin\theta' \quad \text{and} \quad z = f - r\cos\theta = -f + r'\cos\theta', \tag{D.1}$$

as shown in figure D.1. From Watson (1958) page 361 equation 8 we have the following

Graf's addition theorem

$$K_n(lr)\cos n\theta = (-1)^n \sum_{m=-\infty}^{\infty} (-1)^m K_{n+m}(-2lf) I_m(lr')\cos m\theta'. \tag{D.2}$$

Now from Gradshteyn & Ryzhik (1980) page 958 equation 8.432 (1) we have

$$K_{n+m}(-2lf) = \int_0^{\infty} \cosh(n+m)u \; e^{2lf\cosh u} du, \tag{D.3}$$

and substituting this into (D.2) we obtain

$$K_n(lr)\cos n\theta = (-1)^n \sum_{m=-\infty}^{\infty} (-1)^m I_m(lr')\cos m\theta' \int_0^{\infty} \cosh(n+m)u \; e^{2lf\cosh u} du. \tag{D.4}$$

We will now write the summation so that it starts from zero, thus

$$\begin{aligned}
&\sum_{m=-\infty}^{\infty} (-1)^m I_m(lr')\cos m\theta' \cosh(n+m)u \\
&\quad = I_0(lr')\cosh nu + \sum_{m=1}^{\infty} (-1)^m I_m(lr')\cos m\theta'[\cosh(n+m)u + \cosh(n-m)u] \\
&\quad = \cosh nu \sum_{m=0}^{\infty} (-1)^m \epsilon_m I_m(lr')\cos m\theta' \cosh mu,
\end{aligned} \tag{D.5}$$

where $\epsilon_0 = 1$ and $\epsilon_m = 2$ for $m \geq 2$. We can now write (D.4) as

$$\begin{aligned}
&K_n(lr)\cos n\theta \\
&\quad = (-1)^n \int_0^{\infty} \cosh nu \; e^{2lf\cosh u} \left[\sum_{m=0}^{\infty} (-1)^m \epsilon_m I_m(lr')\cos m\theta' \cosh mu\right] du.
\end{aligned} \tag{D.6}$$

From Gray (1978) page 32 equation 2

$$\exp\left[\frac{1}{2}X\left(T+\frac{1}{T}\right)\right] = I_0(X) + \sum_{m=0}^{\infty}\left(T^m + \frac{1}{T^m}\right) I_m(X). \tag{D.7}$$

Putting $X = -lr'$ and $T = e^{u+i\theta'}$ and noting that $I_m(-X) = (-1)^m I_m(X)$, (D.7) becomes

$$\begin{aligned}
&\exp[-lr'(\cosh u\cos\theta' + i\sinh u\sin\theta')] \\
&\quad = \sum_{m=0}^{\infty} (-1)^m \epsilon_m [\cosh mu\cos m\theta' + i\sinh mu\sin m\theta'] I_m(lr').
\end{aligned} \tag{D.8}$$

Taking the real part of (D.8) and substituting into (D.6) we obtain

$$K_n(lr)\cos n\theta = (-1)^n \int_0^{\infty} \cosh nu \; e^{2lf\cosh u} e^{-lr'\cosh u\cos\theta'} \cos(lr'\sinh u\sin\theta') du. \tag{D.9}$$

Finally substituting Cartesian coordinates into the right-hand side gives

$$K_n(lr)\cos n\theta = (-1)^n \int_0^{\infty} \cosh nu\cos(lx\sinh u) e^{-l(z-f)\cosh u} du \qquad z > f. \tag{D.10}$$

By following a similar method the integral representation of $K_n(lr)\sin n\theta$ can be found, which is

$$K_n(lr)\sin n\theta = (-1)^{n+1}\int_0^\infty \sinh nu \sin(lx\sinh u)e^{-l(z-f)\cosh u}du \qquad z > f. \quad \text{(D.11)}$$

Appendix E

Expansions of $K_m(lr_1)\cos m\theta_1$ and $K_m(lr_1)\sin m\theta_1$ in polar coordinates (r_2, θ_2)

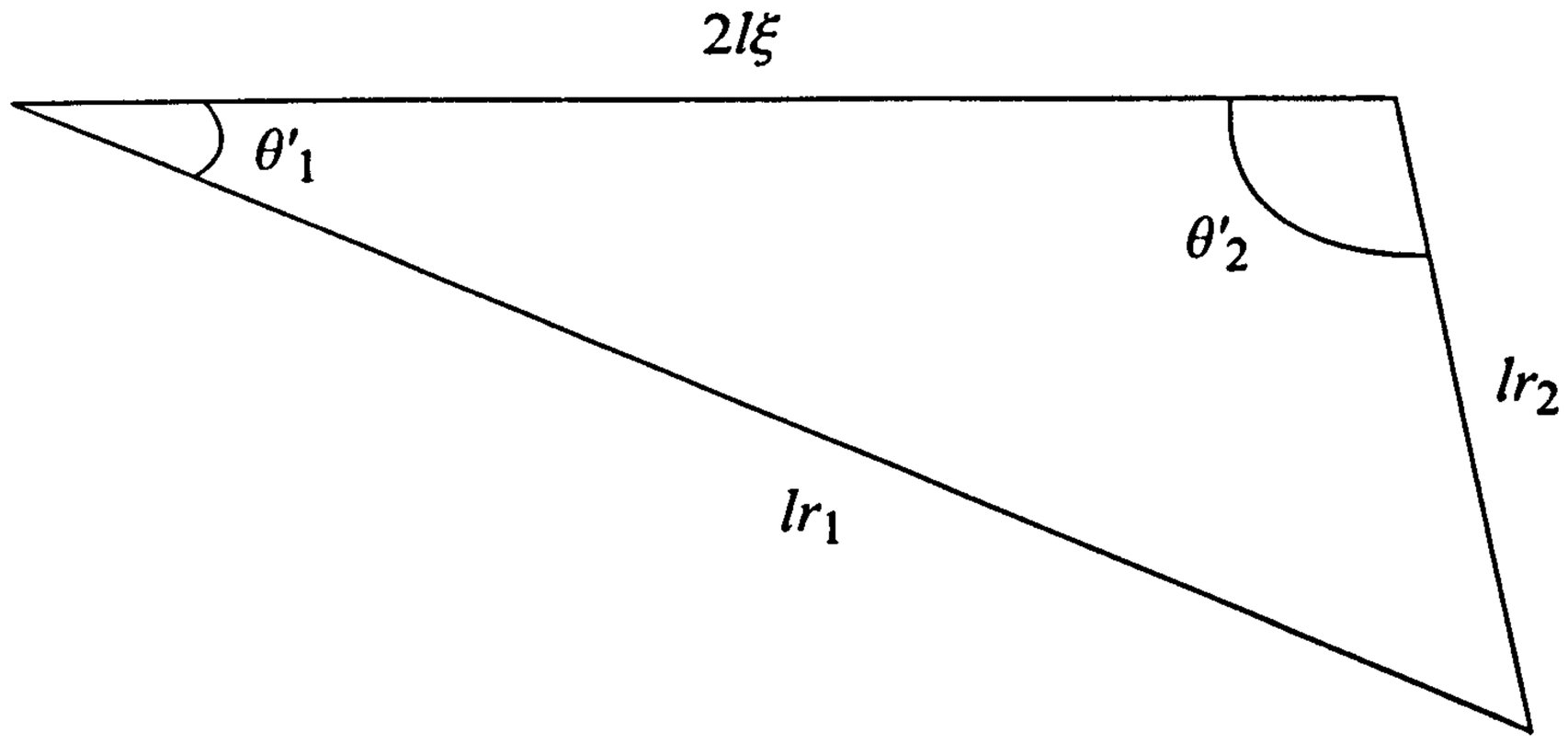

Figure E.1: Definition sketch

Graf's addition theorem can be written as

$$K_m(lr_1)\begin{matrix}\cos\\ \sin\end{matrix} m\theta_1' = \sum_{n=-\infty}^{\infty} K_{m+n}(2l\xi)I_n(lr_2)\begin{matrix}\cos\\ \sin\end{matrix} n\theta_2', \tag{E.1}$$

from Watson (1958) page 361 equation 8 and using figure E.1. From figure 7.1 we can write $\theta_1' = \pi/2 - \theta_1$ and $\theta_2' = \pi/2 + \theta_2$ and substituting these forms into equation (E.1)

and expanding the trigonometric functions we obtain

$$K_m(lr_1)\left[\cos\frac{m\pi}{2}\cos m\theta_1+\sin\frac{m\pi}{2}\sin m\theta_1\right]$$
$$=\sum_{n=-\infty}^{\infty}K_{m+n}(2l\xi)I_n(lr_2)\left[\cos\frac{n\pi}{2}\cos n\theta_2-\sin\frac{n\pi}{2}\sin n\theta_2\right] \quad \text{(E.2)}$$

and

$$K_m(lr_1)\left[\sin\frac{m\pi}{2}\cos m\theta_1-\cos\frac{m\pi}{2}\sin m\theta_1\right]$$
$$=\sum_{n=-\infty}^{\infty}K_{m+n}(2l\xi)I_n(lr_2)\left[\sin\frac{n\pi}{2}\cos n\theta_2+\cos\frac{n\pi}{2}\sin n\theta_2\right]. \quad \text{(E.3)}$$

To obtain an expression for $K_m(lr_1)\cos m\theta_1$ in terms of r_2 and θ_2 we require (E.2)$\times\cos(m\pi/2)$+(E.3)$\times\sin(m\pi/2)$ which gives

$$K_m(lr_1)\cos m\theta_1=\sum_{n=-\infty}^{\infty}K_{m+n}(2l\xi)I_n(lr_2)$$
$$\times\left[\cos\frac{(m-n)\pi}{2}\cos n\theta_2+\sin\frac{(m-n)\pi}{2}\sin n\theta_2\right]. \quad \text{(E.4)}$$

Using (E.2)$\times(\sin m\pi/2)-$(E.3)$\times(\cos m\pi/2)$ we obtain an equivalent expression for $K_m(lr_1)\sin m\theta_1$ which is

$$K_m(lr_1)\sin m\theta_1=\sum_{n=-\infty}^{\infty}K_{m+n}(2l\xi)I_n(lr_2)$$
$$\times\left[\sin\frac{(m-n)\pi}{2}\cos n\theta_2-\cos\frac{(m-n)\pi}{2}\sin n\theta_2\right]. \quad \text{(E.5)}$$

For convenience we require the summations to start from zero and so the expansions now take the form

$$K_m(lr_1)\cos m\theta_1=\sum_{n=0}^{\infty}\frac{\epsilon_n}{2}I_n(lr_2)(K_{m-n}(2l\xi)+(-1)^mK_{m+n}(2l\xi))$$
$$\times\left[\cos\frac{(m+n)\pi}{2}\cos n\theta_2-\sin\frac{(m+n)\pi}{2}\sin n\theta_2\right] \quad \text{(E.6)}$$

and

$$K_m(lr_1)\sin m\theta_1=\sum_{n=0}^{\infty}\frac{\epsilon_n}{2}I_n(lr_2)(K_{m-n}(2l\xi)+(-1)^{m+1}K_{m+n}(2l\xi))$$
$$\times\left[sin\frac{(m+n)\pi}{2}\cos n\theta_2+\cos\frac{(m+n)\pi}{2}\sin n\theta_2\right]. \quad \text{(E.7)}$$

Bibliography

Abramowitz, M. & Stegun, I. A. (1965), *Handbook of Mathematical Functions*, Dover, New York.

Barthélemy, E., Kabbaj, A. & Germain, J. P. (2000), 'Long wave surface by a step in a two-layer fluid', *Fluid Dynamics Research* **26**, 235–255.

Berry, M. V. & Wilkinson, M. (1984), 'Diabolical points in the spectra of triangles', *Proc. Roy. Soc. Lond.* **A392**, 15–43.

Cadby, J. R. & Linton, C. M. (2000), 'Three-dimensional water-wave scattering in two-layer fluids', *J. Fluid Mech.* **423**, 155–173.

Dean, W. R. (1948), 'On the reflexion of surface waves by a submerged circular cylinder', *Proc. Camb. Phil. Soc.* **44**, 483–491.

Endo, H. (1987), 'Shallow-water effect on the motions of three-dimensional bodies in waves', *J. Ship Research* **31**, 34–40.

Evans, D. V. & Linton, C. M. (1989), 'Active devices for the reduction in wave intensity', *Appl. Ocean Res.* **11**, 26–32.

Evans, D. V. & Porter, R. (1998), 'Trapped modes embedded in the continuous spectrum', *Q. Jl Mech. appl. Math.* **52**, 263–274.

Friis, A., Grue, J. & Palm, E. (1991), Application of fourier transform to the second order 2D wave diffraction problem, *in* T. Miloh, ed., 'M. P. Tulins Festschrift: Mathematical Approaches In Hydrodynamics', SIAM, pp. 209–227.

Garrison, C. J. (1985), Interaction of oblique waves with an infinite cylinder, *in* C. A. Brebbia, ed., 'Boundary Element Research', Computational Mechanics Limited.

Gavrilov, N., Ermanyuk, E. & Sturova, I. (1999), Scattering of internal waves by a circular cylinder submerged in a stratified fluid, *in* 'Proc. 22nd Symposium on Naval Hydrodynamics', pp. 907–919.

Gradshteyn, I. S. & Ryzhik, I. M. (1980), *Tables of Integrals, Series and Products*, Academic Press.

Gray, A. & Matthews, G. B. (1952), *A Treatise on Bessel Functions and Their Applications to Physics.*, MacMillan, London.

Gray, E. P. (1978), 'Scattering of surface waves by a submerged sphere', *J. Engng. Math.* **12**, 15–41.

Havelock, T. H. (1955), 'Waves due to a floating sphere making periodic heaving oscillations', *Proc. Roy. Soc. Lond.* **A231**, 1–7.

Hulme, A. (1982), 'The wave forces on a floating hemisphere undergoing forced periodic oscillations', *J. Fluid Mech.* **121**, 443–463.

Iooss, G. (1999), 'Gravity and capillary-gravity periodic travelling waves for two superposed fluid layers, one being of infinite depth', *J. Math. Fluid Mech.* **1**, 24–61.

Kassem, S. E. (1982), 'Multipole expansions for two superposed fluids, each of finite depth', *Math. Proc. Camb. Phil. Soc.* **91**, 323–329.

Kreisel, G. (1949), 'Surface waves', *Quart. Appl. Math.* **7**, 21–44.

Kuznetsov, N. (1993), 'Trapped modes of internal waves in a channel spanned by a submerged cylinder', *J. Fluid Mech.* **254**(8), 113–126.

Lamb, H. (1932), *Hydrodynamics (6th edn).*, Cambridge University Press. Reprinted 1993.

Levine, H. (1965), 'Scattering of surface waves by a submerged circular cylinder', *J. Math. Physics.* **6**(8), 1231–1243.

Linton, C. M. (1991), 'Radiation and diffraction of water waves by a submerged sphere in finite depth', *Ocean Engng* **18**, 61–74.

Linton, C. M. & Kuznetsov, N. G. (1997), 'Non-uniqueness in two-dimensional water wave problems: numerical evidence and geometric restrictions.', *Proc. R. Soc. Lond. A* **453**, 2437–2460.

Linton, C. M. & McIver, M. (1995), 'The interaction of waves with horizontal cylinders in two-layer fluids', *J. Fluid Mech.* **304**, 213–229.

Linton, C. M. & McIver, P. (1998), 'Acoustic resonances in the presence of radial fins in circular cylindrical waveguides.', *Wave Motion* **28**, 99–117.

Martin, P. A. (1989), On the computation and excitation of trapping modes, *in* 'Proc. 4th Intl Workshop on Water Waves and Floating Bodies, Øystese, Norway', pp. 145–147.

McIver, P. & Evans, D. V. (1984), 'The occurance of negative added-mass in free-surface problems involving submerged oscillating bodies', *J. Engng. Math.* **18**, 7–22.

McIver, P. & Evans, D. V. (1985), 'The trapping of surface waves above a submerged, horizontal cylinder', *J. Fluid Mech.* **151**, 243–255.

Mei, C. C. (1983), *The Applied Dynamics of Ocean Surface Waves*, Wiley Interscience, New York.

Milgram, J. H. & Halkyard, J. E. (1971), 'Wave forces on large objects in the sea', *J. Ship Res.* **15**, 115–124.

Newman, J. N. (1976), The interaction of stationary vessels with regular waves, *in* 'Proc. 11th Symp. on Naval Hydrodynamics', London.

Newman, J. N. (1977), *Marine Hydrodynamics*, MIT Press.

Nguyen, T. & Yeung, R. W. (1997), Steady wave systems in a two-layer fluid of finite depth, *in* 'Proc. 9th Intl Workshop on Water Waves and Floating Bodies, Marseille, France', pp. 195–198.

Ogilvie, T. F. (1963), 'First and second order forces on a cylinder submerged under a free surface', *J. Fluid Mech.* **16**, 451–472.

Srokosz, M. A. (1979), 'The submerged sphere as an absorber of wave power', *J. Fluid Mech.* **95**, 717–741.

Stokes, G. G. (1847), 'On the theory of oscillatory waves', *Trans. Camb. Phil. Soc.* **8**, 441–455. Reprinted in *Mathematical and Physical Papers* **1**, 314–326.

Sturova, I. V. (1994), 'Planar problem of hydrodynamic shaking of a submerged body in the presence of motion in a two-layered fluid', *J. Applied Mechanics and Technical Physics* **35**, 670–679.

Sturova, I. V. (1999), 'Problems of radiation and diffraction for a circular cylinder in a stratified fluid', *Fluid Dynamics* **34**(4), 521–533.

Thorne, R. C. (1953), 'Multipole expansions in the theory of surface waves', *Proc. Camb. Phil. Soc.* **49**, 709–716.

Ursell, F. (1950), 'Surface waves on deep water in the presence of a submerged circular cylinder I', *Proc. Camb. Phil. Soc.* **46**, 141–152.

Ursell, F. (1951), 'Trapping modes in the theory of surface waves', *Proc. Camb. Phil. Soc.* **47**, 347–358.

Watson, G. N. (1958), *A Treatise on the Theory of Bessel Functions*, Camb. Press.

Yeung, R. & Nguyen, T. (1999), Radiation and diffraction of waves in a two-layer fluid, *in* 'Proc. 22nd Symposium on Naval Hydrodynamics', pp. 875–891.

Zilman, G. & Miloh, T. (1995), 'Hydrodynamics of a body moving over a mud layer - part 1: wave resistance', *J. Ship Research* **39**(3), 1947–201.